

**UNIVERSITY OF GAZİANTEP  
GRADUATE SCHOOL OF  
NATURAL AND APPLIED SCIENCES**

**CHARACTERIZATION AND UTILIZATION OF  
CALCINED TURKISH KAOLINS FOR IMPROVING  
STRENGTH AND DURABILITY ASPECTS OF  
CONCRETE**

**Ph. D. THESIS  
IN  
CIVIL ENGINEERING**

**BY  
KASIM MERMERDAŞ**

**JANUARY 2013**

**Characterization and Utilization of Calcined Turkish  
Kaolins for Improving Strength and Durability Aspects of  
Concrete**

**Ph. D. Thesis  
in  
Civil Engineering**

**Supervisor  
Assoc. Prof. Dr. Erhan GÜNEYİSİ**

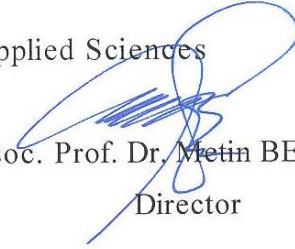
**by  
Kasım MERMERDAŞ  
January 2013**

©2013 [Kasım MERMERDAŞ]

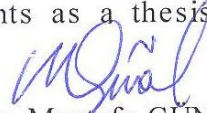
REPUBLIC OF TURKEY  
UNIVERSITY OF GAZİANTEP  
GRADUATE SCHOOL OF NATURAL & APPLIED SCIENCES  
CIVIL ENGINEERING DEPARTMENT

Name of the thesis : Characterization and Utilization of Calcined Turkish  
Kaolins for Improving Durability and Mechanical Aspects of Concrete  
Name of the Student : Kasım MERMERDAŞ  
Exam date : January 22, 2013


Approval of the Graduate School of Natural and Applied Sciences

  
Assoc. Prof. Dr. Metin BEDİR  
Director

I certify that this thesis satisfies all the requirements as a thesis for the  
degree of Doctor of Philosophy

  
Prof. Dr. Mustafa GÜNAL  
Head of Department

This is to certify that we have read this thesis and that in our opinion it is fully  
adequate, in scope and quality, as a thesis for the degree of Doctor of  
Philosophy.

  
Assoc. Prof. Dr. Erhan GÜNEYİSİ  
Supervisor

Examining Comitee Members:

Prof. Dr. Turan ÖZTURAN

Assist. Prof. Dr. Osman KAYA

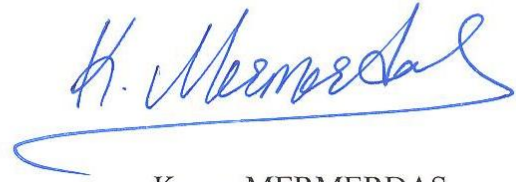
Assoc. Prof. Dr. Erhan GÜNEYİSİ

Assoc. Prof. Dr. Mehmet GESOĞLU

Assoc. Prof. Dr. Hanifi ÇANAKCI

Signature  
  
  
  
  


**I hereby declare that all information in this document has been obtained and presented in accordance with academic rules and ethical conduct. I also declare that, as required by these rules and conduct, I have fully cited and referenced all material and results that are not original to this work.**



Kasim MERMERDAŞ

## ABSTRACT

### CHARACTERIZATION AND UTILIZATION OF CALCINED TURKISH KAOLINS FOR IMPROVING STRENGTH AND DURABILITY ASPECTS OF CONCRETE

MERMERDAŞ, Kasım  
Ph.D. in Civil Engineering  
Supervisor(s): Assoc. Prof. Dr. Erhan GÜNEYİSİ  
January 2013  
200 pages

In this thesis, an experimental investigation on the utilization of calcined impure Turkish kaolins as supplementary cementing material to improve mechanical and durability characteristics of concrete was presented. Microstructural characteristics of the raw kaolins were analyzed and the alteration in microstructural properties were monitored as a result of calcination process. The microstructural features were measured by means of X ray diffraction analysis (XRD), thermal analyses (DTA-TG), scanning electron microscopy (SEM), particle size distribution with laser diffractometer, and Brunauer-Emmet-Teller (BET) nitrogen adsorption specific surface area measurements. Pozzolanic properties of calcined kaolins were evaluated and compared. Furthermore, commercially available high reactivity metakaolin (MK) from Czech Republic was used for comparison. The concretes of different properties including various amounts of calcined kaolins and MK were produced for comparison and evaluation of the effectiveness of the calcined kaolin on the mechanical (compressive and splitting tensile strength) and durability (gas permeability, water permeability, sorptivity, rapid chloride penetration, electrical resistivity, freezing-thawing resistance, drying shrinkage, and corrosion behavior) characteristics of concrete. Finally, an analytical study was carried out to obtain explicit mathematical formulation for estimation of the concrete properties.

**Keywords:** Calcination, Concrete, Durability, Metakaolin, Microstructure, Strength

## ÖZ

### TÜRKİYE KÖKENLİ KALSİNE KAOLENİN BETONUN DAYANIM VE DAYANIKLILIK ÖZELLİKLERİNİ İYİLEŞTİRİLMEDE KULLANIMININ ARAŞTIRILMASI

MERMERDAŞ, Kasım  
Doktora Tezi, İnşaat Mühendisliği Bölümü  
Tez Yöneticisi: Doç. Dr. Erhan GÜNEYİSİ  
Ocak 2013  
200 sayfa

Bu tezde saflaştırılmamış yerli kaolenlerin kalsine edilerek betonun mekanik ve durabilite özelliklerini iyileştirmede bir katkı malzemesi olarak kullanılabilirlikleri üzerine deneysel bir araştırma gerçekleştirilmiştir. Kaolenlerin kalsinasyon öncesi ve sonrası mikro yapıları analiz edilmiş ve kalsinasyonun bu özellikleri nasıl etkilediği incelenmiştir. Ham kaolenlerin mikroyapıları X ışınları kırınımı, lazerli tane boyut dağılımı, Brenaur-Emmet-Teller (BET) özgül yüzey alanı ölçümü ve ısıtma işlem karakterizasyonu yoluyla belirlenmiştir. Üretilen kalsine kaolenlerin puzolanik özellikleri belirlenmiş ve karşılaştırılmıştır. Ayrıca, Çek Cumhuriyeti'nden temin edilen yüksek reaktiviteli ticari metakaolen de karşılaştırma amaçlı kullanılmıştır. Daha sonra üretilen kalsine kaolenler ve metakaolen kullanılarak beton üretimi gerçekleştirilmiş ve betonların sertleşmiş özellikleri incelenmiştir. İncelenen mekanik özellikler basınç ve yarmada çekme dayanımları iken durabilite özellikleri olarak gaz geçirimsizliği, basınçlı su işleme deneyi, kılcal su geçirimsizlik deneyi, elektriksel direnç deneyi, donma-çözünme direnci, korozyon davranışı ve kuruma rötreleri de araştırılmıştır. Deneysel çalışmadan elde edilen sonuçlar kullanılarak analitik modelleme çalışması yapılmış ve beton özelliklerini tahmin etmek için matematiksel ilişkiler sunulmuştur.

**Anahtar Kelimeler:** Beton, Dayanım, Dayanıklılık, Kalsinasyon, Metakaolen, Mikroyapı

*To my wife and sons*  
*Emel, Berkant and Yunus Emre*



## ACKNOWLEDGEMENT

I would like to express my gratitude and deep appreciations to my supervisor, Assoc. Prof. Dr. Erhan GÜNEYİSİ for his invaluable help, advices and directions during this thesis.

Special thanks are reserved for Prof. Dr. Turan ÖZTURAN, Assoc. Prof. Dr. Mehmet GESOĞLU, Assoc. Prof. Dr. Hanifi ÇANAKCI, and Assist. Prof. Dr. Osman KAYA for serving on the committee and their contributions and suggestions to improve the quality of the thesis.

This study received a financial support from Gaziantep University Scientific Research Projects Governing Unit under grant number MF09.04. I also would like to thank to conscientious specialists and technicians of Materials and Chemistry Institutes of TUBITAK Marmara Research Center for conducting microstructural analyses of kaolins.

"Balıkesir-Düvertepe kaolin" was obtained from Matel Hammadde Sanayi ve Ticaret A.Ş., "Balıkesir-Danaçayırı kaolin" was obtained from Cam-Ser Madencilik A.Ş. from Şişecam Group, "Çanakkale-Çan kaolin" was obtained from Kalemaden Endüstriyel Hammaddeler San. ve Tic. A.Ş., "Bursa-Mustafa Kemal kaolin" was obtained from Gökser Madencilik İnşaat Turizm Sanayi ve Ticaret Ltd. Şti. Moreover, the micronization of kaolins was carried out at grinding plant belonging to Gökser Madencilik.

Advices and notifications of Dr. Mining Eng. Mustafa Salih EYGİ about native kaolins were gratefully acknowledged.

I would like to extend my thanks to my colleague Res. Assist. Süleyman İPEK, for his precious helps in experimental phase of the study.

Finally, I would like to express my particular thanks to my family, especially to my wife and my kids for their, patience, support, and tolerance.

## CONTENTS

Page

<b>ABSTRACT</b> .....	i
<b>ÖZET</b> .....	ii
<b>ACKNOWLEDGEMENT</b> .....	iv
<b>TABLE OF CONTENTS</b> .....	v
<b>LIST OF TABLES</b> .....	ix
<b>LIST OF FIGURES</b> .....	xi
<b>LIST OF SYMBOLS/ABBREVIATIONS</b> .....	xix
<b>CHAPTER 1 INTRODUCTION</b> .....	1
1.1 General.....	1
1.2 Outline of the thesis.....	3
<b>CHAPTER 2 LITERATURE REVIEW AND BACKGROUND</b> .....	5
2.1 General .....	5
2.2 Metakaolin as a mineral admixture.....	7
2.2.1 Conversion of kaolin to metakaolin.....	7
2.2.2 Effect of metakaolin on hydration mechanism.....	8
2.3 Effect of MK on the fresh properties of concrete.....	9
2.4 Effect of metakaolin on the hardened properties of concrete.....	11
2.4.1 Mechanical properties.....	13
2.4.2 Time dependent properties.....	16
2.4.3 Durability properties.....	19
<b>CHAPTER 3 EXPERIMENTAL STUDY</b> .....	27
3.1 Stage 1: Examining properties of raw and calcined kaolins.....	27
3.1.1 Materials: Turkish kaolins .....	27
3.1.2 Test methods on microstructural and thermal characterization .....	29
3.1.2.1 X-Ray Diffraction Analysis.....	29

	<u>Page</u>
3.1.2.2 Differential thermal and thermo gravimetric analyses (DTA-TG).....	29
3.1.2.3 Particle Size Distribution .....	30
3.1.2.4 Specific Surface Area.....	30
3.1.2.5 Scanning electron microscopy (SEM).....	30
3.1.2 Heat treatment.....	30
3.1.3 Pozzolanic activity index.....	32
3.2 Stage 2: Experimental study on concrete.....	33
3.2.1 Materials.....	33
3.2.1.1 Cement.....	33
3.2.1.2 Calcined kaolins and commercial metakaolin.....	33
3.2.1.3 Aggregates.....	34
3.2.1.4 Superplasticizer.....	35
3.2.2 Mix proportions .....	35
3.2.3 Test methods.....	38
3.2.3.1 Compressive strength.....	38
3.2.3.2 Splitting tensile .....	38
3.2.3.3 Rapid chloride permeability test (RCPT).....	38
3.2.3.4 Water Permeability.....	40
3.2.3.5 Gas Permeability.....	40
3.2.3.6 Sorptivity.....	43
3.2.3.7 Electrical resistivity.....	44
3.2.3.8 Resistance against freeze-thaw cycles.....	45
3.2.3.9 Ultrasonic pulse velocity.....	46
3.2.3.10 Corrosion current density by linear polarization resistance (LPR) technique.....	48
3.2.3.11 Drying Shrinkage and Weight Loss.....	51
<b>CHAPTER 4 TEST RESULTS AND DISCUSSIONS.....</b>	<b>52</b>
4.1 Results on microstructural characterization and pozzolanic activity of calcined kaolins.....	52
4.1.1 Mineral composition by X –ray diffraction analysis.....	52
4.1.2 Thermal characterization .....	53

	<b><u>Page</u></b>
4.1.3 Pozzolanic activity.....	56
4.1.4 Fineness and particle size distribution.....	59
4.1.5 SEM image analysis.....	62
4.2 Results on mechanical properties of concrete.....	64
4.2.1 Compressive strength development.....	64
4.2.2 Splitting tensile strength .....	72
4.3 Results on permeability and durability related properties of concretes.....	75
4.3.1 Gas permeability.....	75
4.3.2 Water permeability .....	84
4.3.3 Water sorptivity .....	90
4.3.4 Rapid chloride penetration test.....	92
4.3.5 Electrical resistivity.....	95
4.3.6 Freezing and thawing.....	98
4.3.7 Corrosion current density with linear polarization resistance.....	104
4.3.8 Drying Shrinkage and weight loss.....	109
<b>CHAPTER 5 STATISTICAL ANALYSIS AND CORRELATIONS.....</b>	<b>115</b>
5.1 Analysis of variance (ANOVA) study on the experimental data.....	115
5.2 Correlations between properties of concrete.....	120
<b>CHAPTER 6 ANALYTICAL MODELLING.....</b>	<b>128</b>
6.1 Introduction.....	128
6.2 Genetic Programming.....	129
6.3 Multiple linear regression (MLR) .....	131
6.4 Derivation of the mathematical models.....	132
6.5 Prediction performances of the models.....	143
<b>CHAPTER 7 CONCLUSIONS.....</b>	<b>150</b>
7.1 Introduction.....	150
7.2 Microstructural characterization and pozzolanic activity of kaolins.....	150
7.3 Properties of the concretes.....	152
7.4 Mathematical modeling .....	154

	<u>Page</u>
<b>REFERENCES.....</b>	<b>156</b>
<b>APPENDIX A Input and output databases.....</b>	<b>169</b>
<b>APPENDIX B Mathematical models .....</b>	<b>176</b>

## **LIST OF TABLES**

	<b><u>Page</u></b>
Table 2.1 Fresh properties of blended cements with metakaolin (Batis, 2005).....	10
Table 2.2 Electrical indication of chloride penetrability of control and blended concretes (Poon et al., 2006).....	21
Table 3.1 Designation of the experimental codes of the calcined kaolin samples.....	28
Table 3.2 Chemical compositions and specific gravities of the Turkish kaolins.....	29
Table 3.3 Chemical composition of the cement.....	33
Table 3.4 Chemical, physical and mineralogical properties of the calcined Turkish kaolins, commercial metakaolin.....	34
Table 3.5 Properties of the superplasticizer.....	35
Table 3.6 Mix Proportions ( $\text{kg}/\text{m}^3$ ).....	37
Table 3.7 Interpretation of the test results obtained using RCPT test.....	39
Table 4.1. Semiquantitative phase estimation results.....	53
Table 4.2 Compressive strength values of the mortar specimens.....	57
Table 4.3 Particle size distribution of the raw and calcined kaolin samples.....	62
Table 4.4 Compressive strength (MPa) of the concretes.....	67
Table 4.5 Splitting tensile strength (MPa) of the concretes.....	73
Table 4.6 Apparent gas permeability coefficients ( $\times 10^{-16} \text{ m}^2$ ) average of K values for 150, 200, and 300 kPa inlet pressures as recommended per RILEM (1999).....	82
Table 4.7 Water penetration depths (mm) measured at 28 and 90 days.....	86
Table 4.8 28 and 90 days sorptivity values ( $\text{mm}/\text{min}^{1/2}$ ) of concretes.....	90
Table 4.9 Total charge values (Coulombs) measured at 28 and 90 days.....	93
Table 4.10 Electrical resistivity values (Kohm.cm) of the concretes at 28 and 90 days.....	96
Table 4.11 Corrosion rates (mm/yr) of concretes before and after exposure to chloride attack.....	108
Table 5.1 Statistical evaluation of pozzolanic activity index.....	116
Table 5.2 Statistical evaluation of compressive strength of the concretes produced with calcined kaolins.....	117

	<b><u>Page</u></b>
Table 5.3 Statistical evaluation of the gas permeability, RCPT, sorptivity, and water permeability of the concretes .....	118
Table 5.4 Statistical evaluation of electrical resistivity and corrosion rate.....	119
Table 5.5 Statistical evaluation of UPV loss due to 300 freezing and thawing cycles.....	120
Table A1 Input and output database for compressive strength (training set).....	170
Table A2 Input and output database for compressive strength (testing set).....	171
Table A3 Input and output database for splitting tensile strength.....	172
Table A4 Input and output database used for constructing the models for permeability properties.....	173
Table A5 Summary of input and output database used for shrinkage modeling.....	174
Table A6 Input and output database used for electrical resistivity modeling.....	175
Table A7 Summary of input and output database used for corrosion current density modeling.....	175

## **LIST OF FIGURES**

	<b><u>Page</u></b>
Figure 2.1 HRWR dosage for different W/B ratios. (Madandoust and Mousavi, 2012).....	10
Figure 2.2 Differential thermograms of OPC-metakaolin mix hydrated for different periods (Singh and Garg 2004).....	12
Figure 2.3 SEM of OPC-metakaolin mixture hydrated for different periods (a) 3 days, (b) 7 days, (c) 28 days, and (d) 90 days (Singh and Garg 2004).....	12
Figure 2.4 Effect of the percentage of metakaolin on the density of concrete mixes containing 45% glass (Al-Sibahy and Edwards, 2012).....	13
Figure 2.5 Effect of silica fume and metakaolin on compressive strength development of concretes (Güneyisi et al., 2012a).....	15
Figure 2.6 Effect of silica fume and metakaolin on splitting tensile strength of concretes (Güneyisi et al., 2012a).....	15
Figure 2.7 Flexural strength versus replacement with ages (Kim et al., 2007).....	16
Figure 2.8 Total shrinkage of drying concrete specimens (Brooks and Johari, 2001).....	17
Figure 2.9 Influence of metakaolin on total creep of concrete (Brooks and Johari, 2001).....	17
Figure 2.10 Effect of metakaolin and silica fume on free shrinkage of concretes with a w/b ratio of 0.35 (Güneyisi et al., 2012a).....	18
Figure 2.11 Effect of metakaolin and silica fume on the initiation and propagation of restrained shrinkage cracking of concretes having a w/b ratio of 0.35 (Güneyisi et al., 2012a).....	19
Figure 2.12 Levels of decrease in water permeability of concretes in comparison to control specimen.....	21
Figure 2.13 Effect of metakaolin replacement level on different transport properties (Shekarchi et al., 2010).....	22
Figure 2.14 Chloride ions ingress profile test result. (Shekarchi et al., 2010).....	22



	<u>Page</u>
Figure 2.15 Percentage of weight gained of freezing and thawing specimens for all tested SCC.....	23
Figure 2.16 Percentage of pulse velocity reduction of freezing and thawing specimens for all tested SCC.....	24
Figure 2.17 Corrosion potentials of specimens immersed in sodium-chloride solution (Batis et al., 2005) .....	25
Figure 2.18 Electrochemical mass loss of mortar specimens immersed in sodium-chloride solution (Batis et al., 2005).....	25
Figure 2.19 Corrosion rate measurement for concrete specimens with MK. (Parande et al., 2008).....	26
Figure 3.1 The sources of the kaolins used in this study.....	27
Figure 3.2 Photographic views of muffle furnace.....	30
Figure 3.3 Heating and cooling cycles for each heat treatment level.....	31
Figure 3.4 Aggregate grading curves.....	35
Figure 3.5 Schematic presentation of the test set up for RCPT.....	38
Figure 3.6 Photographic view of the RCPT test set up.....	38
Figure 3.7 Water permeability test: a) device and b) measurement of penetration depth.....	39
Figure 3.8 Gas permeability test: a) photographic view of the gas permeability set up, b) schematic presentation of set-up, c) detail of pressure cell and test specimen.....	42
Figure 3.9 Sorptivity test set up.....	43
Figure 3.10 Photographic view of the ER test device.....	44
Figure 3.11 Compressive strength test on freezing-thawing specimen.....	46
Figure 3.12 Schematic presentation of the test set up for UPV.....	47
Figure 3.13 The points for UPV change monitoring due to freezing and thawing.....	48
Figure 3.14 Schematic presentation of the linear polarization resistance test set up..	49
Figure 3.15 Photographic view of the potentiostat/galvanostat test set up.....	50
Figure 3.16 Free shrinkage specimens.....	51
Figure 4.1 XRD patterns and mineralogical compositions of the kaolin samples.....	53
Figure 4.2 DTA curves for the kaolins for observation of the phase transformations.....	55

	<u>Page</u>
Figure 4.3 TG curves of the kaolins.....	55
Figure 4.4 Pozzolanic activity indices of the calcined kaolins.....	57
Figure 4.5 Weight losses of the kaolins due to 3 h calcination process.....	58
Figure 4.6 XRD patterns of the calcined Turkish kaolins.....	59
Figure 4.7 Photographic views of a) Hammer mill, b) Feeding the mill.....	60
Figure 4.8 BET Specific surface area of the raw and calcined kaolin samples.....	60
Figure 4.9 Particle size distribution of the raw and calcined CC.....	61
Figure 4.10 SEM images of calcined kaolins at x500 magnification.....	63
Figure 4.11 SEM images of a) raw, b) calcined DV kaolin at different magnifications.....	63
Figure 4.12 Compressive strength development of the concretes incorporating a) 5%, b) 10%, c) 15% and d) 20% CK or MK.....	69
Figure 4.13 Effect of replacement level of MK or CKs on a) 3 days, b) 7 days, c) 28 days, and d) 90 days relative compressive strength of concretes.....	71
Figure 4.14 Splitting tensile strengths of the plain and mineral admixed concretes at 28 and 90 days.....	73
Figure 4.15 Effect of replacement level on splitting tensile strength of the concretes at a) 28 days, b) 90 days ( $F_{s,plain\ concrete} = 100\%$ ).....	74
Figure 4.16 Typical apparent gas permeability profile of control and MK incorporated concretes with inlet pressure: a) 28 days, and b) 90 days.....	77
Figure 4.17 Typical apparent gas permeability profile of control and calcined DV incorporated concretes with inlet pressure: a) 28 days, and b) 90 days.....	78
Figure 4.18 Typical apparent gas permeability profile of control and calcined DC incorporated concretes with inlet pressure: a) 28 days, and b) 90 days.....	79
Figure 4.19 Typical apparent gas permeability profile of control and calcined CC incorporated concretes with inlet pressure: a) 28 days, and b) 90 days.....	80
Figure 4.20 Typical apparent gas permeability profile of control and calcined BMK incorporated concretes with inlet pressure: a) 28 days, and b) 90 days.....	81
Figure 4.21 Variation of 28 day apparent gas permeability coefficients of the concretes with replacement level of CK and MK.....	83
Figure 4.22 Variation of 90 day apparent gas permeability coefficients of the concretes with replacement level of CK and MK.....	83

	<u>Page</u>
Figure 4.23 Water penetration depths of the plain and mineral admixed concretes at 28 and 90 days.....	86
Figure 4.24 Effect of replacement level on water penetration depth of the concretes at a) 28 days, b) 90 days (Penetration depth for Control concrete is 100%).....	87
Figure 4.25 Water sorptivity test results of the plain and mineral admixed concretes.....	90
Figure 4.26 Effect of replacement level on sorptivity indices of the concretes at a) 28 days, b) 90 days (Sorptivity index for Control concrete is 100%).....	91
Figure 4.27 RCPT test results of the plain and mineral admixed concretes at 28 and 90 days.....	93
Figure 4.28 Effect of replacement level on chloride resistance of the concretes at a) 28 days, b) 90 days (Charge passed for Control concrete is 100%).....	94
Figure 4.29 Electrical resistivity test results of the plain and mineral admixed .....	97
Figure 4.30 Effect of replacement level on electrical resistivity of the concretes at a) 28 days, b) 90 days (Electrical resistivity for Control concrete is 100%).....	98
Figure 4.31 Reduction in UPV values of the concretes at the end of 300 freezing-thawing cycles: a) 5% replacement level vs. control b) 15% replacement level vs. control.....	100
Figure 4.32 Percent decrease in a) flexural and b) compressive strength due to 300 cycles of freezing and thawing.....	101
Figure 4.33 Relative flexural strength of a) Undamaged concretes b) Damaged concretes ( $F_{\text{control}}=100\%$ ).....	102
Figure 4.34 Relative compressive strength of a) Undamaged concretes b) Damaged concretes ( $F_{\text{control}}=100\%$ ).....	103
Figure 4.35 Variation of corrosion current density over 40 weeks of 2% NaCl exposure for the concretes incorporating a) 5% and b) 15% MK and CKs.....	106
Figure 4.36 Variation of corrosion current density over 40 weeks of 5% NaCl exposure for the concretes incorporating a) 5% and b) 15% MK and CKs.....	107
Figure 4.37 Corrosion rates of concretes before and after exposure to 2% NaCl solution .....	108

	<u>Page</u>
Figure 4.38 Corrosion rates of concretes before and after exposure to 5% NaCl solution.....	108
Figure 4.39 Drying shrinkage strain development of a) Control and 5% MK or CK incorporated concretes and b) Control and 15% MK or CK incorporated concretes.....	110
Figure 4.40 Variations in weight loss of a) Control and 5% MK or CK incorporated concretes and b) Control and 15% MK or CK incorporated concretes.....	112
Figure 4.41 Average shrinkage rates of a) Control, b) 5%, and c) 15% MK or CK incorporated concretes.....	114
Figure 5.1 Correlation between compressive and splitting tensile strength of concretes.....	122
Figure 5.2. Correlation between gas permeability and water permeability of concretes.....	123
Figure 5.3 Correlation between gas permeability and sorptivity values of concretes.....	123
Figure 5.4 Correlation between gas permeability and RCPT values of concretes....	124
Figure 5.5 Correlation between UPV loss and compressive strength loss of the concretes exposed to 300 freezing and thawing cycles.....	124
Figure 5.6 Correlation between UPV loss and flexural strength loss of the concretes exposed to 300 freezing and thawing cycles.....	125
Figure 5.7 Correlation between 90 day electrical resistivity and corrosion rate of the concretes 40 weeks of 2% NaCl exposure.....	125
Figure 5.8 Correlation between 90 day electrical resistivity and corrosion rate of the concretes 40 weeks of 5% NaCl exposure.....	126
Figure 5.9 Shrinkage strain vs. weight loss of a) Control, b) 5%, and c) 15% MK or CK incorporated concretes.....	127
Figure 6.1 Flowchart for the genetic programming paradigm. (Koza, 1992).....	130
Figure 6.2 A sample sub-expression tree for a mathematical operation.....	131
Figure 6.3 Components of MLR model.....	131
Figure 6.4 Experimental vs. predicted compressive strength values from gene expression programming (GEP) model: a) Training data set and b) Testing data set.....	133

	<u>Page</u>
Figure 6.5 Experimental vs. predicted compressive strength values from MLR model.....	133
Figure 6.6 Experimental vs. predicted splitting tensile strength values from gene expression programming (GEP) model: a) Training data set and b) Testing data set.....	134
Figure 6.7 Experimental vs. predicted compressive strength values from MLR model.....	134
Figure 6.8 Experimental vs. predicted shrinkage strain values from gene expression programming (GEP) model: a) Training data set and b) Testing data set.....	135
Figure 6.9 Experimental vs. predicted shrinkage strain values from MLR model.....	135
Figure 6.10 Experimental vs. predicted gas permeability values from gene expression programming (GEP) model: a) Training data set and b) Testing data set.....	136
Figure 6.11 Experimental vs. predicted gas permeability values from MLR model.....	136
Figure .12 Experimental vs. predicted sorptivity values from gene expression programming (GEP) model: a) Training data set and b) Testing data set.....	137
Figure 6.13 Experimental vs. predicted sorptivity values from MLR model.....	137
Figure 6.14 Experimental vs. predicted water permeability values from gene expression programming (GEP) model: a) Training data set and b) Testing data set.....	138
Figure 6.15 Experimental vs. predicted water permeability values from MLR model.....	138
Figure 6.16 Experimental vs. predicted total charge values from gene expression programming (GEP) model: a) Training data set and b) Testing data set.....	139
Figure 6.17 Experimental vs. predicted total charge values from MLR model.....	139
Figure 6.18 Experimental vs. predicted resistivity values from gene expression programming (GEP) model: a) Training data set and b) Testing data set.....	140

	<u>Page</u>
Figure 6.19 Experimental vs. predicted resistivity values from MLR model.....	140
Figure 6.20 Experimental vs. predicted UPV loss values from gene expression programming (GEP) model: a) Training data set and b) Testing data set.....	141
Figure 6.21 Experimental vs. predicted UPV loss values from MLR model.....	141
Figure 6.22 Experimental vs. predicted $I_{corr}$ values from gene expression programming (GEP) model: a) Training data set and b) Testing data set.....	142
Figure 6.23 Experimental vs. predicted $I_{corr}$ values from MLR model.....	142
Figure 6.24 Prediction performances of GEP and MLR analytical models for compressive strength.....	144
Figure 6.25 Prediction performances of GEP and MLR analytical models for splitting tensile strength.....	144
Figure 6.26 Prediction performances of a) GEP and b) MLR analytical models for shrinkage strain.....	145
Figure 6.27 Prediction performances of GEP and MLR analytical models for gas permeability.....	146
Figure 6.28 Prediction performances of GEP and MLR analytical models for water sorptivity.....	146
Figure 6.29 Prediction performances of GEP and MLR analytical models for water permeability.....	147
Figure 6.30 Prediction performances of GEP and MLR analytical models for rapid chloride permeability test.....	147
Figure 6.31 Prediction performances of GEP and MLR analytical models for electrical resistivity.....	148
Figure 6.32 Prediction performances of GEP and MLR analytical models for UPV loss after 300 cycles of freezing and thawing.....	148
Figure 6.33 Prediction performances of a) GEP and b) MLR analytical models for corrosion current density ( $I_{corr}$ ) values.....	149
Figure B1 GEP expression tree for prediction of compressive strength.....	177
Figure B2 GEP expression tree for prediction of splitting tensile strength.....	179
Figure B3 GEP expression tree for prediction of gas permeability.....	182

	<b><u>Page</u></b>
Figure B4 GEP expression tree for prediction of water permeability.....	185
Figure B5 GEP expression tree for prediction of water sorptivity.....	187
Figure B6 GEP expression tree for prediction of RCPT.....	190
Figure B7 GEP expression tree for prediction of electrical resistivity.....	192
Figure B8 GEP expression tree for prediction of UPV loss.....	194
Figure B9 GEP expression tree for prediction of corrosion current density.....	197
Figure B10 GEP expression tree for prediction of drying shrinkage.....	199

## LIST OF SYMBOLS/ABBREVIATIONS

$\mu$	Viscosity of oxygen
C	Coulombs
CK	Calcined kaolin
CSH	Calcium silicate hydrate
D	Depth of water penetration
DTA	Differential thermal analysis
FA	Fly ash
$F_c$	Compressive strength
$F_s$	Splitting tensile strength
GEP	Gene expression programming
GGBFS	Ground granulated blast furnace slag
$I_{corr}$	Corrosion current density
ITZ	Interfacial transition zone
K	Apparent gas permeability coefficient
LPR	Linear polarization resistance
MK	Metakaolin
MLR	Multiple linear regression
$P_1$	Outlet pressure (kPa)
$P_2$	Inlet pressure (kPa)
PC	Portland cement
PI	Pozzolanic index
Q	Rate of discharge
R/C	Reinforced concrete
S	Sorptivity index
SCC	Self compacting concrete
SEM	Scanning electron microscopy
SF	Silica fume
TG	Thermo gravimetric analysis



UPV	Ultrasonic pulse velocity
w/b	water-to binder ratio
WA	Water absorption
XRD	X ray diffraction
$\beta_a$	Anodic Tafel slope
$\beta_c$	Cathodic Tafel Slope

# CHAPTER 1

## INTRODUCTION

### 1.1 General

Mechanical and durability properties of the concrete are the key parameters for the beneficiation of this material. Hence, to improve the mechanical and durability properties of the concrete, various supplementary cementing materials have extensively been used for many years (Khatri et al., 1997; Güneyisi et al., 2005; Ramezaniyanpour and Malhotra, 1995; Chindaprasirt et al., 2004). Pozzolans, such as fly ash, silica fume, and slag are the most commonly used mineral admixtures in production of high-performance concrete. These materials provide additional performance to the concrete by reacting with Portland cement hydration products to create additional C-S-H gel, the part of the paste being mainly responsible for the concrete strength (Neville, 1996).

Being the most important raw material for various industrial fields, kaolin is converted to metakaolin (MK) through a heat treatment which chemically drives off bound water and alters the crystalline structure (Shvarzman et al., 2003; Kakali et al., 2001; Badogiannis et al., 2005). Unlike industrial by-products such as fly ash, silica fume, and blast-furnace slag, MK is refined carefully to lighten its color, remove inert impurity, and control particle size. Metakaolin is also known as calcined kaolin due to calcination process. Calcined kaolin has extensively been studied since the mid 1990's for improving the mechanical and durability properties of concrete (Sabir et al., 2001; Güneyisi and Mermerdaş, 2007; Güneyisi et al., 2008; Güneyisi et al., 2010; Ding and Li, 2002; Kim et al., 2007). Research has generally been focused on the heat treatment parameters for dehydroxylation or amorphization processes of the kaolinite (Shvarzman et al., 2003). Another field of interest regarding the calcined kaolin related studies is the improvement of concrete properties by using this material at various replacement levels by weight of the total binder. In the literature,

it is emphasized that the influence of calcined kaolin on cement paste is the pore size refinement by micro-filling effect and provision of additional C-S-H gel by secondary hydration reactions (Poon et al., 2006; Wild and Khatib, 1996).

Kaolin clay is generally used in paint, paper, and ceramic industries as coating and filler material. Crude kaolins contain colored impurities such as iron oxide. To comply with the specifications required by the industry kaolin has to be cleaned of all impurities aiming to have kaolinite content up to 100%. However, Shvarzman et al. (2003) demonstrated that useful properties of metakaolin are preserved even at a reduced content (down to 30%) of kaolinite in the raw mix.

There are various kaolin deposits in Turkey with different morphological origins. Due to the distinctions in the formation of these deposits, the mineralogical and chemical properties of the raw materials are somehow different. Geological formation conditions, location, mineralogical and geochemical properties, capacity, quality, origin, and economical conditions of kaolin deposits are the main factors affecting the exploitation of raw kaolin. (Yanık et al., 2010). Kaolin production in Turkey mainly serves the ceramic industry and there has not yet been a proper investigation for the utilization of Turkish kaolins in the form of metakaolin for construction industry. Western region of Turkey provides large kaolin deposits with different geological formations. In this study, four types of unprocessed Turkish kaolins obtained from the same geographic region having the majority of the kaolin beds were experimentally investigated. The experimental program was separated into two stages:

In the first stage, microstructural characteristics such as mineralogical composition and fineness of the materials before and after calcination process were determined by means of X ray diffraction analysis (XRD), thermal analyses (DTA-TG), scanning electron microscopy (SEM), particle size distribution with laser diffractometer, and Brenaur-Emmet-Teller (BET) nitrogen adsorption specific surface area measurements. In order to specify a proper heat treatment to obtain calcined kaolins, the pozzolanic activity indices of the calcined Turkish kaolins were tested and compared.

Second stage of the experimental study covers various mechanical, permeability and durability testing of the concretes. The concretes were produced by incorporation of CKs at four different replacement levels up to 20% of the weight of cement. Moreover, commercially available high reactivity metakaolin (MK) from Czech Republic was also utilized for comparison purpose. Therefore, considering one plain mix as control concrete, totally 21 different mixes were produced for mechanical and permeability testing. The strength development of the concretes were tested up to 90 days while the durability related permeability testing of the concretes were conducted at the ends of 28 and 90 days. Furthermore, the concretes exposed to 300 freezing-thawing cycles were tested for the change in ultrasonic pulse velocity, flexural strength, and compressive strength. Corrosion behavior of steel bar embedded in concretes was monitored through variation of corrosion current density over 40 weeks of exposure to NaCl solution with different concentrations.

## **1.2 Outline of the thesis**

The thesis comprises of 7 chapters. A detailed literature review and general background information about thermally treated kaolins and their effects on the fresh, mechanical, and durability properties of concrete were presented in Chapter 2. The conversion processes of kaolin to metakaolin as well as corresponding alterations in microstructural properties were also explained.

Chapter 3 includes the experimental program carried out in this study. Properties of Turkish kaolins, cement, aggregates, and chemical admixture used in the concrete production were given. Moreover, the details of tests on mechanical, permeability, and durability properties of concretes are described.

Chapter 4 provides the test results of testing program performed. The presented results cover microstructural alterations and pozzolanic properties of Turkish kaolins as well as detailed discussions of test result obtained from concrete testing.

Chapter 5 presents the statistical analyses of the experimental results. Moreover, the correlations between the properties of concretes were presented.

The general information and literature review about genetic programming (GEP) and multiple linear regression (MLR) were introduced in Chapter 6. Mathematical models obtained from GEP and MLR were presented in this chapter. In this section, the performances of explicit formulations of concrete properties were also evaluated.

Chapter 7 contains the summary of the conclusions obtained from experimental and analytical studies presented in this thesis.

## **CHAPTER 2**

### **LITERATURE REVIEW AND BACKGROUND**

#### **2.1 General**

Concrete is the most widely used materials of construction due to its mechanical and durability properties incorporated with lower cost and proper workability. Concrete is therefore an important element of the infrastructure and well-designed concrete can be a durable construction material. The performance of concrete can be determined by its durability and strength. In order to enhance the mechanical and durability properties of the concrete, some supplementary cementing materials have extensively been used for many years (Aldea, 2000; Neville, 1996). These materials, such as silica fume, fly ash, and slag are the most commonly used ones in production of high-performance concrete. Pozzolanic materials impart additional performance to the concrete by reacting with Portland cement hydration products to create extra C-S-H gel as a result of secondary hydration. This gel is the part of the paste which is mainly responsible for the concrete strength.

In last decade, there has been a soaring interest in the utilization of high-reactivity metakaolin (MK) as a supplementary cementitious material in concrete related studies (Sabir et al., 2001; Batis et al., 2005; Güneyisi and Mermerdaş, 2007; Güneyisi et al., 2008; Güneyisi et al., 2012a). MK is an ultrafine pozzolanic material, produced by calcining high purity kaolin clay at temperature ranging from 700 to 900 °C to drive off the chemically bound water and alter the crystalline structure (Sabir et al., 2001; Brooks and Johari, 2001; Snyder, 2000). Being different from industrial by-products such as fly ash, silica fume, and blast-furnace slag, it has to be processed carefully to lighten its color, remove inert impurity, and control particle size. The particle size of commercially available high reactivity metakaolin (MK) is generally less than 2 µm, which is considerably smaller than that of cement particles, though not as fine as silica fume (Bisonette et al., 1999). The studies in the utilization of MK

has been concentrated on the consumption of calcium hydroxide (CH) formed in cement hydration which is associated with low durability. Thus, the use of metakaolin improves long-term strength development and durability. Additionally, it is also possible to obtain early strength enhancement through the filling effect (Cook, 1986).

According to the literature, it has been stated that concrete including metakaolin reveals superior-level engineering properties that can be compared to silica fume concrete (Ding and Li 2002; Güneyisi et al., 2012a). This results from its chemical composition, fineness, and poorly crystalline nature (Frias and Cabrera, 2002). The research works about the use of metakaolin can be classified in two main areas. In the first one, the heat treatment parameters, the dehydroxylation/amorphization process of the kaolinite, and the formation of the metakaolinite have been studied (Frias and Cabrera, 2002; Gamiz et al., 2005; Shvarzman et al., 2003; Kakali et al., 2005; Arıkan et al., 2008). The second field of interest concerns the filling and pozzolanic behavior of metakaolin and its influence on cement and concrete properties (Caldarone et al., 1994; Zhang and Malhotra, 1995; Wild et al., 1996; Ding and Li, 2002; Mermerdaş, 2006; Güneyisi and Mermerdaş, 2007; Güneyisi et al., 2008; Güneyisi et al., 2012a). Research related to the effect of metakaolin on the performance of concrete is in progress due to the fact that metakaolin is a relatively new supplementary cementing material for concrete industry. Metakaolin is also considered as an alternative pozzolana for utilization in production of special types of concrete. It is comparable to silica fume in pozzolanic reactivity, but is relatively lower in price (Poon et al., 2001; Revilla et al., 2005; Güneyisi et al., 2012a).

It is generally agreed that penetration of aggressive species into concrete causes, in many structures, to long-term deterioration. The performance of concrete depends mainly on the environmental conditions, the microstructures, and the chemistry of the concrete. So, the continuation of hydration reactions in Portland cement is essential to improve the potential strength and durability of concrete. This continuation is based on the type (chemical composition) and fineness of cement, the type and the amount of cementitious material available, the w/cm ratio and the curing condition, especially at early ages (Khatri et al., 1997). It is evident that those parameters are essential to obtain long lasting concrete structures.

## **2.2 Metakaolin as a mineral admixture**

There are several aspects of utilization of metakaolin as a supplementary cementing material (or mineral admixture) in concrete (Siddique, 2008). These are;

- High strength concrete-enhanced compressive and tensile strengths,
- Durable concrete- reduced permeability, increased resistance to chemical attack, reduced effects of alkali-silica reactivity (ASR), reduced time dependent deformation due to particle packing,
- Precast-prestressed concrete for industrial structures,
- Architectural concrete elements- reduced potential for efflorescence,
- Mortars, repair material, pool plasters- enhanced workability and finishing of concrete.

### **2.2.1 Conversion of kaolin to metakaolin**

Kaolinite is a dioctahedral 1:1 layer silicate mineral with well-formed six-sided flakes, generally with a prominent elongation in one direction. Kaolin is a type of fine, white, clay mineral that has been mostly used in the ceramic industry. Kaolinite is the mineralogical term that can be used for kaolin clays. Kaolinite is defined as a common mineral, hydrated aluminum disilicate, the most common ingredient of kaolin. The meta prefix is a term used to designate alteration. In the case of metakaolin, the change that occurs is dehydroxylation, brought on by the application of heat during a specified period of time. The behavior of clay minerals on heating depends on their microstructural features, such as size of crystal and degree of crystallinity. At just above 100 °C, clay minerals lose most of their adsorbed water (Siddique, 2008). The temperature at which kaolinite loses water by dehydroxylation is in the range of 500–800 °C. This process provides thermal activation which is also known as calcination.

The calcination process alters the particle shape and size of kaolin and increases its hardness. Fully calcined kaolin has the following properties: high color retention, excellent thermal stability, and the absorption of UV light by dissipating the energy as heat. Calcined kaolin contributes to opacity by replacing up to 15-25% of TiO<sub>2</sub>



pigments in most applications. The low surface hydroxyl content of calcined kaolin causes in low moisture pick up which gives excellent performance in moisture sensitive applications (Ramezaniapour and Malhotra, 1995).

### 2.2.2 Effect of metakaolin on hydration mechanism

Strength of concrete is mainly gained as a result of the hydration of alite and belite in Portland cement to form C-S-H. Alite hydrates quickly to form C-S-H and is mainly responsible for early strength gain; belite, on the other hand, has a slower hydration rate and is responsible for the long term strength developments (Taylor, 1997).



When alite and belite hydrate they generate a by-product, calcium hydroxide (CH), which crystallizes around the aggregate to create a weak zone called the interfacial transition zone (ITZ) (Neville, 1996). Concrete paste has a higher porosity and lower strength than the surrounding paste and allows the greatest penetration of harmful containments at ITZs.

Reactivity ability of MK can be examined by Chapelle test (Kostuch et al., 1993; Asbridge et al., 1994). Asbridge et al., (1994) reported a comparison of reactivity level of MK with silica fume (SF) and fly ash (FA) with respect to consumption rate of CH per gram of pozzolans. Based on the results 427, 875, and 1050 mg of Ca(OH)<sub>2</sub> were consumed per 1 g of FA, SF, and MK, respectively.

The amount of CH in hardened concrete can be determined by thermogravimetric analysis (TG) and differential thermal analysis (DTA) (Siddique, 2008). Besides, the reactivity of pozzolans can also be assessed by chemical determination of unreacted pozzolan in hydrated PC-pozzolan pastes. Kostuch et al., (1993) have reported that:(i) CH was considerably reduced with age for all replacement levels (0, 10, and 20%); and (ii) 20% replacement of cement by MK was required for full removal of all of the portlandite in concrete at 28 days where as Oriol and Pera (1995) reported

that between 30 to 40% MK is required to remove all the CH in MK-PC paste at a water-binder ratio of 0.5 when cured in lime-saturated water for 28 days.

### **2.3 Effect of MK on the fresh properties of concrete**

Metakaolin provide improvement in the workability and constructability, and has a positive effect on the time and energy in finishing and pumping of concrete, provided that proper amount of superplasticizers are used (Shekarchi et al., 2010). In the study of Brooks et al. (2000) it was reported that a 30% reduction of slump when using 15% metakaolin in concrete followed by a 20% retardation of setting times was observed. Moulin et al. (2001) and Badogiannis et al. (2005) stated retardation in a range of 0–95% in initial setting time as well as 14–64% for final setting time using 20% of different types of metakaolin. These discrepancies could be attributed to the fineness of different metakaolins and the amount and performance of different chemical admixtures in each test.

In the study of Shekarchi et al. (2010), MK was replaced with cement up to 15 % in production of concrete. They pointed out that use of metakaolin accelerated the initial set time of concrete; however the final set time remained unchanged. Effects of MK on setting time and consistency of mortars were also determined by Batis et al. (2005). They observed that MK blended cements required significantly more water than the plain cement which was also attributed to the high fineness of metakaolin. The increase of the metakaolin content causes a considerable increase of the water demand. 10% MK (MK-10) blended system revealed the lowest water demand, compared with the other blended cements. The initial and final setting times of metakaolin cements were reported to be longer than that of pure cement. Table 2.1 shows the results from the study of Batis et al. (2005) on the water demand for normal consistency and setting times of the blended cements with metakaolin.

Table 2.1 Fresh properties of blended cements with metakaolin (Batis, 2005)

Sample	Water Demand (%)	Setting time (min)	
		Initial	Final
PC	27.5	105	140
MK-10	32.5	155	180
MK-20	41.0	205	230
MKC-20	37.5	140	170

Fresh properties of self compacting concrete (SCC) have paramount importance affecting its utilization in construction industry. Due to its viscosity modifying property several researchers has benefited from MK in SCC production (Melo and Carneiro, 2010; Güneysi et al., 2010; Vejmelkova et al., 2011; Madandoust and Mousavi, 2012). In the study of Madandoust and Mousavi (2012), self compacting concretes with 3 different w/b ratios and various replacement levels of MK were produced. It was reported that increasing the amount of MK resulted in significant increase in the amount of high range water reducing admixture to provide slump flow between 6600-715 mm (Fig 2.1).

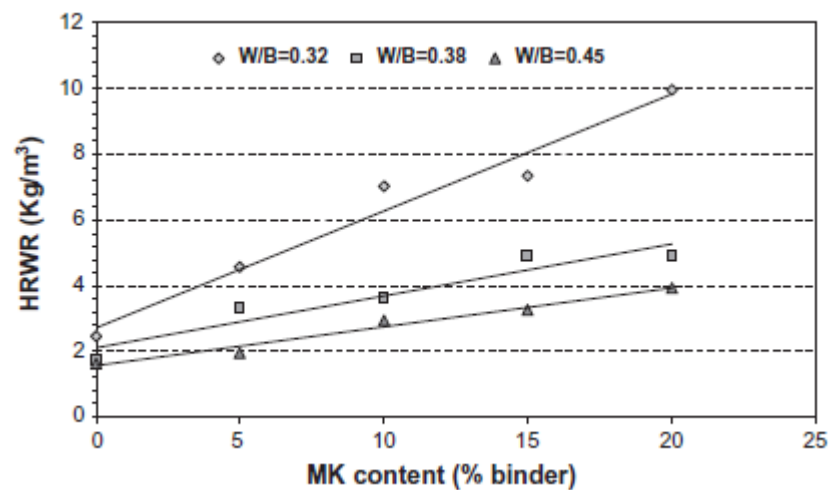


Figure 2.1 HRWR dosage for different w/b ratios (Madandoust and Mousavi, 2012).

## 2.4 Effect of metakaolin on the hardened properties of concrete

One of the most significant effects of the pozzolans is pore size refinement. Filling up large capillary pores is critical in terms of enhancement of the strength and permeability of the concrete (Moon and Shin, 2007). Therefore, modifiers should be used to provide refinement in average pore size and its distribution in concrete.

In the study conducted by Bredy et al. (1989), porosity together with pore size distribution of the pastes containing MK were studied. The pastes containing MK between 0–50% at different water to binder (w/b) ratios to obtain the similar consistency were produced. They concluded that the total porosity of paste reduced if the MK content was lower than 20%. However, beyond 30%, porosity was increased. Larbi and Bijen (1992) reported that at the end of hundred days of curing, the pore volume of mortar and the threshold diameter decreased as a result of pore refinement property of metakaolin. Khatib and Clay (2003) pointed out a slight rise in pore volume for pastes containing up to 15% MK as partial replacement of cement at a constant water/binder, and this increase was based on the amount of MK. The presence of MK, however, results in refinement in pore structure, so that for the pastes including MK the threshold diameter was reduced while the percentage of small pores were increased.

In the study of Singh and Garg (2006), the microstructure of the metakaolin modified mortar has been reported. The influence of addition of metakaolin up to 25% in the Portland cement mortars was examined. An increase in compressive strength and decrease of porosity and pore diameter of cement mortars containing metakaolin (10%) was reported over the cement mortars without metakaolin. The hydration of metakaolin blended cement mortars was investigated by differential thermal analysis (DTA) and scanning electron microscopy (SEM). DTA of hydrated cement revealed (Fig. 2.2) formation of endotherms of major hydraulic products such as C-S-H (130–135 °C), hexagonal calcium aluminate hydrate ( $C_4AH_{13}$ ) (180–200 °C), and  $Ca(OH)_2$  (480–500 °C) due to their decomposition reactions. The endotherms at 750–770 °C were due to decomposition of calcium carbonate ( $CaCO_3$ ). An increase in peak areas of C-S-H and  $C_4AH_{13}$  was observed with increase in metakaolin up to 10%. SEM (Fig. 2.3) indicated formation of dense subhedral to euhedral crystals of C-S-H and

$C_4AH_{13}$  interspersed with short length ettringite at 3 days (a) of curing. Appearance of partially hydrated amorphous  $SiO_2$  and  $Al_2O_3$  can also be seen. At 7 and 28 days of hydration (b and c), well-crystallized CSH formed. With the increase in curing period (d), well-developed euhedral CSH crystals with little unhydrated metakaolin are formed. The formation of these crystals is responsible for increase in strength of OPC–metakaolin mortar than the plain OPC mortar. Replacement of metakaolin with silica fume (up to 5%) did not show appreciable enhancement in compressive strength of the cement.

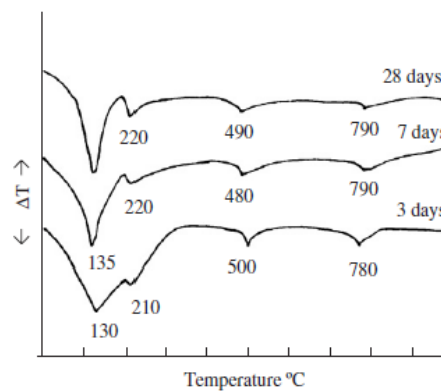


Figure 2.2 Differential thermograms of OPC-metakaolin mix hydrated for different periods (Singh and Garg, 2006)

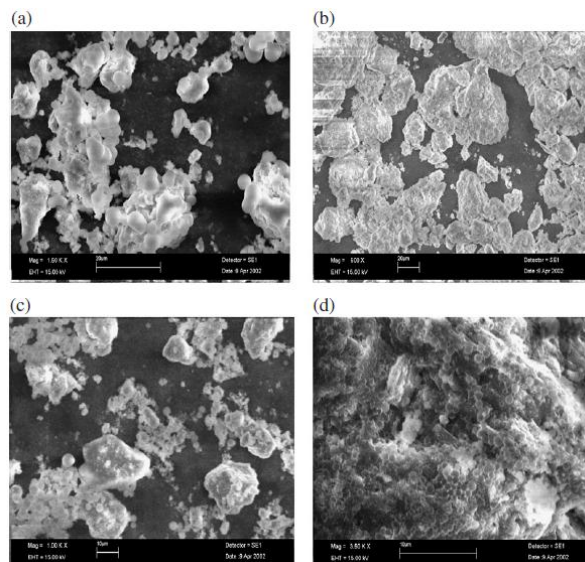


Figure 2.3 SEM of OPC-metakaolin mixture hydrated for different periods (a) 3 days, (b) 7 days, (c) 28 days, and (d) 90 days (Singh and Garg, 2006)

Al-Sibahy and Edwards (2012) performed a study on mechanical and thermal properties of a new type lightweight concrete containing recycled glass and metakaolin. In the study, for the lightweight concretes containing 45% recycled glass an increase in the density was observed (Fig. 2.4).

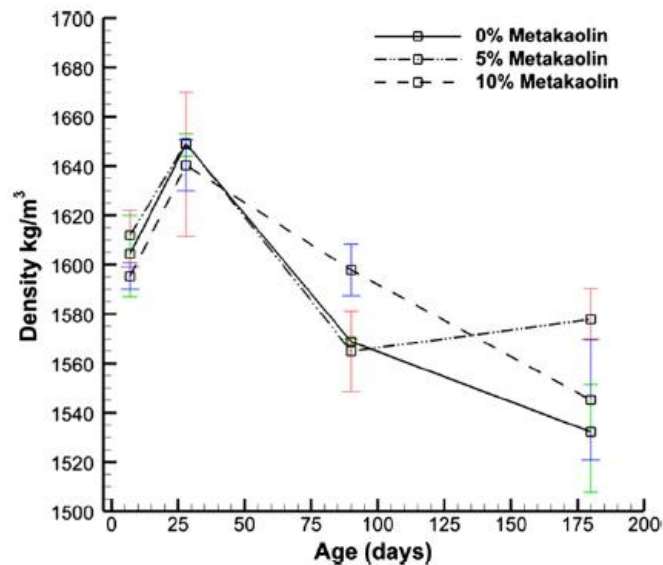


Figure 2.4 Effect of the percentage of metakaolin on the density of concrete mixes containing 45% glass (Al-Sibahy and Edwards, 2012)

### 2.4.1 Mechanical properties

The use of MK is reported to increase the concrete strength especially during the early ages of hydration (Zhang and Malhotra, 1995, Mermerdaş et al., 2012; Güneysi et al., 2012a). In metakaolin blended cement concretes, metakaolin contributes to the strength of concrete not only at early ages mainly by the filling effect, but also at later ages due to the fast pozzolanic reaction (Poon et al., 2006). Very high strength concrete can be obtained through incorporation of metakaolin (Kim et al., 2007). Naveen et al. (2006) reported the results of an experimental study wherein metakaolin, fly ash and their blends were utilized as fillers in production of self-compacting concrete (SCC). They concluded that SCC can be produced with cement content, as low as  $200 \text{ kg/m}^3$  of concrete together with rest of the powder coming from fly ash.

The increase in compressive strength of MK concrete is known to be due to the filling effect where MK particles fill the space between cement particles, acceleration

of cement hydration and pozzolanic reaction of MK. This influence is similar to that of silica fume. Although the pore volume slightly increases in pastes containing MK, the pore structure of paste, however, is found to be refined (Khatib and Wild, 1996). The improvement in pore structure of the paste is increased when the amount of MK increases up to at least 20% as partial substitution of PC (Khatib and Hibbert, 2005). The portlandite content in MK paste and mortar is reduced due to the reaction between PC hydration products and MK (Wild and Khatib, 1997).

In order to evaluate and compare the mechanical properties of the concrete incorporating metakaolin, Kim et al. (2007) carried out an experimental study on compressive, splitting tensile and flexural strength properties of concretes using various replacements of silica fume and metakaolin. Based on the results demonstrated in the study it was found out that the level of compressive strength enhanced due to the increase in replacement ratios of MK and SF from 5% to 20%. A replacement ratio of 15% was seen to improve the development of compressive strength, but such effect appears to reduce for 20%. In other words, the most remarkable strengths were developed for replacement ratios from 10 to 15%, with poor improvement effect for a replacement ratio of 15% compared to 20%. Similarly, in the study of Güneyisi et al. (2012a), concretes incorporated with 5% and 15% replacement level of MK showed relatively higher strength than that of plain concretes at two different water-to-cementitious material (w/cm) ratios (Figs. 2.5). The splitting tensile strengths measured at 3, 7 and 28 days were presented in Fig. 2.6. The highest splitting tensile strengths were obtained for the concretes incorporated with 15% replacement of SF and MK for w/cm ratios of 0.25 and 0.35, respectively. Moreover, based on the test results obtained in that study, it was observed that the splitting tensile strength development of the concretes had similar tendency with compressive strength. However, the differences between plain and blended concretes were not as high as compressive strength.

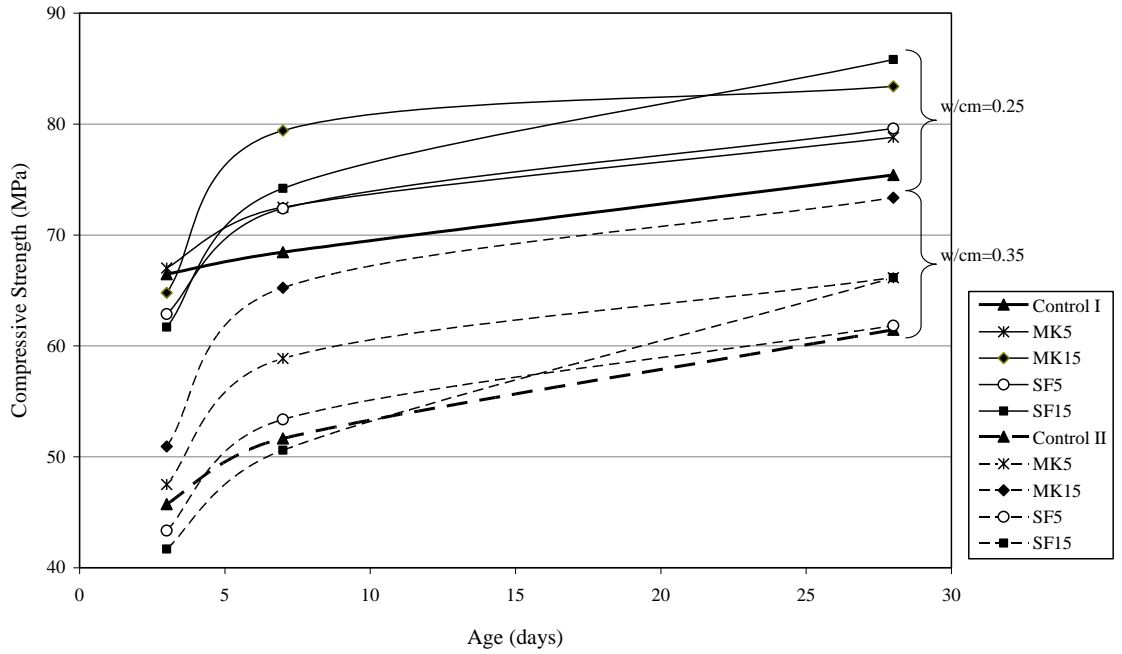


Figure 2.5 Effect of silica fume and metakaolin on compressive strength development of concretes (Güneyisi et al., 2012a)

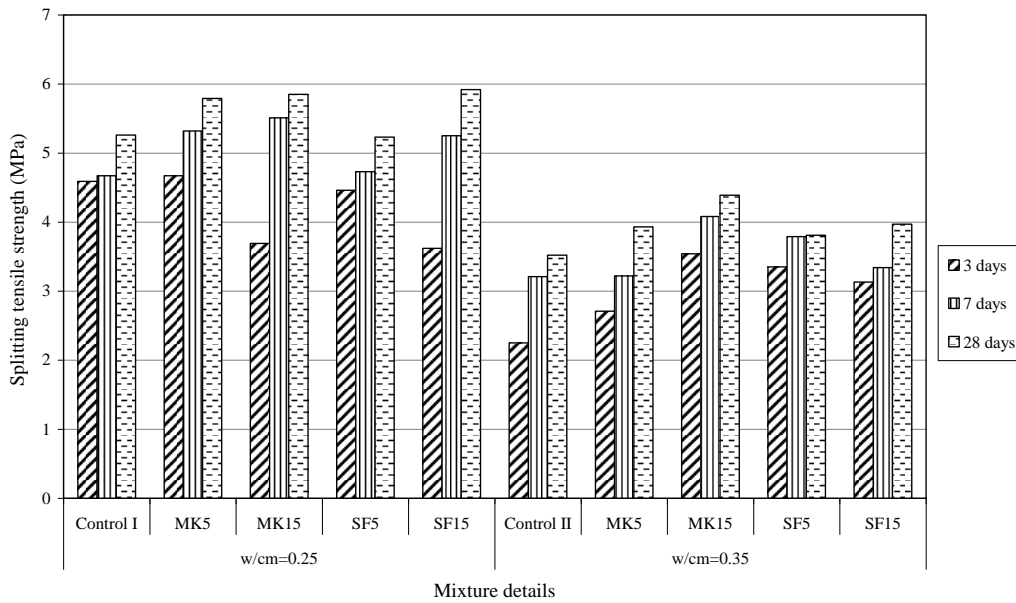


Figure 2.6 Effect of silica fume and metakaolin on splitting tensile strength of concretes (Güneyisi et al., 2012a)

The flexural strength values presented in the study of Kim et al. (2007) were measured at 1, 3, 7, 28, 56 and 91 days and shown in Fig. 2.7. Test results indicated that the increase in the replacement ratio of the binder employed provided



improvement of the flexural strength. It can be verified that the values of the flexural strength reached about 10% of the compressive strength.

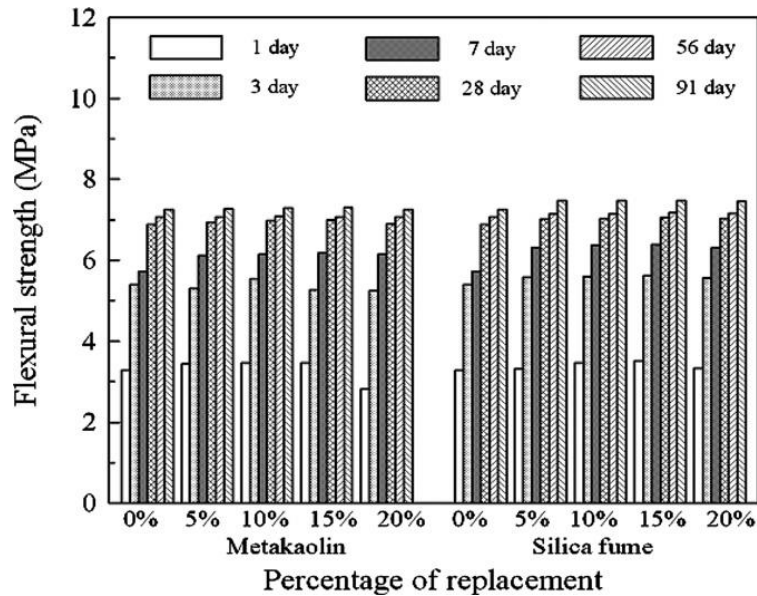


Figure 2.7 Flexural strength versus replacement with ages

#### 2.4.2 Time dependent properties

One of the most important properties of the concrete is time dependent behaviors, which are known as shrinkage and creep. Brooks and Johari (2001) studied the effect of MK on the creep and shrinkage of properties of concrete mixes. The levels of MK replacement were assigned as 0%, 5%, 10% and 15% by weight of cement. Based on the results, the early age autogenous shrinkage measured from the time of initial set of the concrete was reduced as a result of inclusion of MK, however long-term autogenous shrinkage measured from the age of 24 h was increased. At 5% replacement level, the effect of MK was to increase the total autogenous shrinkage considered from the time of initial set. While at replacement levels of 10% and 15%, it reduced the total autogenous shrinkage. The total shrinkage (autogenous plus drying shrinkage) measured from 24 h was decreased by the use of MK, while the drying shrinkage was considerably less for the MK concretes than for the control concrete. The total creep, basic creep together with drying creep was significantly reduced especially at higher MK replacement levels. Compared with predicted values, total creep of all concretes was overpredicted, particularly in the mixes including the higher values of MK. For basic creep, estimates for low levels of MK

were acceptable but, for the higher levels, creep was overpredicted. Fig. 2.8 indicates the influence of MK replacement levels on total shrinkage of concrete specimens. In Fig. 2.9, the effect of metakaolin on total creep of concrete loaded to an initial stress/strength ratio of 0.20 at the age of 28 days was demonstrated.

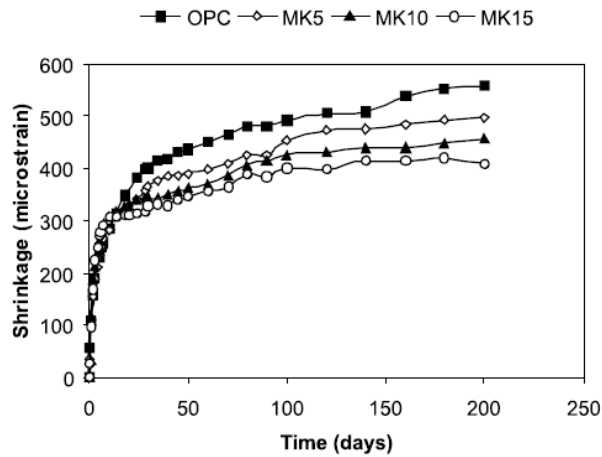


Figure 2.8 Total shrinkage of drying concrete specimens from 24 h (Brooks and Johari, 2001)

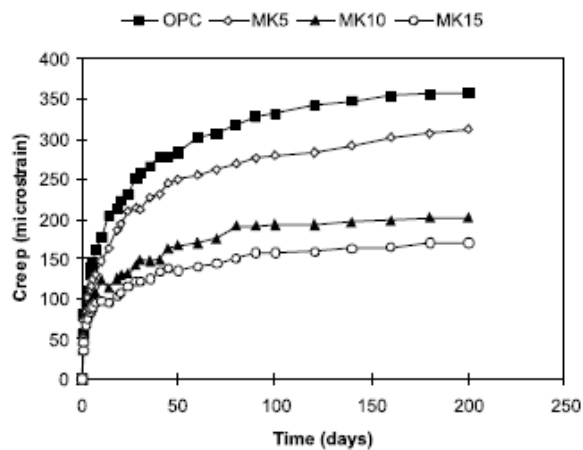


Figure 2.9 Influence of metakaolin on total creep of concrete (Brooks and Johari, 2001)

Comparison of effectiveness of MK and SF on the shrinkage properties of high strength concretes were presented by Güneysi et al. (2012a). In the study, concrete with water to binder ratio of 0.35 were produced. MK and SF were used as mineral admixtures replaced with cement by weight with the levels of 5 and 15% to assess

restrained and free shrinkage of concrete. For both replacement levels, MK and SF incorporated concretes demonstrated lower drying shrinkage in comparison to the plain concretes (Fig. 2.10). The lowest shrinkage strains were observed at the concrete containing 15% SF and 15% MK. The drying shrinkage rates of the concretes had a decreasing trend as the time passed, especially for the MK and SF concretes.

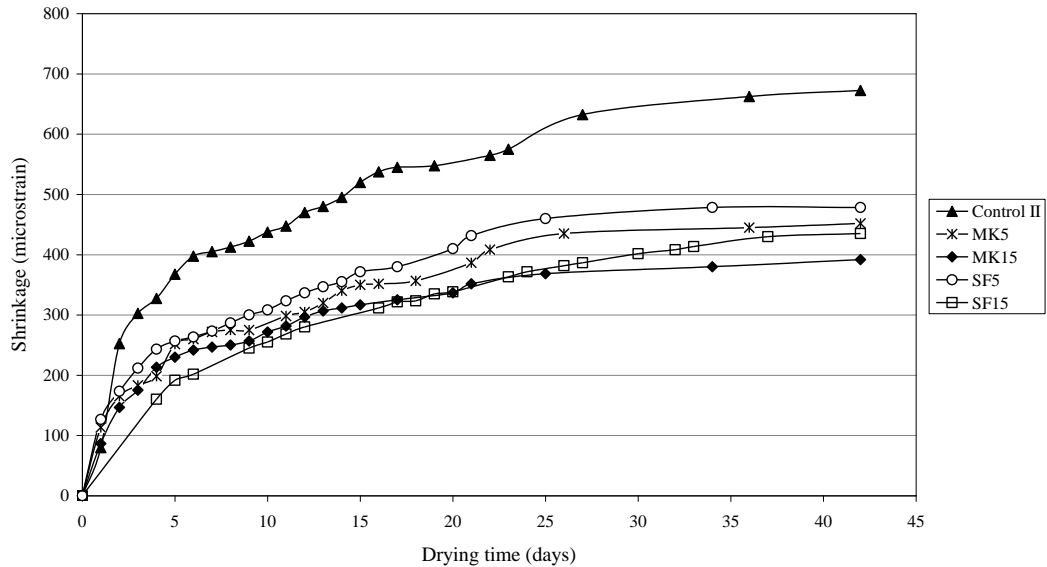


Figure 2.10 Effect of metakaolin and silica fume on free shrinkage of concretes with a w/b ratio of 0.35 (Güneyisi et al., 2012a)

Moreover, based on the result obtained from restrained shrinkage test, they stated that although initial crack formation was detected on the same day (8<sup>th</sup> day) for control and MK concretes, the final crack widths of MK concretes were relatively lower than that of control concrete. However, incorporation of SF delayed the crack initiation and propagation. The initial cracks were observed at 9<sup>th</sup> and 10<sup>th</sup> day for SF5 and SF15 concretes, respectively. As can be seen from Fig. 2.11, the maximum crack width was measured at control concrete as 0.69 mm, while the lowest was measured as 0.33 mm at SF15 concrete (Güneyisi et al., 2012a).

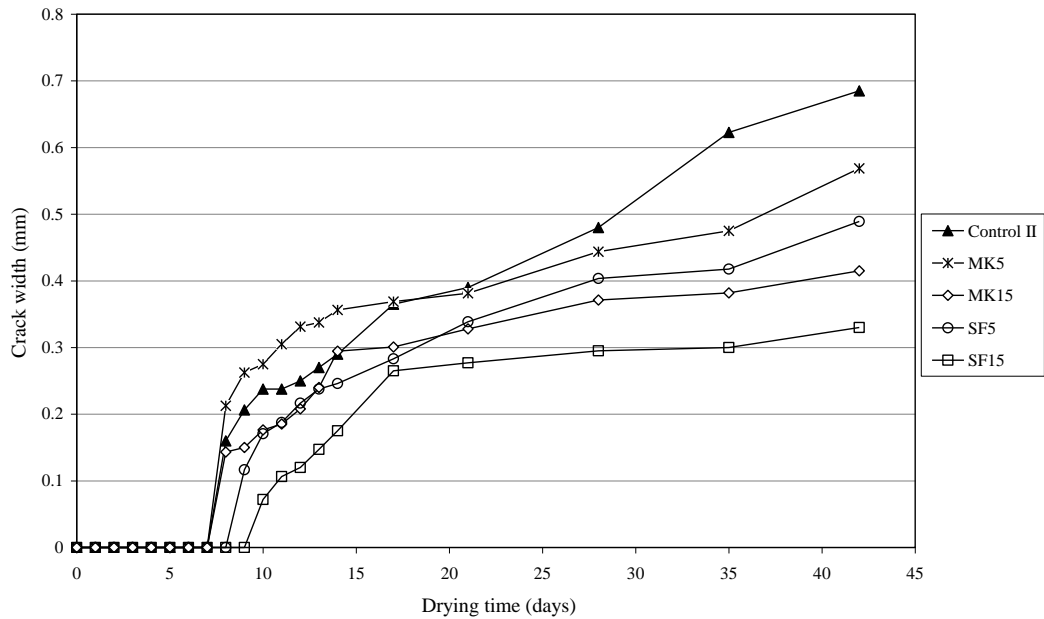


Figure 2.11 Effect of metakaolin and silica fume on the initiation and propagation of restrained shrinkage cracking of concretes having a w/b ratio of 0.35 (Güneyisi et al., 2012a)

### 2.4.3 Durability properties

Permeability of concrete is one of the most important factors affecting the long term durability. The permeability of concrete is defined as the property that measures the flow of fluid throughout concrete under a pressure gradient. It has such an importance for concretes used in water-retaining structure. Some reinforced concrete (R/C) structures might be exposed to aggressive environmental effects such as sulfate and chloride attack, abrupt climatic changes. These detrimental effects may lead to the deterioration of structures, hence losing their serviceability or being exposed to catastrophic damages under instantaneous superimposed loads. Therefore, the permeability characteristics should carefully be considered for concretes having environmental deterioration risk (Khatib and Clay, 2004). Therefore, it can be said that permeability has a significant impact on a wide variety of processes in manufacture of high performance concrete. It has been known that mineral admixtures contribute to mechanical and durability performance for the concretes by either physical and/or chemical refinement of the pore structure. Providing the refinement of porosity reduces the permeability of the hardened cement matrix. Various supplementary cementing materials have extensively been used for many

years for improving the permeability related durability properties of the concrete as well as mechanical performance (Ramezani pour and Malhotra, 1995; Khatri et al., 1997). Fly ash (FA), silica fume (SF), and ground granulated blast furnace slag (GGBFS) are examples of most commonly used pozzolanic mineral admixtures in production of high performance concrete. They provide additional performance to the concrete by reacting with Portland cement hydration products to create additional C-S-H gel, the part of the paste being mainly responsible for the concrete strength (Neville, 1996).

For the last two decades, there has been a growing interest for the beneficiation of metakaolin (MK) as a supplementary cementing material in the production of concrete with enhanced transport and mechanical features (Cassagnabère et al., 2009; Ding and Li, 2002; Güneyisi and Mermerdaş, 2007; Güneyisi et al., 2008; Güneyisi et al., 2010; Güneyisi et al., 2011; Güneyisi et al., 2012a; Kim et al., 2007; Poon et al., 2006; Sabir et al., 1996; Sabir et al., 2001; Wild and Khatib, 1996). The major difference between MK and other types of pozzolans is that MK is the primary product obtained at the end of the series of processes such as purification, grinding, thermal characterization, and calcination. However, other artificial pozzolans like GGBFS, FA, and SF are disposal materials or by-products of some heavy industrial processing plants. Therefore, it can be said that MK can be produced with a controlled process to achieve the desired properties such as fineness and/or high reactivity.

Poon et al. (2006) investigated the chloride penetrability of the concretes in terms of the charge passed according to ASTM C1202 (2012). The concretes were modified with MK or SF at different water-to-binder ratios. They reported that both MK and SF modified concretes showed total charge passed lower than the control. The concrete with low w/b ratio (0.3) incorporating 10% MK replacement showed the best performance while at the high w/b ratio (0.5), concrete with 20% replacement was the best. Their results were given in Table 2.2.

Table 2.2 Electrical indication of chloride penetrability of control and blended concretes (Poon et al., 2006)

Series	w/cm	Mix	Total Charge passed (C)			
			3 days	7 days	28 days	90 days
1	0.30	Control	2461	2151	1035	931
		5% MK	1327	1244	862	646
		10% MK	417	347	199	135
		20% MK	406	395	240	124
		5% SF	1060	945	665	426
		10% SF	567	445	360	336
2	0.50	Control	5312	4054	2971	2789
		5% MK	4215	3765	2079	1065
		10% MK	1580	1247	918	752
		20% MK	751	740	640	580
		5% SF	3156	2047	1641	1235
		10% SF	3140	1877	1523	1053

Güneyisi et al. (2011) used some mineral admixtures to improve the water permeability of self-compacting concretes. They observed that the use of fly ash, slag, and metakaolin remarkably reduced the water permeability of concretes up to 80% (Fig. 2.12).

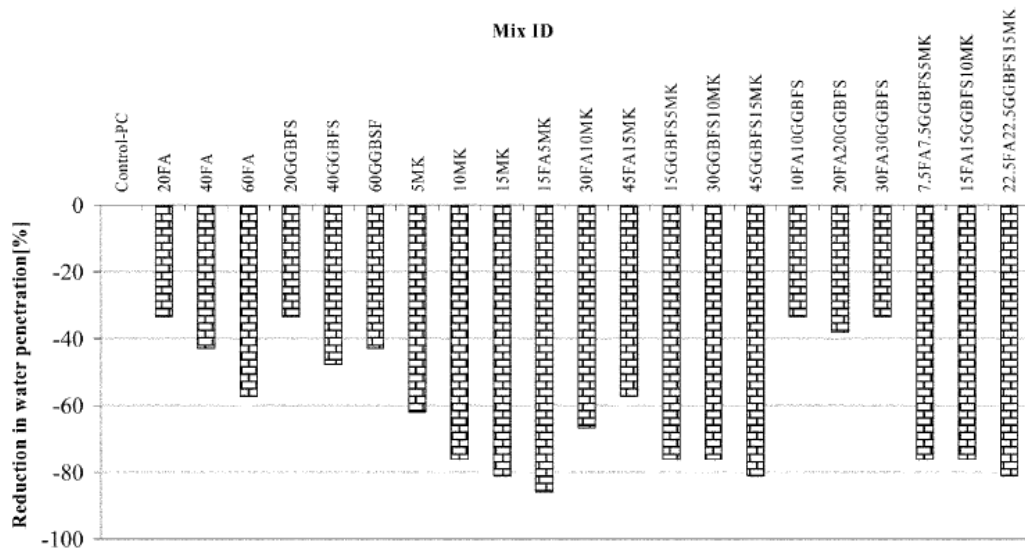


Figure 2.12 Level of decrease in water permeability of concretes with respect to control specimen (Güneyisi et al., 2011)

Shekarchi et al. (2010) reported the results of an experimental study. Transport properties measured in terms of water penetration (WP), gas permeability (GP), water absorption (WA), electrical resistivity (ER), and ionic diffusion were improved up to 50%, 37%, 28%, 450%, and 47%, respectively (Figs. 2.13 and 2.14).

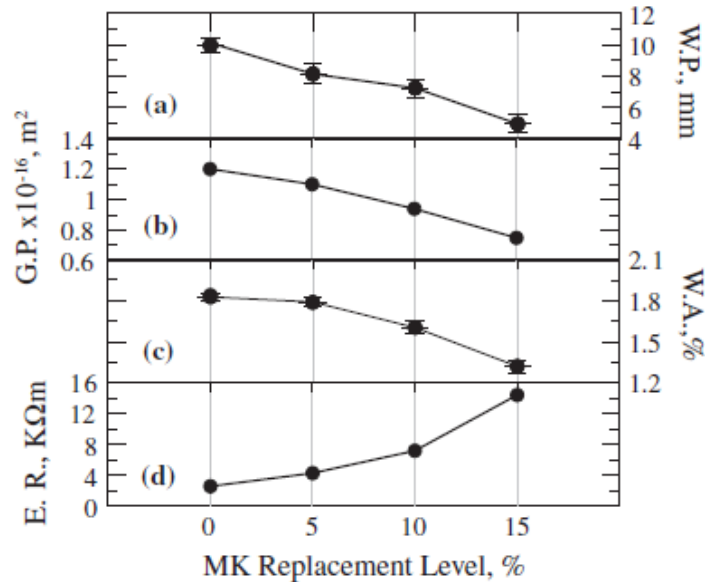


Figure 2.13 Effect of metakaolin replacement level on different transport properties (Shekarchi et al., 2010)

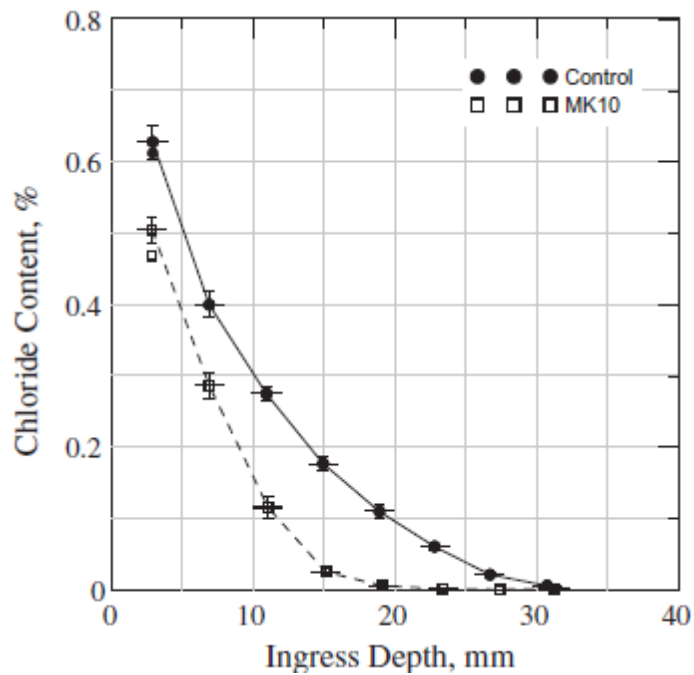


Figure 2.14 Chloride ions ingress profile test result (Shekarchi et al., 2010)

In the study of Hassan et al. (2012), freezing-thawing resistances of MK modifies concretes were evaluated through weight change and pulse velocity. The weight change was used to show the amount of moisture that had been absorbed due to cracking caused by expansion of the cement paste. At the end of each cycle; weight gain and pulse velocity reduction percentages for each cycle were determined and presented in Figs. 2.15 and 2.16. They concluded that the weight of the samples and the reduction in pulse velocity increased as the number of cycles rose. The optimum percentage of MK was determined to be 20%. As the percentage of MK went up to 20%, weight gain and reduction of pulse velocity increased. However, the performance of 25MK through 300 cycles was observed to be very close to that of 20MK. The 20MK mixture demonstrated the lowest weight gain and reduction of pulse velocity amongst all tested mixtures. This indicated that 20MK absorbed less water and had fewer internal cracks. Also, all MK incorporating specimens with more than 5% MK did not break up to the end of the test (300 cycles).

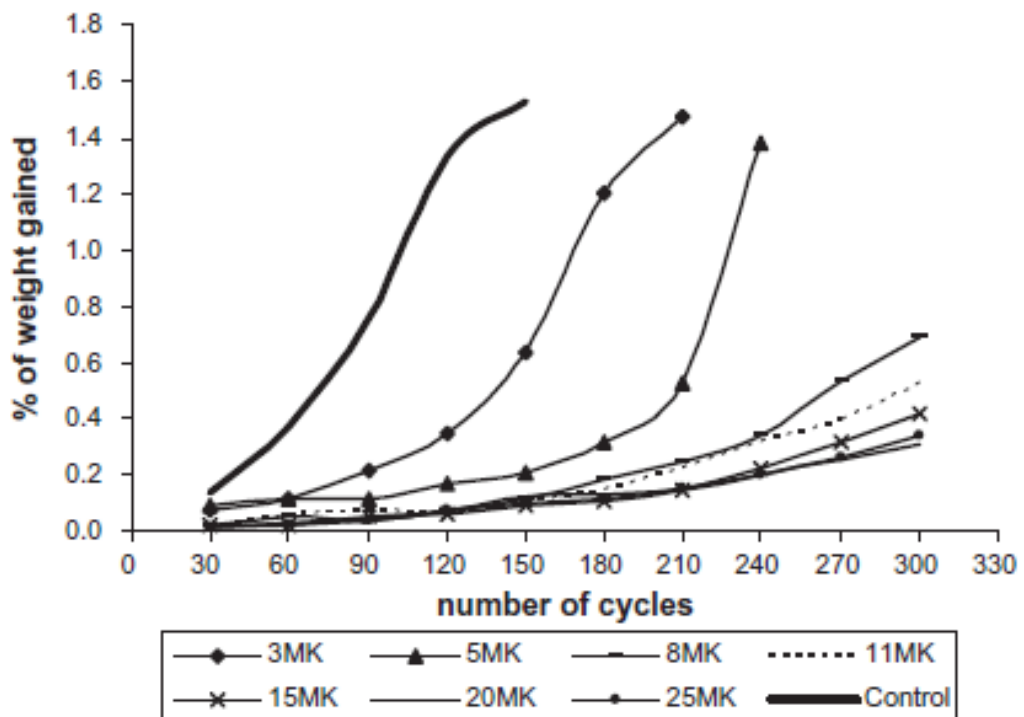


Figure 2.15 Percentage of weight gained of freezing and thawing specimens for all tested SCC



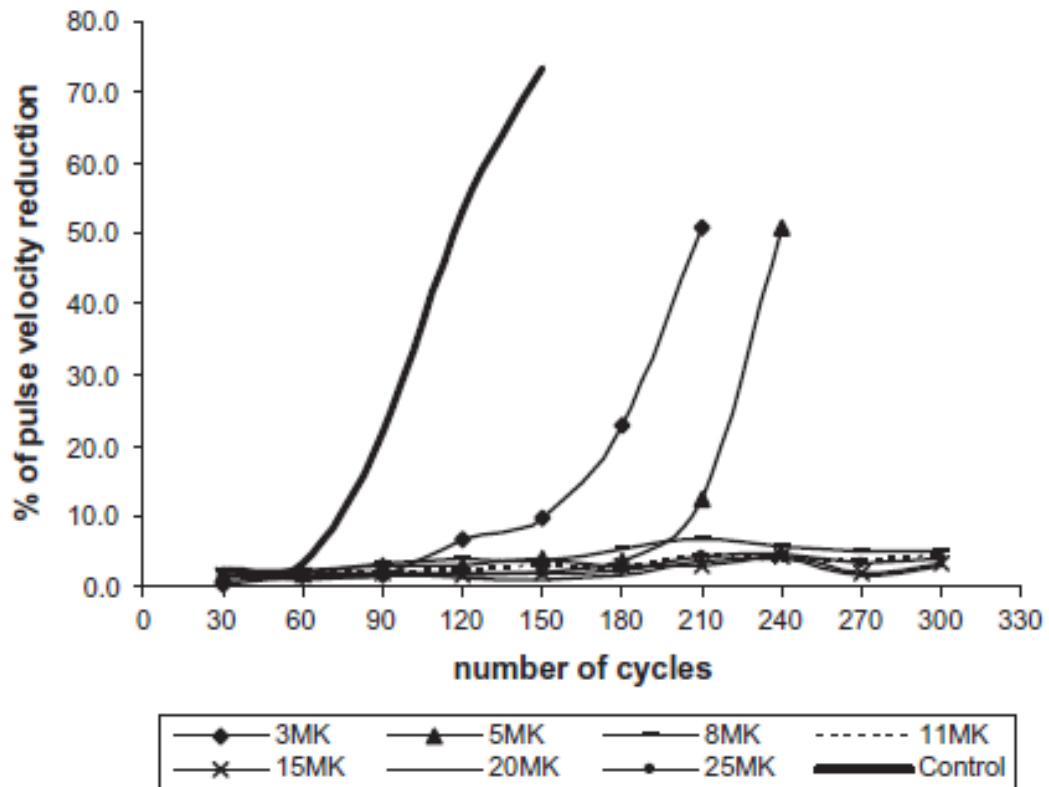


Figure 2.16 Percentage of pulse velocity reduction of freezing and thawing specimens for all tested SCC

Corrosion of reinforcement can be considered as one of the most important disadvantages of the reinforced concrete structural elements. Particularly, in marine structures or in such environments where chloride contamination risk exist this problem gains much importance. The studies regarding the effect of MK on the corrosion resistance of the cementitious composites, such as mortar and concrete is very limited (Batis et al., 2005; Güneyisi et al., 2012b). Batis et al. (2005) conducted a study on the effect of metakaolin on the corrosion behavior of mortars. They prepared several mixtures where metakaolin replaced either sand or cement. They exposed the mortar specimens to the corrosive environment of either partial or total immersion in 3.5% NaCl solution. According to the test results, they concluded that the use of metakaolin, either as a sand replacement up to 20%, or as a cement replacement up to 10%, enhanced the corrosion behavior of mortar specimens. However, in case of using greater percentages of metakaolin had no positive effect (Figs 2.17 and 2.18).

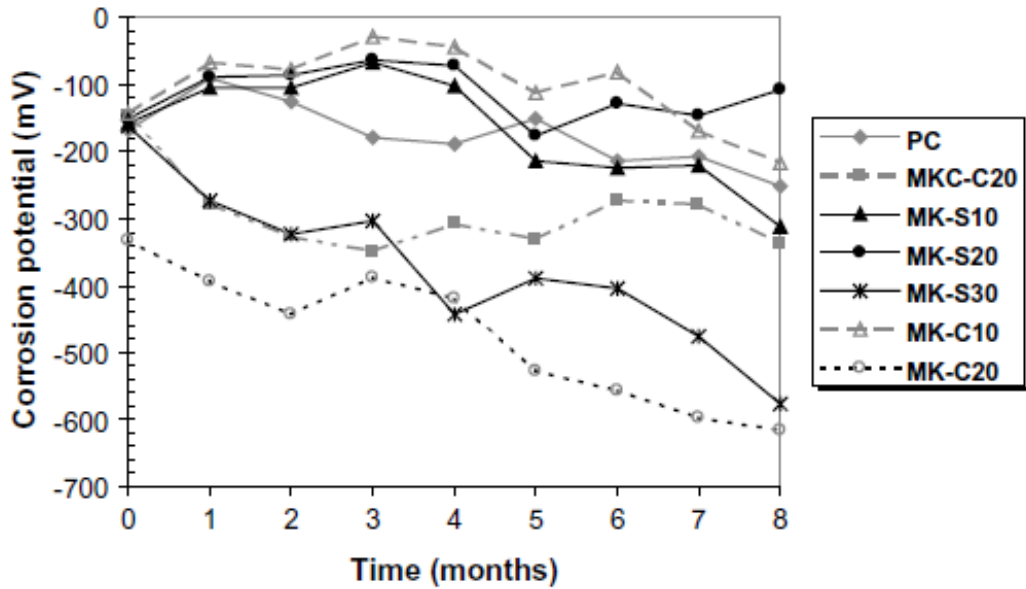


Figure 2.17 Corrosion potentials of specimens immersed in sodium-chloride solution (Batis et al., 2005)

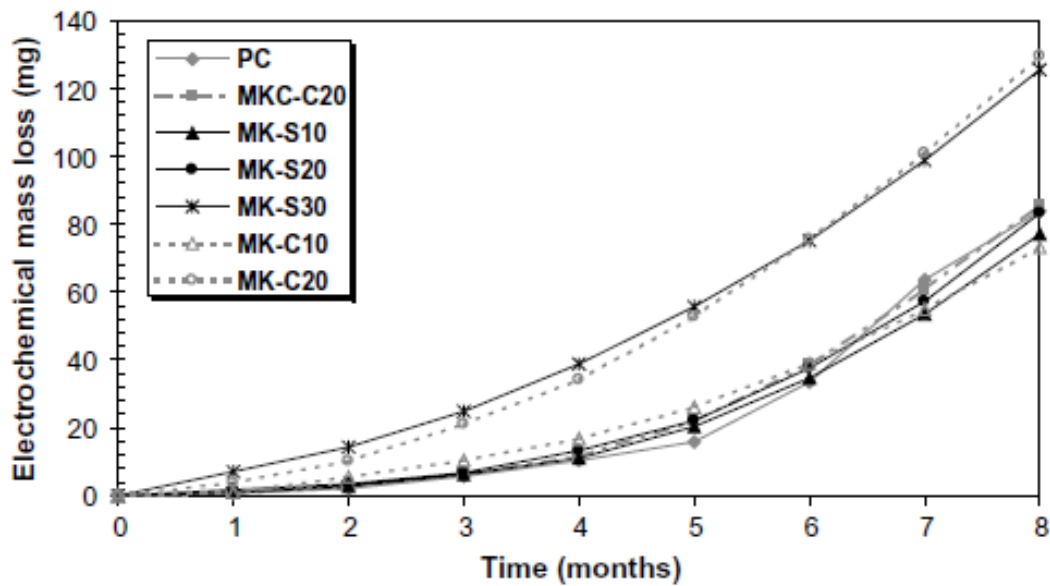


Figure 2.18 Electrochemical mass loss of mortar specimens immersed in sodium-chloride solution (Batis et al., 2005)

Similar result was also presented in the study of Parende et al. (2008). Corrosion behavior of carbon steel embedded in concrete which was produced using metakaolin (5–20%) as partial replacement in ordinary Portland cement (OPC). The corrosion

rate in concretes is represented in Fig. 2.19. The addition of metakaolin above 15% showed higher corrosion rate when compared to other systems. In 5% MK addition, corrosion rate was observed to be slightly higher than the control system. But at the end of exposure period the corrosion rate for 5% was found to be lower than that of control system. In case of 10% and 15% MK, lower corrosion rate was observed till the end of exposure period. Nevertheless, 20% MK addition showed higher corrosion rate from initial to final.

Batis et al. (2005) attributes this phenomenon mainly to the pH decrease of the pore solution, due to the pozzolanic reaction and the following consumption of the  $\text{Ca}(\text{OH})_2$ .

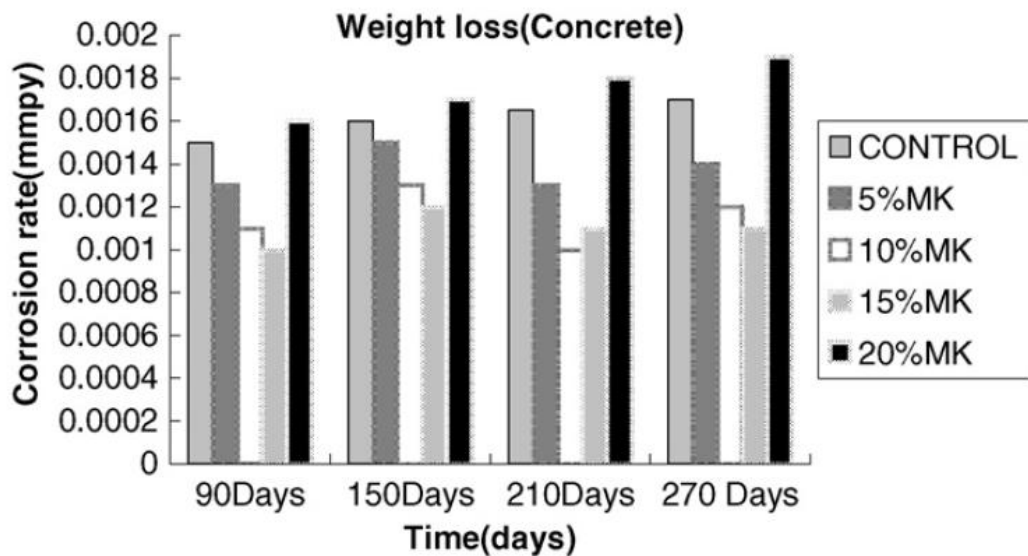


Figure 2.19 Corrosion rate measurement for concrete specimens with MK (Parande et al., 2008)

## **CHAPTER 3**

### **EXPERIMENTAL STUDY**

The overall experimental study was undertaken in two stages. The first stage consists of microstructural, thermal, and pozzolanic characterization studies on unprocessed and/or calcined Turkish kaolins. The alterations in microstructural properties of the kaolins as a result of the calcination process were monitored and evaluated. The experimental work in this stage covers qualitative mineralogical phase identification via X ray diffraction analysis, particle size analysis with laser diffractometer, specific surface area measurements by nitrogen adsorption method (BET), differential and thermogravimetric analyses (DTA-TG), and pozzolanic reactivity index as per ASTM C311 (2005).

In the second stage of the experimental study, plain concrete and concretes incorporating calcined impure kaolins (CK) produced within the scope of this work. Moreover, commercially available high reactivity metakaolin (MK) obtained from Czech Republic was also used in the production of concretes for comparison purpose. The hardened properties of the concretes were evaluated in terms of some mechanical and durability properties.

#### **3.1 Stage 1: Examining properties of raw and calcined kaolins**

##### **3.1.1 Materials: Turkish kaolins**

Representative Turkish kaolins used in this study were obtained from four different kaolin deposits with different geological formations. The suppliers are located in three cities (Fig. 3.1). Table 3.1 shows the sources and experimental codes of the kaolins investigated in this study. Almost half of the total kaolin deposits are located in Balıkesir city. Therefore, two types of kaolins (DV and DC) from different quarries located in this city were investigated in this study. On the other hand,

kaolins from neighboring cities Bursa and Çanakkale were also studied for evaluating the effect of mineralogy and chemical composition. The chemical properties of the kaolins used in this study are given in Table 3.2.

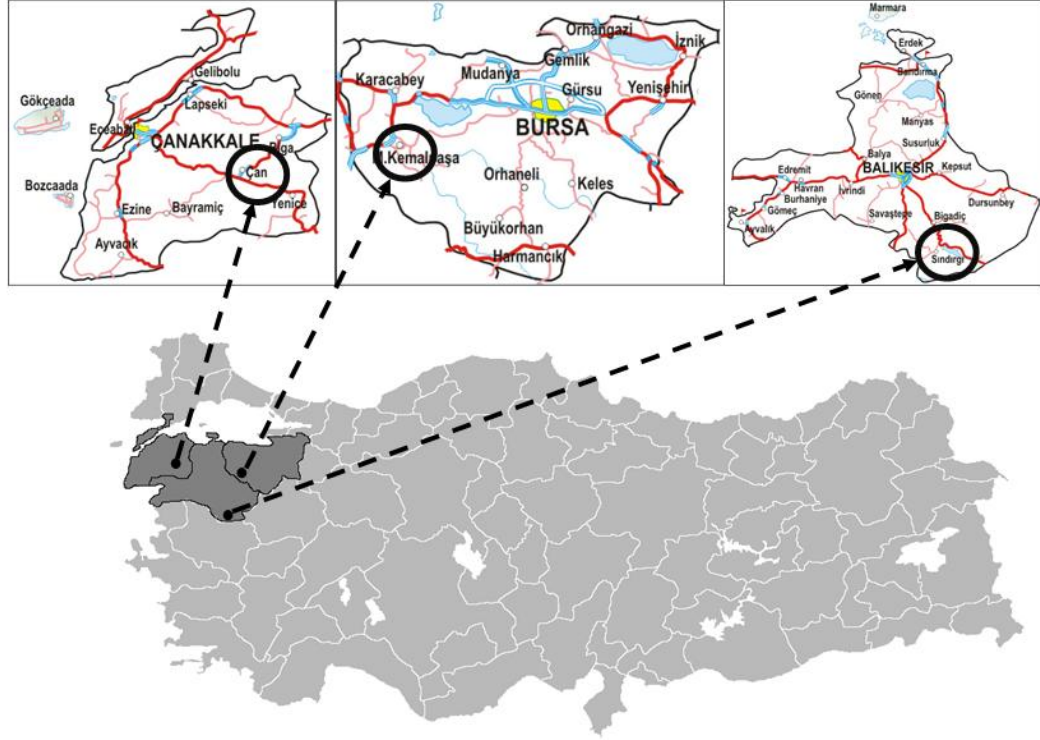


Figure 3.1 The sources of the kaolins used in this study

Table 3.1 Designation of the experimental codes of the calcined kaolin samples

Sample no	Location of the quarry		Experimental codes
	City	Location	
1	Balıkesir	Sındırgı-Düvertepe	DV
2	Balıkesir	Sındırgı-Danaçayırı	DC
3	Bursa	Mustafa Kemal Paşa	BMK
4	Çanakkale	Çan-Semedeli	CC

Table 3.2 Chemical compositions and specific gravities of the Turkish kaolins

<b>Chemical Composition (%)</b>	<b>DV</b>	<b>DC</b>	<b>BMK</b>	<b>CC</b>
<b>CaO</b>	2.03	2.90	2.03	1.69
<b>SiO<sub>2</sub></b>	63.73	73.29	44.76	62.90
<b>Al<sub>2</sub>O<sub>3</sub></b>	22.06	15.14	26.70	23.61
<b>Fe<sub>2</sub>O<sub>3</sub></b>	0.628	0.826	0.362	1.206
<b>MgO</b>	0.81	0.74	0.90	0.86
<b>TiO<sub>2</sub></b>	0.450	0.337	0.73	0.460
<b>K<sub>2</sub>O</b>	0.23	0.053	3.1	0.45
<b>LOI</b>	10.23	6.50	19.70	9.15
<b>SO<sub>3</sub></b>	0.772	0.19	10.50	1.49
<b>Specific gravity</b>	2.60	2.64	2.67	2.55

### 3.1.2 Test methods on microstructural and thermal characterization

#### 3.1.2.1 X-Ray diffraction analysis

Mineralogical compositions of raw and calcined kaolins were determined by X-ray diffraction analysis (XRD). The semiquantitative mineralogical estimation was carried out to calculate the approximate percentage compositions of the kaolins. The estimation is based on the characteristic X-ray diffraction (XRD) peaks of each mineral, in combination with the bulk chemical analysis of the samples (Kakali et al., 2001).

#### 3.1.2.2 Differential thermal and thermo gravimetric analyses (DTA-TG)

Thermal characterizations of the kaolins were evaluated by the differential thermal and thermo gravimetric analysis (DTA-TG). DTA curve provides data on the transformations that have occurred in the microstructure of the material such as glass transitions, crystallization, melting, and sublimation. On the other hand, thermo gravimetric analysis (TG) is a type of testing that is performed on samples to determine changes in weight in relation to change in temperature. To evaluate the thermal properties of the native kaolins handled in this study, DTA-TG analysis were

carried out. The device used for analysis is Perkin Elmer Pyris1 operating within the range of 20-900 °C with a rate of 10 °C/min.

### **3.1.2.3 Particle size distribution**

A device called “Mastersizer 2000” was utilized in order to observe the change in the particle size distribution of the Turkish kaolins before and after calcination process. The working principal of the device is based on the laser light scattering technique. The kaolin samples were dissolved in water for observation of the particle sizes.

### **3.1.2.4 Specific surface area**

The BET method is widely used in surface science for the calculation of surface areas of solids by physical adsorption of gas molecules. Previous studies (Kakali et al., 2001; Badogiannis et al., 2005) showed that when heated above a certain temperature crystal structure of the kaolin changes resulting in a coarse texture. Furthermore, metakaolin is known to have an important filling effect due to its high degree of fineness. For this purpose, multipoint BET specific surface area measurements were carried out. The device named Quantachrome Instruments Nova 4000E was utilized for testing. The samples were dried at 150 °C for 16 hours and the test was conducted at degase chamber of the device by absorption of nitrogen at 300 °C for approximately 5 hours.

### **3.1.2.5 Scanning electron microscopy (SEM)**

Scanning electron microscopy (SEM) image analysis was carried out to observe the changes in particle size, shape, and surface texture as a result of the calcination procedure adopted.

### **3.1.2 Heat treatment**

Calcination temperatures from 550 to 850 °C were used in this study. For this purpose, seven heat treatment levels (550, 600, 650, 700, 750, 800 and 850 °C) were chosen based on the findings of the DTA-TG analyses. These heat treatments were

applied to the kaolin specimens for determination of the suitable temperature level for calcination. A muffle furnace having internal volume of 100 lt was used for the calcination process (Fig 3.2). The maximum temperature that the furnace can reach is 1200 °C. Heating and cooling cycles which were adopted by the furnace for each heat treatment level were presented in Fig. 3.3. Each of the kaolins were first heated to the target temperature level, after keeping at that temperature for 3 hours, left to cool to the room temperature. As it can be seen from the Fig 3.3, the device is able to reach the target temperature within short time for the temperatures less than 550 °C. However, from this point forward the heating capacity gradually decreases and the maximum temperature of 850 °C can be achieved at about 60 minutes. Approximately cooling periods took about 5 hours for almost all of the cycles.



a)



b)

Figure 3.2 Photographic views of a) kaolins under calcination process and b) general view of muffle furnace



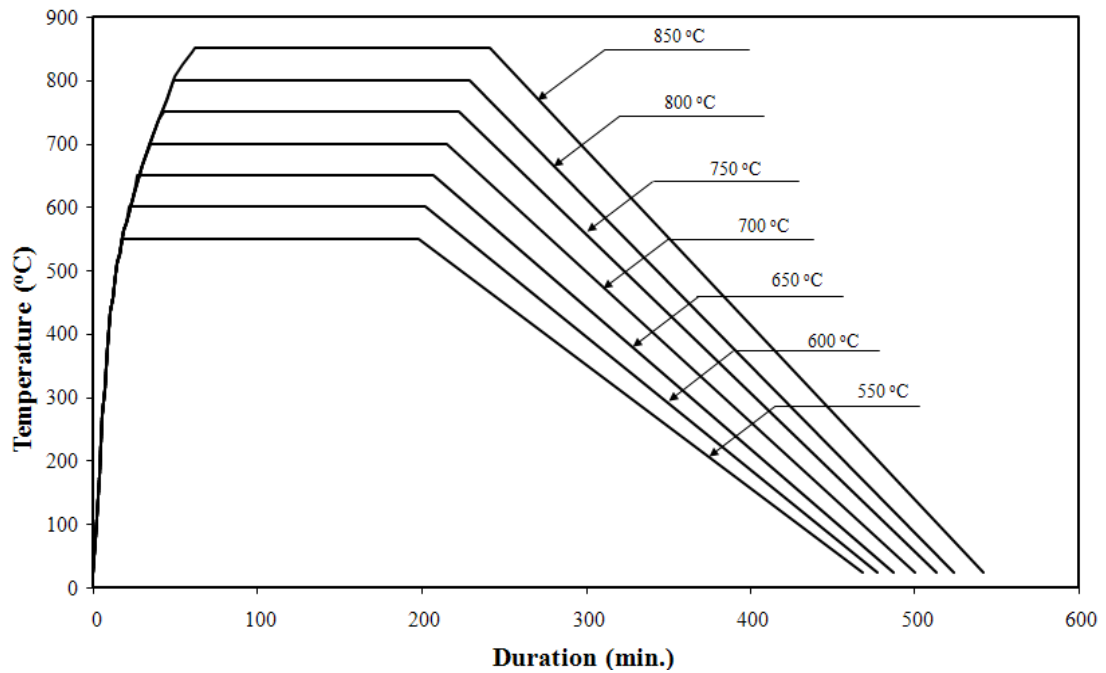


Figure 3.3 Heating and cooling cycles for each heat treatment level

### 3.1.3 Pozzolanic activity index

A standard test method ASTM C311 (2005) was applied to evaluate the pozzolanic reactivity of the produced materials. The test for the pozzolanic activity is considered to be a suitable means of evaluating the strength contribution potential of a mineral admixture. The strength activity index is determined as the ratio of the compressive strength of standard mortar cubes, prepared with 80% reference cement plus 20% additive by mass, to the compressive strength of standard mortar cube prepared with reference cement only, tested at the same age. The water to binder ratio (w/b) was 0.50. Sand-to-cement ratio (S/C) of 3 was used. Cube samples of 50-mm size were cast from the mortars mixed with a pan mixer. The specimens were demolded after 24 h and cured in lime-saturated water at 20 °C until testing at 28 days.

## 3.2 Stage 2: Experimental study on concretes

### 3.2.1 Materials

#### 3.2.1.1 Cement

CEM I 42.5 R type portland cement having specific gravity of 3.14 and Blaine fineness of 327 m<sup>2</sup>/kg was utilized for preparing the mortar specimens used in determination of pozzolanic activity index and concrete production for mechanical and durability testing. The chemical composition of the cement is shown in Table 3.3.

Table 3.3 Chemical composition of the cement

Chemical composition of the cement (%)								
CaO	SiO <sub>2</sub>	Al <sub>2</sub> O <sub>3</sub>	Fe <sub>2</sub> O <sub>3</sub>	MgO	SO <sub>3</sub>	K <sub>2</sub> O	Na <sub>2</sub> O	LOI
62.58	20.25	5.31	4.04	2.82	2.73	0.92	0.22	1.02

#### 3.2.1.2 Calcined kaolins and commercial metakaolin

The heat treatment level providing highest pozzolanic activity index and full dehydroxilation was selected as calcination temperature. The properties of the calcined kaolins were given in Table 3.4. Metakaolin (MK) used in this study is a white powder with a Dr Lange whiteness value of 87. It has a specific gravity of about 2.60, and specific surface area (Nitrogen BET Surface Area) of 18000 m<sup>2</sup>/kg. Physical and chemical properties of MK used in this study are also given in Table 3.4. MK used in this study was obtained from Czech Republic.

Table 3.4 Chemical, physical and mineralogical properties of the calcined Turkish kaolins, commercial metakaolin

	<b>Item</b>	<b>DV</b>	<b>DC</b>	<b>BMK</b>	<b>CC</b>	<b>MK</b>
<b>Chemical properties</b>	CaO (%)	2.22	3.07	2.42	1.86	0.5
	SiO <sub>2</sub> (%)	69.78	77.7	59.9	68.19	53
	Al <sub>2</sub> O <sub>3</sub> (%)	24.16	16.04	29.32	25.58	43
	Fe <sub>2</sub> O <sub>3</sub> (%)	0.69	1.01	0.43	1.32	1.2
	MgO (%)	0.89	0.78	1.07	0.95	0.4
	TiO <sub>2</sub> (%)	0.49	0.36	0.88	0.50	0.8
	LOI (%)	0.73	0.50	0.5	0.65	0.4
<b>Physical properties</b>	Specific gravity	2.60	2.64	2.67	2.55	2.60
	Fineness (cm <sup>2</sup> /g)	7340	6450	7430	4450	18000

### 3.2.1.3 Aggregates

Fine sand used for production of mortars is the mixture of crushed and natural river sand with specific gravities of 2.42 and 2.66, respectively. In addition, two types of coarse aggregates namely, No I (4-16 mm) and No II (16-22 mm) were utilized in concrete production. The grading of the aggregates was kept constant for concrete production. Fig 3.4 demonstrates the gradation curves of the each aggregate and aggregate mix in comparison to reference curves (A32, B32, C32).

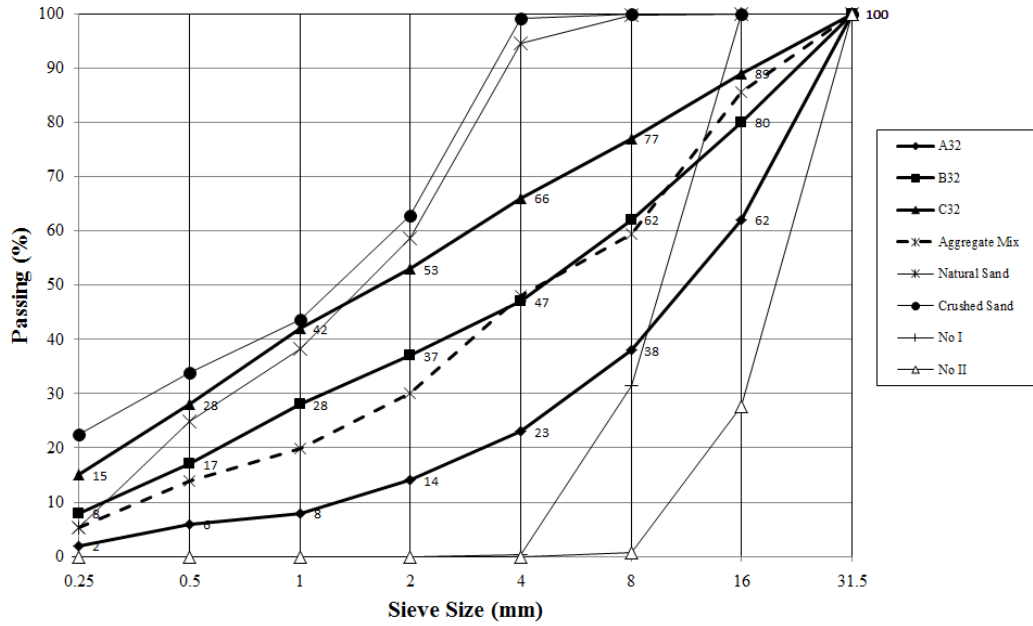


Figure 3.4 Aggregate grading curves

### 3.2.1.4 Superplasticizer

A commercially available sulphonated naphthalene formaldehyde-based superplasticizer was used to give a consistent workability. The properties of the superplasticizer are given in Table 3.5. It was supplied by Grace Chemical Corp.

Table 3.5 Properties of the superplasticizer

<b>Color</b>	<b>Dark brown</b>
<b>State</b>	<b>Liquid</b>
<b>Specific gravity</b>	<b>1.19</b>
<b>Freezing point</b>	<b>-4 °C</b>
<b>Chloride content</b>	<b>None</b>
<b>Nitrate content</b>	<b>None</b>

### 3.2.2 Mix proportions

Concrete mixtures with water-to-cementitious material (w/cm) ratio of 0.40 and MK replacement levels from 5% to 20% were designed. To develop the metakaolin

modified concrete mixtures, the Portland cement was partially replaced with MK as 5%, 10%, 15% and 20% by weight of the total binder content. As well as mineral incorporated concrete, one plain concrete group were produced as the control. Thus, totally 21 different concrete mixtures with and without pure and/or impure calcined kaolins were produced. Details of the mixtures are given in Table 3.6.

The concrete groups were designated with the name of calcined kaolin and replacement level. For example, the concrete containing calcined CC kaolin with 5% replacement was coded as CC5.

Table 3.6 Mix Proportions (kg/m<sup>3</sup>)

Type of Calcined Kaolin	Replacement Level (%)	Mix ID	Materials kg/m <sup>3</sup>							
			Cement	Calcined Kaolin	Water	No I (4-16 mm)	No II (16-22 mm)	Natural sand	Crushed Sand	SP <sup>f</sup>
None	0	Control	350	0	140	695.5	397.4	794.9	99.4	3.5
DV <sup>a</sup>	5	DV5	332.5	17.5	140	693.9	396.5	793.0	99.1	4.2
	10	DV10	315	35	140	692.0	395.4	790.9	98.9	5.3
	15	DV15	297.5	52.5	140	690.1	394.3	788.7	98.6	6.3
	20	DV20	280	70	140	688.5	393.4	786.8	98.4	7.4
DC <sup>b</sup>	5	DC5	332.5	17.5	140	694.0	396.6	793.1	99.1	4.1
	10	DC10	315	35	140	692.2	395.5	791.1	98.9	5.0
	15	DC15	297.5	52.5	140	690.4	394.5	789.0	98.6	6.1
	20	DC20	280	70	140	688.9	393.6	787.3	98.4	7.2
CC <sup>c</sup>	5	CC5	332.5	17.5	140	693.8	396.4	792.9	99.1	4.0
	10	CC10	315	35	140	691.7	395.3	790.6	98.8	4.8
	15	CC15	297.5	52.5	140	689.7	394.1	788.3	98.5	5.9
	20	CC20	280	70	140	688.0	393.1	786.3	98.3	7.0
BMK <sup>d</sup>	5	BMK5	332.5	17.5	140	694.1	396.6	793.2	99.2	4.2
	10	BMK10	315	35	140	692.4	395.6	791.3	98.9	5.5
	15	BMK15	297.5	52.5	140	690.7	394.7	789.3	98.7	6.6
	20	BMK20	280	70	140	689.2	393.8	787.7	98.5	7.7
MK <sup>e</sup>	5	MK5	332.5	17.5	140	693.9	396.5	793.0	99.1	6.5
	10	MK10	315	35	140	692.0	395.4	790.9	98.9	7.4
	15	MK15	297.5	52.5	140	690.1	394.3	788.7	98.6	8.1
	20	MK20	280	70	140	688.5	393.4	786.8	98.4	8.7

a: Calcined Balıkesir-Düvertepe kaolin, b: Calcined Balıkesir-Danaçayırı kaolin, c: Calcined Çanakkale-Çan kaolin, d: Calcined Bursa Mustafa Kemal Paşa kaolin, e: Commercial high reactivity kaolin from Czech Republic, f: Superplasticiser

### **3.2.3 Test methods**

#### **3.2.3.1 Compressive strength**

For compressive strength measurement of concretes, 150x150x150 mm cubes was tested according to ASTM C39 (2012) by means of a 3000 kN capacity testing machine. The test was performed on the test specimens at the ages of 3, 7, 28, and 90 days to monitor the compressive strength development. The compressive strength was computed from average of three specimens at each testing age.

#### **3.2.3.2 Splitting tensile strength**

Splitting tensile strength of the concretes was measured on 100x200 mm cylinder specimens at 28 and 90 days as recommended by ASTM C496 (2011). The splitting tensile strength reported herein is the average of three cylinders.

#### **3.2.3.3 Rapid chloride permeability test (RCPT)**

The rapid chloride permeability test (RCPT) was conducted in order to determine the resistance of the concretes to the penetration of chloride ions according to ASTM C1202 (2012). Three specimens for each mortar mixture will be tested simultaneously at each testing age (28, 90 days). After curing, a 50 mm thick disc sample is cut from the middle of each Ø100x200 mm cylinder and moisture conditioned as mentioned in ASTM C1202 (2012). Then, the disc specimens are transferred to the test cell in which one face of the specimen is in contact with 0.30 N NaOH solution and the other face is with 3% NaCl solution (Figs. 3.5 and 3.6). A direct voltage of  $60.0 \pm 0.1$  V is applied across the faces. A data logger registered the current passing through the concrete specimen over a period of 6 hours. Terminating the test after 6 hours, current (in amperes) versus time (in seconds) are plotted for each concrete and the area underneath the curve is integrated to obtain the charge passed (in coulombs). ASTM C1202 (2012) classifies the chloride permeability into five classes from 'High' to 'Negligible' on the basis of the coulombs calculated (Table 3.7).

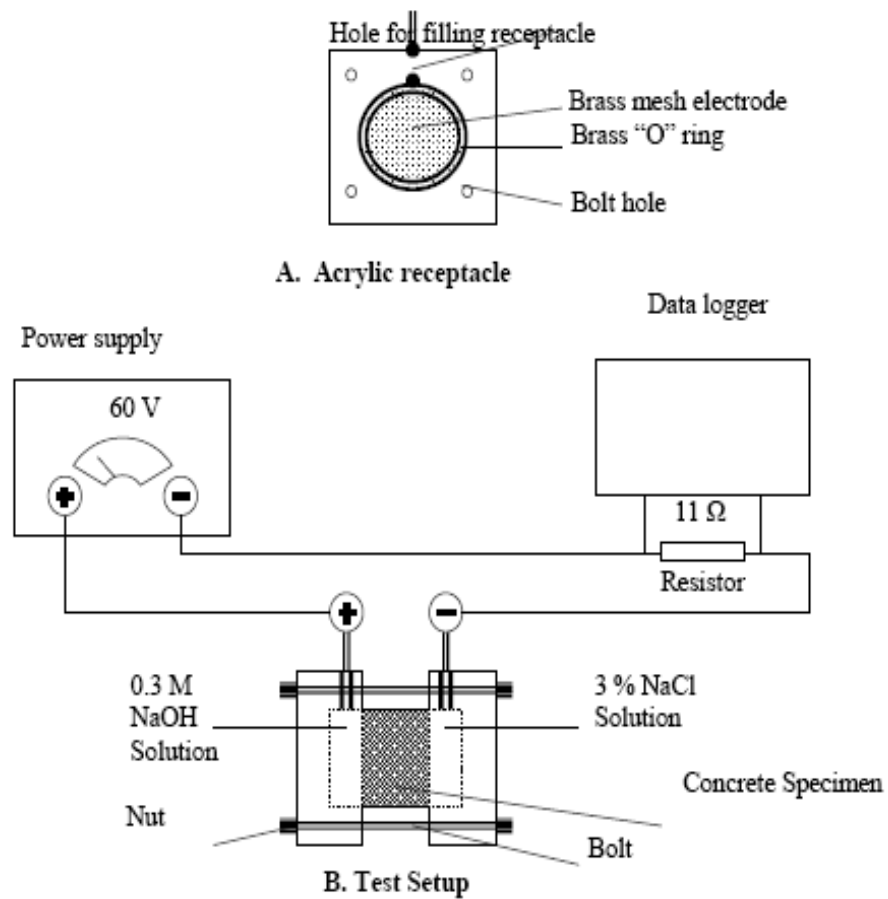


Figure 3.5 Schematic presentation of the test set up for RCPT



Figure 3.6 Photographic view of the RCPT test set up

Table 3.7 Interpretation of the test results obtained using RCPT test  
(ASTM C1202, 2012)

Charge passed (Coulombs)	Chloride permeability
>4000	High
2000-4000	Moderate
1000-2000	Low
100-1000	Very low
<100	Negligible



### 3.2.3.4 Water permeability

TS EN 12390-8 was followed in determining the water permeability of concretes. For this, a  $500 \pm 50$  KPa downward pressure is applied on the specimens for 72 hrs. Drinkable water is used for the test. At the end of 72 hrs period, the test specimens are split in the middle and the greatest penetration depth of water is measured in mm. In order to characterize the concrete resistant to the chemical attack, water does not penetrate to a depth of more than 50 mm in concrete likely to come in contact with slightly aggressive media and not more than 30 mm if concrete is likely to come in contact with aggressive media. A photograph of the water permeability test equipment is given in Fig. 3.7.



Figure 3.7 Water permeability test: a) device and b) measurement of penetration depth

### 3.2.3.5 Gas Permeability

Gas permeability of concrete is a problem closely relating to the microstructure of this heterogeneous material. Under loading and high temperature effect, micro cracks appear in critical zones of concrete. Finally, macro cracks are generated and increase the porosity of concrete matrix. As a consequence, the permeability becomes higher and depends on stress level of concrete during loading process. The gas permeability test set up and schematic presentation of the operation were presented in Fig. 3.8. The test was applied at the end of 28 and 90 days of curing.

The steps of the gas permeability test are as follows;

1. Measure the diameter of the test specimen in 4 positions (two perpendicular diameters in both top and bottom faces) with a precision of 0.1 mm. The diameter  $D$  is the mean value of the four readings. The thickness  $L$  of the test specimen is determined in four positions equally distributed along the perimeter.
2. Place the test specimen in the cell and assemble the apparatus (Fig. 3.8c).
3. Build up a minimum lateral pressure of 7 bar (0.70 MPa) on the rubber tube.
4. Select 3 pressure stages: start with 1.5 bar (0.15 MPa) and increase to 2.0 (0.20 MPa) and then 3.0 bar (0.30 MPa) absolute gas pressure. Correct the input pressure of gas if necessary within 10 minutes.
5. Wait for 30 minutes before measuring the first flow.
6. Measure the flow at each pressure stage until it becomes constant, as follows:
  - a. Moisten the capillary of the soap bubble flow meter 1 minute before creating the bubble for measurement.
  - b. Always start the time measurement when the bubble is at the lowest marking of the calibrated tube.
  - c. Select the measuring volume by choosing the appropriate soap bubble flow meter such that the time reading is more than 20 seconds.
  - d. Take provisional readings of the flow rate. If the difference between successive readings within 5 to 15 minutes is less than 3%, take at least 2 readings in quick succession and determine the flow rate  $Q_i$ :  $Q_i = V/t_i$  ( $m^3/s$ ) for the given pressure stage. If this condition is not reached within 3 hours (no constant flow is attained, *e.g.* very low-permeability concretes), take the previous value of the flow rate.
7. Increase the pressure to the next pressure level and repeat the procedure with steps (6a) through (6d). Ensure that there are no leaks during the tests: the coefficient  $K_i$  should decrease when the pressure increases. If this is not the case, check the test setup for possible leaks and repeat the measurements.

$$K_i = \frac{2P_2QL\mu}{A(P_1^2 - P_2^2)} \quad (3.1)$$

Where,

K: Gas permeability coefficient ( $m^2$ )

$P_1$ : Inlet gas pressure ( $N/m^2$ )

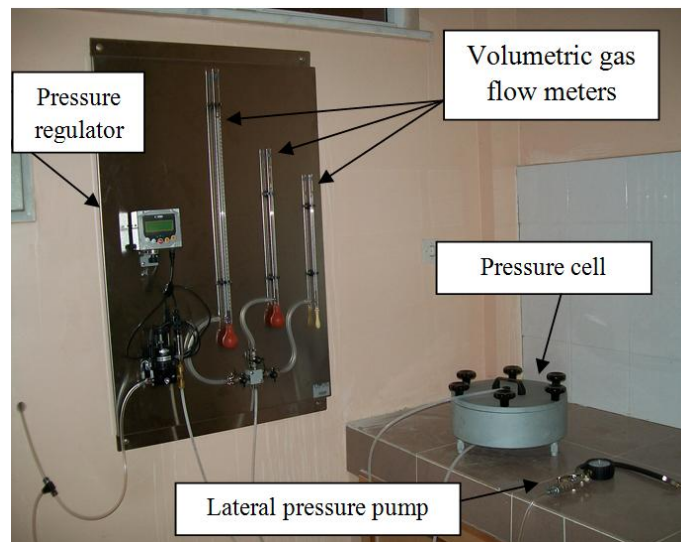
$P_2$ : Outlet gas pressure ( $N/m^2$ )

A: Cross-sectional area of the sample ( $m^2$ )

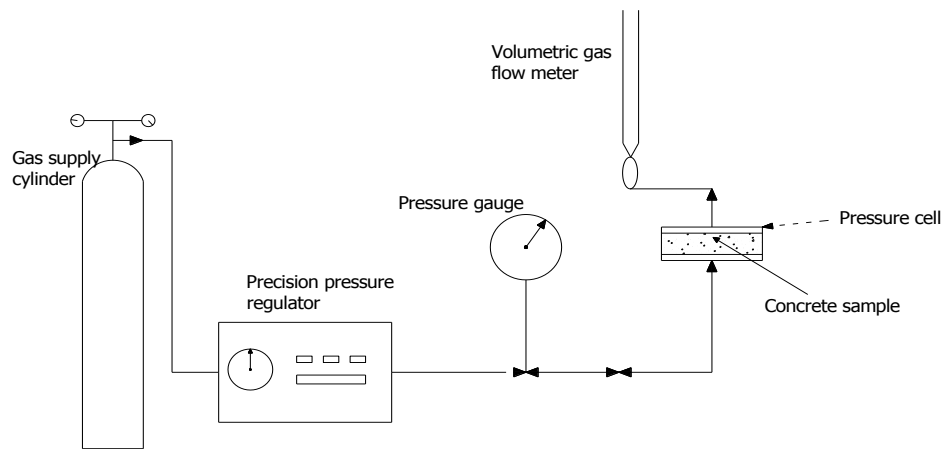
L: Height of sample (m)

$\mu$ : Viscosity of oxygen ( $2.02 \times 10^{-5} \text{ Nsn}/m^2$ )

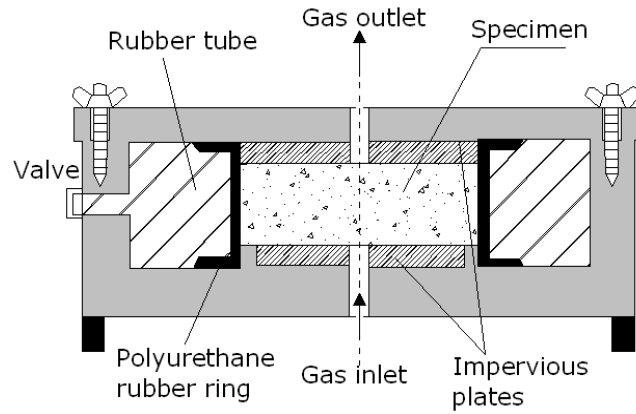
Q: Rate of flow of air bubble ( $m^3/sn$ )



a)



b)



c)

Figure 3.8 Gas permeability test: a) photographic view of the gas permeability set up, b) schematic presentation of set-up, c) detail of pressure cell and test specimen

### 3.2.3.6 Sorptivity

The sorptivity test measures the rate at which water is drawn into the pores of concrete. For this, three test specimens having a dimension of  $\text{Ø}100 \times 50$  mm are employed. The specimens are dried in an oven at about  $50^\circ\text{C}$  until constant mass and then allowed to cool to the ambient temperature in a sealed container. Afterwards, the sides of the specimens are coated by paraffin and as shown in Fig. 3.9, the sorptivity test is carried out by placing the specimens on glass rods in a tray such that their bottom surface up to a height of 5 mm is in contact with water. This procedure is considered to allow free water movement through the bottom surface. The total surface area of water within the tray should not be less than 10 times that of the specimen cross-sectional area. The specimens are removed from the tray and weighed at different time intervals up to 1 hour to evaluate mass gain. The volume of water absorbed is calculated by dividing the mass gained by the nominal surface area of the specimen and by the density of water. These values are plotted against the square root of time. The slope of the line of the best fit is defined as the sorptivity coefficient of concrete. For each test, the measurements are obtained from three specimens and the average values are reported. The test was conducted at the ages of 28 and 90 days.

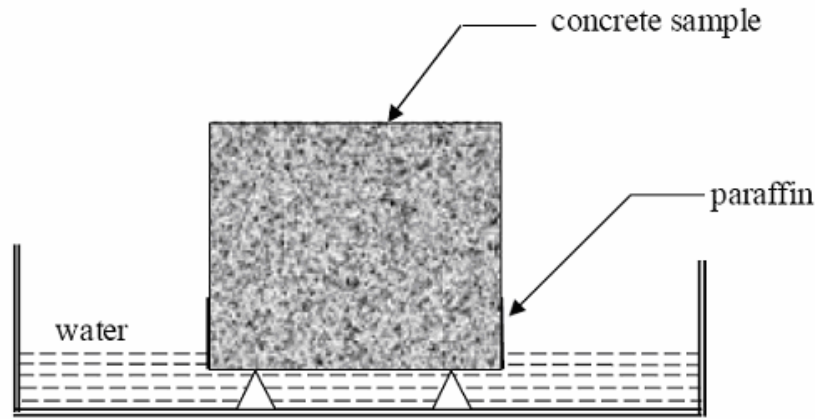


Figure 3.9 Sorptivity test set up

### 3.2.3.7 Electrical resistivity

Commercially available non-destructive testing RM-8000 model resistivity meter was used for evaluating the resistivity of concretes. The test will be performed on Ø100x200 mm cylinder specimens. For this purpose, two electrodes of the resistivity meter are placed in the holes drilled to a depth of 8 mm in concrete and filled with conductive gel. The spacing between electrodes is 50 mm for the present study. During the test, a small alternative current is applied between probes and the resultant potential difference is measured across the probes (Fig. 3.10). The resistivity  $R$  of the concrete, for a semi-infinite geometry, is then determined. Two measurements are taken on the side face of each cube, and the averages of four readings on the three specimens are reported at each testing age.



Figure 3.10 Photographic view of the ER test device

### 3.2.3.8 Resistance against freeze-thaw cycles

This test method covers the determination of the resistance of concrete specimens to rapidly repeated cycles of freezing and thawing in the laboratory according to ASTM C666-03 Procedure A, "Rapid Freezing and Thawing in Water". ASTM C666 specifies various sizes of specimens for testing. However, the dimensions presented are not less than 75 mm in cross-section and 280 mm in length. Therefore, in this study, 100x100x300 mm prisms were used for freezing-thawing testing. In order to observe the effectiveness of CK and MK the concretes were water cured for 90 days before subject to freezing-thawing test. Flexural tensile strength test was applied to the undamaged concretes to obtain reference values. After taking ultrasonic pulse velocity (UPV) readings, the remaining specimens are transferred into tap water freezing-thawing cyclic exposures. The specimens were exposed to 300 freezing-thawing cycles each of which lasts approximately 4 hours between the temperatures of +4.4 °C and -17.7 °C. At the end of each 60 cycles UPV measurement were carried out till the end whole test. At the end of 300 cycles the specimens tested for flexural strength to evaluate the resistances of concretes to freezing-thawing. Moreover, the specimens were also tested for compressive strength to observe the change due to freezing-thawing. For this, 3x100x100 mm steel plates were used as it is shown in Fig. 3.11. This test was applied to the concretes incorporating 5% and 15% CK or MK as well as control.

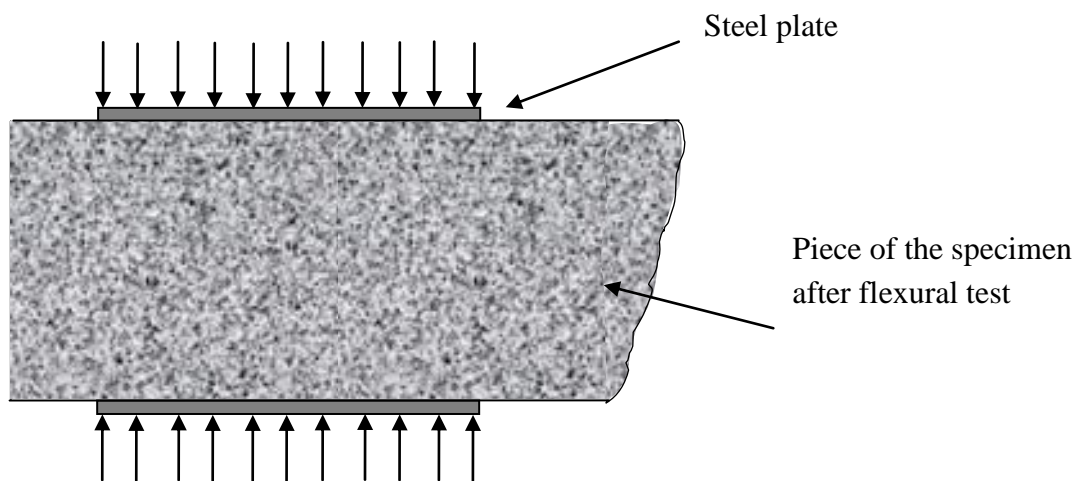


Figure 3.11 Compressive strength test on freezing-thawing specimen

### 3.2.3.9 Ultrasonic pulse velocity

Ultrasonic measurements are used to determine material properties, to detect defects, and to assess deterioration. As it is a non-destructive test method, a long term monitoring on the same specimens is possible. The test was applied to the specimens that were exposed to freezing-thawing cycles.

The test instrument consists of a means of producing and introducing a wave pulse into the concrete (pulse generator and transmitter) and a means of sensing the arrival of the pulse (receiver) and accurately measuring the time taken by the pulse to travel through the concrete. The equipment may also be connected to an oscilloscope, or other display device, to observe the nature of the received pulse. A schematic diagram of this test is shown in Fig. 3.12 complete description is provided in ASTM Test Method C597 (2010).

In this study, UPV measurement were taken for the specimens tested for freezing-thawing. The pulse velocity readings were taken at three points around the perimeter of the specimen specified in Fig. 3.13 at the end of each 50 cycle until 300 cycles. the average value was recorded as the reading value for the specified cycle. This test was applied to the concretes incorporating 5% and 15% CK or MK as well as control.

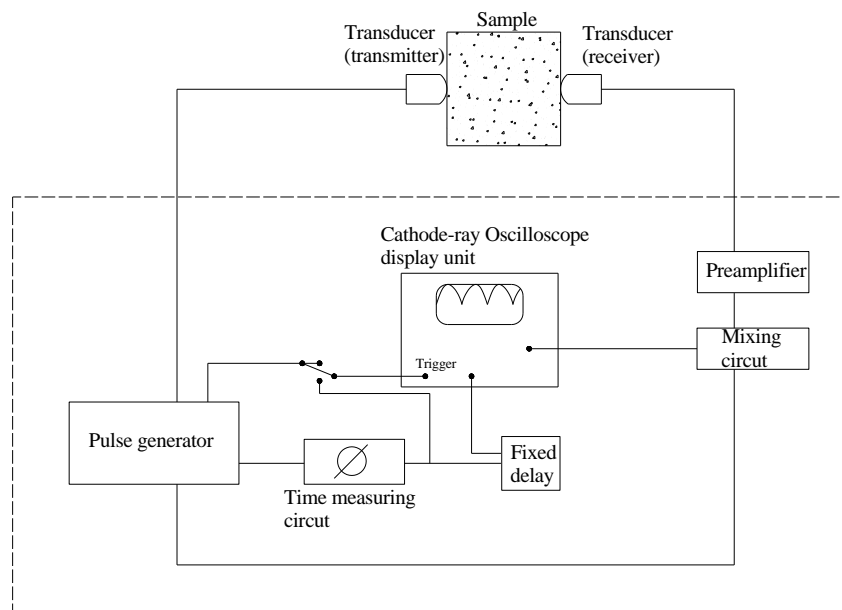


Figure 3.11 Schematic presentation of the test set up for UPV

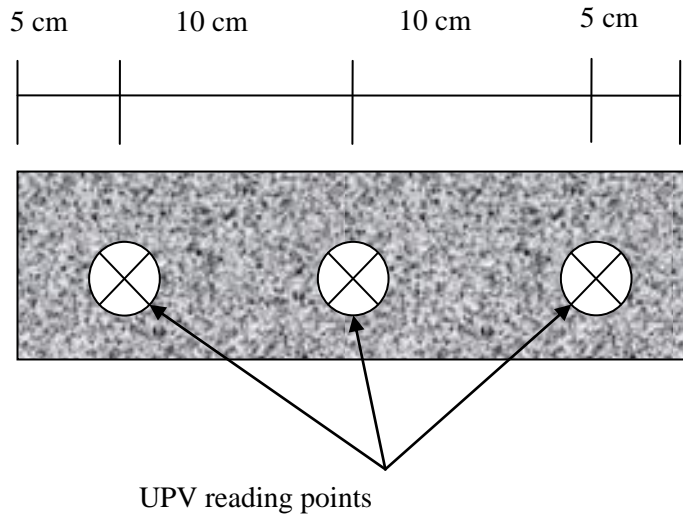


Figure 3.12 The points for UPV change monitoring due to freezing and thawing

### 3.2.3.10 Corrosion current density by linear polarization resistance (LPR) technique

The existence of chlorides within reinforced concrete accelerates the initiation of reinforcement corrosion and results in severe deterioration of concrete structures. Once the chloride content at the reinforcement reaches a threshold value and enough oxygen and moisture are present, the reinforcement corrosion will be initiated (Chen and Mahadevan, 2008). When corrosion is initiated, active corrosion results in a volumetric expansion of the rust around the reinforcing bars against the surrounding concrete (Tuutti, 1982). It is known that, in well designed and high quality concrete, the risk of corrosion is expected to be minimal since it provides chemical and physical conservation to the embedded steel reinforcement bars. The corrosion of rebar in concrete is generally considered as an electrochemical process (Maheswaran and Sanjayan, 2004; Elsener, 2004, El-Gelany; 2001; Liu and Weyers, 1998; Hope et al., 1986). Hence, the use of electrochemical techniques for the appraisal of corrosion behavior of R/C in this regard, becomes a prominent field of durability study. Therefore in this study, an electro-chemical corrosion monitoring technique named linear polarization resistance test was applied to measure the corrosion current density and corresponding corrosion rates of concretes exposed to chloride attack.



The term linear polarization refers to the linear regions of the polarization curve, in which slight changes in current applied to corroding metal in an ionic solution cause corresponding changes in the potential of the metal (Liu, 1996). This technique uses a single voltage scan or ramp programmed from an initial potential to a final potential (range generally limited to +/- 20mV vs. open circuit at  $E_{corr}$ ) that progresses at a defined step height per step time. Technique also referred to as LPR, provides capability to calculate corrosion rate. The linear polarization resistance method has been considered to be a relatively simple and reliable technique to assess the rate of corrosion reinforcement in concrete (Maslehuddin and Al-Amoudi 1992; Andrade et al., 1986).

Corrosion current density ( $I_{corr}$ ) value of less than  $0.1 \mu A/cm^2$  indicates negligible corrosion, while a value greater than  $0.3 \mu A/cm^2$  indicates active corrosion (Rodriguez et al., 1994). Therefore, in this investigation, an  $I_{corr}$  value of  $0.3 \mu A/cm^2$  was considered as the threshold criterion for corrosion initiation. The corrosion current density was measured using the DC linear polarization resistance method with lower potentials. The resistance to polarization ( $R_p$ ) was determined by conducting a linear polarization scan in the range of  $\pm 25$  mV of the open circuit potential at a scan rate of 0.1 mV per second. The corrosion current density ( $I_{corr}$ ) will be then calculated using the Stern–Geary Formula (Eqn 1) (Stern and Geary, 1957). B is calculated by the formula given in Eqn (2).

$$I_{corr}=B/R_p \quad (1)$$

$$B= (\beta_a \cdot \beta_c)/(2.303(\beta_a + \beta_c)) \quad (2)$$

Where B is a constant based on the anodic and cathodic Tafel constants ( $\beta_a$  and  $\beta_c$ ) and  $R_p$  is polarization resistance (Stern and Geary, 1957). The value of B was taken as 26 mV considering steel in active condition (Maslehuddin and Al-Amoudi 1992).

Lambert et al. (1991) have indicated a good correlation between the corrosion current density determined by the linear polarization resistance method and gravimetric weight loss using these values. According to Faraday's law, the following equation

(Eqn 3) can be applied to calculate the corrosion rate (CR) in mm/yr (Ismail and Ohtsu, 2006).

$$CR=3.27 \times I_{\text{corr}} \times E.W./d \quad (3)$$

Where E.W. is the equivalent weight of steel in gm and d is the density of reinforcing bar in gm/cm<sup>3</sup>.

In this study, VersaSTAT 3 a potentiostat/galvanostat with an optional frequency response analyzer (FRA) contained in a single unit was used to polarize the steel at a rate of 0.1 mV/s. Tafel constants were utilized in the calculation of the corrosion current density. As well as corrosion current density, CR values of each mixture were also calculated and presented. The test set up is schematically illustrated in Fig. 3.14.

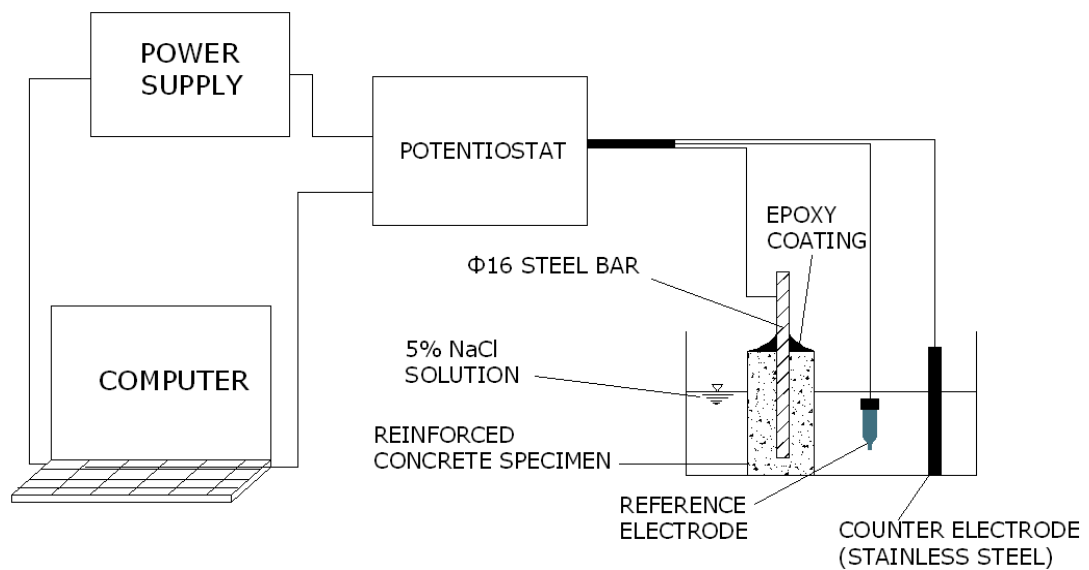


Figure 3.14 Schematic presentation of the linear polarization resistance test set up

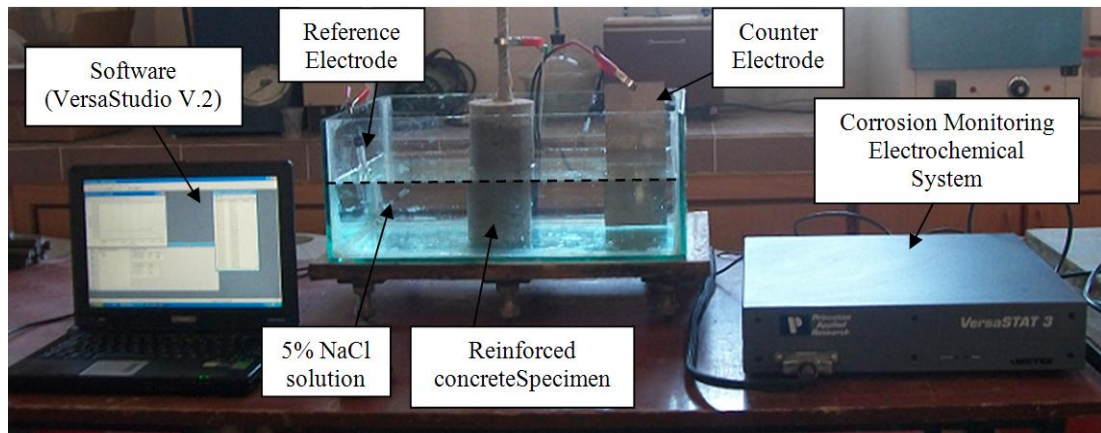


Figure 3.15 Photographic view of the potentiostat/galvanostat test set up

In Fig. 3.15, the photographic view of the potentiodynamic test set up was also presented. This test was applied to the concretes incorporating 5% and 15% CK or MK as well as control. Moreover, two different chloride exposure regimes were adopted. After 7 days of initial water curing, the concrete specimens were separated in two parts. One part was transferred to 2% NaCl solution, while the other part was put in 5% NaCl solution. Corrosion rate monitoring through linear polarization resistance method was carried out over 40 weeks of exposure.

### 3.2.3.11 Drying shrinkage and weight loss

Free shrinkage test specimens having a dimension of 70x70x280 mm for each mixture were cured for 24 h at 20 °C and 100% relative humidity and then were demoulded. After that, the specimens were exposed to drying in a humidity cabinet at  $23 \pm 2$  °C and  $50 \pm 5\%$  relative humidity, as per ASTM C157 for about 60 days. The length change was measured by means of a dial gage extensometer with a 200 mm gage length. The shape of the shrinkage specimens as well as the location of the reference pins are shown in Fig. 3.16. Measurements were carried out every 24 h for the first 3 weeks and then 3 times a week. At the same time, weight loss measurements were also performed on the same specimens. Variations in the free shrinkage strain and the weight loss were monitored during the 60-day drying period (at  $23 \pm 2$  °C and  $50 \pm 5\%$  relative humidity) and the average of three prism specimens were used for each property.

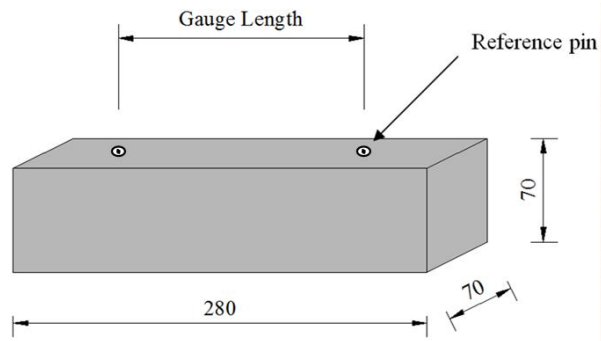


Figure 3.16 Free shrinkage specimens

This test was applied to the concretes incorporating 5% and 15% CK or MK as well as control.

## **CHAPTER 4**

### **TEST RESULTS AND DISCUSSIONS**

Test results and discussion section was presented in three parts. The first part presents the findings obtained from microstructural, thermal, and pozzolanic properties of unprocessed and/or calcined kaolins. In the second part, mechanical properties of plain, thermally treated kaolins (CKs) and commercially available metakaolin (MK) incorporated concretes were discussed in terms of compressive and splitting tensile strength developments. The results on durability related properties of the concretes were given in the third part. This part contains the results of gas permeability, water permeability, water sorptivity, rapid chloride permeability, electrical resistivity, freezing thawing cycles, drying shrinkage, and corrosion behavior of different concretes.

#### **4.1 Results on microstructural characterization and pozzolanic activity of calcined kaolins**

##### **4.1.1 Mineral composition by X –ray diffraction analysis**

The XRD patterns of the raw kaolins are illustrated in Fig. 4.1. In Table 4.1, the semiquantitative mineralogical estimation of the materials is presented. It was proposed that clays containing more than 35% of kaolinite can be directly processed into pozzolanic additives using thermal activation, eliminating the purification stage (Arikan et al., 2009). Therefore, it can be inferred that all of the kaolins used in this study can have pozzolanic property by proper heat treatment. It is seen from Table 4.1 that the content of alunite which requires high temperature for proper decomposition was the maximum for BMK kaolin. In the study of Badogiannis et al. (2005), it was also reported that, in the case of kaolin with high alunite content (22%), the required thermal treatment in order to remove undesirable SO<sub>3</sub> was far higher than for those having low alunite content (5-7%).

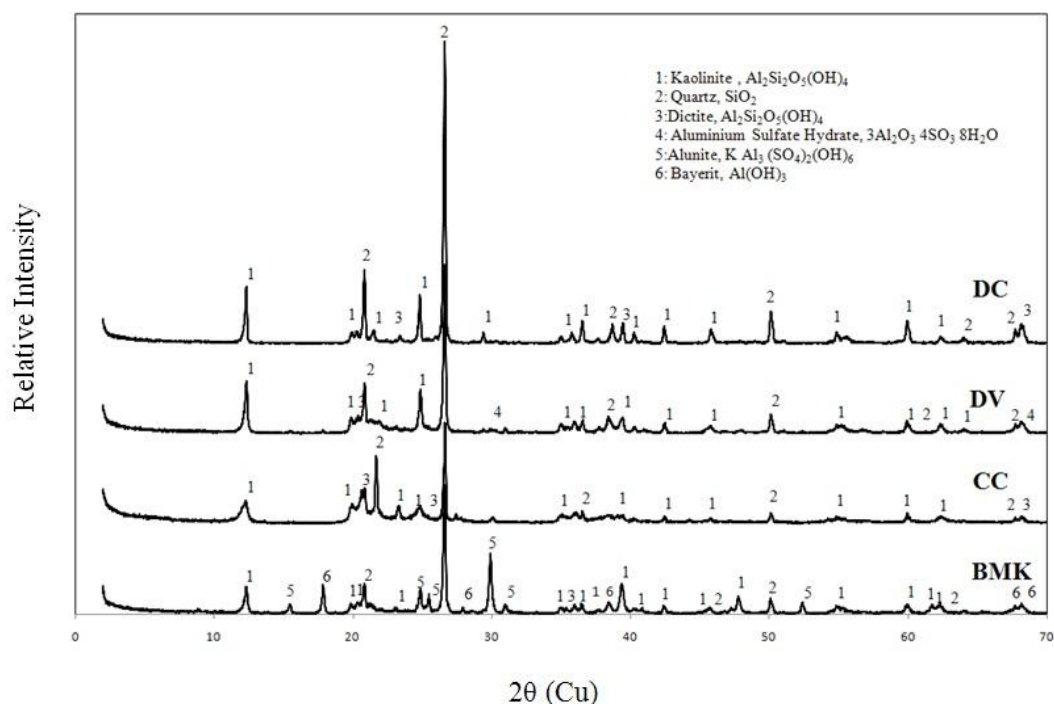


Figure 4.1. XRD patterns and mineralogical compositions of the kaolin samples

Table 4.1 Semiquantitative phase estimation results

Mineralogical composition	Kaolin Type				
	DV	DC	BMK	CC	MK
Kaolinite	54	38	46	54	>95
Quartz	36	55	23	32	-
Alunite	2	0.5	28	4	-
Others	8	6.5	3	10	<5
Convenience for heat treatment	<b>YES</b>	<b>YES</b>	<b>YES</b>	<b>YES</b>	<b>YES</b>

#### 4.1.2 Thermal characterization

In kaolin related studies, differential thermal analysis (DTA) and thermo gravimetric (TG) analysis are commonly used to characterize the thermal behavior of kaolins. For example, Arıkan et al. (2009) used the results of DTA-TG analyses to determine the thermal activation temperatures for the unprocessed kaolins. They determined the suitable thermal treatment temperature as 750 °C at which the DTA-TG curves reached to an asymptote. But, such a direct determination for calcination temperature was observed to be incoherent by the findings of other researchers. For example, Badogiannis et al. (2005) presented the results of XRD and DTA-TG analyses as

well as the pozzolanic activity index for supporting the results. Shvarzman et al. (2003) investigated the effect of heat treatment parameters on the dehydroxylation/amorphization process of the kaolinite-based materials such as natural and artificial kaolin clays with different amounts of amorphous phase (metakaolin). The production of artificial kaolins was achieved by providing amorphous phase contents at varying levels up to 75%. The process of dehydroxylation/amorphization of kaolinite was characterized by DTA/TGA with mass-spectrometry and X-ray powder diffraction.

Characteristic DTA-TG curves of the kaolins are given in Figs. 4.2 and 4.3. Fig. 4.2 reveals that, BMK kaolin experiences two different phase formations at 580 °C and 780 °C. Kakali et al. (2001) reported that the decomposition of alunite takes place in two stages between 480-620 °C ( $2\text{KAl}_3(\text{SO}_4)_2(\text{OH})_6 \rightarrow 2\text{KAl}(\text{SO}_4)_2 + 2\text{Al}_2\text{O}_3 + 6\text{H}_2\text{O}$ ) and 770-900 °C ( $2\text{KAl}(\text{SO}_4)_2 \rightarrow \text{K}_2\text{SO}_4 + \text{Al}_2\text{O}_3 + 3\text{SO}_3$ ). However, one endothermic peak occurred for DC, CC, and DV kaolins at 675, 500, and 545 °C, respectively. In thermal analyses, the first endothermic reaction at 580°C concerns alunite water loss while the third at 877°C corresponds to the decomposition of sulfates for BMK kaolin. An endothermic reaction is also visible between 650 and 680°C for BMK and DC samples. This may indicate the presence of dickite (Arazi and Krenkel 1970). To determine a proper calcination process for each type of kaolin, these endothermic peaks can be considered as threshold values where the alteration of the crystal structure of the kaolins begins. When observing the weight losses in Fig. 4.3, kaolins DC, CC, and DV seemed to reach to complete decomposition at about 750 °C. The variations in weight loss values of the kaolins beyond this temperature remained almost unchanged. On the other hand, the weight loss of BMK kaolin was observed to be constantly changing up to 900 °C due to its well-ordered crystalline structure and high alunite content. Nevertheless, BMK seems to reach its loss of ignition capacity (19.7%) presented in Table 3.2.

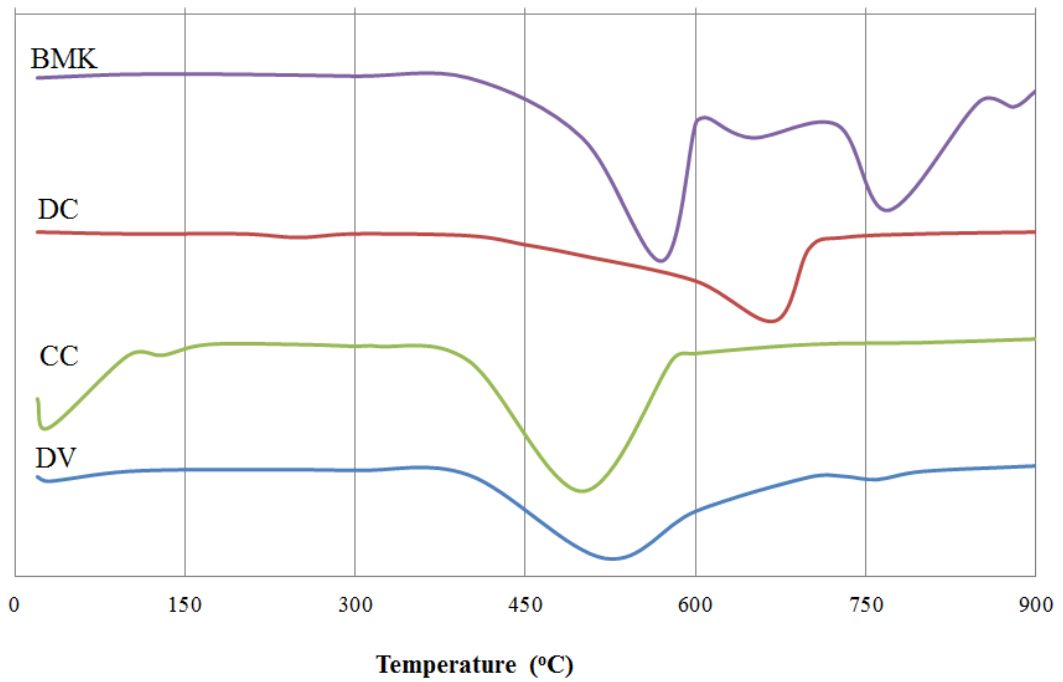


Fig. 4.2 DTA curves for the kaolins for observation of the phase transformations

It is stated that thermal exposure beyond 850 °C will result in sintering and the formation of mullite, which is dead burnt and not reactive (Kakali et al., 2001; Badogiannis et al., 2005). This situation results in a decline of material reactivity. Therefore it is important that kaolin should be optimally altered to a metakaolin state.

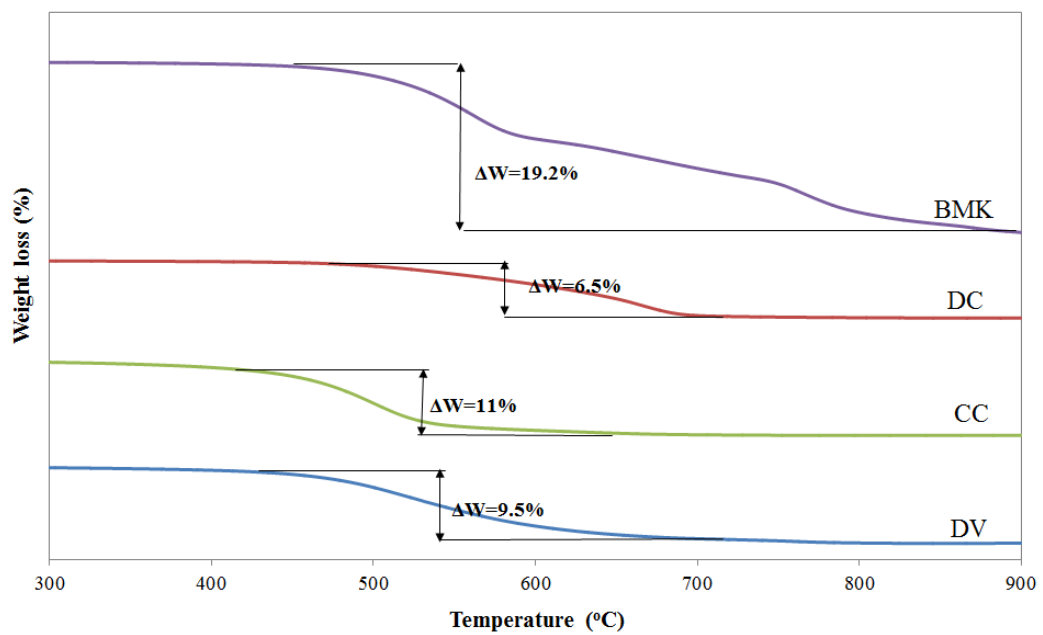


Figure 4.3 TG curves of the kaolins



### 4.1.3 Pozzolanic activity

According to the results obtained by DTA-TG analyses and the literature background, it was determined that the kaolins should be calcined for 3 hours at temperatures between 550-850 °C with 50 °C increments. After production of the calcined kaolin samples, they were tested for pozzolanic activity index per ASTM C311 (2005). Compressive strengths of the mortars at 28 days are given in Table 4.2. The plain mortar specimens (without calcined kaolin minerals) had 62 MPa compressive strength at the end of 28 days, while the compressive strength of the mortars varied between 49.6-66.6 MPa, depending mainly on the type of the calcined kaolin used and the calcination temperature. The corresponding pozzolanic activity index values of the calcined kaolins are presented in Fig. 4.4, where the ASTM C618 (2008) limit was also shown. ASTM C618 specifies that the pozzolanic index (PI) of a pozzolan-containing mortar after 28 days of curing should exceed 75%. The kaolins used in this study all satisfied the ASTM C618 (2008) limit at each calcination temperature between 550-850 °C. This may be considered to indicate the convenience of the calcination period.

According to the results presented in Fig. 4.4, it can be observed that kaolins DC, CC, and DV had the highest PI values at 750 °C, while BMK kaolin reached its maximum PI value at 850 °C. Kakali et al. (2001) stated that absolute value of the slope of the DTA curve corresponding to dehydroxylation is sharper for the well-crystallized samples. Moreover, in the study of Murat (1983), it is stated that the starting of decomposition of kaolinite in well crystallized samples occurs at higher temperature. Therefore, considering these highlighting facts, it can be inferred that by increasing the temperature up to 850 °C, the conversion of kaolinite to metakaolinite was mostly accomplished for BMK. The higher the amount of metakaolinite, the higher amount of additional CSH gel was formed due to secondary hydration reactions. The maximum PI values at 750 °C were calculated as 107% for DV and CC, 104% for DC. For BMK kaolin calcined at 850 °C, maximum PI value was calculated as 102%. For DC, CC, and DV kaolins at calcination temperatures over 750 °C PI values decreased due to reduction in pozzolanic property. This can be attributed to the decrease in chemical vulnerability as a result of overheating of the kaolins. Consequently, 750 °C can be considered as the most convenient calcination

temperature for DC, CC, and DV kaolins. Since calcination over 850 °C results in mullite formation, the calcination temperature for BMK kaolin was taken as 850 °C.

Table 4.2 Compressive strength values of the mortar specimens

Calcination Temperature (°C)	28 day compressive strength result (MPa)			
	DV	DC	BMK	CC
550	51.0	49.6	51.8	54.0
600	63.7	56.0	60.1	58.3
650	64.1	58.4	61.3	63.8
700	64.5	60.4	61.7	62.7
750	66.4	64.8	62.5	66.6
800	62.5	62.3	62.6	57.8
850	59.3	59.4	63.4	55.2
Control	62.0			

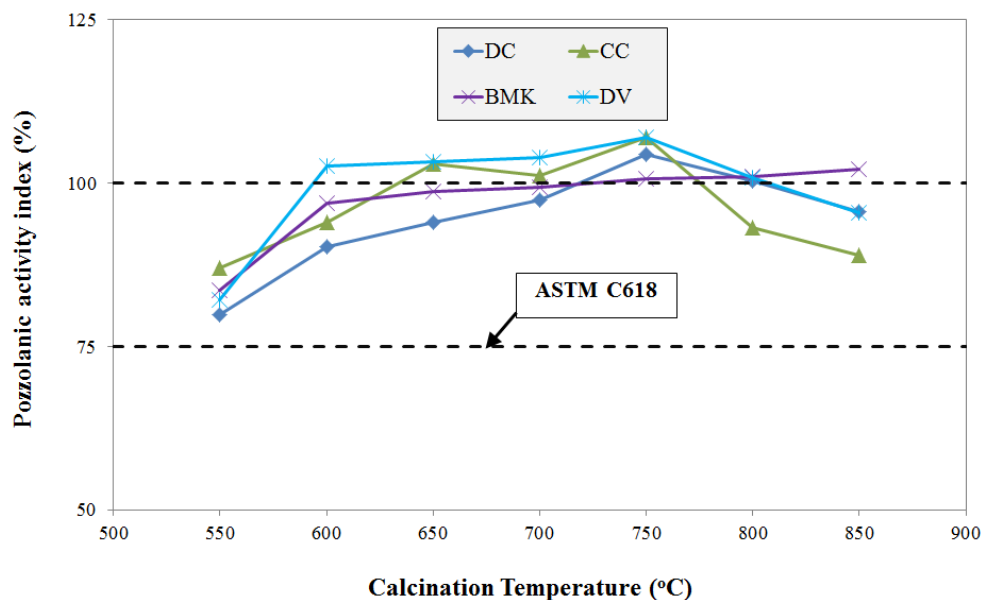


Figure 4.4 Pozzolanic activity indices of the calcined kaolins

The principal reaction takes place between the metakaolinite, ( $\text{Al}_2\text{O}_3 \cdot 2\text{SO}_2$ ) or  $\text{AS}_2$ , and the CH derived from cement hydration, in the presence of water. This reaction forms additional, cementitious aluminum containing CSH gel, together with crystalline products, which include calcium aluminate hydrates and aluminosilicate hydrates (i.e.,  $\text{C}_2\text{ASH}_8$ ,  $\text{C}_4\text{AH}_{13}$  and  $\text{C}_3\text{AH}_6$ ) (Sabir et al., 2001).

Fig. 4.5 shows the weight losses of the samples exposed to 3-hour thermal treatment at each calcination temperature. As it can be clearly seen from Fig. 4.5, the temperature increase above 750°C does not cause any noticeable further mass loss in

samples DV, DC, and CC. This indicates that the kaolinite to metakaolinite conversion in these samples is almost complete, after thermal treatment at 750°C for 3 h. However, BMK kaolin shows a continuous mass loss up to 850°C, due to the decomposition of alunite and the removal of sulfates.

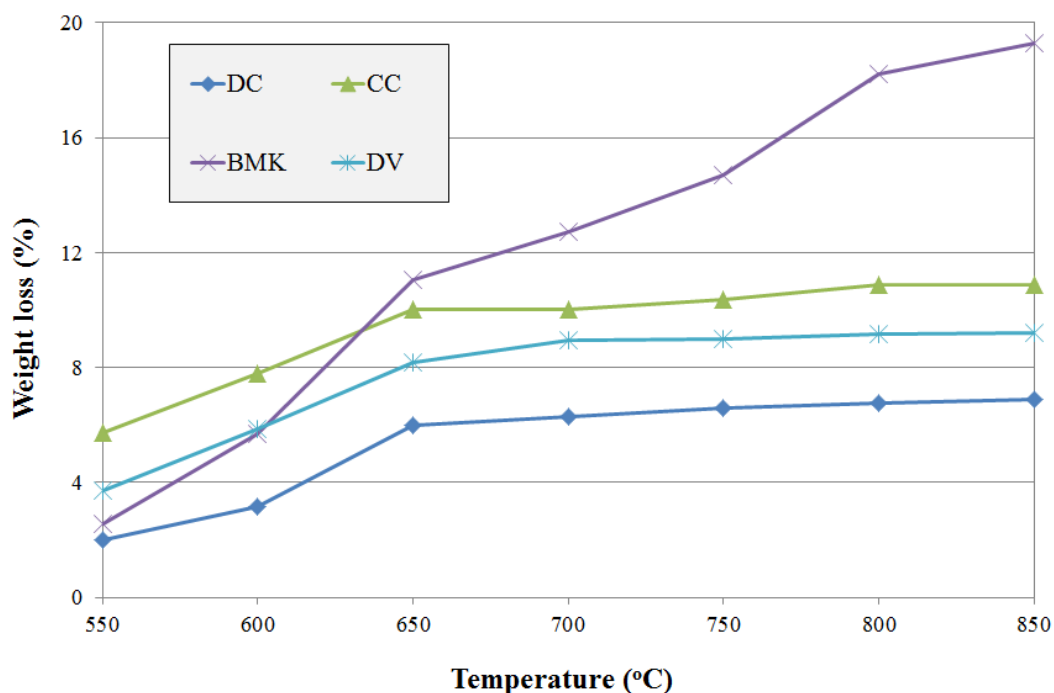


Figure 4.5 Weight losses of the kaolins due to 3 h calcination process

In order to check the disappearance of the characteristic peaks of kaolinite and alunite, XRD analysis was carried out on the calcined samples and the results are shown in Fig. 4.6. The XRD patterns of the calcined samples revealed that the consumption of kaolinite was achieved in all of the samples as a result of transformation to metakaolinite. Furthermore, in calcined BMK sample, due to complete decomposition of the alunite phase, the characteristic peaks of alunite were disappeared as well.

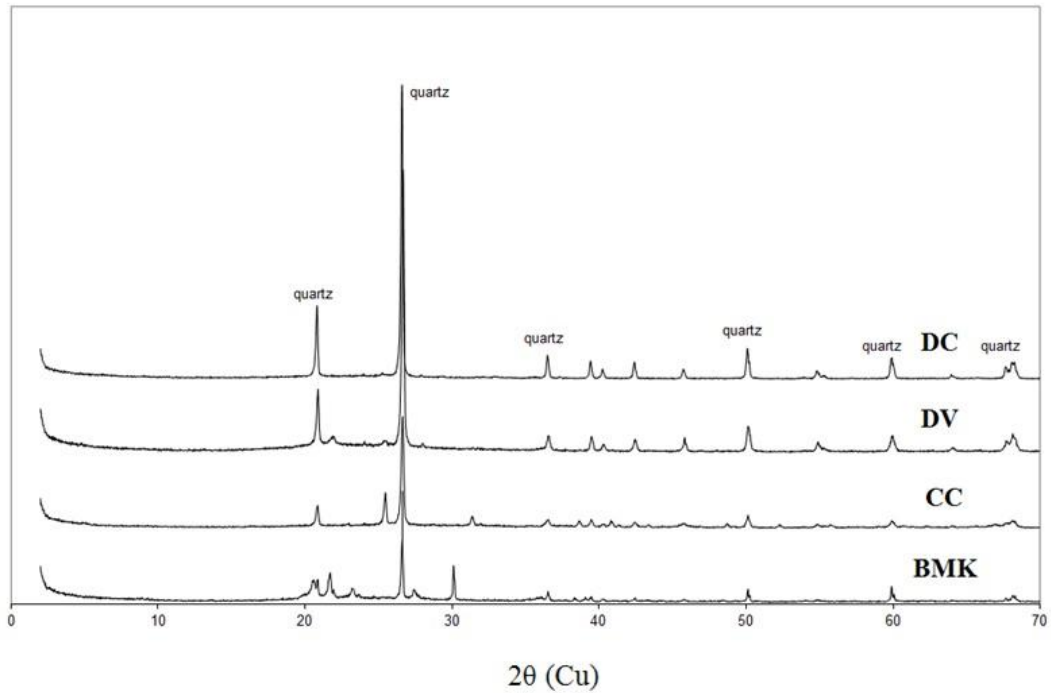


Figure 4.6 XRD patterns of the calcined Turkish kaolins

#### 4.1.4 Fineness and particle size distribution

Specific surface area (SSA) of kaolin is related to the particle shape and size. As the particle size decreases, surface roughness, angularity and thus the surface area increase. Increased surface area provides chemical vulnerability to the calcined kaolin when it is introduced to the hydration process (Cassagnabère et al., 2009). SSA of calcined kaolin has a paramount importance when the contribution of the mineral admixture on the concrete properties is taken into consideration.

The raw kaolins in this study were ground by industrial type hammer mill system (Fig. 4.7). Since exactly the same grinding process was applied to each raw kaolin, the measured SSA values were close to each other. BET SSA values of the raw and calcined kaolins were presented in Fig. 4.8. SSA of the kaolins were measured to range between 5500-8300 m<sup>2</sup>/kg and 4400-7400 m<sup>2</sup>/kg for raw and calcined kaolins, respectively. The differences in the SSA of the kaolins may be due to the variations in hardness of the materials, surface roughness, and porosity of the particles (Kaloumenau 1999). It must be remembered that the samples contained various amounts of kaolinite therefore the differences can come from the composition of the

remaining minerals. Heat treatment of the kaolins resulted in clustering of the particles (Vizcayno et al., 2010). As a result, the specific surface area of the calcined kaolins decreased. As seen in Fig. 4.8, SSA of the CC kaolin showed a decrease of about 20% while the others experienced about 10% reduction through calcination.

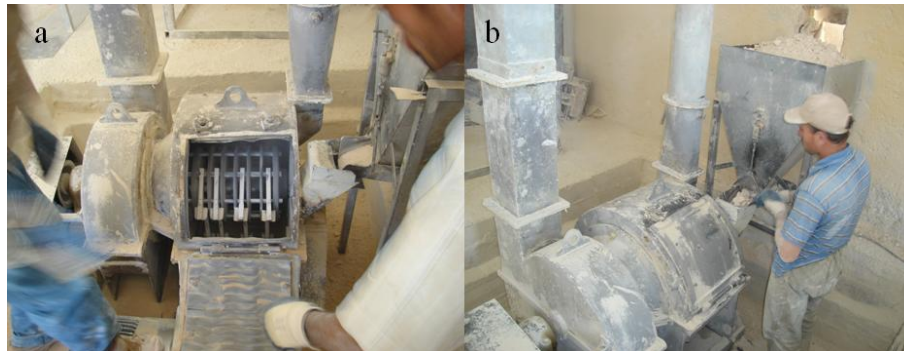


Figure 4.7 Photographic views of a) Hammer mill, b) Feeding the mill

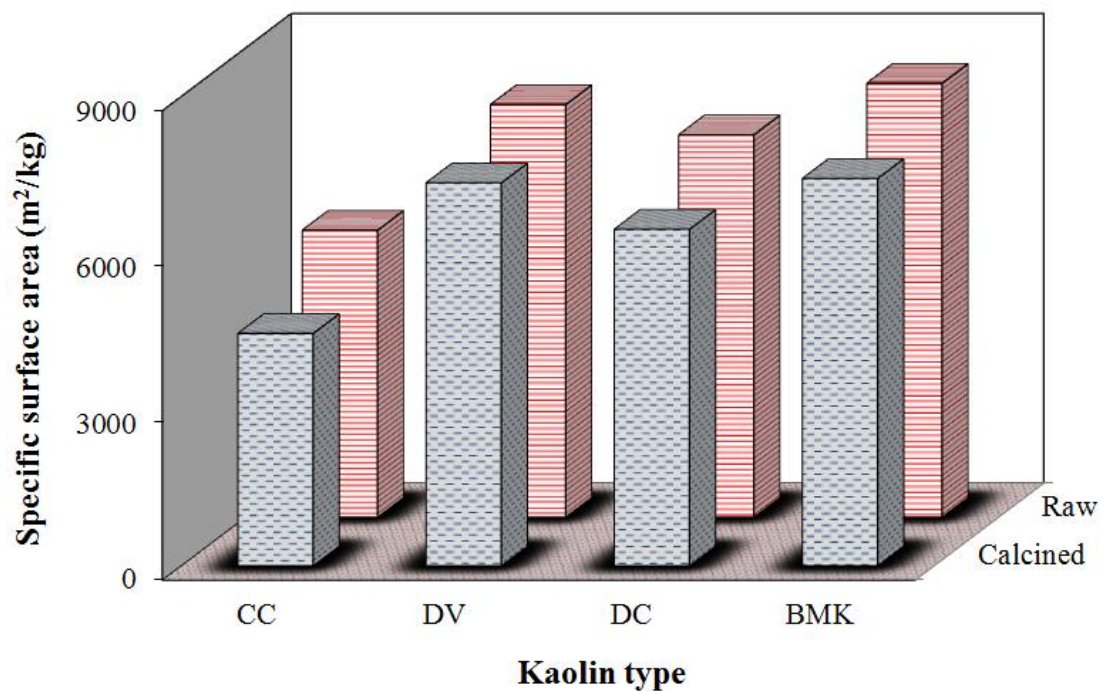


Figure 4.8 BET specific surface area of the raw and calcined kaolin samples

Particle size distribution of calcined clay is a crucial parameter affecting its microfilling ability. The calcined kaolin shows a higher microfilling effect as the particle size gets smaller. Typical particle size distribution curves of raw and calcined CC kaolins are illustrated in Fig. 4.9. The figure shows that relatively coarser particulate formation occurs due to calcination. The percentiles  $D_{50}$  and  $D_{90}$

represent, respectively, the particle size at which 50% and 90% of the volume is finer and they are used to characterize the particle size distribution of the kaolins before and after calcination (Table 4.3). Test results indicate that there is a substantial increase in the particle size of the kaolins as a result of calcination. The quantity of the coarse fraction increases with temperature in all of the samples. During calcination, aggregate structures are formed by the partial fusion of the clay particles which is most importantly affected by the size distribution of the particles (Chandrasekhar 2002). The extreme change was observed at CC kaolin, while the minimum change was detected in the DC kaolin. When fineness of the calcined kaolins are compared, it seems that BMK and DV kaolins have almost the same average particle sizes. Critical observation of Fig. 4.9 and Table 4.3 indicates that there is not a linear relationship between the particle size distribution and the specific surface area.

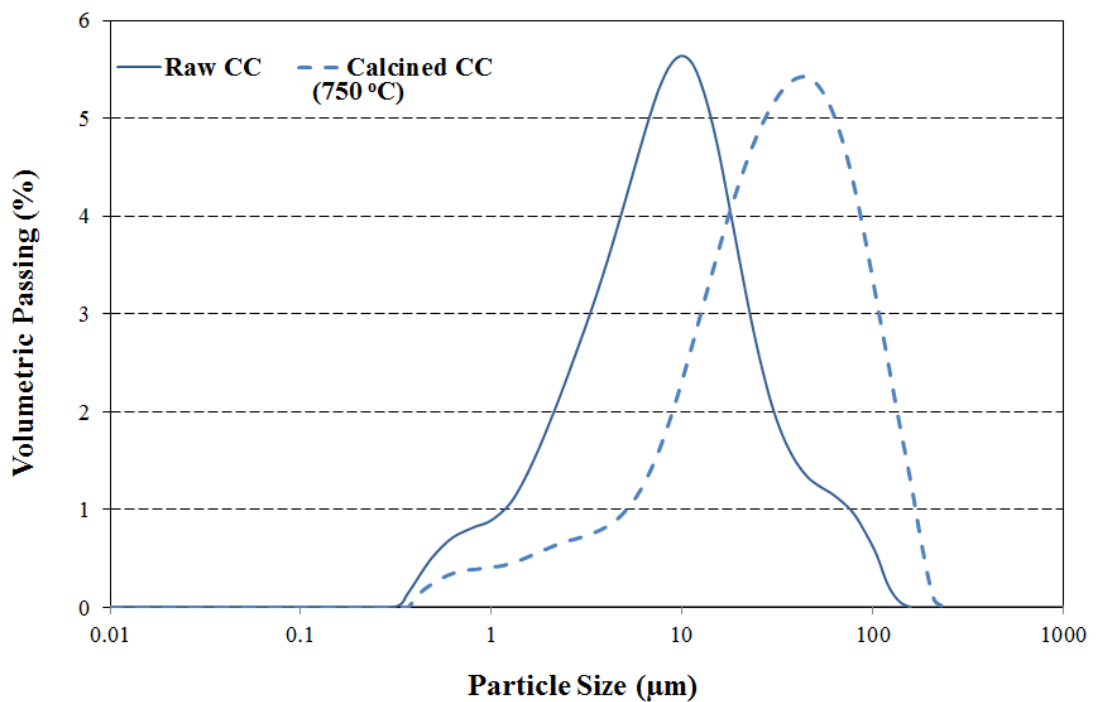


Figure 4.9 Particle size distribution of the raw and calcined CC

Table 4.3 Particle size distribution of the raw and calcined kaolin samples

Sample	Particle size distribution ( $\mu\text{m}$ )		
	$D_{50}$	$D_{90}$	
<b>DV</b>	Calcined	8.5	33.5
	Raw	6.5	26
<b>DC</b>	Calcined	6.3	10.9
	Raw	5.9	9.8
<b>BMK</b>	Calcined	8.4	21
	Raw	7.4	17.6
<b>CC</b>	Calcined	33.2	85
	Raw	9.2	32.5

#### 4.1.5 SEM image analysis

SEM images of the calcined kaolins at x500 magnification are demonstrated in Fig. 4.10, for visualizing the comparative particle size distributions. As an example to the agglomeration and change in the crystalline order kaolins, SEM images of DV kaolin before and after calcination are presented at x2500 and x30000 magnifications in Fig. 4.11. Fig. 4.11 also illustrates that, the quantity of the coarse fraction increases as a result of calcination (a-1 vs. b-1).

The crystalline order of the kaolinite seems to be altered due to the calcination. It is known that the ordered phase of pseudo-hexagonal plates of kaolins intercalates but the highly disordered kaolinite does not. Therefore, it can be concluded that irregular arrangement and broken edges of the kaolinite platelets indicate the disordered phase. As can be seen from Fig. 4.11, a more disordered phase occurred as a result of thermal treatment (a-2 vs. b-2).

It can be seen in Fig. 4.10 that CC kaolin has coarser particles whereas the other three has similar particle size distribution. In that respect it was seen that SEM image analysis is compatible with the BET surface area measurements and laser diffraction analysis.

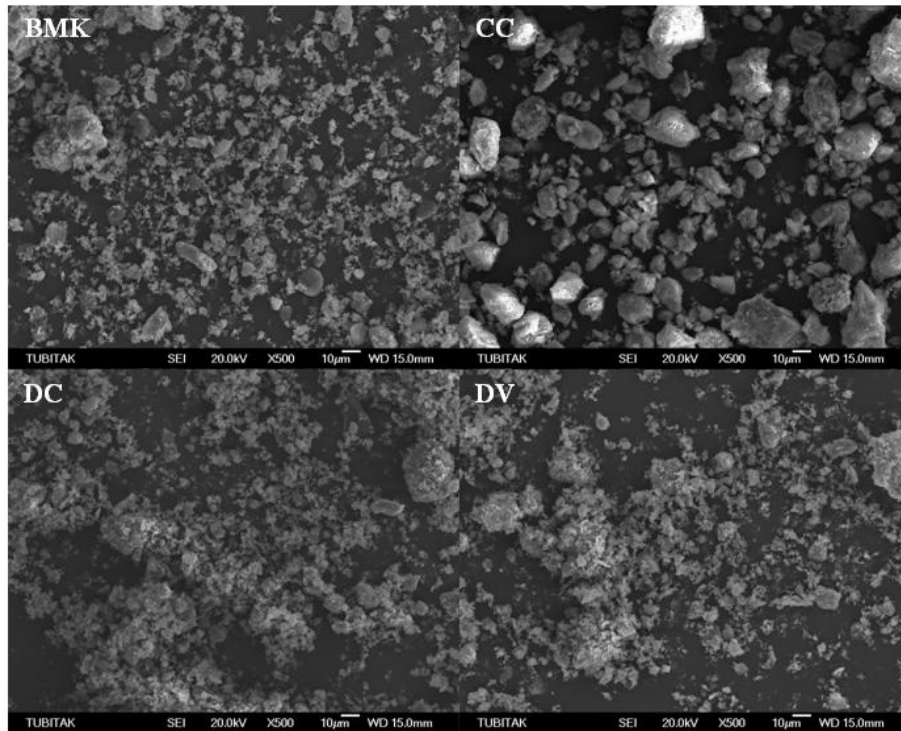


Figure 4.10 SEM images of calcined kaolins at x500 magnification

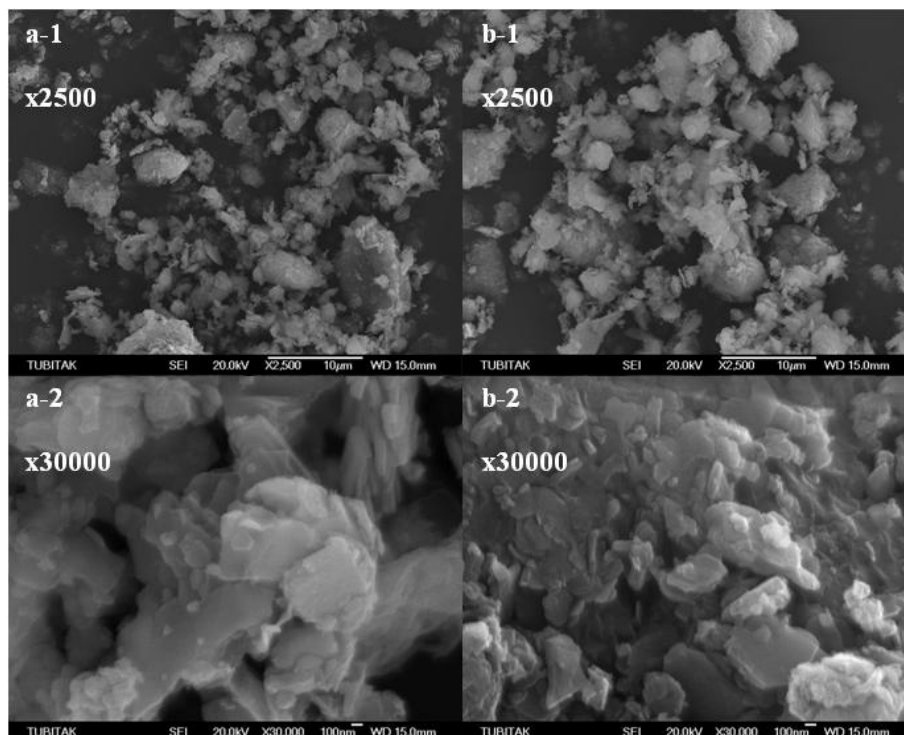


Figure 4.11 SEM images of a) raw and b) calcined DV kaolin at different magnifications



## 4.2 Results on mechanical properties of concrete

### 4.2.1 Compressive strength development

The compressive strength development of the concretes produced with calcined Turkish kaolins (CK) and the commercial metakaolin (MK) are shown in Table 4.4 and graphically presented in Fig. 4.12. Fig. 4.13 shows the effect of replacement level on the compressive strength of the concretes relative to the control. Relative strength is the percentage of the strength of the metakaolin concrete by the strength of the plain concrete at each specified curing time. The rate of development in the strength for the concrete without MK or CK is based mainly on the hydration rate of Portland cement, whereas in cement– metakaolin systems, it depends on the combination of cement hydration and the pozzolanic reaction of MK. Wild et al. (1996) state that the relative strength–time plots provide an insight into the rates of reaction in the blended system relative to the plain ordinary Portland cement system.

Fig. 4.12 shows that, the compressive strength of the control concrete varied between 40-56 MPa while compressive strength of CK and MK incorporated concretes ranged between 23-64 MPa and 35-67 MPa, respectively, mainly depending on the age and replacement level. At 5% replacement level, compressive strength development of the CK and MK modified concretes were observed to have close trends.

It seems that at this replacement level, all of the concretes had almost same compressive strengths at 3 days of curing (Fig. 4.12a). Nevertheless, as the time passed the difference in strength became clearer. At later ages, especially at 90 days, the difference in compressive strength of MK and CK concretes were not too distinct at all. For example, 90 day compressive strength of the concretes were measured as 60.0, 58.2, 59.6, 58.0, 56.5 MPa for MK5, DV5, DC5, CC5, and BMK5 concretes, respectively. It was observed from Fig. 4.12b that MK10 concrete had a greater compressive strength development even at early ages. Its 7 day compressive strength was 52.5 MPa, while the others were in the range of 43-47 MPa, including control concrete strength. However, at 28 days, the strength of 10% CK incorporating concrete reached to that of MK10 concrete. Moreover, the range of the variation of the compressive strength of the concretes was very narrow at that age (53-56 MPa).

Observation of Fig. 4.12c indicated that the lowest compressive strength was observed at DC15 concrete at 3 days of curing. However, at 90 days, the compressive strength of DC15 was far higher than control concrete.

Due to its high reactivity and fineness, MK concretes had relatively higher compressive strength development than control and CK concretes. But through the whole curing period the compressive strength development of DV15, DC15, and CC15 concretes demonstrated a very close trend to that of MK15 concrete even at early ages. For example, at 7 days of curing MK15 had 47.5 MPa compressive strength, however, DC15 concrete had 44 MPa compressive strength. The highest compressive strength was measured at MK20 concrete at 90 days of curing (67 MPa). But at 20% replacement level, 3 day compressive strengths of the mineral admixed concretes were not much higher than that of control concrete. At 20% replacement level the compressive strength development trend of the CK concretes were slightly irregular compared to the other replacement levels.

The relative compressive strength of the concrete is calculated by division of compressive strength of each mineral admixture incorporated concrete by the compressive strength of the control concrete at the same age. When observing Fig. 4.13, it was found out that at early ages, especially at the end of 3 days, pozzolanic or micro-filling effect of the calcined kaolins did not able to compensate the decrease in the compressive strength as a result of reduction in the cement content. Fig. 4.13a reveals that 3 day compressive strength of the concretes with increasing amount of mineral admixture fall below the control concrete. However, at 20% replacement level of MK the relative strength was measured to be 104% at 3 days. This can be attributed to the high degree of fineness of MK. When considering 7 days of curing, 5% replacement level showed the highest relative strength compared to other replacement levels, except for MK concrete. MK concrete had highest 7 day compressive strength at 10% replacement level also.

Superior enhancement in early age compressive strength of MK blended concretes may also be due to the high reactivity of this material. In the study of Poon et al. (2001), the degree of pozzolanic reactions of high-performance cement paste blended with metakaolin and silica fume (SF) were compared. They prepared the MK

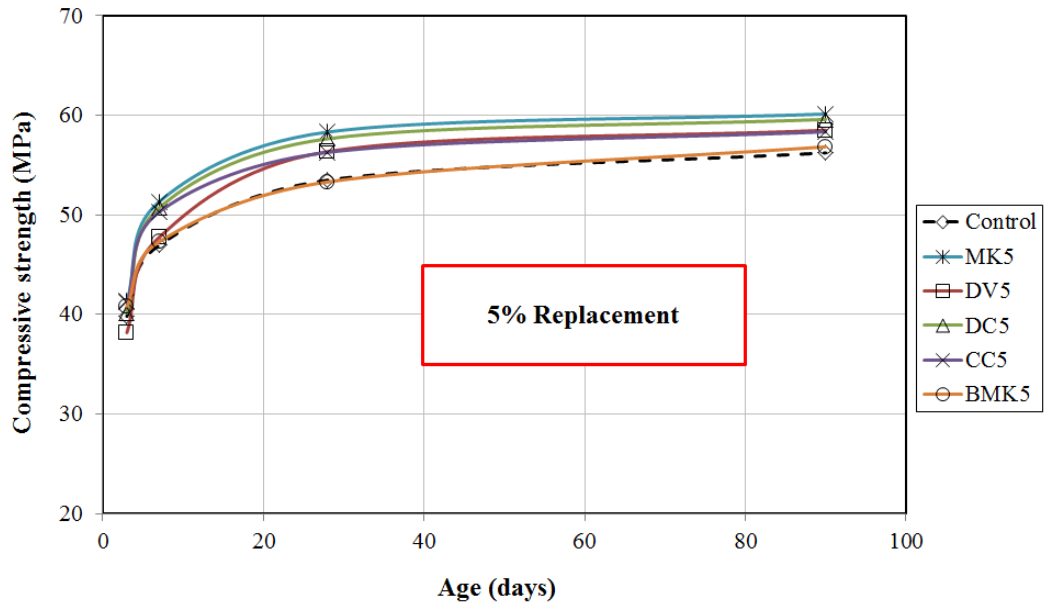
blended cement pastes with MK contents of 5, 10, and 20%, SF-blended pastes with SF contents of 5% and 10%, and a control paste without any mineral admixture. At 3 days, the degree of pozzolanic reaction of MK in the pastes at the MK replacement levels of 5 and 10% was 20.6% and 15.3%, which were 30% and 49% higher than that of SF in the corresponding blended cement pastes. The high reactivity of MK is due to its high purity which, in turn, corresponds to higher metakaolinite content. Since the CKs used in this study have been obtained by calcination of non-purified local kaolins, the decrease in the early age compressive strength of the concretes as the amount of admixture increases was observed.

Although increasing amount of CK showed a decreasing tendency, the relative strength values were generally within -10% limits. Relative strength values at 28 days showed that at almost all of the replacement levels concrete compressive strengths were higher than control concrete. The highest 28 day relative strength values for CK and MK concretes were achieved at 15% and 20% replacement levels, respectively. Fig. 4.13d showed that, all of the concretes had significantly higher compressive strength than the plain concrete. Only BMK concrete did not exceed +10% limit at all replacement levels. This can be explained by the distinction of the chemical composition and mineralogy of this material.

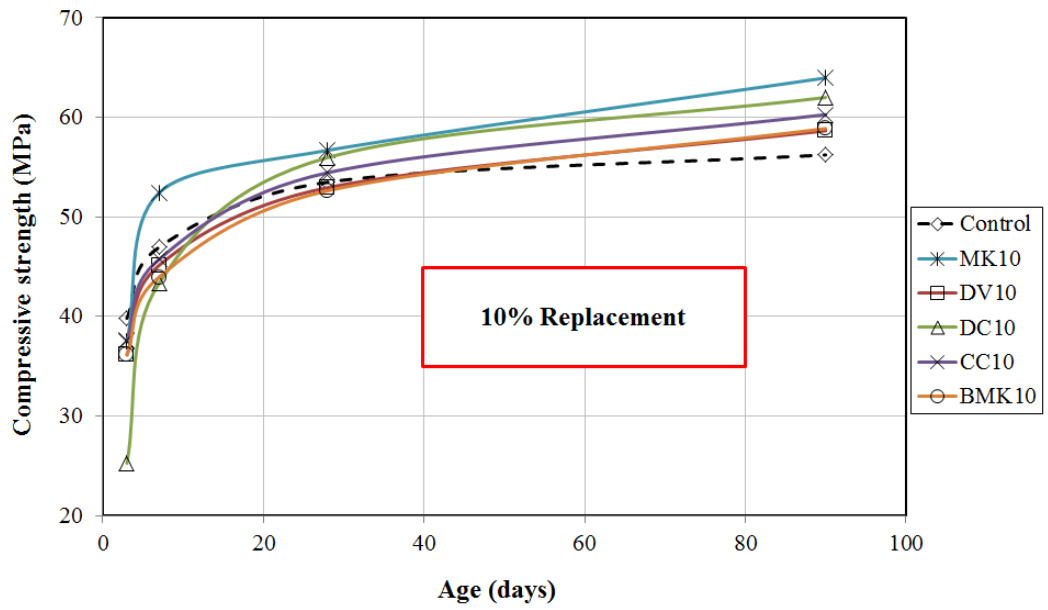
Observing Fig. 4.13c and Fig. 4.13d, it can be concluded that the best replacement level for CK and MK used in this study seemed to be 15% and 20%, respectively. Wild et al. (1996) investigated the effect of metakaolin (MK) on the compressive strength of concrete mixtures at 0, 5, 10, 15, 20, 25, and 30% replacement levels of ordinary Portland cement (OPC). Compressive strength tests were conducted up to the age of 90 days. It was concluded that inclusion of MK as partial replacement of cement improved the compressive strength of concrete at all ages, but the optimum replacement level of OPC by MK to give maximum long term strength enhancement was about 20%.

Table 4.4 Compressive strength (MPa) of the concretes

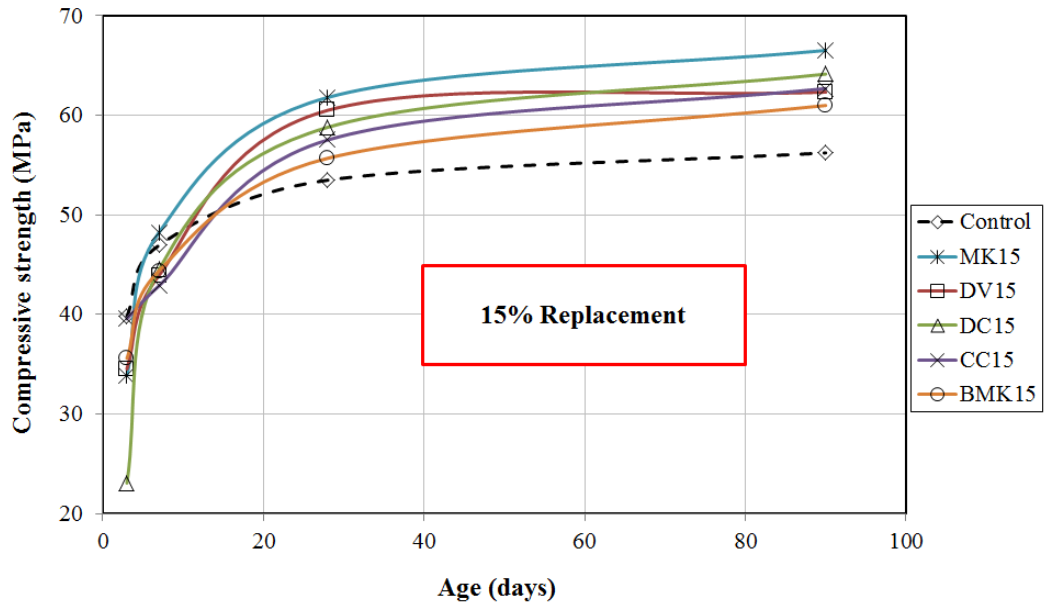
Mix	Replacement level (%)	Age (days)			
		3	7	28	90
Control	0	39.8	46.9	53.5	56.2
	5	38.2	47.7	56.4	58.5
DV	10	36.1	45.1	52.9	58.7
	15	34.5	43.9	60.5	62.3
	20	25.9	42.9	55.7	60.5
	5	40.2	50.7	57.6	59.6
DC	10	25.3	43.3	56.0	62.0
	15	23.1	44.5	58.8	64.1
	20	35.3	47.2	56.0	63.0
	5	41.2	50.3	56.3	58.3
CC	10	37.6	45.7	54.4	60.3
	15	39.6	42.9	57.5	62.7
	20	41.5	48.5	55.8	59.1
	5	40.8	47.3	53.3	56.8
BMK	10	36.2	43.9	52.6	58.9
	15	35.6	44.4	55.7	61.0
	20	33.9	46.0	53.3	60.0
	5	41.3	51.3	58.3	60.1
MK	10	37.4	52.4	56.7	64.0
	15	33.8	48.2	61.8	66.5
	20	35.0	48.4	61.9	66.9



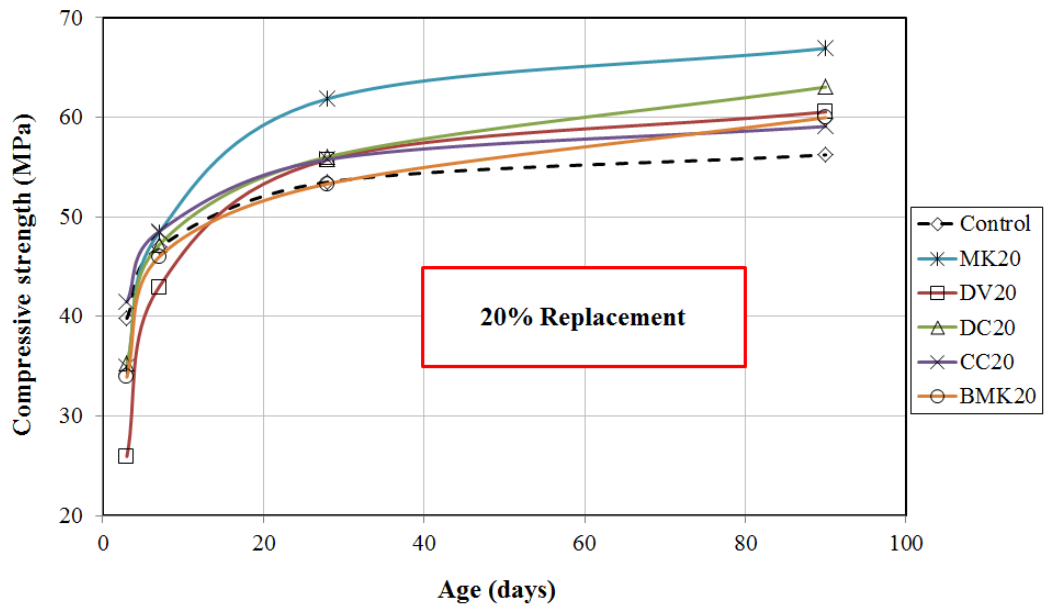
a)



b)

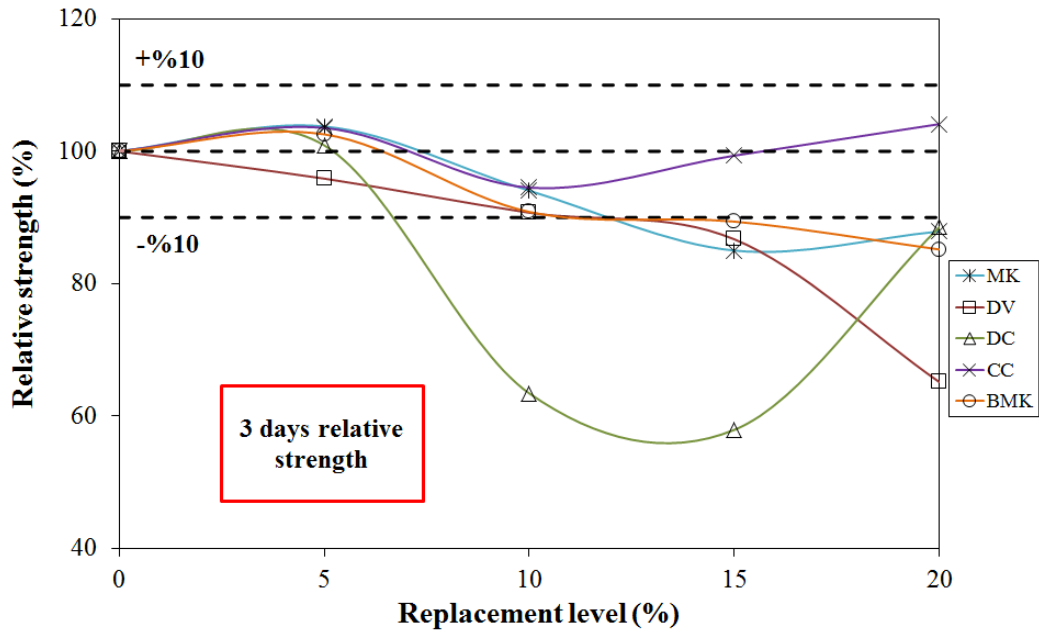


c)

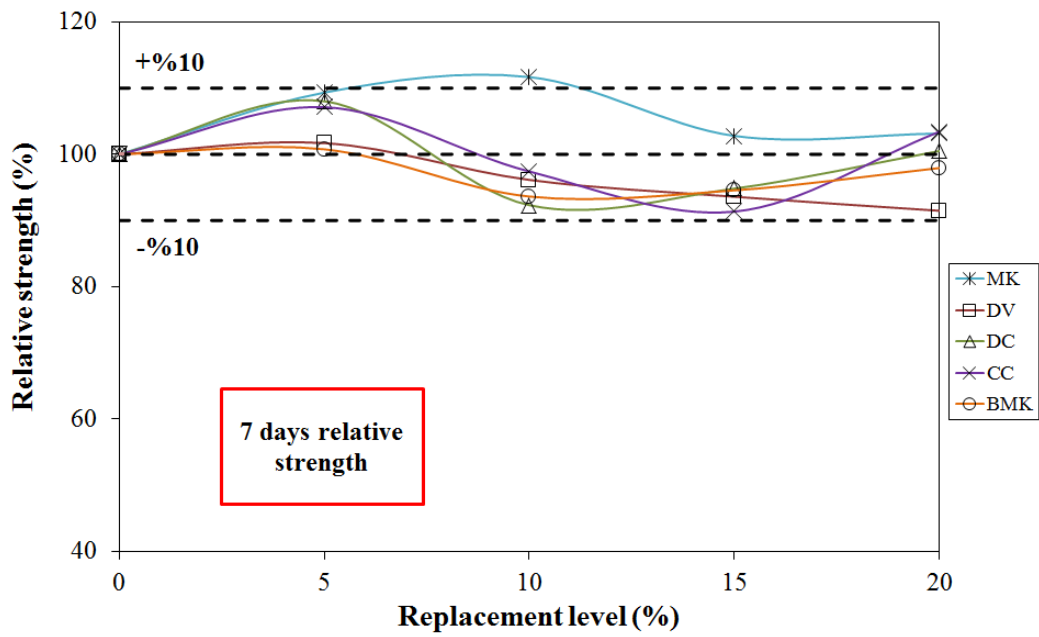


d)

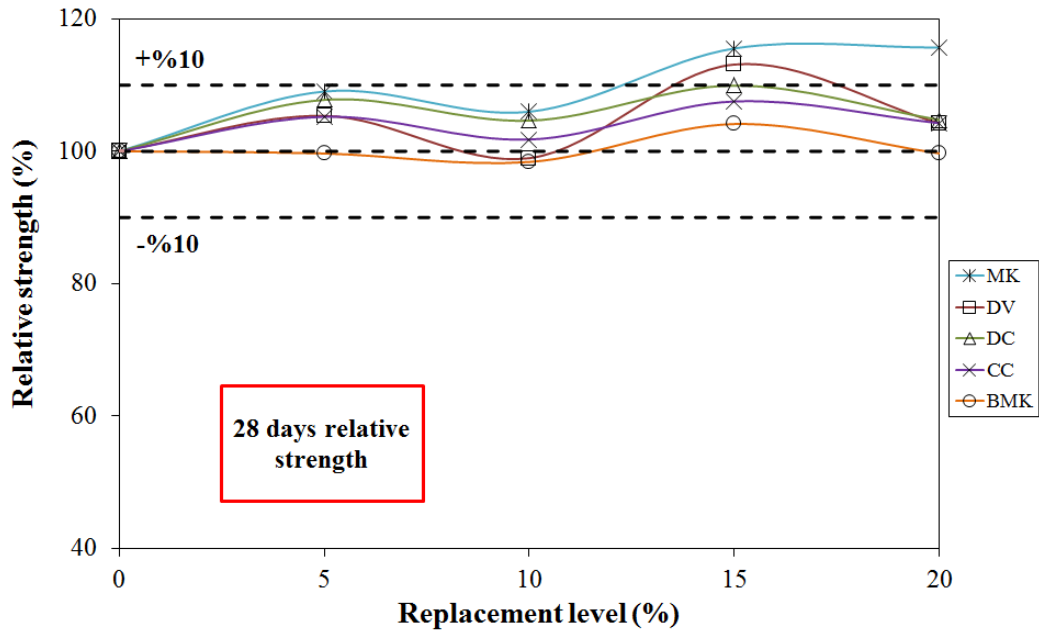
Figure 4.12 Compressive strength development of the concretes incorporating a) 5%, b) 10%, c) 15%, and d) 20% CK or MK.



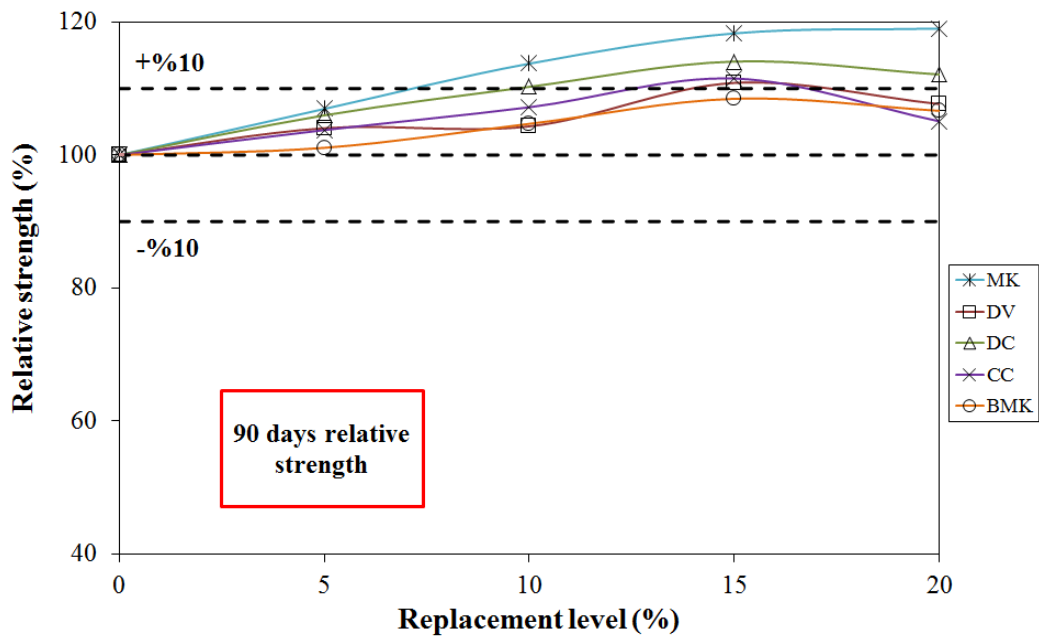
a)



b)



c)



d)

Figure 4.13 Effect of replacement level of MK or CKs on a) 3 days, b) 7 days, c) 28 days, and d) 90 days relative compressive strength of concretes.



#### 4.2.2 Splitting tensile strength

Splitting tensile strength values measured at 28 and 90 days were given in Table 4.5. The variations of these values were also graphically presented in Fig. 4.14. Moreover relative splitting tensile strength values were presented in Fig. 4.15. The lowest 28 and 90 day values were measured for control concrete as 3.20 and 3.40 MPa, respectively. However the maximum strength values were obtained for MK concretes at both ages as 4.28 and 4.68 MPa. It was found out that 15% replacement level provided best enhancement for MK and CK incorporated concretes. On the other hand at 90 days MK15 and MK20 had same splitting tensile strengths.

Based on the results obtained at 28 days the behavior of concretes in terms of splitting tensile strength with the increase of the replacement was similar for MK, DV, and BMK concretes. However, DC and CC incorporated concretes revealed a different trend for 10% replacement level (Fig. 4.14a). When observing, Fig 4.14b, it was found out that only BMK concretes had different tendency than the others; such that BMK20 concrete had almost same splitting tensile strength value as BMK15. Besides, when considering the overall splitting tensile strength variation, it can be determined that the influence of MK and CK on splitting tensile strength development of concretes somehow similar to that of compressive strength. For example, the highest strength gain in concrete was due to MK incorporation while the poorest was observed at BMK.

The number of studies regarding the tensile strength of concretes are very limited (Güneyisi et al., 2008; Kim et al., 2007; Siddique, 2008; Qian and Li, 2001) Qian and Li (2001) investigated 28 day direct tensile strength of concrete prisms incorporating 0, 5, 10, and 15% metakaolin as partial replacement of cement. The results showed that tensile strength of concrete increased systematically with increasing metakaolin replacement level. The average tensile strength increases were 7% (5% metakaolin), 16% (10% metakaolin), and 28% (15% metakaolin), and the average ultimate strain increases were 3% (5% metakaolin), 19% (10% metakaolin), and 27% (15% metakaolin).

Table 4.5 Splitting tensile strength (MPa) of the concretes

Mixtures	Replacement Level (%)	28 days	90 days
Control	0	3.20	3.40
	5	3.77	4.01
DV	10	3.93	4.20
	15	4.02	4.46
	20	3.68	4.55
	5	3.30	3.81
DC	10	3.26	4.04
	15	4.17	4.26
	20	3.66	4.03
	5	3.79	4.07
CC	10	3.22	4.18
	15	4.08	4.53
	20	3.50	4.16
	5	3.31	3.94
BMK	10	3.88	4.25
	15	3.81	3.96
	20	3.32	3.94
	5	3.94	4.14
MK	10	4.04	4.53
	15	4.28	4.68
	20	3.91	4.68
	5	3.94	4.14

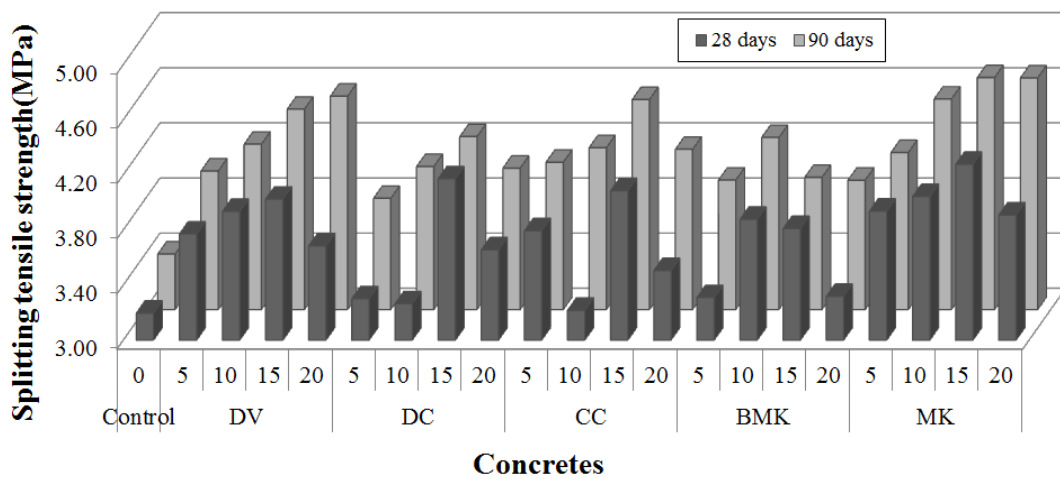
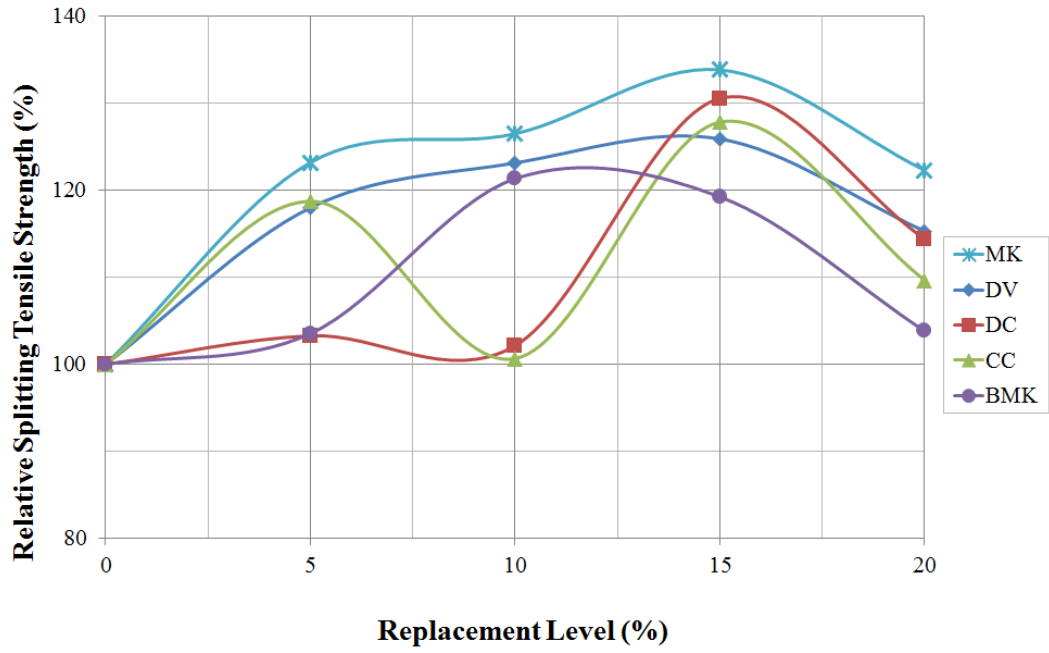


Figure 4.14 Splitting tensile strengths of the plain and mineral admixed concretes at 28 and 90 days



a)

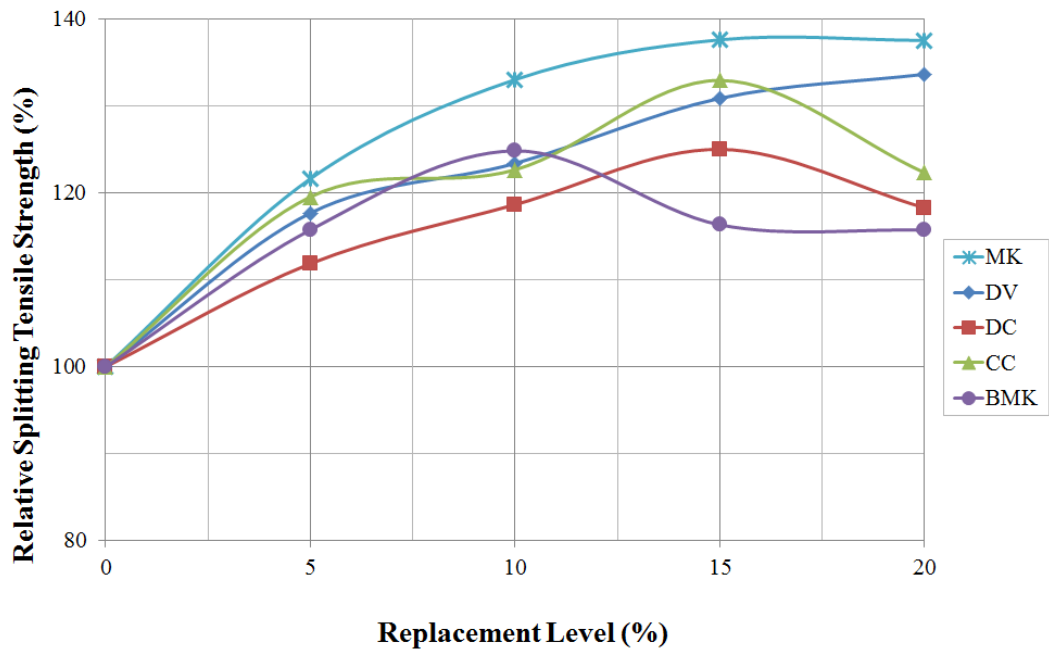


Figure 4.15 Effect of replacement level on splitting tensile strength of the concretes at a) 28 days, b) 90 days ( $F_{s,plain\ concrete} = 100\%$ )

### 4.3 Results on permeability and durability related properties of concretes

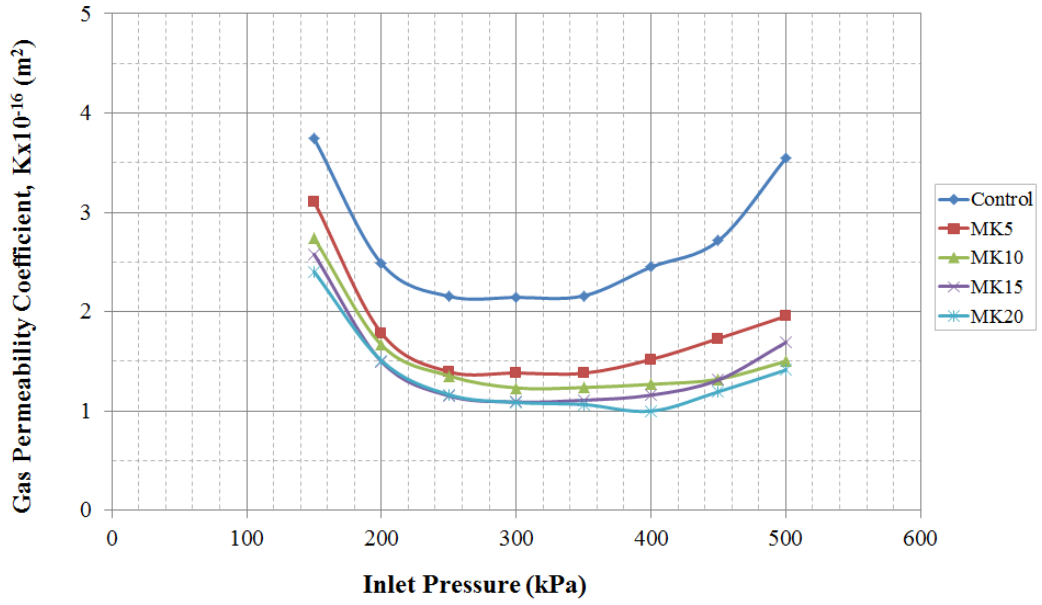
#### 4.3.1 Gas permeability

Variation of the apparent gas permeabilities of concrete with respect to the inlet pressure head ( $P_1$ ) from 150 to 500 kPa are given in Figs. 4.16 through 4.20 for the plain and mineral admixture incorporated concretes. It was observed from those figures that the gas permeability coefficient had a tendency to diminish sharply from 150 to 250 kPa 300 and then stayed stable up to 350 kPa being followed by an increase with a gentle slope up to 500 kPa, especially for MK included concretes. The gas permeability coefficient seemed to be strongly depended on the inclusion of MK and replacement the level. The gas permeability profiles drawn for 90 days showed more stability due to the enhancement in pore structure of the concretes.

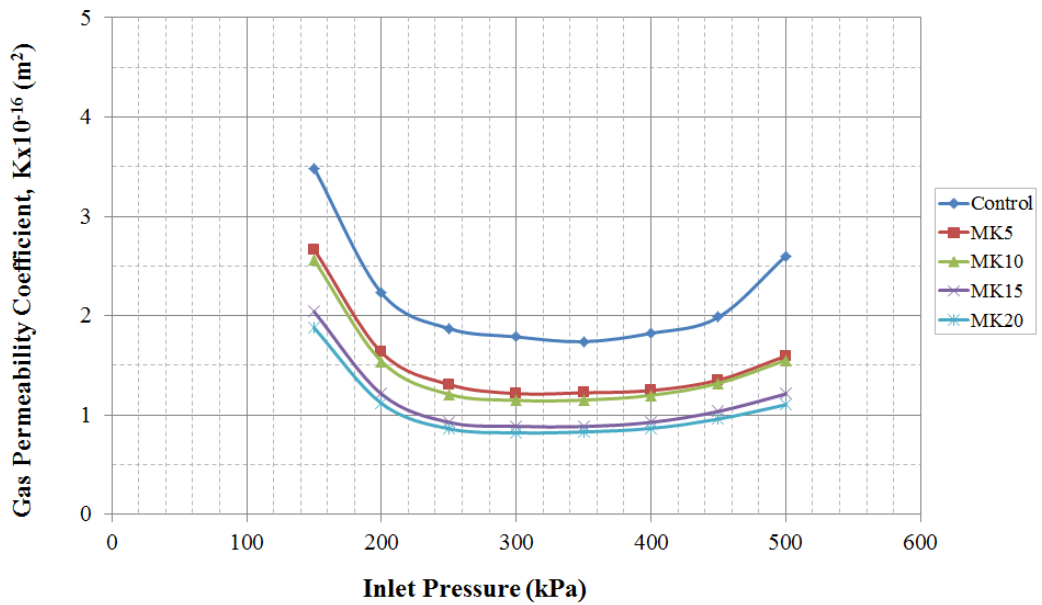
RILEM (1999) recommends using 150, 200, and 300 kPa inlet pressures for determining the average gas permeability coefficient. Therefore, the apparent gas permeability coefficients of the control and mineral admixed concretes measured at 28 and 90 days were determined accordingly and given in Table 4.6. Moreover, Figs. 4.21-4.22, graphically illustrate the variation of average gas coefficients of concretes cured for 28 and 90 days, respectively. The highest gas permeability coefficients ( $K$ ) at 28 and 90 days were measured at control concrete as  $2.78 \times 10^{-16} \text{ m}^2$  and  $2.50 \times 10^{-16} \text{ m}^2$ , respectively. Variation of the  $K$  values for MK and CK incorporated concretes were observed to range between  $1.27 \times 10^{-16}$ - $2.09 \times 10^{-16} \text{ m}^2$  and  $1.76 \times 10^{-16}$ - $2.69 \times 10^{-16} \text{ m}^2$ , respectively, depending mainly on the testing age. Increasing amount of CK or MK resulted in a systematic decrease in  $K$  values. All of the  $K$  values measured for CK incorporated concretes fell between control and MK incorporated concretes for all replacement levels. At 90 days, the concretes incorporating CK seemed to have a more consistent variation of the  $K$  values with the change in replacement level than  $K$  values of 28 days. For example, DC5 and DC10 had moderate and the highest  $K$  values when compared to 5% and 10% CK containing concretes, but DC15 and DC20 had the lowest  $K$  values when compared to others. However, when considering 90 days test results the concretes incorporating calcined DV kaolin had the lowest  $K$  values at all replacement levels. Therefore, it can be inferred from Fig. 4.22 that, of all CK incorporated concretes DV group revealed a close trend to MK

concretes at 90 days. The fluctuation of the K values in 28 days, on the other hand, may be due to the differences in fineness and chemical compositions of the CKs used. Although calcined DV and CC kaolins had similar chemical and mineralogical compositions, the concretes containing DV had lower K values at 90 days. This may be attributed to the pore size refinement of the concretes as a result of higher specific surface area ( $7340 \text{ cm}^2/\text{gr} > 4450 \text{ cm}^2/\text{gr}$ ). This is also more pronounced for the concretes including MK owing to its high degree of fineness and high reactivity resulting from high purity (kaolinite content >95%). However, it should be noticed that, although there are noticeable differences between plain and mineral admixed concretes, the fluctuations of the apparent gas permeability values among CK concretes may not be statistically different.

Enhanced gas permeability of concrete may have a critical significance when considering the industrial concretes to be used for long term underground nuclear waste storage structures (Chen et al., 2012). Chen et al. (2012) assessed the influence of concrete microstructure upon water retention and relative gas permeability via porosity measurements, analysis of the BET theory from water retention properties, and MIP. Finally, they proposed a single relative gas permeability curve for concretes they observed, based on Van Genuchten–Mualem's statistical model, to be used for continuous modelling approaches of concrete structures, both during drying and imbibition.

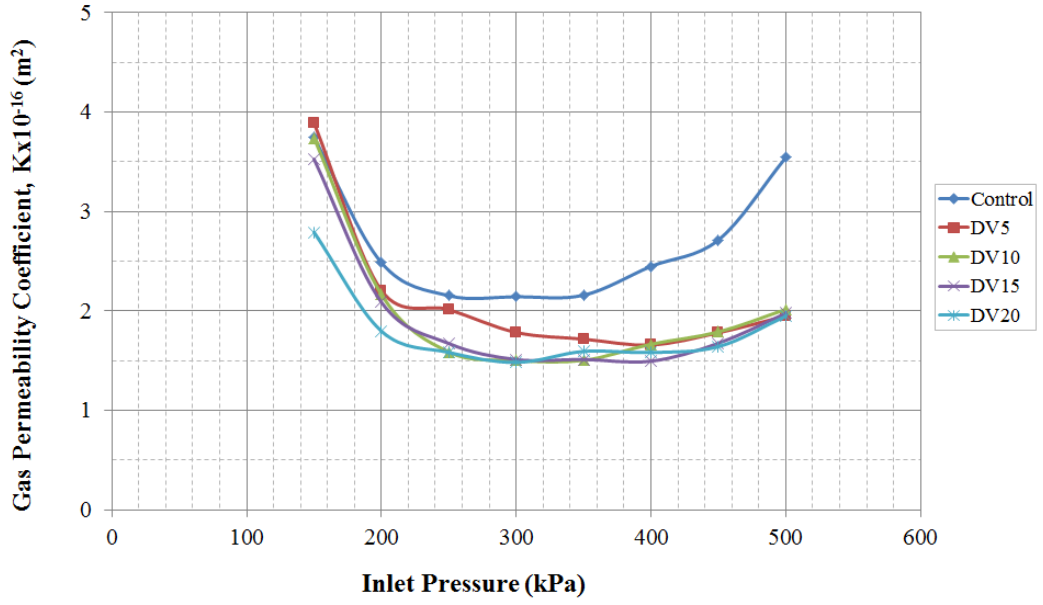


a)

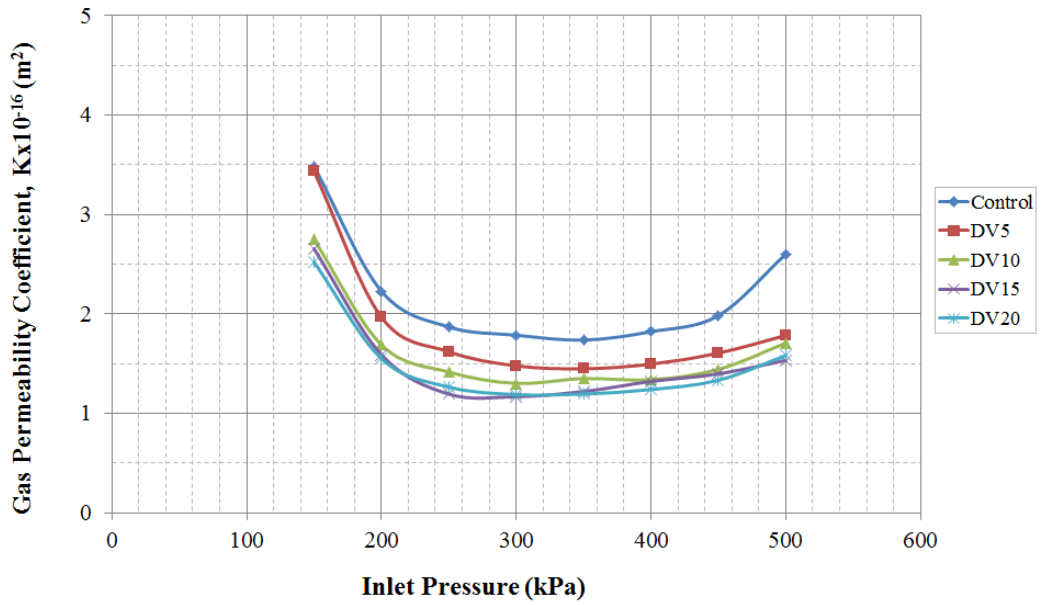


b)

Figure 4.16 Typical apparent gas permeability profile of control and MK incorporated concretes with inlet pressure: a) 28 days and b) 90 days

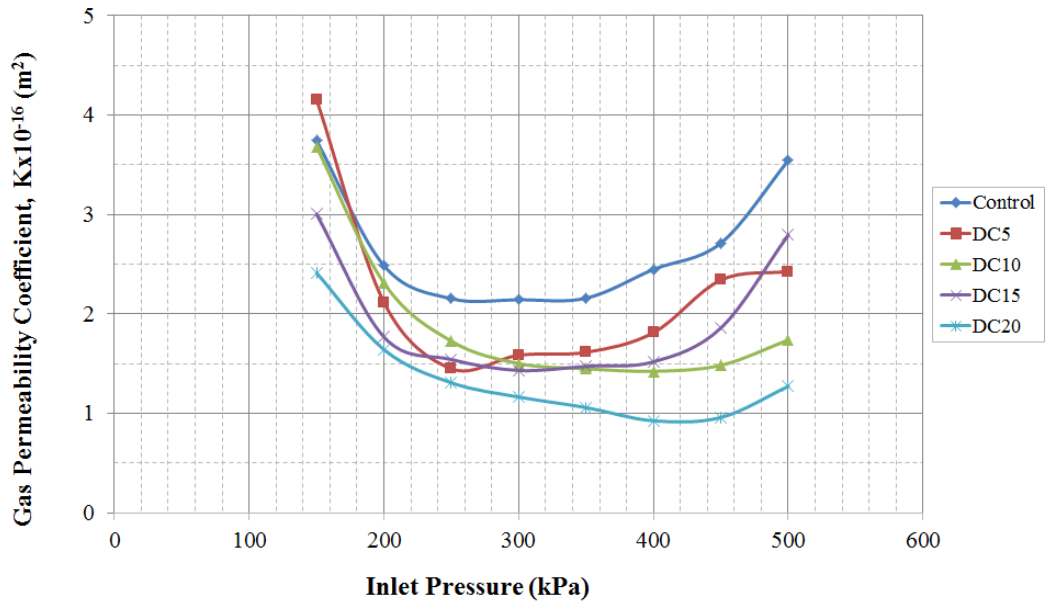


a)

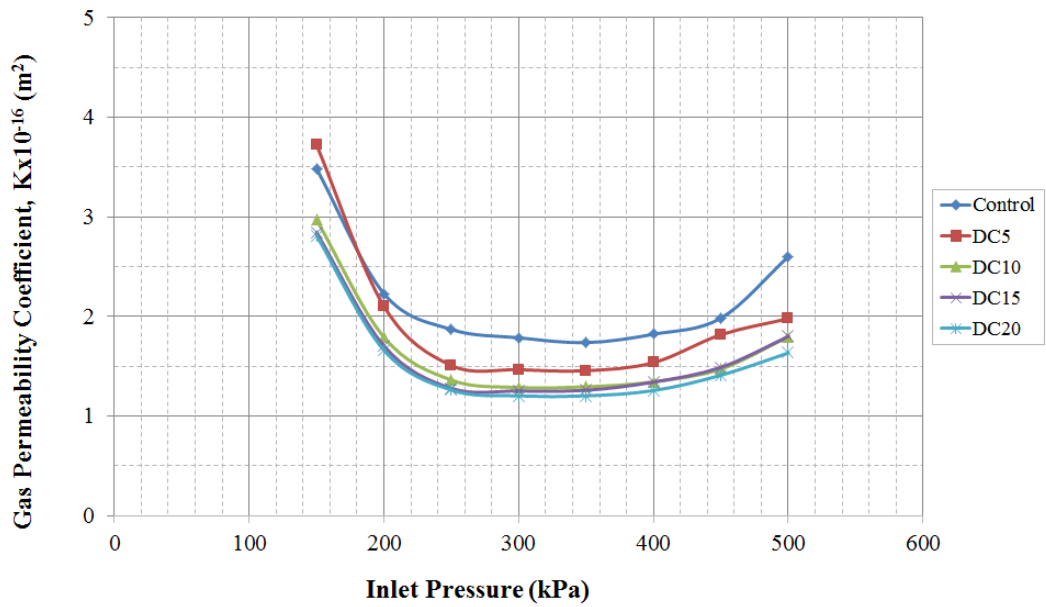


b)

Figure 4.17 Typical apparent gas permeability profile of control and calcined DV incorporated concretes with inlet pressure: a) 28 days and b) 90 days



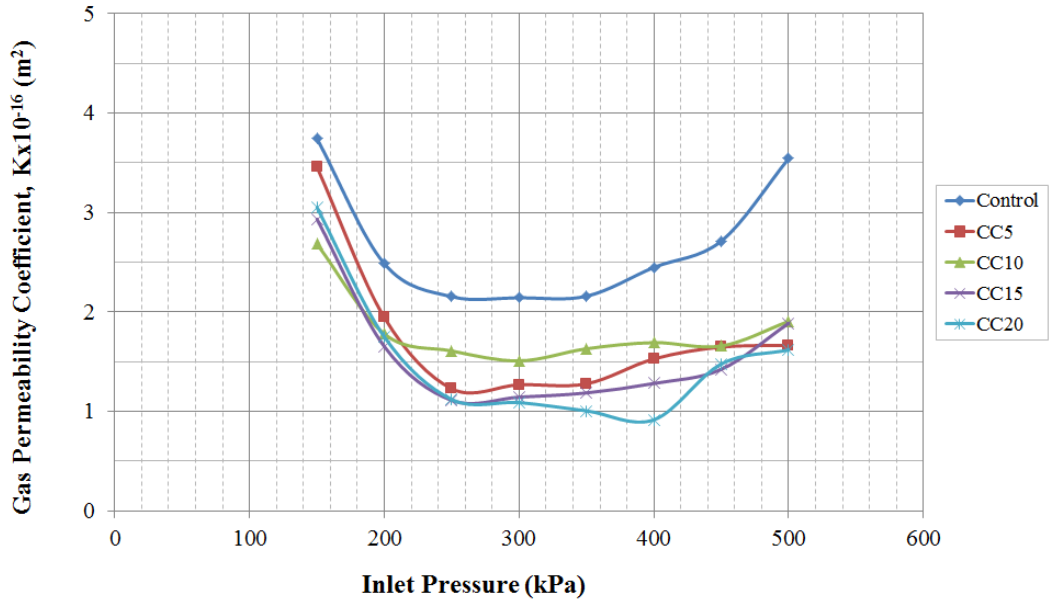
a)



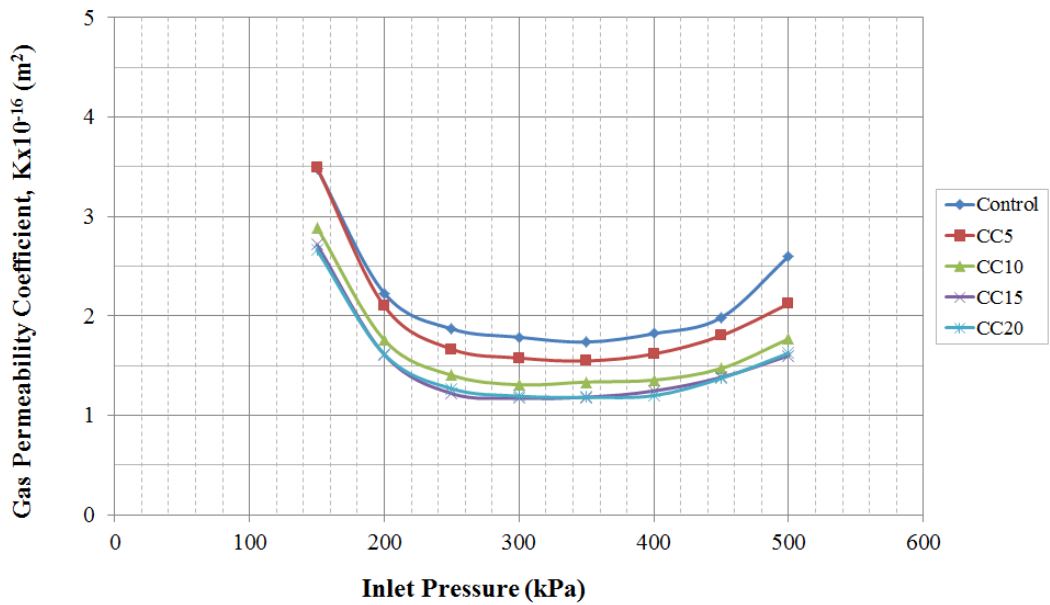
b)

Figure 4.18 Typical apparent gas permeability profile of control and calcined DC incorporated concretes with inlet pressure: a) 28 days and b) 90 days



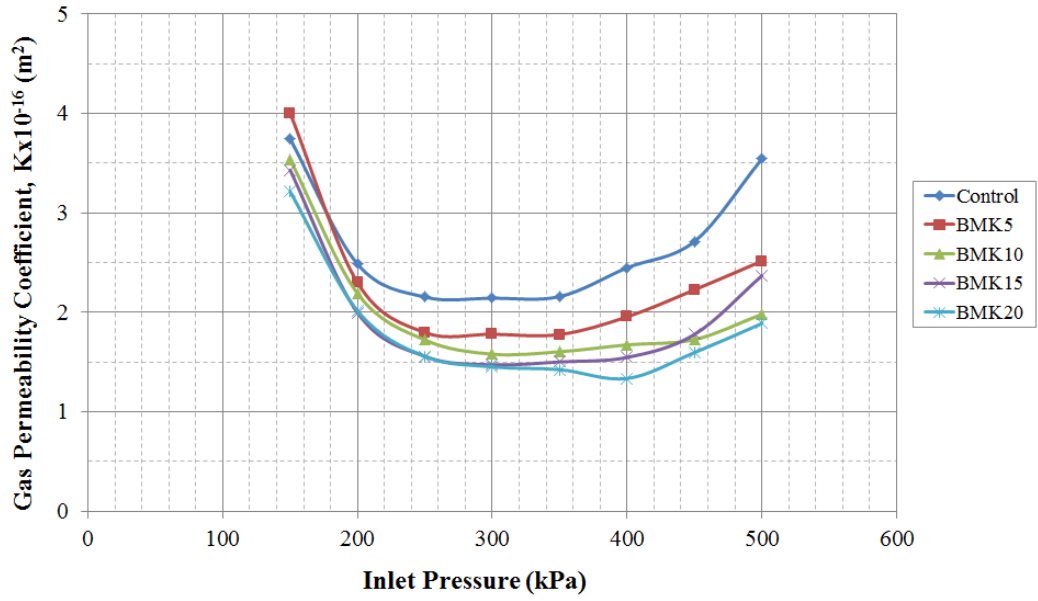


a)

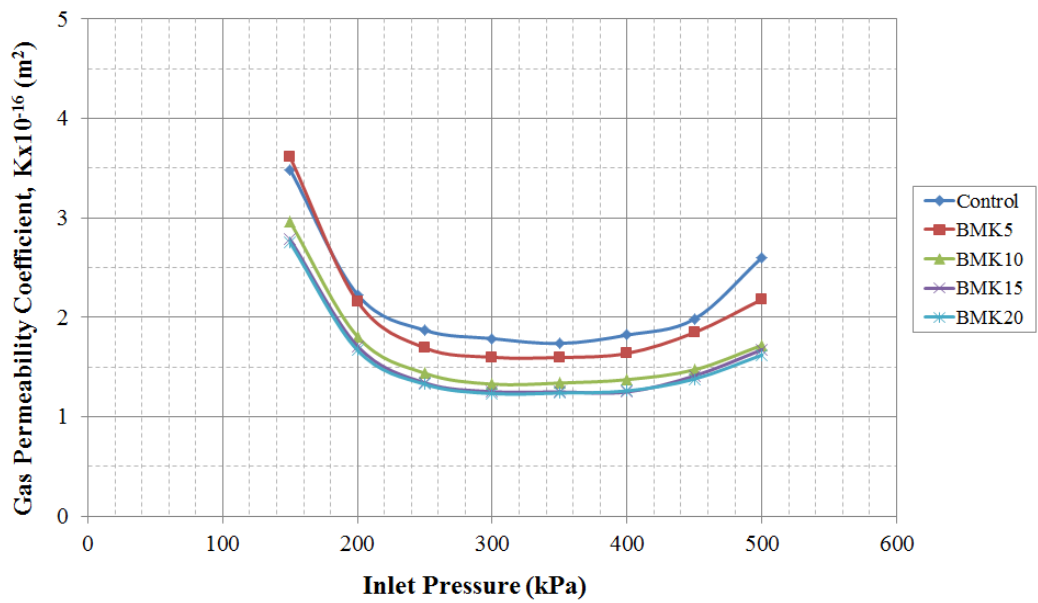


b)

Figure 4.19 Typical apparent gas permeability profile of control and calcined CC incorporated concretes with inlet pressure: a) 28 days and b) 90 days



a)



b)

Figure 4.20 Typical apparent gas permeability profile of control and calcined BMK incorporated concretes with inlet pressure: a) 28 days and b) 90 days

Table 4.6 Apparent gas permeability coefficients ( $\times 10^{-16} \text{ m}^2$ ) average of K values for 150, 200, and 300 kPa inlet pressures as recommended per RILEM (1999)

<b>Mixtures</b>	<b>Replacement level (%)</b>	<b>28 days</b>	<b>90 days</b>
<b>Control</b>	0	2.79	2.50
<b>DV</b>	5	2.63	2.29
	10	2.47	1.91
	15	2.38	1.81
	20	2.03	1.76
<b>DC</b>	5	2.62	2.43
	10	2.50	2.02
	15	2.07	1.93
	20	1.74	1.89
<b>CC</b>	5	2.22	2.39
	10	1.99	1.99
	15	1.91	1.84
	20	1.96	1.83
<b>BMK</b>	5	2.69	2.46
	10	2.44	2.03
	15	2.30	1.92
	20	2.23	1.89
<b>MK</b>	5	2.09	1.84
	10	1.88	1.75
	15	1.72	1.38
	20	1.67	1.27

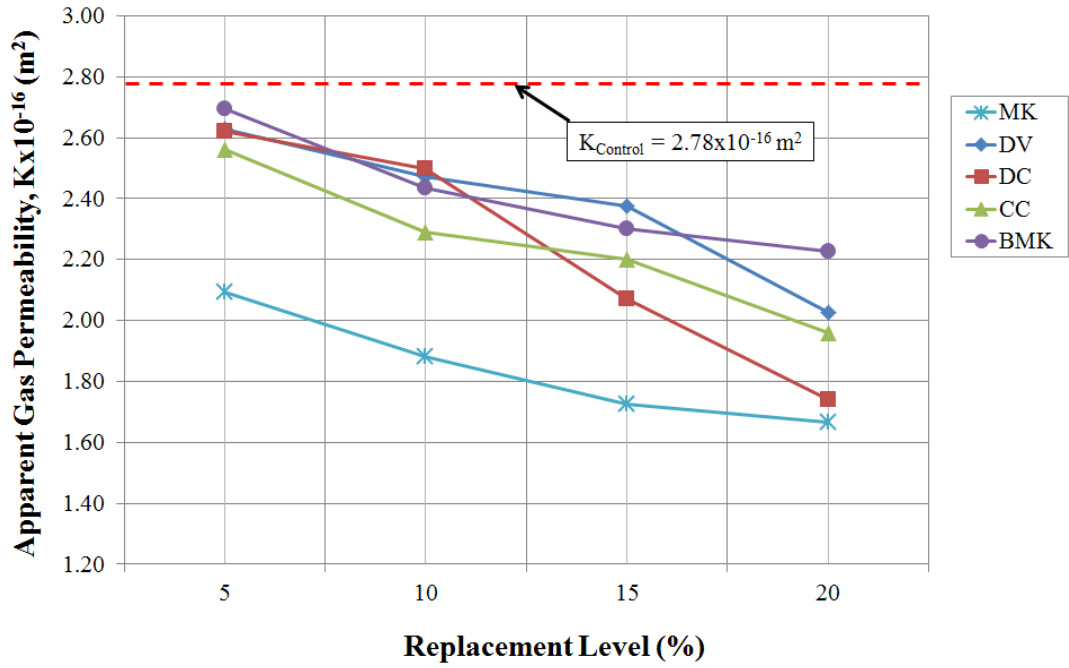


Figure 4.21 Variation of 28 day apparent gas permeability coefficients of the concretes with replacement level of CK and MK

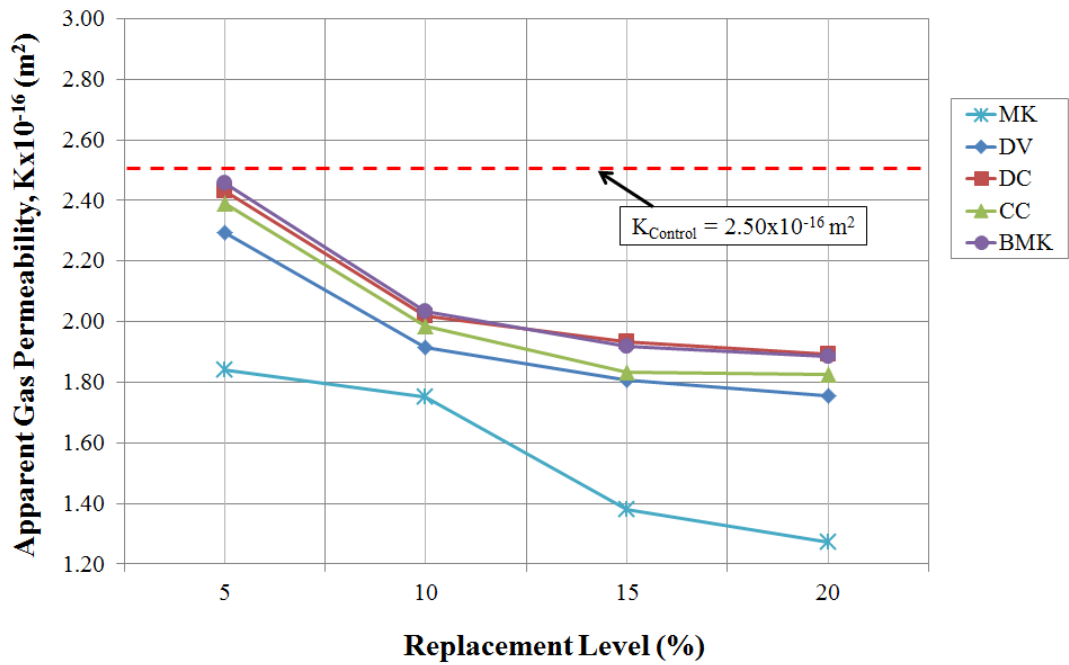


Figure 4.22 Variation of 90 day apparent gas permeability coefficients of the concretes with replacement level of CK and MK

### 4.3.2 Water permeability

Water permeability test represents the ease with which a fluid may flow throughout a permeable body as a result of differential pressure and measures the depth (D) of the water penetration of into the concrete. The variation in the water permeability of the concretes is given in Table 4.7 and graphically demonstrated in Fig. 4.23. Additionally, the relative changes in water penetration depths of the MK and CK modified concretes with respect to the plain control specimens are depicted in Fig. 4.24. Test results clearly demonstrated that substitution of the Portland cement with thermally treated kaolins considerably diminished the water permeability of the concretes, depending on the type of mineral admixture used and the replacement level. The highest penetration depths were measured for control concrete as 26.5 mm and 18.5 mm whereas the lowest penetration depths were measured for MK20 concrete as 10.8 mm and 7.8 mm at 28 and 90 days, respectively. Güneyisi et al. (2011) showed that up to 80% reduction in water permeability can be possible through utilization of binary, ternary, and quaternary blends of MK, FA, and GGBFS in concrete. They also reported that the results of the water permeability test displayed a similar pattern to that observed in the rapid chloride permeability test (RCPT). They observed the highest water permeability of 21 mm for the control concrete which has w/c ratio of 0.32 and cement content of 550 kg/m<sup>3</sup>.

Physicochemical properties of the CKs, substitution level of mineral admixture, and mix design parameters of the concretes affect the permeability behavior. Due to its high alunite content, the calcination process required for BMK kaolin can be different from the others. This may result in a poor pozzolanic property. As can be seen from Fig. 4.24a, the variation of the water penetration depth of the BMK containing concretes at 28 days was somehow different from the others. The results showed that there is improvement at all replacement levels except at 20%. Additionally, the highest reduction in penetration depth was achieved at 15% replacement level of BMK while 20% replacement provided the highest reduction for the others.

Due to formation of additional CSH gel as a result of pozzolanic reactions, the concretes including CK and MK illustrated better performance at later ages. The

results of the water permeability test indicated that the substantial reductions in water penetration depths were obtained at 90 days. Besides, the concretes containing CKs exhibited a comparable performance with MK modified concretes at 90 days. For example, the relative penetration depth for MK20 was reduced to 38.5% while 45.9%, 51.3%, 41.9%, and 68.9% were measured for DV20, DC20, CC20, and BMK20, respectively.

The water permeability test may also provide some information about the pore structure of the concrete, the continuity of the pores, and concrete's potential durability against the aggressive media. According to DIN 1048 (1991) and TS EN 12390/8 (2002) guidelines, concretes can be considered resistant to chemical attacks if the water penetration depth was less than 30 mm when in contact with aggressive media. Therefore, it can be inferred from the water permeability test results that all concretes examined in this study including control are resistant against aggressive chemicals.

The enhancement of the water permeability of concretes due to incorporation of various mineral admixtures has also been reported by previous researchers. Khatri et al. (1997) pointed out that the addition of silica fume to Portland cement (PC) significantly reduced the water permeability, and concretes produced with high slag blended cement had less permeability than those prepared with PC.

Table 4.7 Water penetration depths (mm) measured at 28 and 90 days

Mixtures	Replacement Level (%)	28 days	90 days
Control	0	26.5	18.5
DV	5	21.0	16.5
	10	15.8	13.5
	15	14.3	10.3
	20	12.0	8.5
DC	5	21.0	16.5
	10	23.0	13.6
	15	20.8	11.0
	20	16.5	9.5
CC	5	18.0	16.3
	10	17.0	13.8
	15	15.5	9.4
	20	12.5	7.8
BMK	5	22.5	16.8
	10	25.0	14.3
	15	20.5	13.3
	20	26.0	12.8
MK	5	18.5	13.0
	10	11.8	10.9
	15	13.3	8.0
	20	10.8	7.1

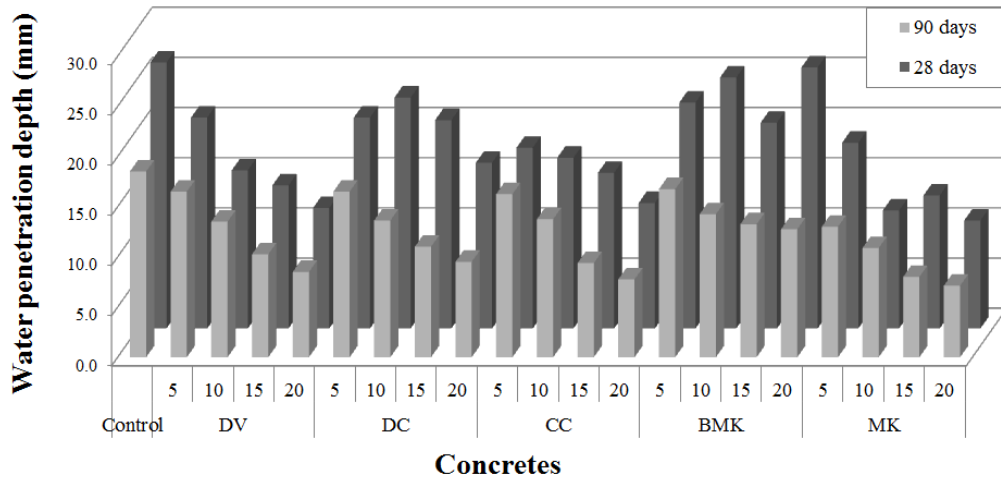
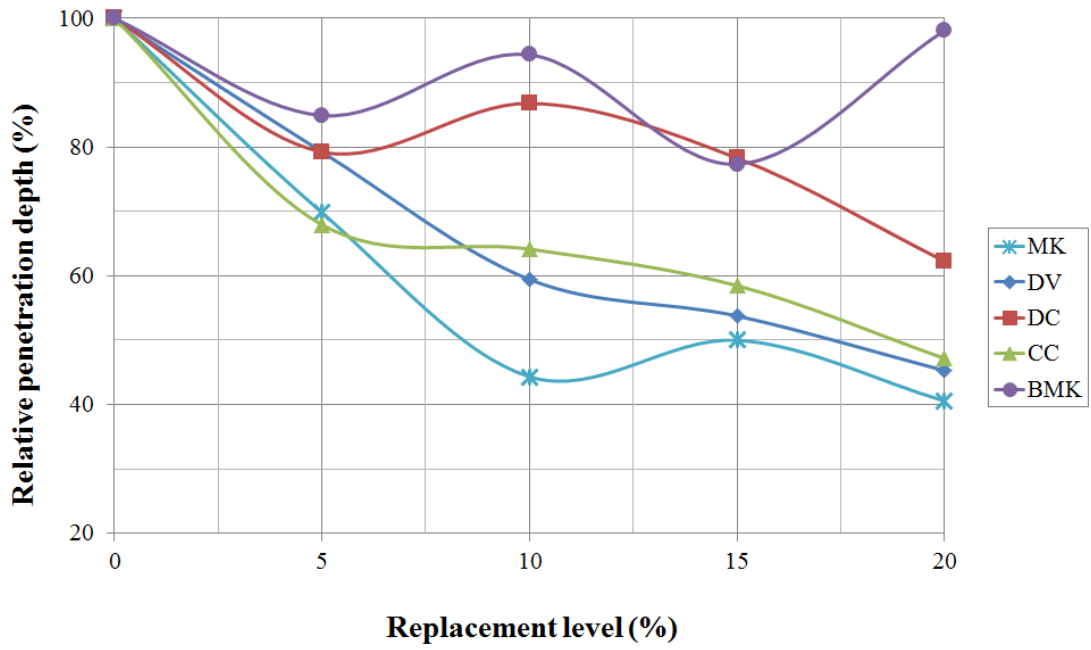
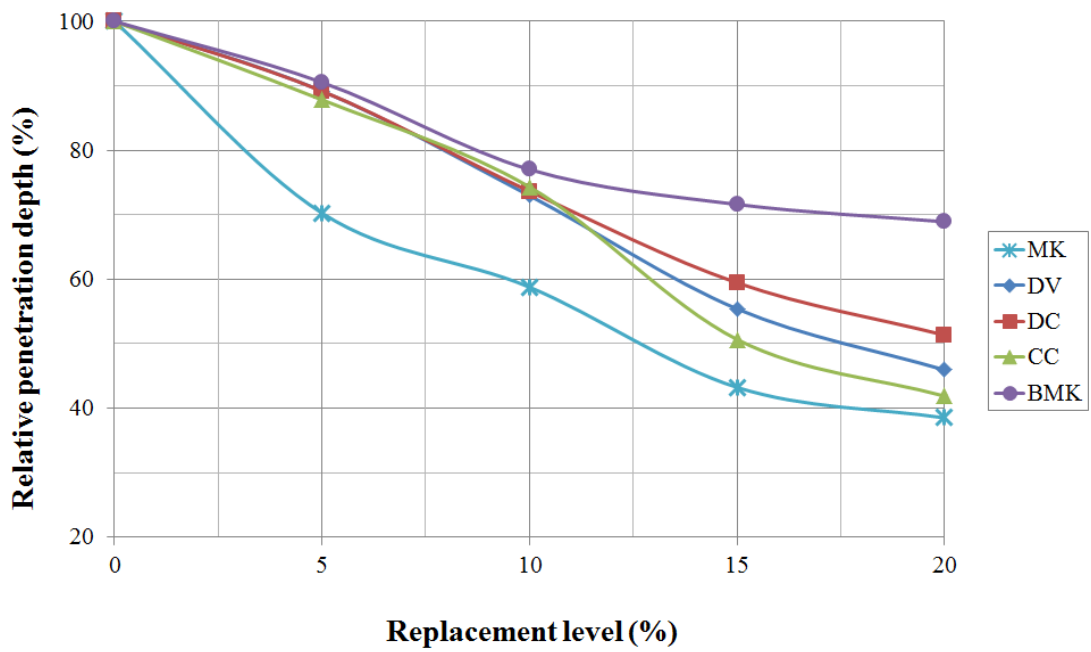


Figure 4.23 Water penetration depths of the plain and mineral admixed concretes at 28 and 90 days



a)



b)

Figure 4.24 Effect of replacement level on water penetration depth of the concretes at a) 28 days, b) 90 days (Penetration depth for Control concrete is 100%)



### 4.3.3 Water sorptivity

Being a relative measure of permeability, the water sorptivity test is based on the water flow into the concrete by capillary action. The relation used for calculation of sorptivity is given below (Eq. 4.1).

$$I = S\sqrt{t} \quad (4.1)$$

where  $S$  is sorptivity ( $\text{mm}/\text{min}^{1/2}$ ) and  $I$  is cumulative infiltration (mm) at time  $t$  (min)

The water sorptivity coefficients ( $S$ ) of the plain and thermally treated kaolin incorporating concretes are shown in Table 4.8 and Fig. 4.25. Fig. 4.26 demonstrates the variation of relative  $S$  values according to the replacement level of the concretes. Concretes containing MK revealed systematic decrease in  $S$  values by increasing replacement level at both ages. However, the trend was different for the CK modified ones. For instance, BMK containing concretes had higher 28 day  $S$  values at 15% and 20% replacement levels. The maximum 28 day sorptivity coefficient was observed at BMK20 concrete as  $0.123 \text{ mm}/\text{min}^{1/2}$ , while the lowest value was measured as  $0.0575 \text{ mm}/\text{min}^{1/2}$  for MK20 concrete. The concretes with 5% replacement level had almost same 28 day  $S$  values except BMK5 concrete. BMK5 had approximately the same  $S$  value ( $S_{\text{relative}}=98.7\%$ ) as the control concrete. As can be seen from Fig. 26a, among the CK incorporated concretes, only the CC concretes revealed a steady decrease at 28 day. Fig. 26b clearly showed that the enhancement of the sorptivity at 90 days was more regular than that of 28 days as the amount of the MK or CK increased. DV and CC incorporated concretes had almost same  $S$  values which were also very close to those of MK concretes, at that age. For example, 90 day relative  $S$  values were 64.3%, 61.8%, and 58.9% for the DV5, CC5, and MK5 concretes. On the other hand, despite having the highest fineness among four types of CKs, BMK was not as effective as the others. In the same line, although the fineness of MK varied between 2.4 to 4 times the CKs, the variation trend in  $S$  values of MK concretes was quite close to those having DV and CC. These findings point out that the contribution of the CKs on the sorptivity of the concretes at later

age is dominantly due to the chemical reactivity of the CKs or MK rather than their physical improvement due to fineness.

In the study of Khatib and Clay (2004), the water sorptivity characteristics of the MK-blended concrete was reported. They stated that the improvement effect of MK on reduction of the sorptivity was apparent even from the visual inspection at the end of the capillary absorption test. After the test ended, the water could be seen on the top surface of the samples for the control mixture. For the mixtures containing 15 and 20% MK, however, no water on the top surface was observed. This behavior was attributed to the discontinuity of pores (that is the pore-blocking effect) when cement was partially replaced with MK. Güneyisi and Mermerdaş (2007) produced concretes with 10% and 20% MK as well as the control. They applied two different curing type namely, water curing and air curing. They reported that the concretes modified with MK, especially at 20% replacement, showed far better performance than control. Moreover, for the fixed amount of MK (10% or 20%), the sorptivity enhancement of the water cured concretes was more pronounced than that of air cured ones for 28 and 90 days. This indicates that the concretes with MK have significant progressive hydration even at later ages.

Decreased sorptivity portrays a finer pore structure that would, for instance, restrain the ingress of aggressive elements into the pore system (Chan and Ji, 1998). Therefore, minimizing sorptivity is important in order to reduce the entry of chloride-containing or sulphate-containing water into concrete, which can cause serious deterioration (Chindaprasirt, 2007). Moreover, a decrease in total porosity can be associated with an increase in mechanical performance. For example, in the study of Menadi et al. (2009) it was reported that a good correlation ( $R^2 = 0.85$ ) was observed between the total porosity and the compressive strength.

Table 4.8 28 and 90 days sorptivity values (mm/min<sup>1/2</sup>) of concretes

Mixtures	Replacement Level (%)	28 days	90 days
Control	0	0.1047	0.0933
DV	5	0.0803	0.0600
	10	0.0676	0.0535
	15	0.0763	0.0480
	20	0.0827	0.0443
DC	5	0.0825	0.0690
	10	0.0863	0.0590
	15	0.0933	0.0497
	20	0.0795	0.0463
CC	5	0.0827	0.0577
	10	0.0767	0.0535
	15	0.0723	0.0490
	20	0.0626	0.0473
BMK	5	0.1033	0.0842
	10	0.0960	0.0763
	15	0.1203	0.0657
	20	0.1230	0.0653
MK	5	0.0838	0.0550
	10	0.0666	0.0516
	15	0.0591	0.0444
	20	0.0575	0.0428

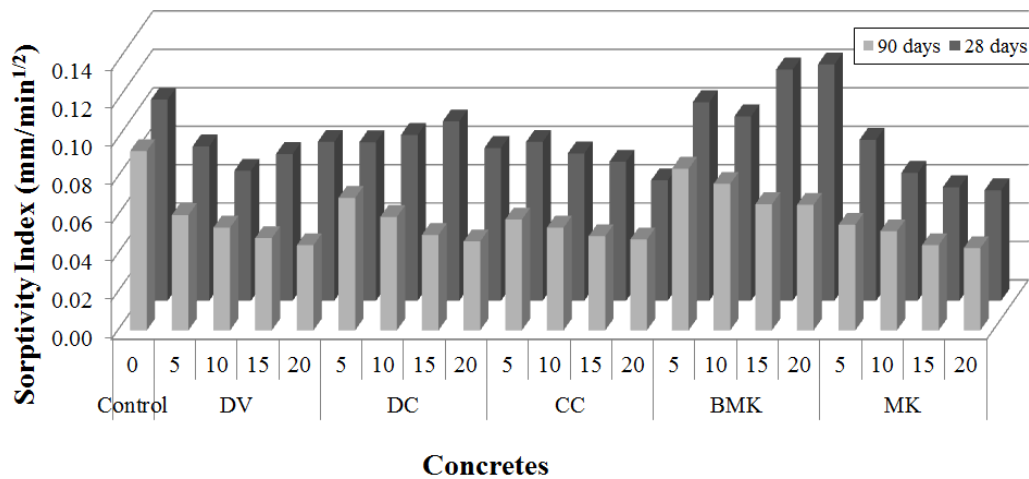
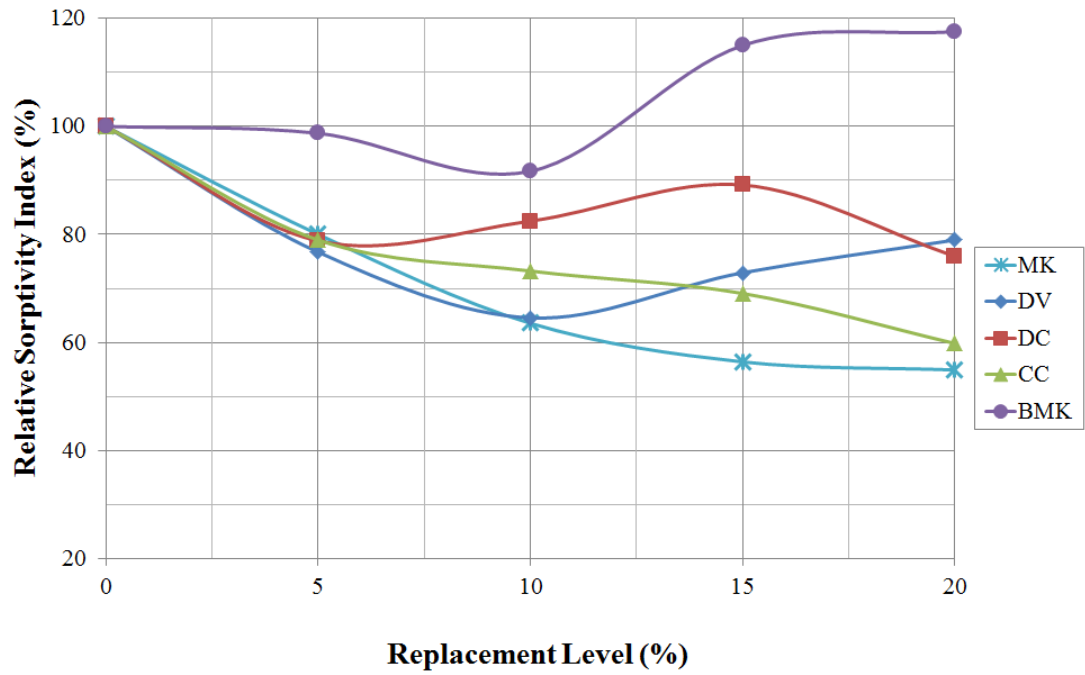
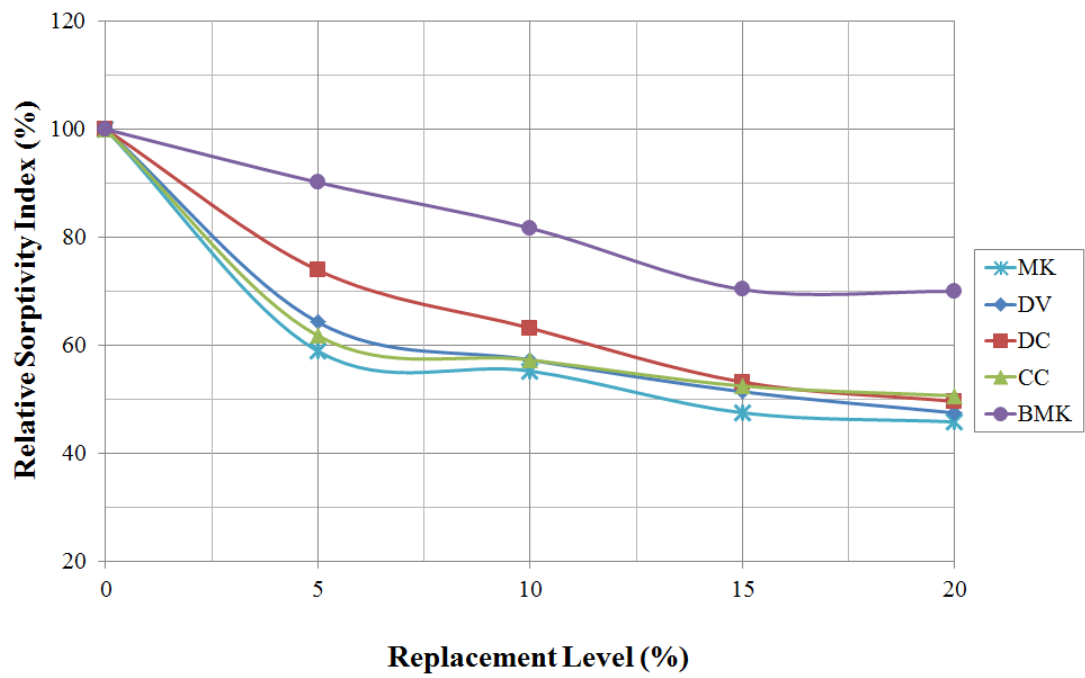


Figure 4.25 Water sorptivity test results of the plain and mineral admixed concretes at 28 and 90 days



a)



b)

Figure 4.26 Effect of replacement level on sorptivity indices of the concretes at a) 28 days and b) 90 days (Sorptivity index for control concrete is 100%)

#### 4.3.4 Rapid chloride penetration test

The resistance of the concretes against chloride ion penetration as a function of electro-migration was indicated in terms of the total charge passed (C). The variation of the C values with respect to the type of concrete was given Table 4.9 and graphically presented in Fig. 4.27. The change in the relative C values of the CK or MK incorporated concretes was also demonstrated in Fig. 4.28. Control concrete had the highest C values 2778 and 1989 Coulombs at 28 and 90 days, respectively. However, the C values measured for the concretes incorporated with thermally treated kaolin were in the ranges between 1009-1854 Coulombs and 657-1764 Coulombs, 28 and 90 days, respectively. The utilization of MK appeared to be the more effective in the reduction of chloride ion permeability than CKs, especially as when increasing MK content. Like the previous results presented above, the variation in 28 days test results of CK incorporated concretes was somewhat irregular when compared to those of 90 days. Nonetheless, the effectiveness of MK was observed to be persistent at both ages. For example, increasing the replacement level from 15% to 20% caused increase in C values of DC, CC, and BMK concretes at 28 days, whereas the increase was observed at 90 days for these concretes. However, MK incorporated ones steadily decreased at both ages. Besides, the CK addition to the concretes was proved to be effective in diminishing C values of the concretes. For example, 15% replacement resulted in the drop of C values between 48-68% at 90 days. This remarks that the utilization of CK can be as effective as MK in protecting the concretes against chloride attacks.

The results presented herein are consistent with the findings of previous researches. Zhang and Malhotra (1995) states that the resistance of MK concrete to chloride ion penetration was significantly higher than the control concrete when considering the durability aspects. Kostuch et al. (1993) studied the influence of MK on the microstructure and diffusion properties of mortar. They reported that the mean pore size was meaningfully decreased when the cement was substituted with 20% MK. It was also established that MK appeared to be efficient in the reduction of the rate of diffusion of  $\text{Cl}^-$  and  $\text{Na}^+$  ions in mortar.

Table 4.9 Total charge values (Coulombs) measured at 28 and 90 days

Mixtures	Replacement Level (%)	28 days	90 days
<b>Control</b>	0	2778	1989
	5	1678	1431
<b>DV</b>	10	1744	1334
	15	1473	969
	20	1115	835
	5	1680	1513
<b>DC</b>	10	1403	1168
	15	1277	1176
	20	1498	985
	5	1604	1376
<b>CC</b>	10	1454	1050
	15	1319	1035
	20	1345	1100
	5	1854	1764
<b>BMK</b>	10	1619	1519
	15	1373	1360
	20	1776	1213
	5	1327	1066
<b>MK</b>	10	1248	910
	15	1082	771
	20	1009	657

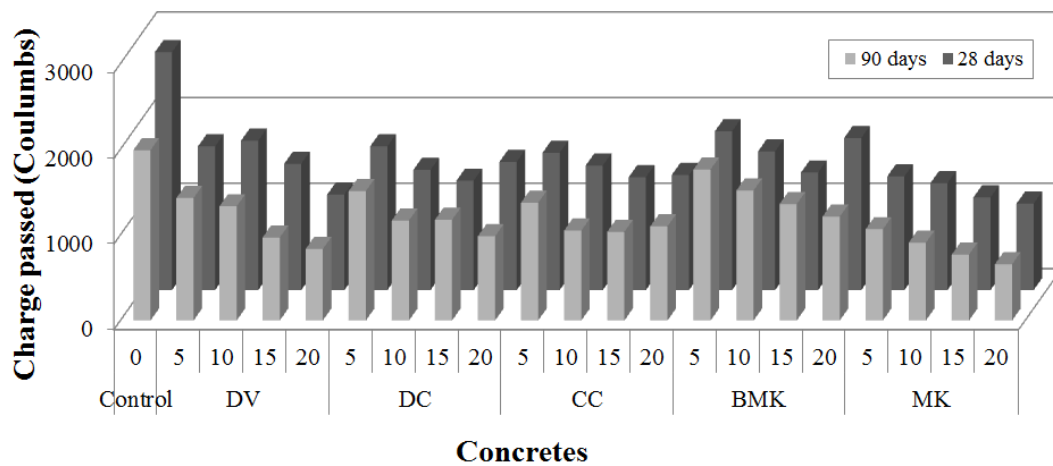
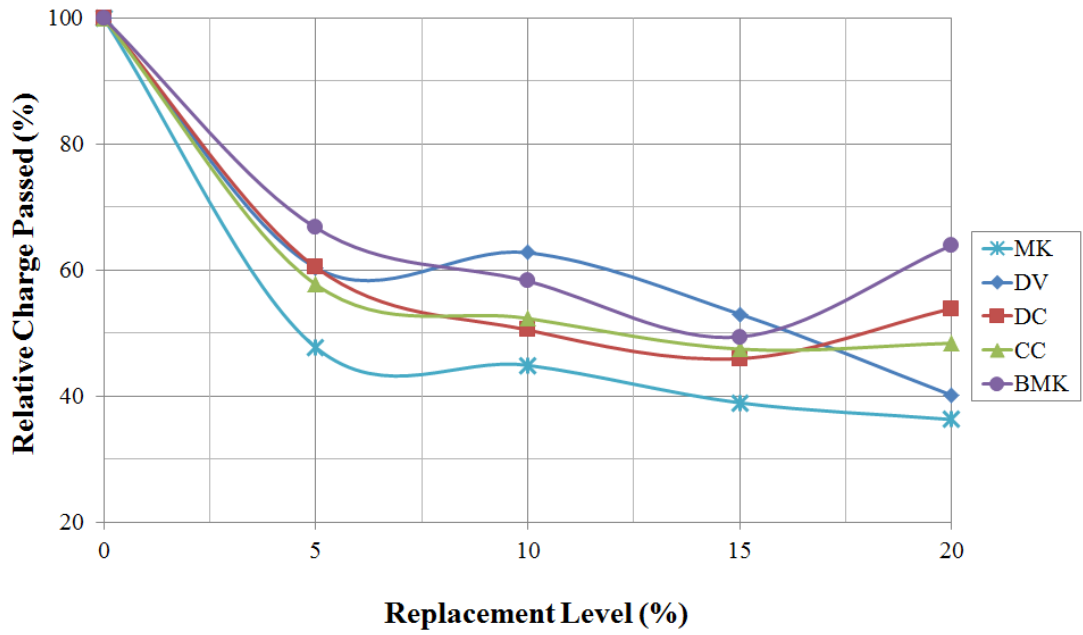
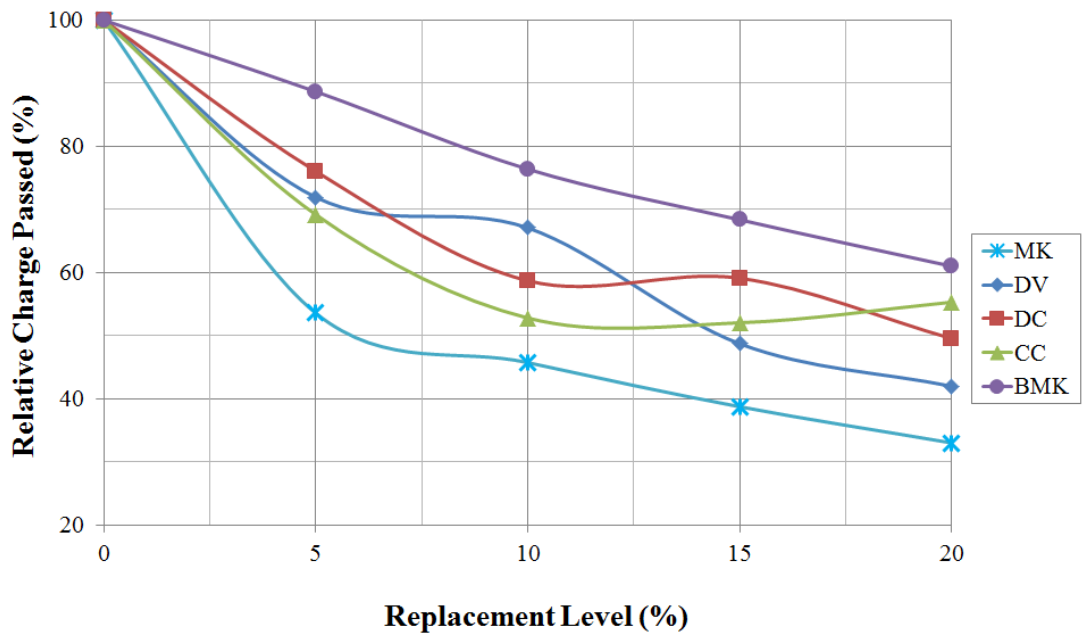


Figure 4.27 RCPT test results of the plain and mineral admixed concretes at 28 and 90 days



a)



b)

Figure 4.28 Effect of replacement level on chloride resistance of the concretes at a) 28 days and b) 90 days (Charge passed for control concrete is 100%)

#### 4.3.5 Electrical resistivity

The electrical resistivity of concrete can be considered as an important component of reinforcing steel corrosion cells, as high resistivity of the concrete leads decrease in corrosion currents, and thus slowing down the rate of corrosion. The surface electrical resistance of the concretes ( $R$ ) for control and thermally activated kaolin incorporated concretes were measured at the end of 28 and 90 days. The results were presented in Table 4.10 and Fig. 4.29. The variations in the relative  $R$  values of the CK or MK incorporating concretes were also demonstrated in Fig. 4.30 for both 28 days and 90 days.

It was observed that there is a systematic increase in  $R$  values as the replacement level increased at both ages. The lowest and highest 28 day  $R$  values were measured as 6.5 kohm.cm and 15.9 kohm.cm for BMK5 and MK20 concretes, respectively. However, 9.4 kohm.cm for the former and 25.8 kohm.cm for the latter was measured at 90 days. The variation can also more clearly be observed from Fig. 4.30. The results obtained for 28 days revealed that, the trend in variation of  $R$  was uniform for CK incorporated concretes. However at 90 days there were slight fluctuation in  $R$  values BMK5 concrete had 78% and 89% relative  $R$  values compared to control concrete at 28 and 90 days, respectively. the most significant change was observed at MK including concretes especially at 90 days. Calcined DV kaolin incorporated concretes showed the best performance at 10 and 15% replacement levels at 90 days compared to other CK incorporated concretes. At both ages, 20% replacement generally provided the maximum  $R$  values (the exemption is the result for DV20 at 90 day).

CEB-192 (Comite Euro-International du Beton) proposes that the likely corrosion rate is negligible for concrete with resistivity higher than 200  $\Omega$ .m (20 kohm.cm), low for resistivity values in the range of 100 to 200  $\Omega$ .m (10 to 20 kohm.cm), high for resistivity values in the range of 50 to 100  $\Omega$ .m (5 to 10 kohm.cm), and very high for concrete with resistivity lower than 50  $\Omega$ .m (5 kohm.cm) (Mehta, 1997).

Electrical resistivity of concrete represents moving ions (such as chloride ions) in pore solution. Concrete resistivity is dependent on both the microstructural properties



of the concrete and the conductivity of the pore solution (Ramezaniapour and Jovein, 2012). The conductivity feature of the concrete is mainly controlled by the chemical characteristics of the pore solutions, although also influenced by the pore structure of the concrete (Krieg, 2008). It can specially be used on concretes when a large portion of their cementitious chemical reactions have been completed such as those concretes made with silica fume or metakaolin (Ramezaniapour et al., 2011). MK also provides a denser structure to concrete by microfilling and secondary pozzolanic reactions (Wild et al., 1996; Poon et al., 2006). Güneyisi et al. (2005) stated that the increase in the electrical resistivity with strength of concrete was mainly due to the denser microstructure of concrete.

Table 4.10 Electrical resistivity values (Kohm.cm) of the concretes at 28 and 90 days

<b>Mixtures</b>	<b>Replacement Level (%)</b>	<b>28 days</b>	<b>90 days</b>
<b>Control</b>	0	8.4	10.5
<b>DV</b>	5	10.0	11.0
	10	10.6	12.5
	15	12.3	17.8
	20	15.3	16.7
<b>DC</b>	5	8.7	12.7
	10	10.2	11.8
	15	11.9	18.5
	20	15.5	19.3
<b>CC</b>	5	8.9	11.9
	10	9.2	18.1
	15	10.1	18.6
	20	14.0	19.4
<b>BMK</b>	5	6.5	9.4
	10	7.8	13.3
	15	9.9	13.1
	20	11.3	16.3
<b>MK</b>	5	10.4	16.8
	10	12.4	21.2
	15	15.2	23.8
	20	15.9	25.8

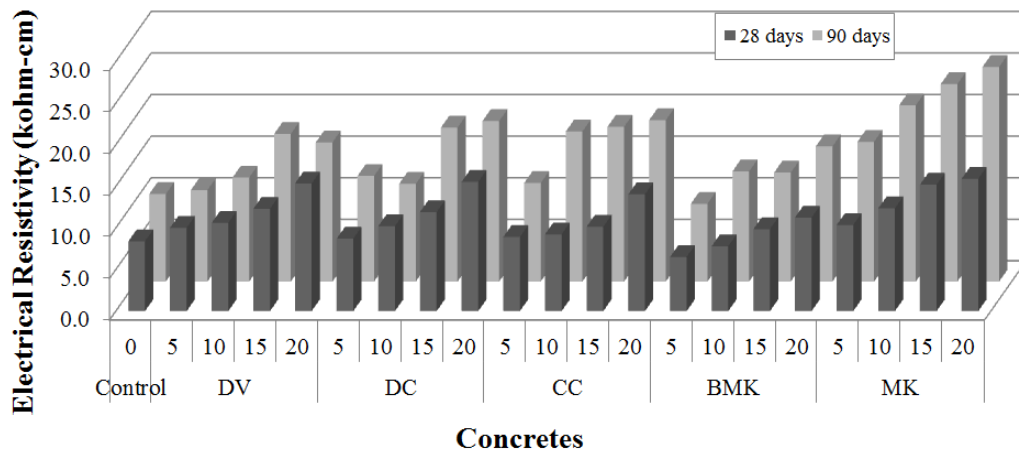
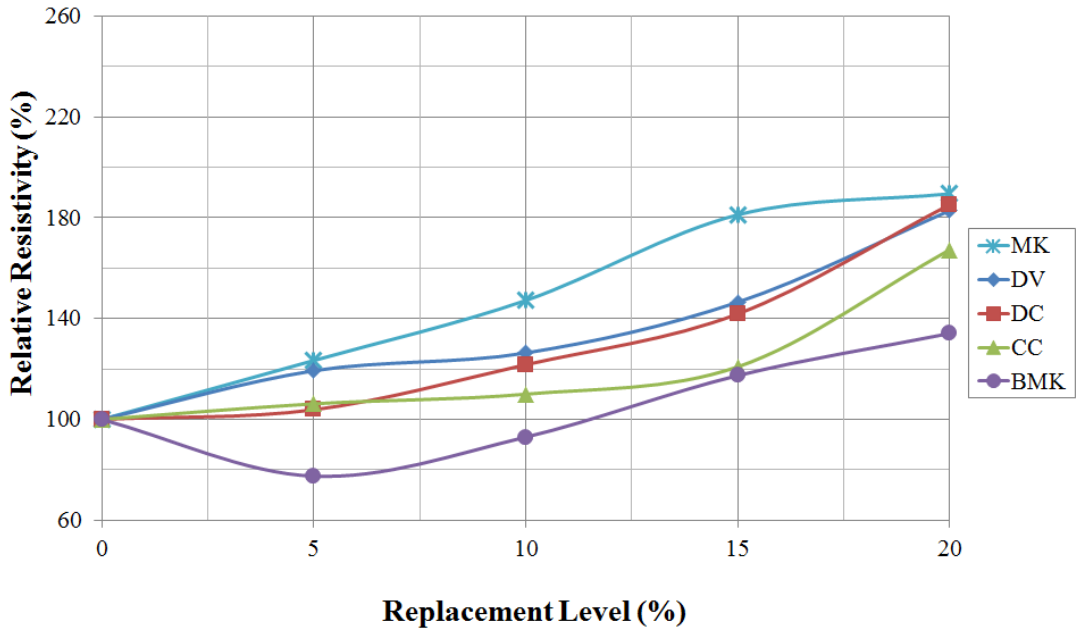
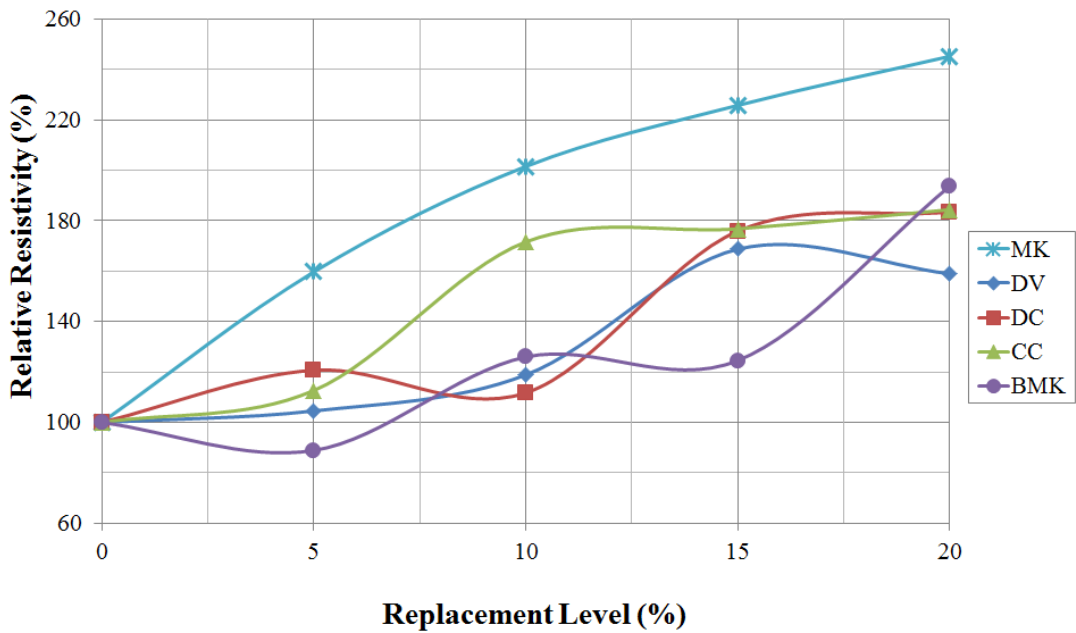


Figure 4.29 Electrical resistivity test results of the plain and mineral admixed concretes at 28 and 90 days



a)



b)

Figure 4.30 Effect of replacement level on electrical resistivity of the concretes at a) 28 days and b) 90 days (Electrical resistivity for control concrete is 100%)

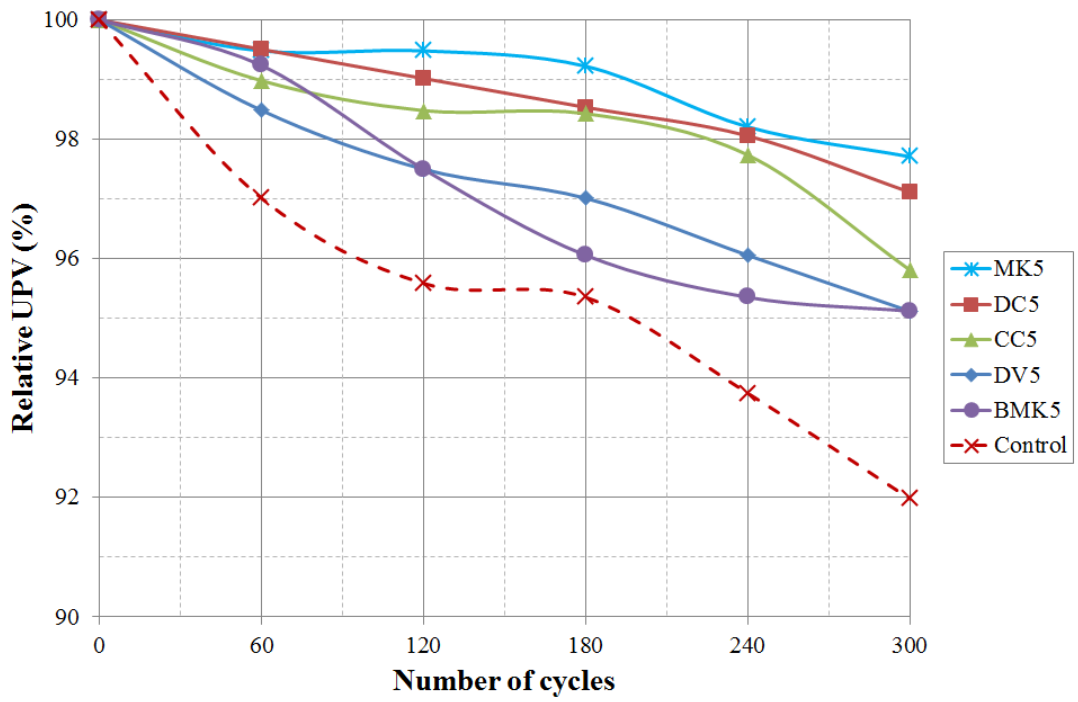
#### 4.3.6 Freezing and thawing

Freezing and thawing resistances of the concretes were monitored through change in UPV values (Fig. 4.31) and strength reductions (Fig. 4.32). Fig. 4.33 illustrates the

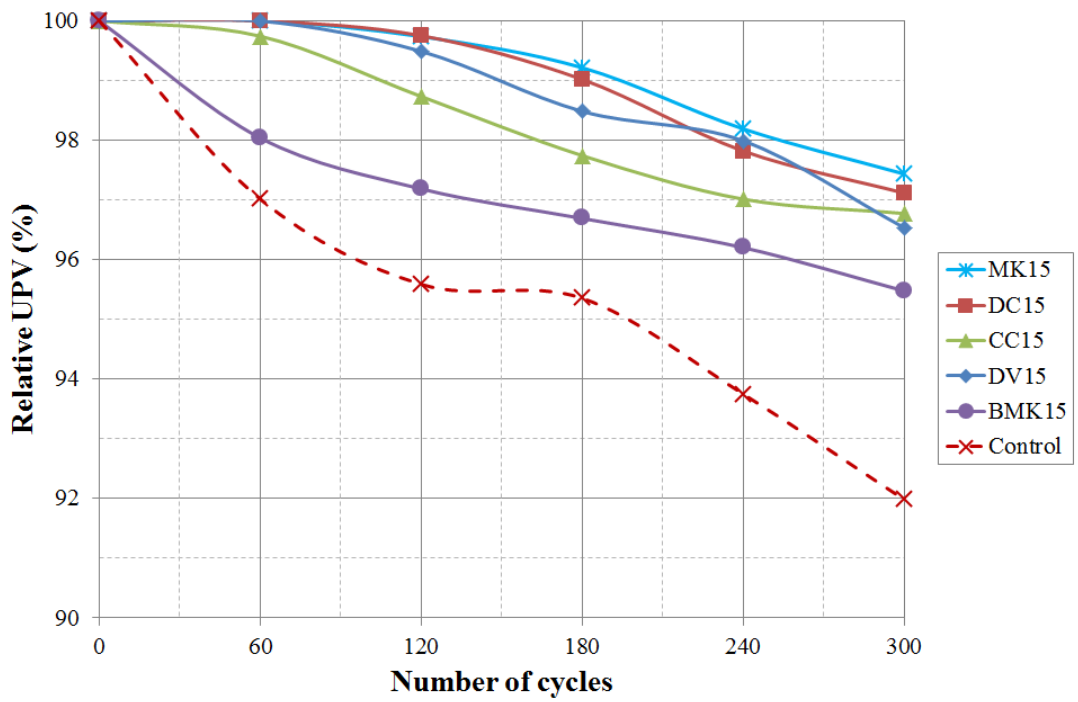
relative flexural strengths of the undamaged and damaged concretes in comparison to control concrete. In the same manner the relative compressive strengths of the undamaged and damaged concretes were also presented in Fig. 4.34. The maximum decrease in UPV values were observed for control concrete as 8%. However no significant change was observed for MK or CK incorporated concretes. The ranges of reduction were 2.30-4.90% for 5% replacement level while 2.5-4.5% for 15% replacement level depending on type of mineral admixture. On the other hand serious reductions in flexural strength (Fig 4.32a) were measured for the concretes. For example control concrete lost about 47% of its flexural strength while the losses for MK or CK incorporated concretes were ranged between 29-46% mainly depending on the replacement level. Although, concretes underwent great reduction in flexural strength, the change in compressive strength was not as high as flexural strength. The highest reduction was observed at control as 12.53% while the lowest was 2.06% for MK15. Utilizing 15% CK was seemed to be effective for providing resistance to concrete against freezing and thawing. Especially DV15 concrete appeared to be best among CK incorporated ones, since it demonstrated similar behavior as MK concrete.

Critical observation of Figs 4.33 and 4.34 indicated that the inclusion of MK and CK played an important role in inhibiting the deterioration of mechanical properties. For example 7-40% higher flexural strength was measured in undamaged CK or MK incorporated concretes, while this difference was observed to be 31-88% in damaged concrete.

Similar conclusion was presented by Hassan et al. (2012) They reported that the incorporation of MK to SCC mixtures enhances resistance to freezing and thawing. As the percentage of MK increased, resistance was also increased as well. The best performance was obtained at replacement level of 20%. They also stated that freezing and thawing resistance was higher with MK than SF at the same level of addition.

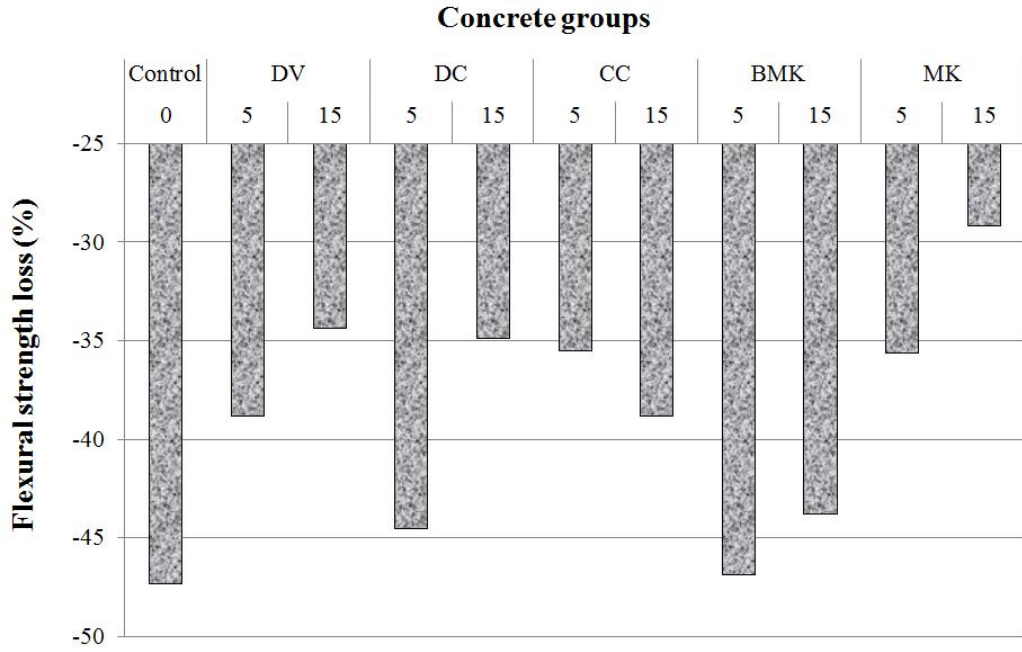


a)

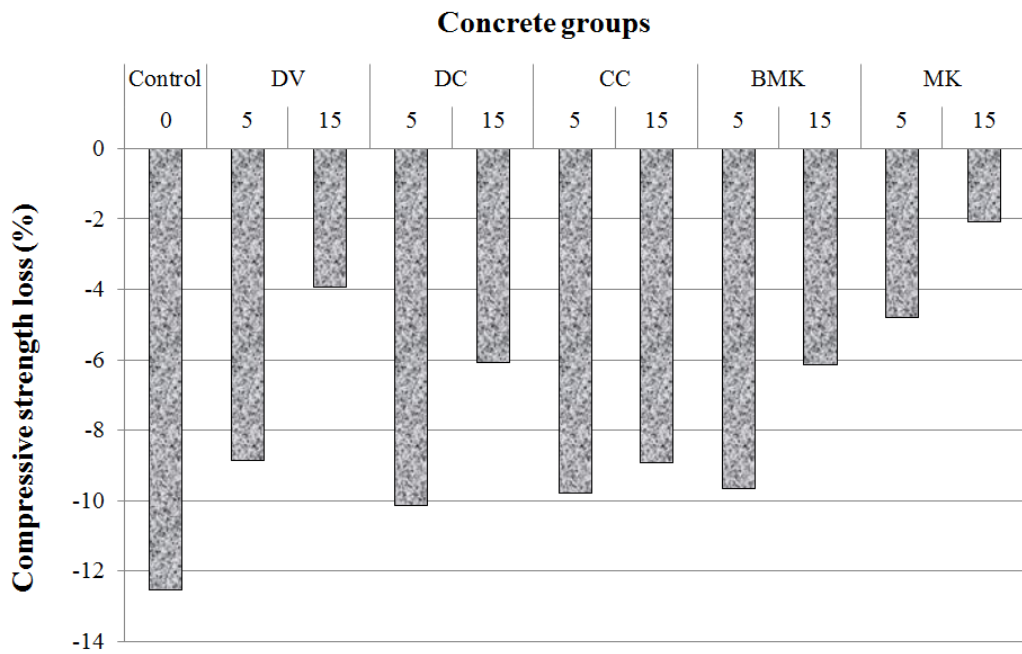


b)

Figure 4.31 Reduction in UPV values of the concretes at the end of 300 freezing-thawing cycles: a) 5% replacement level vs. control and b) 15% replacement level vs. control

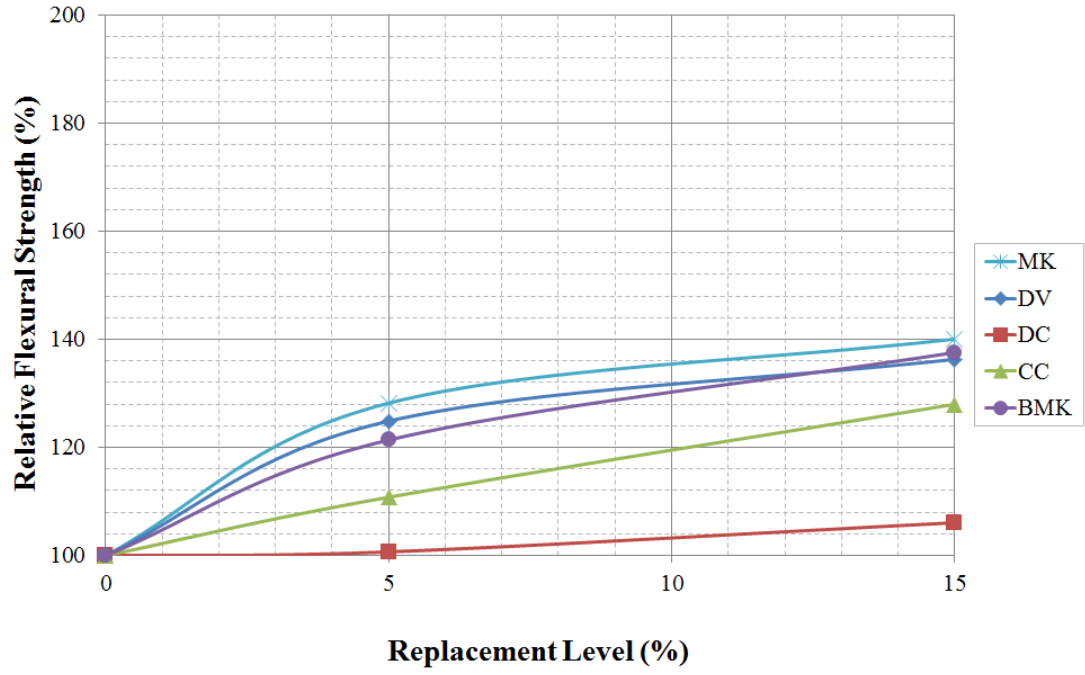


a)

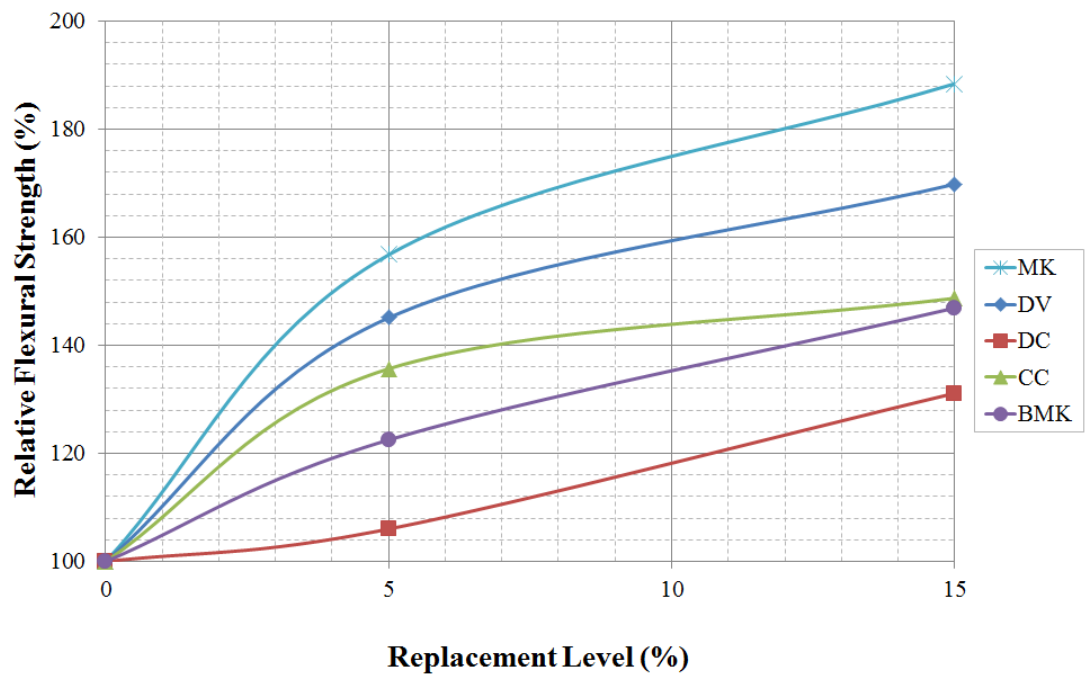


b)

Figure 4.32 Percent decrease in a) flexural and b) compressive strength due to 300 cycles of freezing and thawing

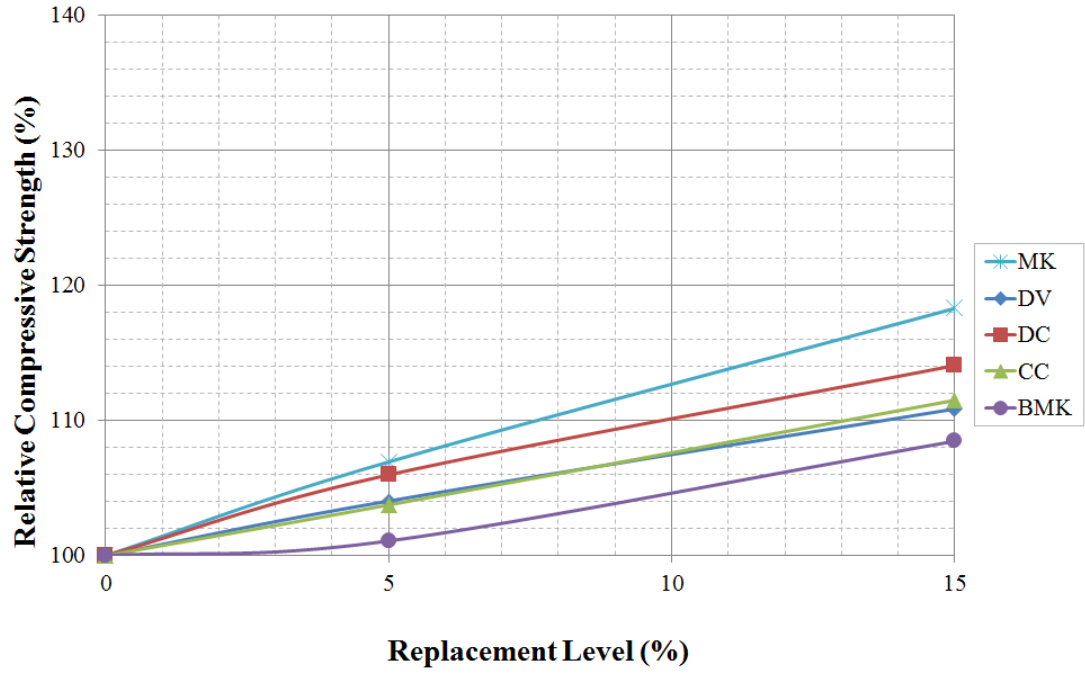


a)

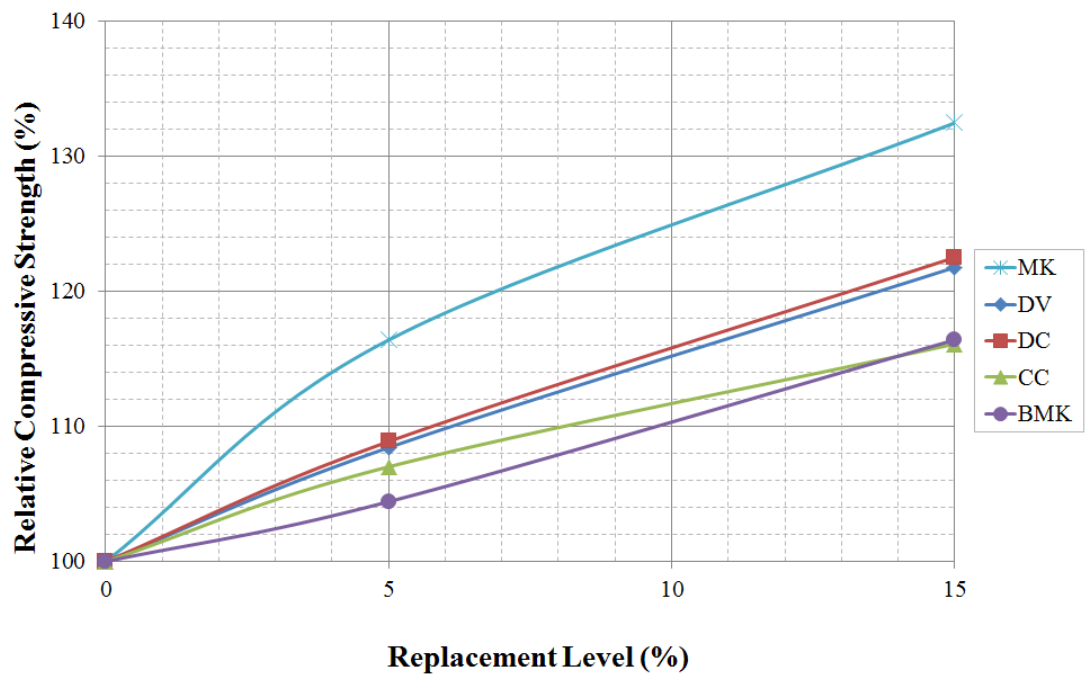


b)

Figure 4.33 Relative flexural strength of a) undamaged concretes and b) damaged concretes ( $F_{\text{control}}=100\%$ )



a)



b)

Figure 4.34 Relative compressive strength of a) undamaged concretes and b) damaged concretes ( $F_{\text{control}}=100\%$ )



#### 4.3.7 Corrosion current density with linear polarization resistance

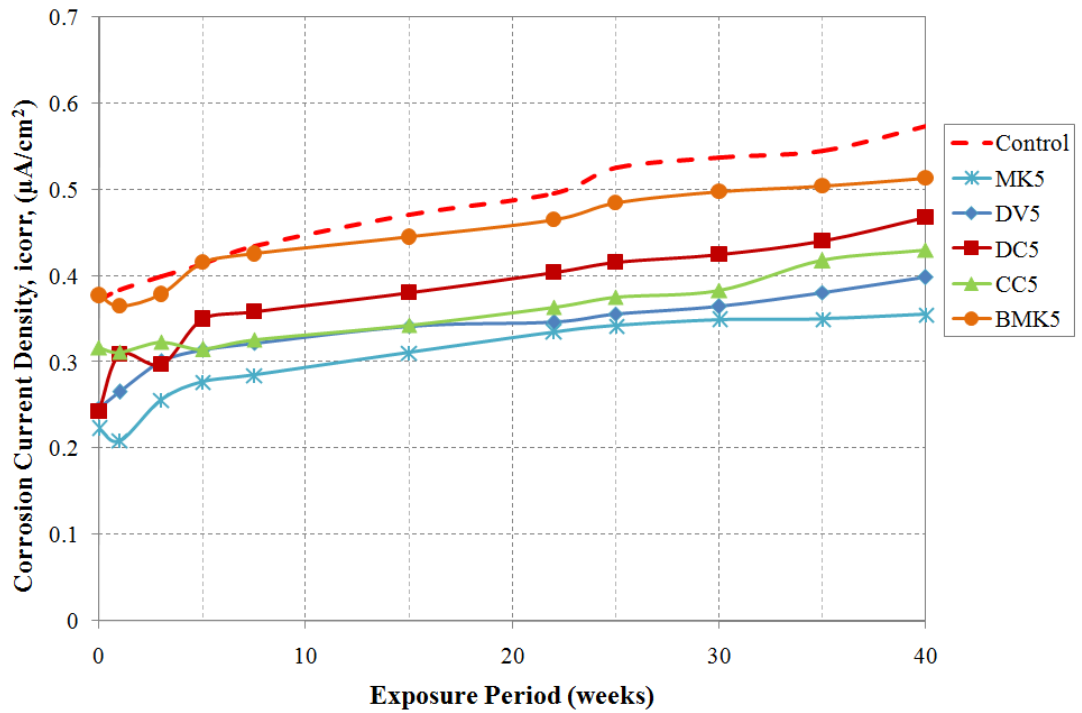
The variation in corrosion current densities ( $I_{\text{corr}}$ ) of the concretes over 40 weeks of 2% and 5% NaCl exposure were shown in Fig. 4.35 and 4.36. The rates of corrosion in mm/yr for each type of concrete before and after NaCl exposure regime were given Table 4.11. Moreover, in order to observe effect of chloride concentration on the corrosion rate visually, Figs. 4.37 and 4.38 were illustrated for 2% and 5% NaCl exposures, respectively.

At both exposure conditions, control concrete revealed the lowest performance, while MK incorporation provided significant reduction in  $I_{\text{corr}}$  values. Variation of  $I_{\text{corr}}$  values appeared to be similar at both exposure conditions for control concrete. However, the difference in behavior of concretes incorporating MK and CK can be observed more clearly. For example, DC5 concrete had  $0.55 \mu\text{A}/\text{cm}^2$  and  $0.46 \mu\text{A}/\text{cm}^2$   $I_{\text{corr}}$  values for NaCl exposure solutions of 5% and 2%, respectively. Moreover, increasing the amount of CKs generally provided better performance when considering the overall exposure period. The highest and lowest  $I_{\text{corr}}$  values were measured as  $0.57 \mu\text{A}/\text{cm}^2$  for control and  $0.28 \mu\text{A}/\text{cm}^2$  for MK15 concrete irrespective of concentration of the solution. Kayalı and Zhu (2004) carried out an experimental study on chloride diffusion and corrosion activity of reinforced silica fume–cement concrete slabs after partial immersion in a 2% chloride solution. Continuous increase in  $I_{\text{corr}}$  values with slight fluctuations was observed. The highest  $I_{\text{corr}}$  was measured as  $0.72 \mu\text{A}/\text{cm}^2$  at the end of 575 days (82 weeks).

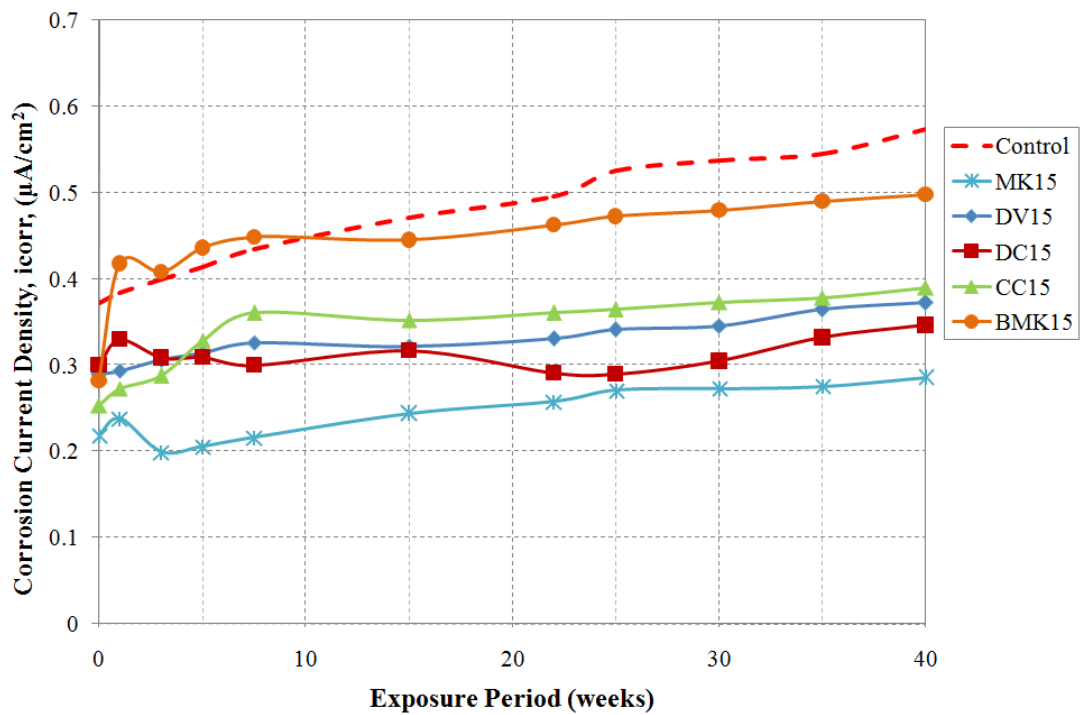
In the literature, there have been different discussions on the corrosion behavior of steel bar embedded in concrete based on the value of the corrosion current density result. Several researchers have determined that current density values which are greater than  $0.3 \mu\text{A}/\text{cm}^2$  may be indicative of active corrosion (Andrade et al., 1990; Al-Amoudi et al., 2003). Andrade and Alonso (2001) have reported a set of data for the levels of corrosion rates. They stated that corrosion current density between  $0.1 \mu\text{A}/\text{cm}^2$  and  $0.5 \mu\text{A}/\text{cm}^2$  can be considered as low and the values between  $0.5$ – $1 \mu\text{A}/\text{cm}^2$  are moderate. However, the current density values greater than  $1 \mu\text{A}/\text{cm}^2$  are considered high while the values below  $0.1 \mu\text{A}/\text{cm}^2$  are assumed to be negligible (Gonzales et al., 1996; Andrade and Alonso, 2001). Gonzalez et al. (1996) claimed

that corrosion current density less than  $0.2 \mu\text{A}/\text{cm}^2$  would be acceptable with no durability risks. Other researchers have nominated the value of  $0.3 \mu\text{A}/\text{cm}^2$  as the threshold for active reinforcement corrosion (Al-Amoudi et al., 2003). However, rates that are above the value of  $1 \mu\text{A}/\text{cm}^2$  are considered as hazardous (Rodriguez et al., 1994). In accordance with the comments presented above, utilizing MK or CK can effectively slow down the corrosion process depending on the replacement level and chloride exposure environment.

It is known that the presence of chloride ions R/C plays a major role in reinforcement corrosion and hence for the durability and service life of R/C structures (Pradhan and Bhattacharjee, 2009). Increasing the concentration of solution resulted in rise in the corrosion current density values. This can be attributed to the case that the higher the ionic conductivity due to the introduction of chloride ions, the lower the electrical resistivity resulting in the susceptibility to initiation of corrosion. Wee et al. (2000) explained the lower chloride permeability of concretes containing mineral additives in terms of the lower ionic conductivity ( $\text{OH}^-$  ions) of the pore fluid and the denser microstructure of the cement paste which may also explain the higher electrical resistivity of these concretes. However, it should be noted that use of MK provides an enhancement in electrical resistivity of the concretes as a result of not only providing denser structure but also chloride binding property (Thomas et al., 2012). Thomas et al. (2012) reported that the cement pastes incorporating MK had remarkable chloride binding capacity due to high alumina content (45%  $\text{Al}_2\text{O}_3$ ). Vejmelková et al. (2010) reported that the high performance concretes incorporating 10% MK revealed 30% more chloride binding property. This reduced the risk of embedded steel corrosion which otherwise would be increased by the decrease of alkalinity of pore solution. Another supporting result to this phenomenon can be found in the study of Coleman and Page (Coleman and Page, 1997). It was reported that utilizing MK up to 20% caused a substantial reduction in the concentrations of free chloride ions that were retained in the pore solution phase of paste specimens in which 1% chloride (by weight of total solids) had been included as a mix contaminant (Coleman and Page, 1997).

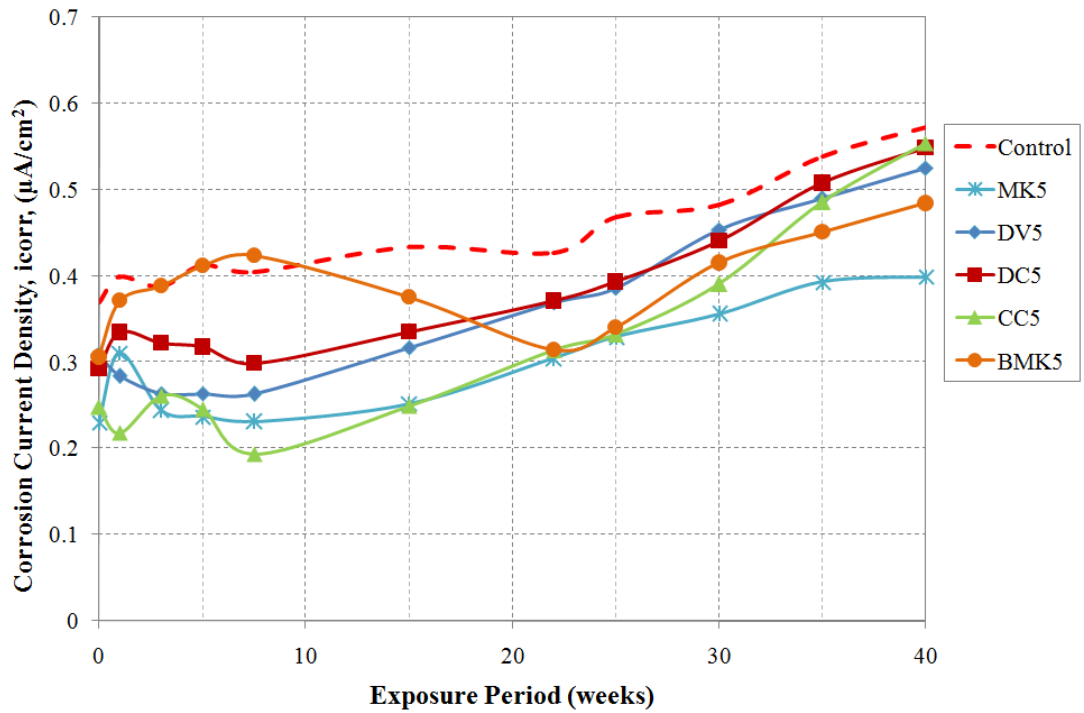


a)

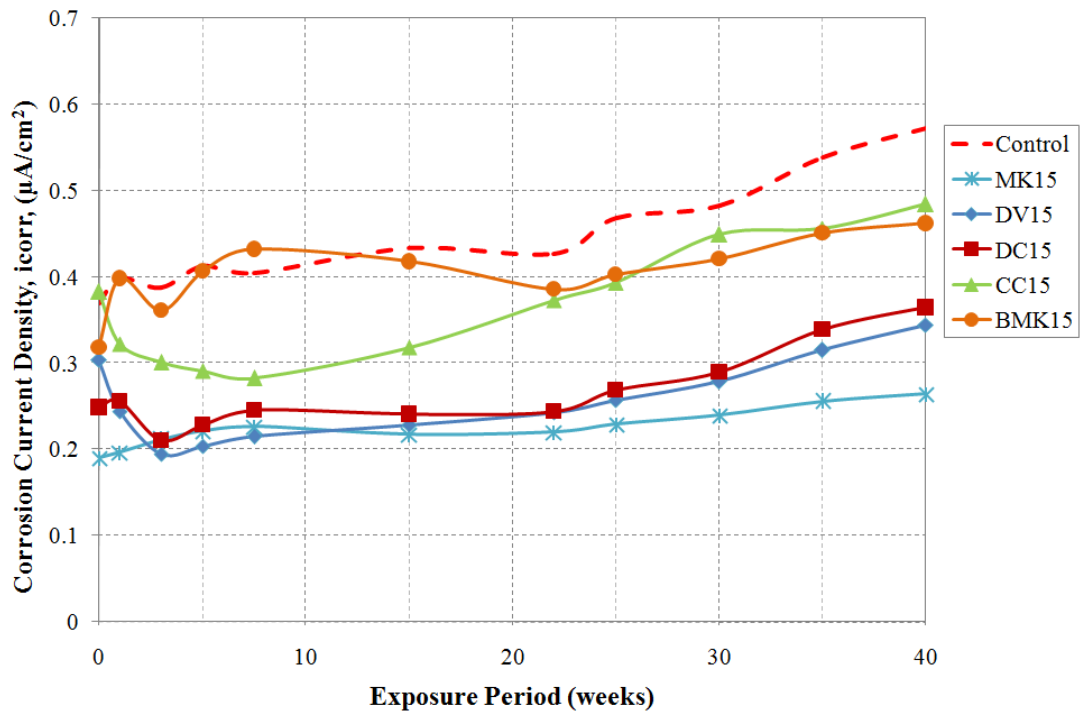


b)

Figure 4.35 Variation of corrosion current density over 40 weeks of 2% NaCl exposure for the concretes incorporating a) 5% and b) 15% MK and CKs



a)



b)

Figure 4.36 Variation of corrosion current density over 40 weeks of 5% NaCl exposure for the concretes incorporating a) 5% and b) 15% MK and CKs

Table 4.11 Corrosion rates (mm/yr) of concretes before and after exposure to chloride attack

Mix ID	Replacement level	2% NaCl solution		5% NaCl solution	
		Before exposure	After exposure	Before exposure	After exposure
Control	0	0.004327	0.006664	0.004295	0.006646
	5	0.002871	0.004626	0.003593	0.0061
DV	15	0.003369	0.004327	0.003532	0.003999
	5	0.002823	0.005434	0.003394	0.00637
DC	15	0.003483	0.004025	0.002891	0.004237
	5	0.003686	0.004996	0.002881	0.006436
CC	15	0.002943	0.004525	0.004449	0.005626
	5	0.004385	0.005966	0.003556	0.005627
BMK	15	0.00328	0.00579	0.003697	0.00537
	5	0.002597	0.004128	0.002677	0.00464
MK	15	0.002546	0.00332	0.002211	0.003076

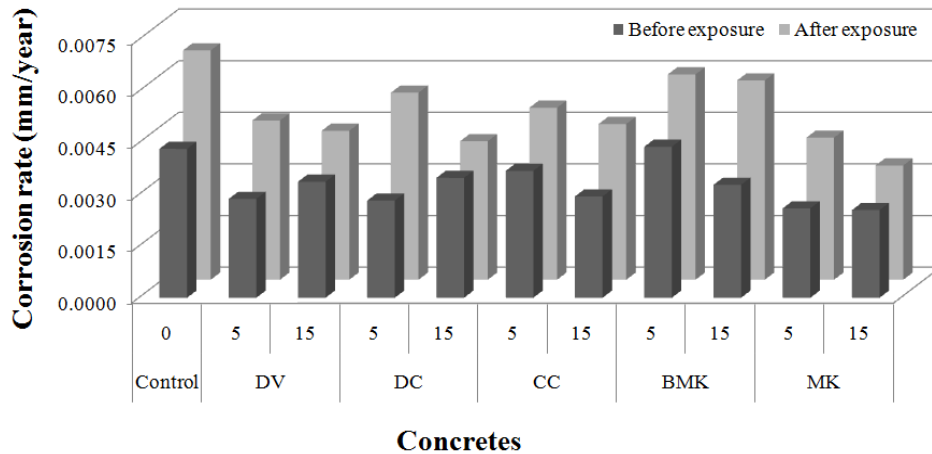


Figure 4.37 Corrosion rates of concretes before and after exposure to 2% NaCl solution

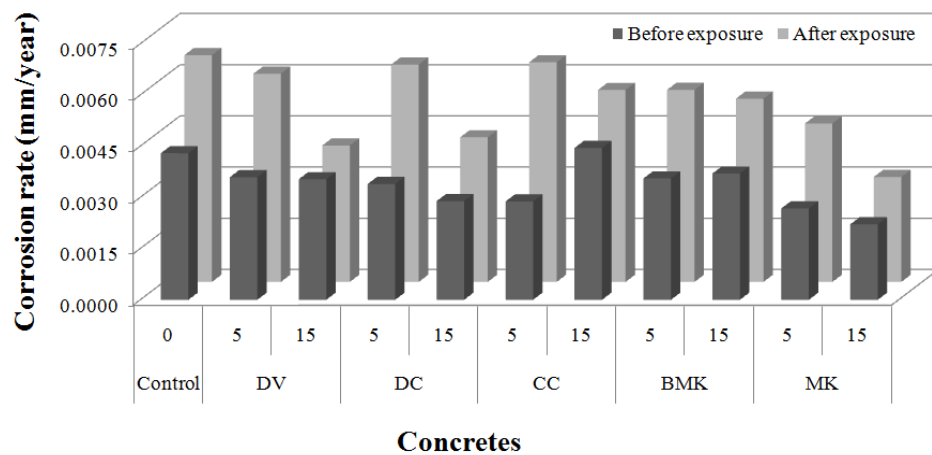
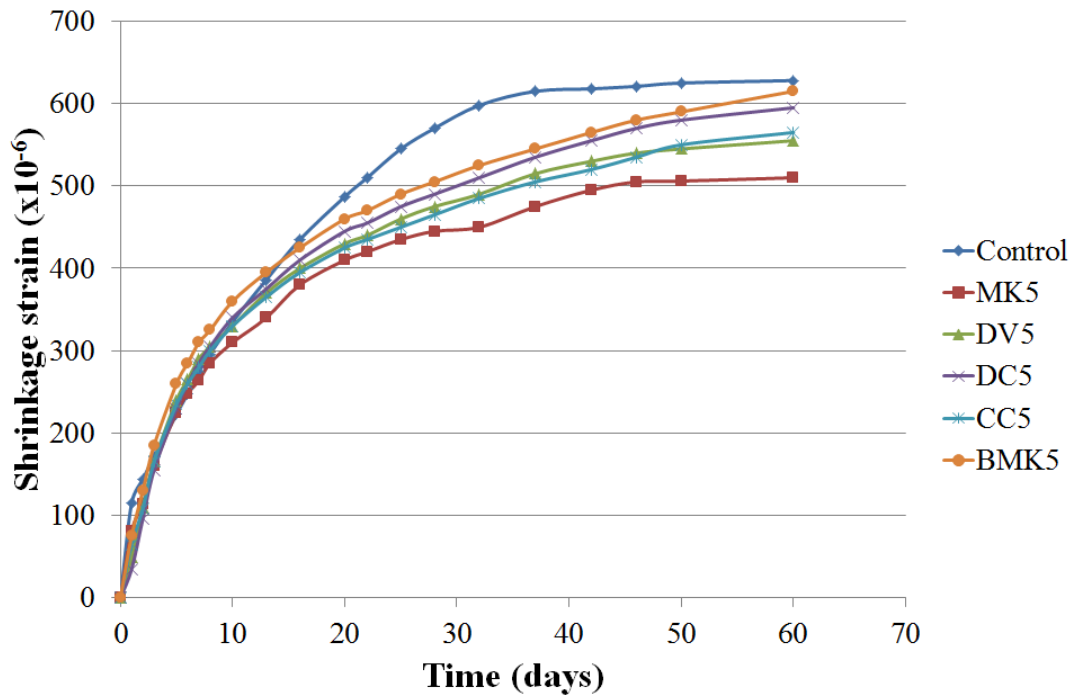


Figure 4.38 Corrosion rates of concretes before and after exposure to 5% NaCl solution

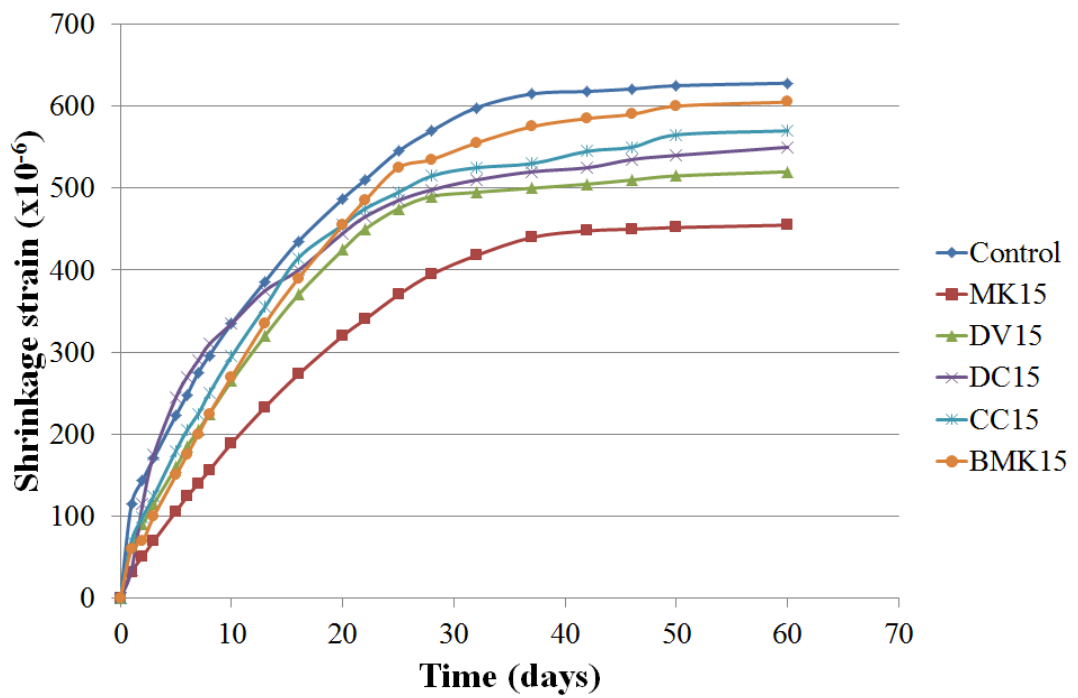
#### 4.3.8 Drying Shrinkage and weight loss

Free shrinkage strain developments of the concretes are depicted in Fig. 4.39. The shrinkage strain values of the CK incorporated concretes varied between control and MK concretes for both replacement levels. For example, 60 day shrinkage strains of 628, 605, 570, 550, 520, and 455 microstrain were measured for control, BMK15, CC15, DC15, DV15, and MK15 concretes, respectively. Due to its high reactivity, even at early ages, MK incorporated concretes had relatively lower shrinkage strains, particularly at 15% replacement level. However, the effects of inclusion of CKs were only clearly pronounced especially after 3 weeks of drying at both replacement levels (Fig. 4.39b).

The shrinkage strain development curves of CK incorporated concretes at 15% replacement level were clearly distinguished from each other, while no distinguishable difference were detected between DV and CC incorporated concretes at 5% replacement. Although exhibiting a very close trend to control for the first three weeks, BMK5 concrete yielded slightly less shrinkage strain than plain concrete at 60 days. However, increasing the amount of BMK resulted in lower shrinkage strain development even at early ages. The poor behavior of BMK incorporated concretes when compared to the others may be attributed to its pozzolanic property. Due to its high alunite content (see Table 2), BMK kaolin requires much more heat for full alteration of crystal structure exhausting  $SO_3$  (Arazi and Krenkel, 1970; Badogiannis et al., 2005). As a result of such a heat treatment, lower pozzolanic activity is obtained.



a)



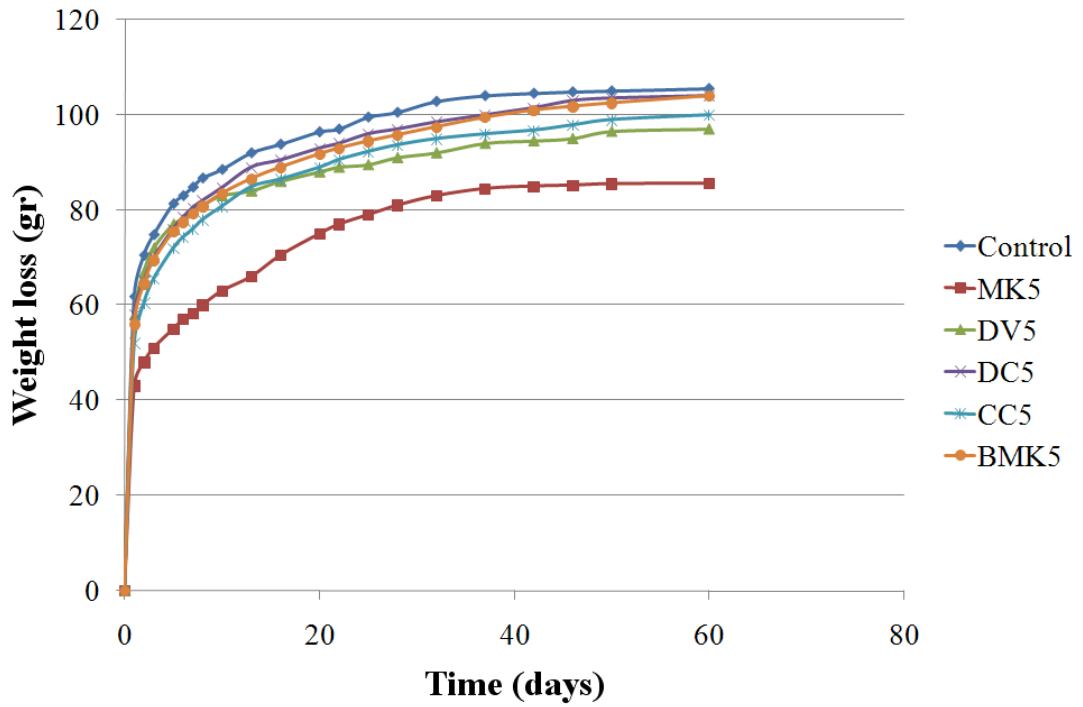
b)

Figure 4.39 Drying shrinkage strain development of a) Control and 5% MK or CK incorporated concretes and b) Control and 15% MK or CK incorporated concretes

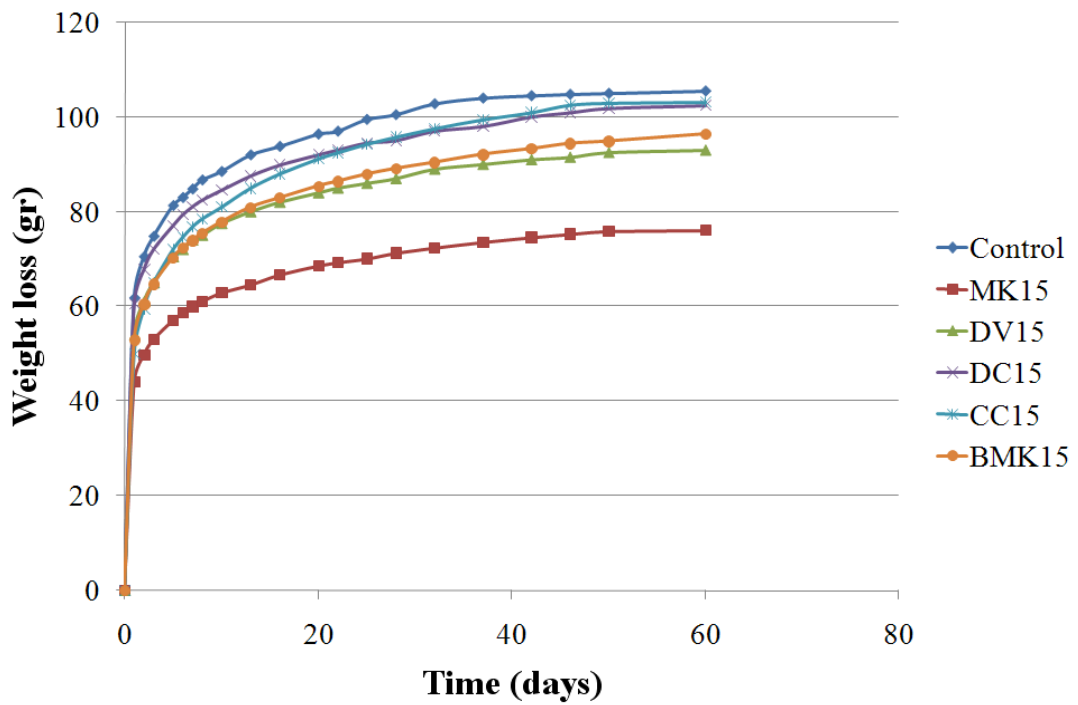
Weight losses of the concretes for 60 days of drying period are illustrated in Fig. 4.40. The maximum weight loss of 105.5 gr was observed in control concrete while the minimum was observed at MK15 concrete as 76 gr. As can be seen from Fig. 4.40, incorporation of CKs reduced the weight loss being lesser with increasing the amount of CKs. Of all CK incorporated concretes, the ones including DV were better than the others.

In CK modified concretes, BMK incorporated ones showed considerable decrease in weight loss when the replacement level increased from 5% to 15%, which may be due to the higher specific surface area of BMK. Actually, BMK and DV calcined kaolins have very close specific surface areas, 7.45 and 7.34 m<sup>2</sup>/gr, respectively. Observing from Fig. 4.40b, it is evident that BMK15 and DV15 had close weight loss values. Therefore, it may be claimed that weight loss behavior at high replacement levels is dominated by physical improvement due to microfilling effect of the mineral admixture. The foregoing trends support that the MK concretes have lower porosity and finer pore structure which encourage loss of water by self desiccation rather than by diffusion to the outside environment (Brooks and Johari, 2001; Wiegrink et al., 1996).





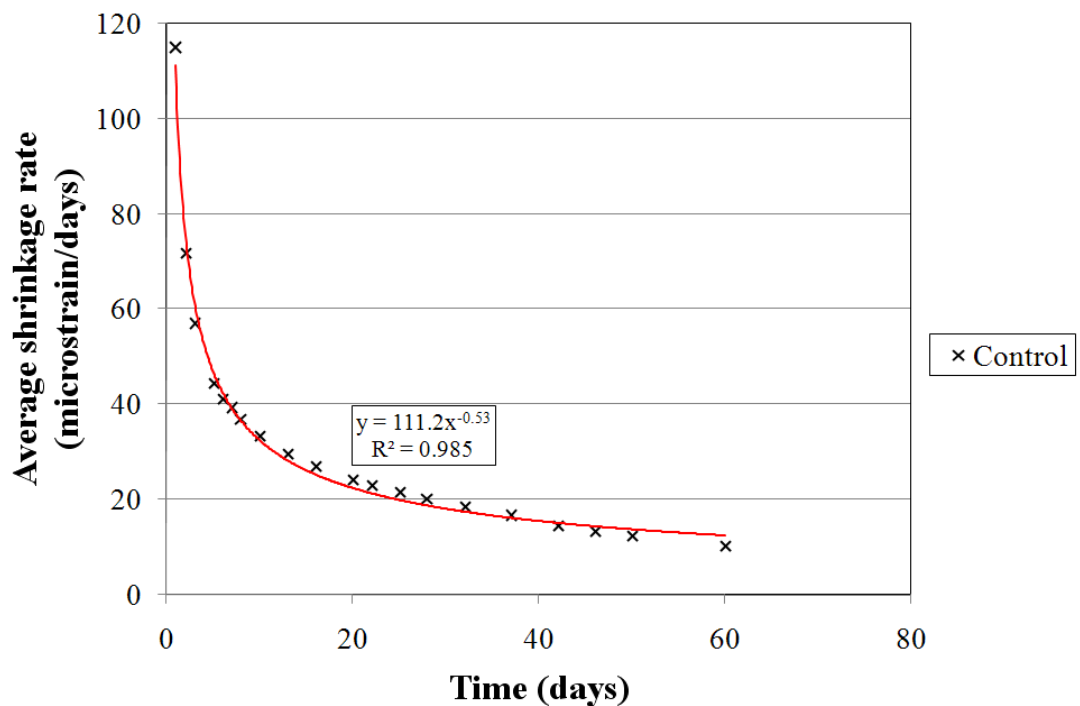
a)



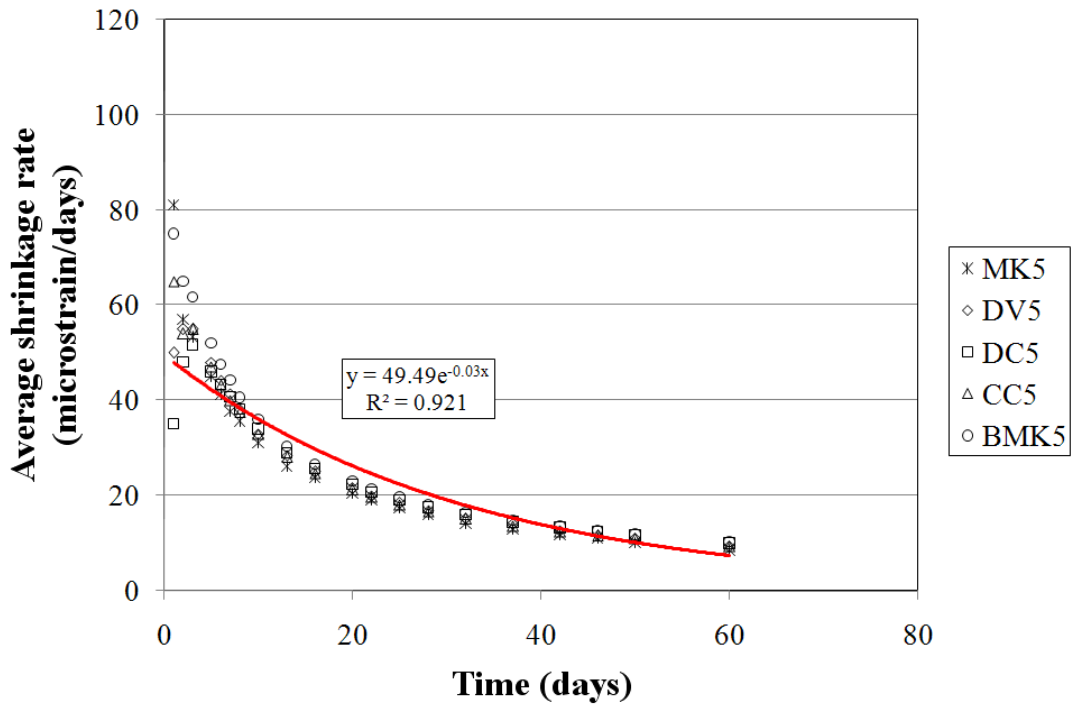
b)

Figure 4.40 Variations in weight loss of a) Control and 5% MK or CK incorporated concretes and b) Control and 15% MK or CK incorporated concretes

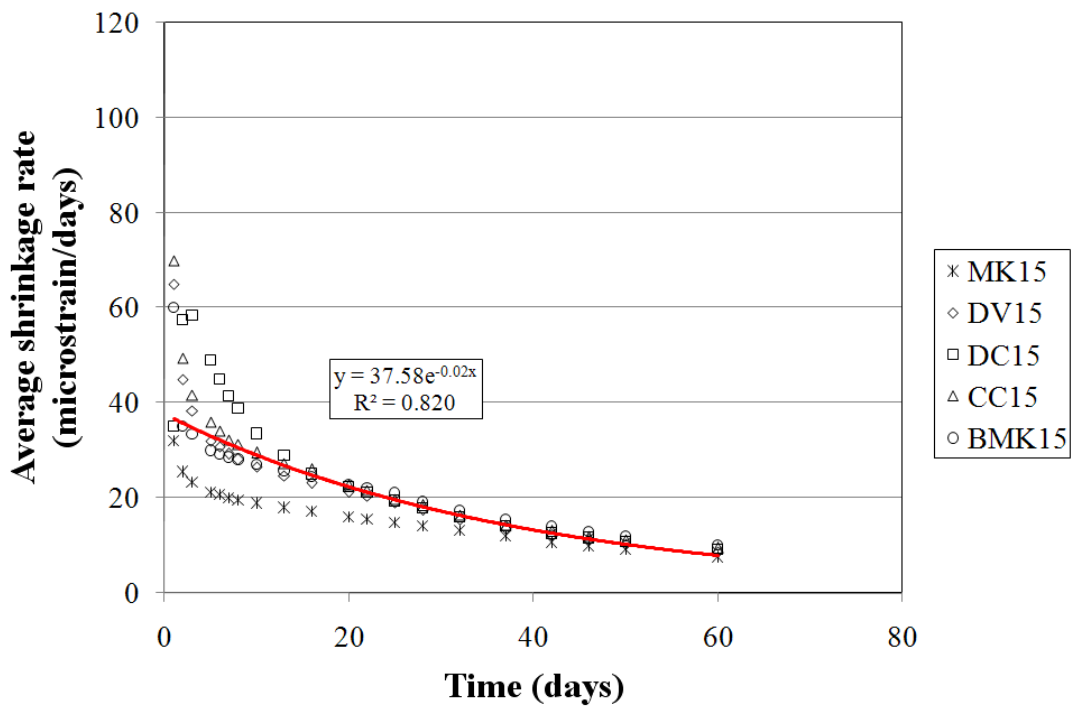
The reason that lies behind the lower shrinkage strain in MK or CK modified concretes is surely due to the decrease in the rate of shrinkage of concrete as a result of mineral admixture incorporation (Güneyisi et al., 2008). The average rates of shrinkage strains were calculated and presented in Fig. 4.41. Shrinkage rates sharply decreased early ages. Since MK showed relatively lower shrinkage strain development, as the amount of MK increased the correlation between the shrinkage rate and drying period decreased. As can be seen from Fig. 4.41 that shrinkage strain rate is strictly dependent on the type and amount of the mineral admixture which is observed more clearly at 15% replacement level.



a)



b)



c)

Figure 4.41 Average shrinkage rates of a) Control, b) 5%, and c) 15% MK or CK incorporated concretes

## CHAPTER 5

### STATISTICAL ANALYSIS AND CORRELATIONS

#### 5.1 Analysis of variance (ANOVA) study on the experimental data

In order to assess the statistical significance of the experimental test parameters, general linear model analysis of variance (GLM-ANOVA) was performed at 0.05 level of significance. GLM-ANOVA is an important statistical analysis and diagnostic tool which helps in reducing the error variance and quantifies the dominance of a control factor. In this analysis, the total sum of squares was calculated, which was partitioned into the sum of squares (SS) for individual factors and the SS for the residual random error. Next, the mean squares (MS) of the factors were calculated by dividing their corresponding SS by the associated degrees of freedom (DF). Then, the effect of individual factors was evaluated by testing the hypothesis of the equality of variances, which was the test of null hypothesis or simply the significance test at a particular probability level (Pradhan Bhattacharjee, 2009; Hicks, 1982).

The experimental data presented in "Chapter 4" were examined using the GLM-ANOVA technique by means of a software called "Minitab" at a 0.05 level of significance to analyze the variation in the tested properties of the concretes.

To determine statistical significance of kaolin type and calcination temperature on the pozzolanic activity index of the kaolins GLM-ANOVA was applied and the results were presented in Table 5.1. In the analysis, kaolin type and calcination temperature were assigned as the dependent variables while the pozzolanic activity index was selected as the independent factor. The general linear model analysis of variance was performed and the effective test parameter and/or parameters and their percent contributions on the above mentioned properties of calcined kaolins were

determined. The p-values in Table 5.1. show the significance of the given test parameters on the test results. As it can be seen in Table 5.1, the p-value of the parameters were less than 0.05, indicating that the variability of experimental test results can be explained in terms of test parameters. Therefore, it can be said that, the type of kaolin and the level of calcination temperature are both effective on the pozzolanic indices of the mortars.

Table 5.1 Statistical evaluation of pozzolanic activity index

Dependent variable	Source of variation	Statistical parameters				Significance
		Sequential sum of square	Mean square	F	p-value	
Pozzolanic Activity Index	Kaolin Type	16121.7	5373.7	330.7	0.000	YES
	Calcination Temperature	1710.4	285.1	17.5	0.000	YES
	Error	292.5	16.3			

In the analysis, the compressive and splitting tensile strengths were assigned as the dependent variables while the experimental test parameters were selected as the independent factors. The independent factors are type of calcined kaolin, replacement level, and age of concrete. The resulting p-values shown in Table 5.2 indicate the significance of test parameters on the compressive strength development. As can be seen in Table 5.2, the effects of all parameters on compressive strength were determined to be statistically significant, while type of thermally treated kaolin seemed to have no statistically significant effect in splitting tensile strength. That may be attributed to the narrow range of the variation of the data.

Table 5.2 Statistical evaluation of compressive strength of the concretes produced with calcined kaolins

Source of variation	Parameters	Statistical parameters				Significance
		Sequential sum of squares	Mean square	F	p-Value	
Compressive strength	Type of calcined kaolin	15.86	48.63	5.18	0.003	YES
	Replacement level	7801.45	2612.46	278.41	0.000	YES
	Age of Concrete	229.35	57.34	6.11	0.000	YES
	Error	647.7	9.38			
	Total	8694.12				
Splitting tensile strength	Type of calcined kaolin	1.259	0.12208	2.35	0.076	NO
	Replacement level	0.9176	0.30585	5.89	0.003	YES
	Age of Concrete	1.827	1.827	35.18	0.000	YES
	Error	1.609	0.05192			
	Total	5.613				

For statistical analysis of the permeability properties the independent variables were considered as type of thermally treated kaolins (MK and CKs), age of concrete, and replacement level of mineral admixtures. The results of the analysis were given in Table 5.3. Table 5.3 indicated that the independent parameters evaluated have been proved to be effective on permeability properties of the concretes. The utilization of mineral admixture is attributed to the replacement level considered for the statistical analysis. Similar findings were presented by Güneyisi et al. (2011). They used multisystem blends of FA, MK, and GGBFS to examine some permeability properties of concretes. They reported that the use of mineral admixtures appeared to be statistically significant in reducing the permeability of the concretes in terms of chloride ion permeability, water permeability, and sorptivity. Among the mineral admixtures used, MK was found to be the most effective in enhancing the permeability resistance of the concretes.

Table 5.3 Statistical evaluation of the gas permeability, RCPT, sorptivity, and water permeability of the concretes

Dependent Variable	Independent variable	Statistical parameters				Significance
		Sequential Sum of Squares	Mean Square	F	p-value	
Gas permeability	Type of Mineral Admixture	1.16814	0.292035	14.47	0.000	YES
	Age	0.81349	0.81349	40.31	0.000	YES
	Replacement level	4.49707	1.1242675	55.7	0.000	YES
	Error	0.80733	0.02018325	-	-	-
	Total	7.28603	-	-	-	-
RCPT	Type of Mineral Admixture	953749	238437.25	7.49	0.000	YES
	Age	1821950	1821950	57.27	0.000	YES
	Replacement level	10522814	2630703.5	82.69	0.000	YES
	Error	1272533	-	-	-	-
	Total	14571046	-	-	-	-
Sorptivity	Type of Mineral Admixture	0.004594	0.0011485	10.68	0.000	YES
	Age	0.0066261	0.0066261	61.6	0.000	YES
	Replacement level	0.0076808	0.0019202	17.85	0.000	YES
	Error	0.0043026	-	-	-	-
	Total	0.0232035	-	-	-	-
Water permeability	Type of Mineral Admixture	198.24	49.56	9.47	0.000	YES
	Age	468.18	468.18	89.43	0.000	YES
	Replacement level	643.29	160.8225	30.72	0.000	YES
	Error	209.41	-	-	-	-
	Total	1519.12	-	-	-	-

Statistical analyses of electrical resistivity and corrosion testing were shown in Table 5.4. Since corrosion current density can be converted to corrosion rate by a mathematical relation (Güneyisi et al., 2012b), only corrosion rate was used for statistical analysis. The factors considered for electrical resistivity were type of thermally treated kaolin (CK or MK), age of concrete, and replacement level of CK or MK. However for analysis of corrosion rate, concentration of NaCl solution and

exposure period were also considered. The statistical analyses have shown that the factors tested for these properties were all statistically effective.

Table 5.4 Statistical evaluation of electrical resistivity and corrosion rate

Dependent Variable	Independent variable	Statistical parameters				Significance
		Sequential Sum of Squares	Mean Square	F	p-value	
Electrical resistivity	Type of Mineral Admixture	188.39	47.096	16.35	0.000	YES
	Age	259.59	76.303	26.49	0.000	YES
	Replacement level	228.909	76.303	26.49	0.000	YES
	Error	89.295	-	-	-	-
	Total	766.18	-	-	-	-
Corrosion rate	Type of Mineral Admixture	0.0000769	0.0000192	72.43	0.000	YES
	NaCl concentration	0.0000031	0.0000031	11.50	0.001	YES
	Replacement level	0.0000105	0.0000105	39.45	0.000	YES
	Exposure period	0.0000598	0.0000060	22.52	0.000	YES
	Error	0.0000539	-	-	-	-
	Total	0.00002041	-	-	-	-

Since the number of data is limited for flexural and compressive strength loss due to 300 freezing and thawing cycles, these parameters were not statistically analyzed as the result may be misleading. Instead, change in UPV values corresponding to each cycle were considered to be appropriate for statistical analysis. For this, independent factors were assigned as type of thermally treated kaolin, number of freezing-thawing cycles and replacement level of MK or CK (Table 5.5). The results revealed that all of the parameter was statistically significant on the variation of UPV loss values.



Table 5.5 Statistical evaluation of UPV loss due to 300 freezing and thawing cycles

Dependent Variable	Independent variable	Statistical parameters				Significance
		Sequential Sum of Squares	Mean Square	F	p-value	
UPV loss	Type of Mineral Admixture	29.346	7.336	28.29	0.000	YES
	Number of cycles	53.126	13.282	51.22	0.000	YES
	Replacement level	2.488	2.489	9.60	0.004	YES
	Error	10.372	0.2593	-	-	-
	Total	95.333	-	-	-	-

## 5.2 Correlations between properties of concrete

Correlating the experimental data is one of the common practices among the researchers for appraisal of the findings reported. Hypothetically, the principal elements controlling the mechanical and transport features of concrete are the relative volume fractions of paste matrix and aggregate, the texture of the pore structure of the matrix and the interfacial transition zone around the aggregate particles. As mentioned in the previous section lower permeability reflects refined pore structure of the cement paste. Some researchers pointed out the relation between the permeability and other properties of concretes. For example, Hui-Sheng et al. (2009) performed a study on mechanical, carbonation, and gas permeability of concretes incorporated by-product mineral admixtures, namely fly ash and slag. It was reported that gas permeability of concretes had strong relation with mechanical and durability properties, such as the concretes with higher compressive strength had lower gas permeability coefficients. Boel et al. (2008) reported that there is a rather good correlation between the capillary porosity and the gas permeability. Based on the facts presented above to specify the possible correlation between the properties of control and thermally treated kaolin modified concretes, the correlation coefficients (R) between the investigated properties were calculated and presented in Figs. 5.1 through 5.7. The data used for these figures cover the entire test results obtained at 28 and 90 days for compressive and splitting tensile strengths as well as transport properties. However for freezing and thawing test the UPV and strength losses at the end of 300 cycles were used. Moreover, for the correlation of the corrosion rates of

the concretes exposed to 2% and 5% NaCl solutions were performed using 90 day electrical resistivities of the concretes.

The correlation between compressive and splitting tensile strength yielded correlation coefficient of 0.619. MK incorporated concretes demonstrated the closest trend to best fit line while the others had no uniform scatter around the line.

Fig. 5.2 demonstrates that the correlation between gas permeability and water permeability of MK modified concretes is generally better than that of CK included ones. However DV and CC included ones have also proved to have similar trend that MK concretes did. Correlating gas permeability data with RCPT test results had the highest correlation coefficient ( $R^2=0.812$ ) among permeability properties. 28 day water permeability test result of control concrete was seen far divergent from the general tendency of the others in Fig. 5.3. Fig. 5.4 demonstrated that the weakest correlation among permeability properties has taken place between gas permeability and sorptivity. This may be due to the fact that the sorptivity test is based on the free movement of the water as a result of the capillary action of the continuous pores, while in gas permeability test there is an impressed pressure head dominating the movement of the oxygen molecules through the concrete.

The correlation among UPV loss and strength losses appeared to have similar correlations as shown in Figs. 5.5 and 5.6. However the correlation between UPV loss and compressive strength loss is slightly greater than flexural strength loss ( $0.475>0.454$ ).

Figs. 5.7 and 5.8 reveal the relation between 90 day electrical resistivity and corrosion rates at the end of 40 weeks 2% and 5% NaCl of exposure regimes, respectively. From the figures it can be inferred that there is a close relation between the electrical resistance and corrosion behavior of the concretes. Correlation coefficients of 0.754 and 0.770 were calculated for the concretes exposed to 2% and 5% NaCl solution. MK and CKs presented similar trends in this property.

Fig. 5.9 presents the relations between the shrinkage strain and weight loss developments polynomial, logarithmic, and exponential expressions. The correlation

coefficients are quite high revealing a strong relation between the shrinkage strain and weight loss. One important point that should be notified is the tendencies of MK5 and MK15 in Figs. 5.9b and 5.9c, which are far divergent from CK incorporated ones. For example, MK15 concrete had 65 gr weight loss for 300 microstrain while CK incorporated ones had approximately 80 gr weight loss for the same shrinkage strain (Fig. 5.9c).

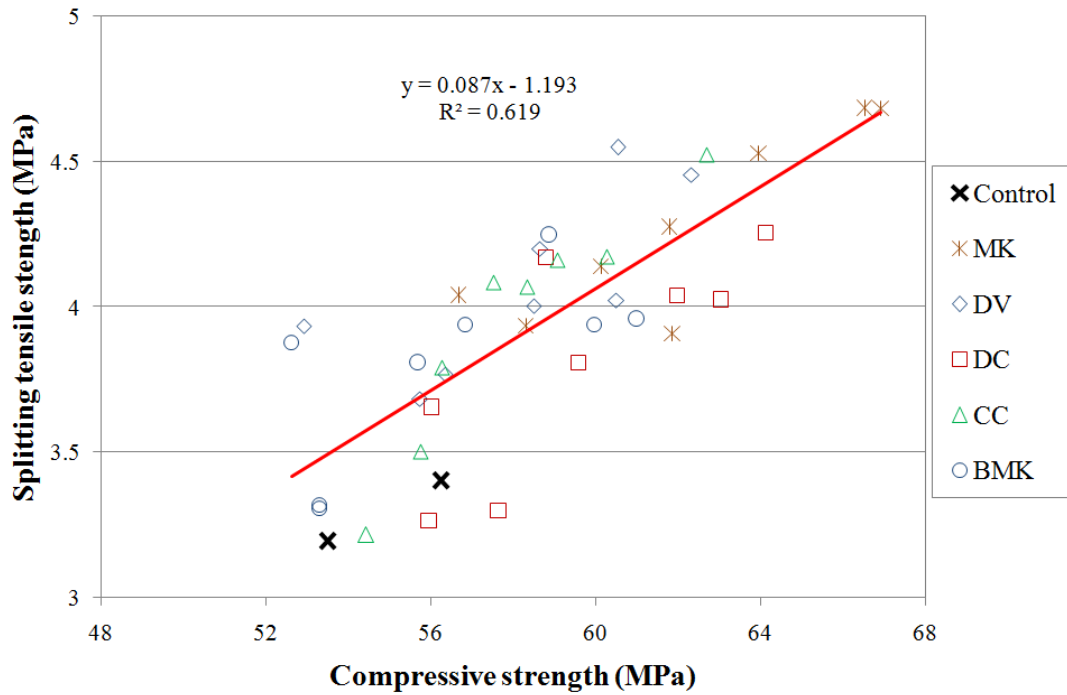


Figure 5.1 Correlation between compressive and splitting tensile strength of concretes

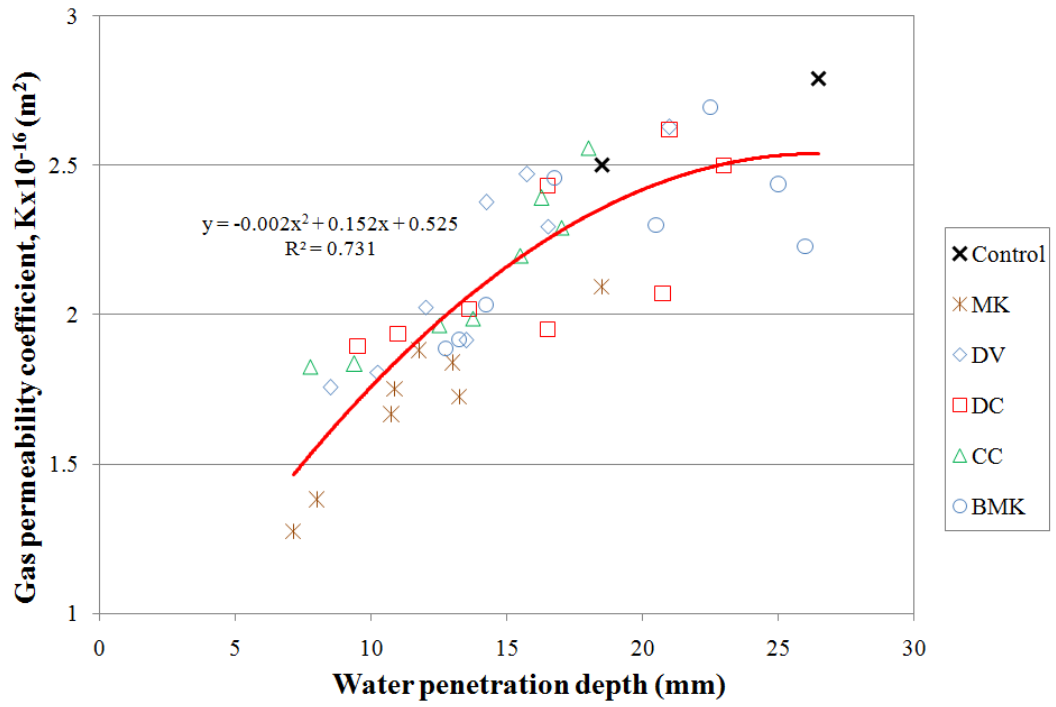


Figure 5.2 Correlation between gas permeability and water permeability of concretes

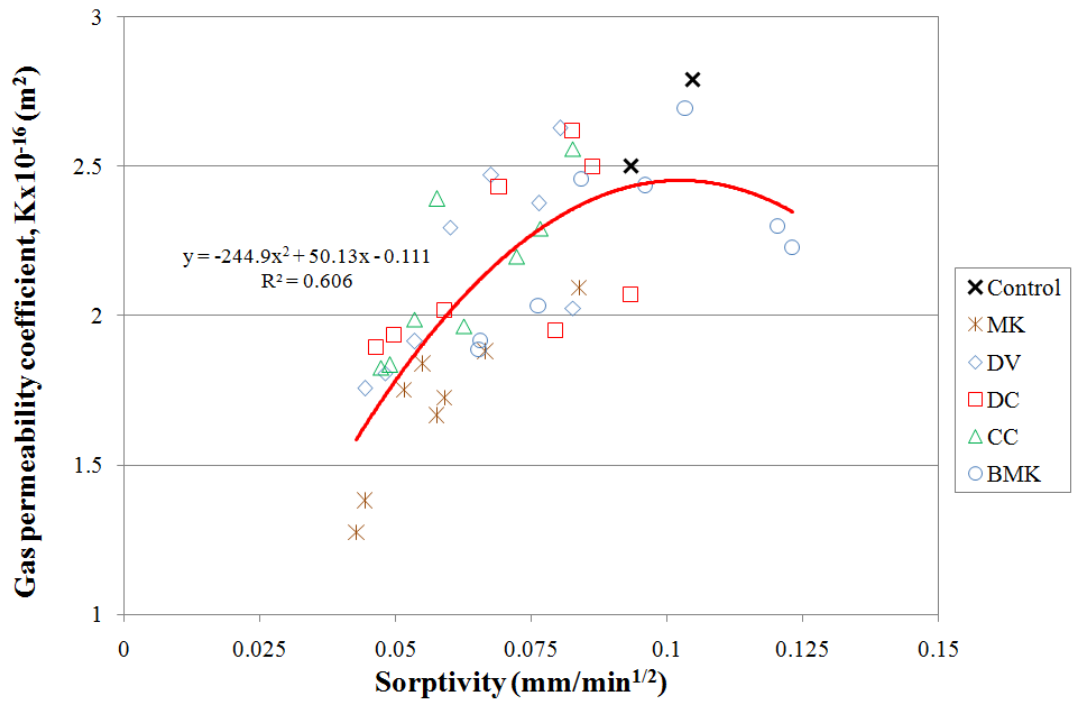


Figure 5.3 Correlation between gas permeability and sorptivity values of concretes

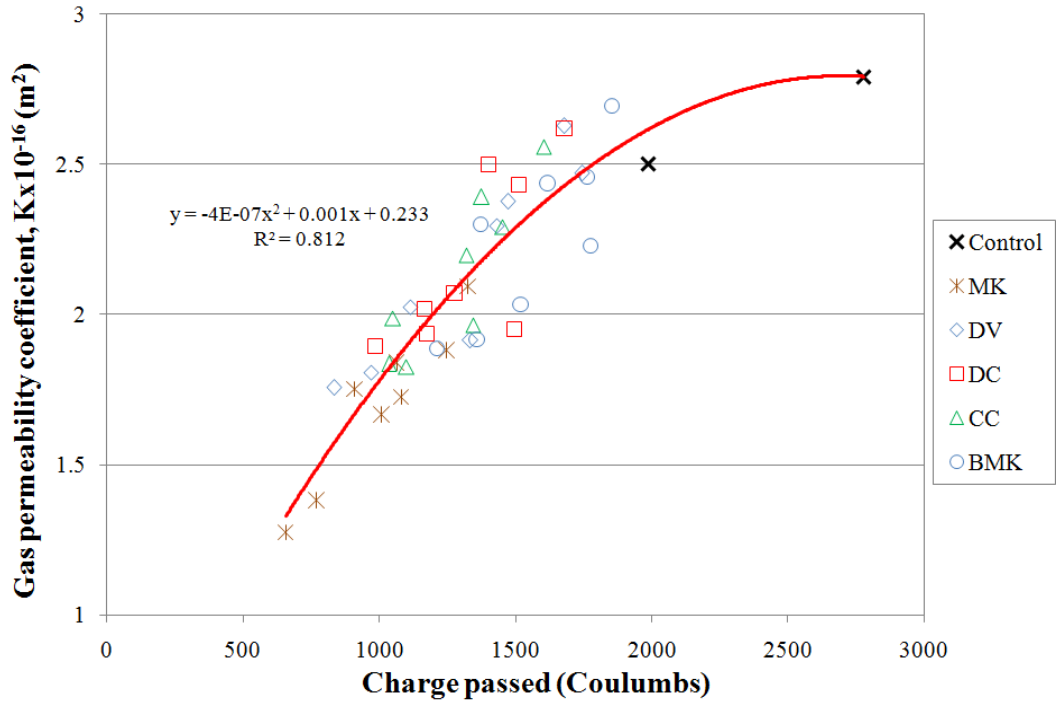


Figure 5.4 Correlation between gas permeability and RCPT values of concretes

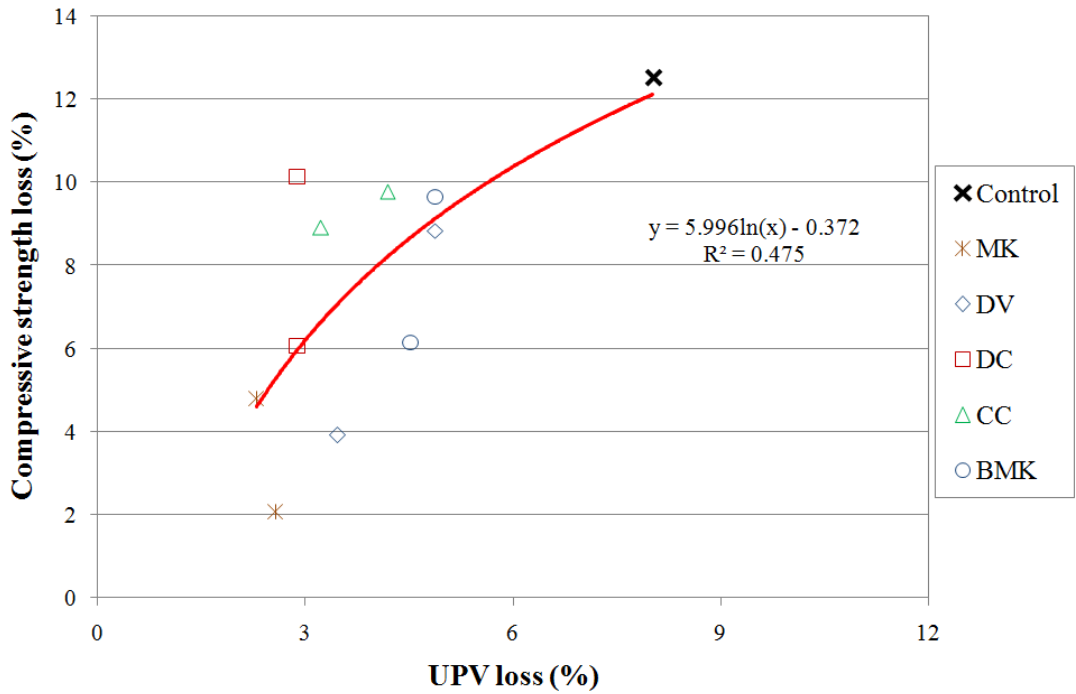


Figure 5.5 Correlation between UPV loss and compressive strength loss of the concretes exposed to 300 freezing and thawing cycles

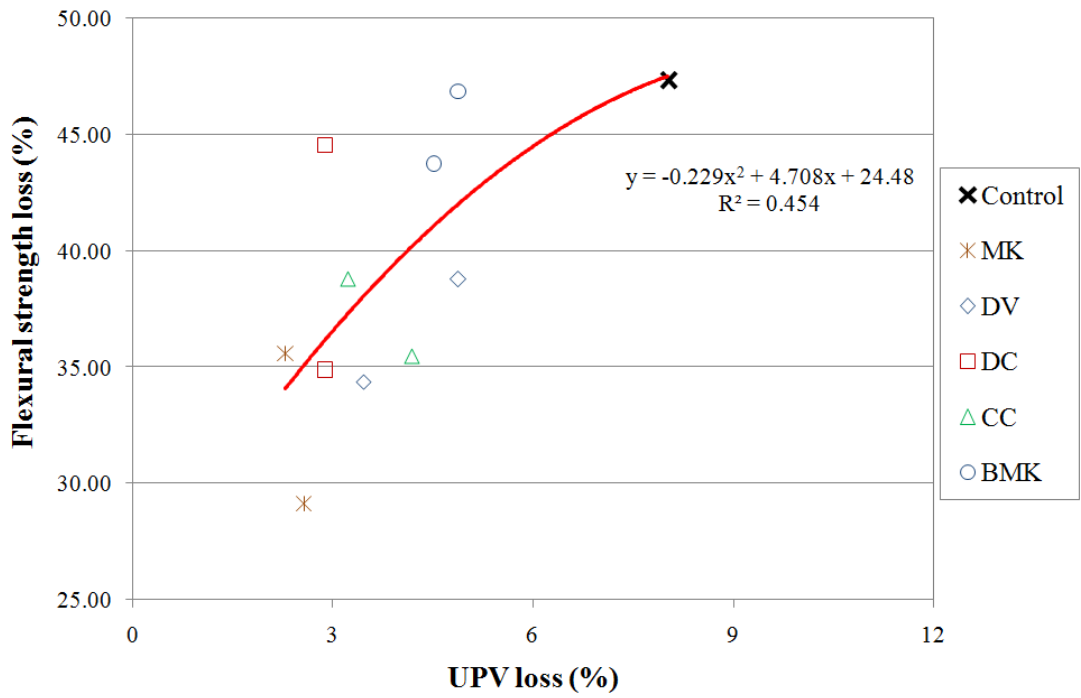


Figure 5.6 Correlation between UPV loss and flexural strength loss of the concretes exposed to 300 freezing and thawing cycles

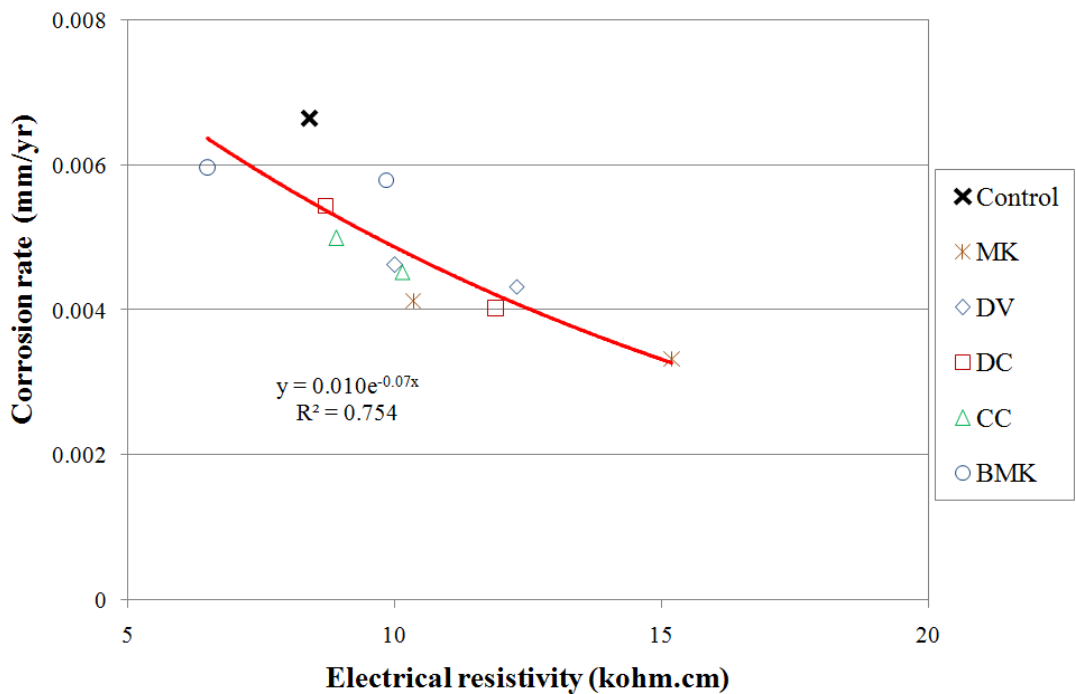


Figure 5.7 Correlation between 90 day electrical resistivity and corrosion rate of the concretes 40 weeks of 2% NaCl exposure

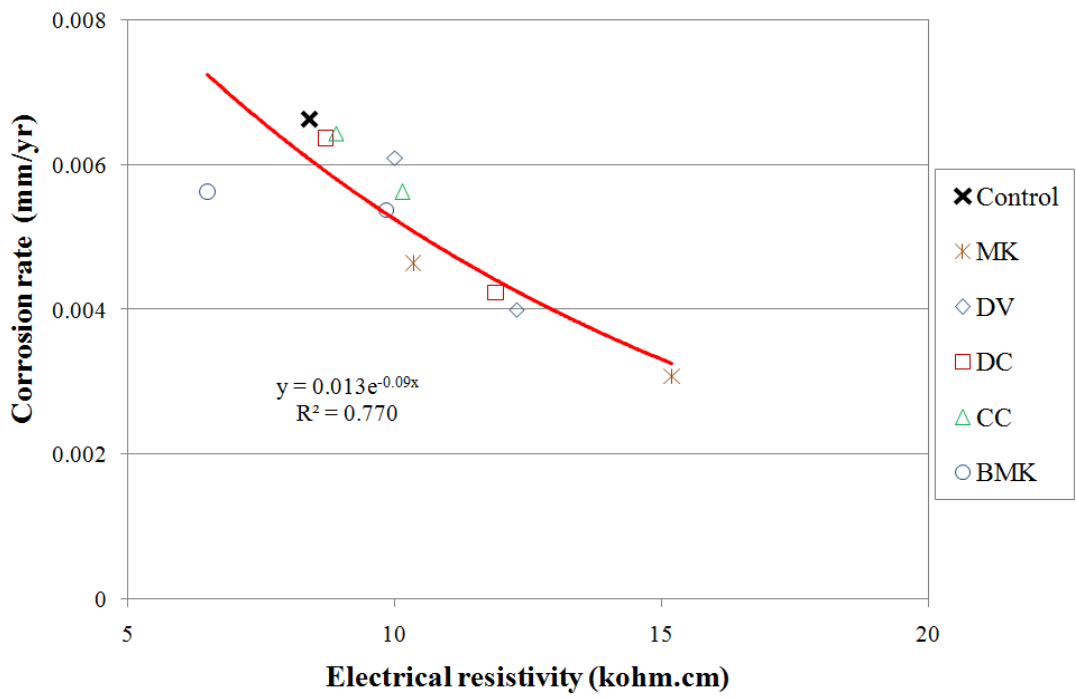
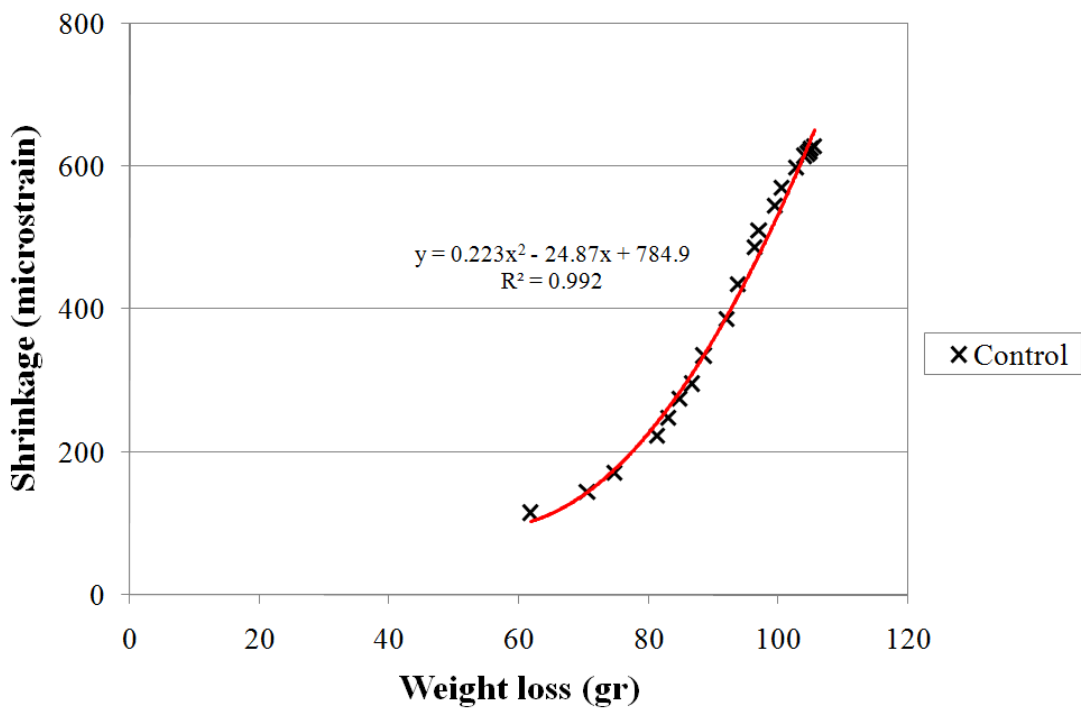
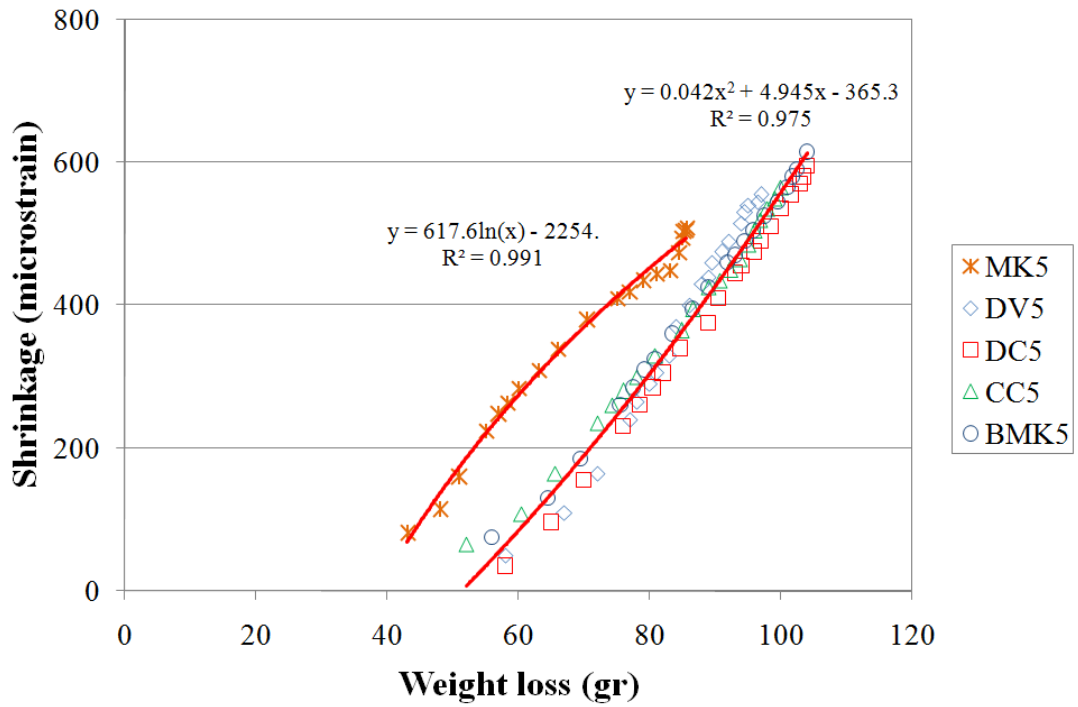


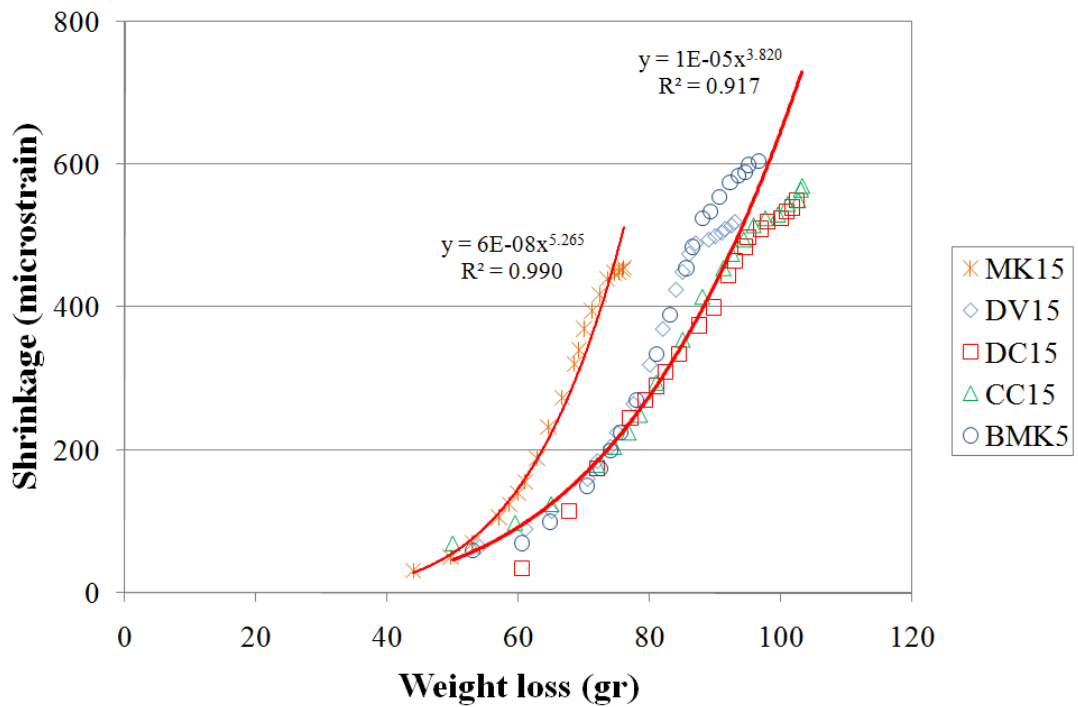
Figure 5.8 Correlation between 90 day electrical resistivity and corrosion rate of the concretes 40 weeks of 5% NaCl exposure



a)



b)



c)

Figure 5.9 Shrinkage strain vs. weight loss of a) Control, b) 5%, and c) 15% MK or CK incorporated concretes



## **CHAPTER 6**

### **ANALYTICAL MODELLING**

#### **6.1 Introduction**

An analytical model is a description of a system using mathematical concepts and language. The process of developing a mathematical model is termed mathematical modeling. Mathematical models are used not only in the natural sciences and engineering disciplines but also in the social sciences. Researchers use mathematical models most extensively. A model may help to explain a system and to study the effects of different components, and to make predictions about behaviour (Wikipedia, 2008).

Artificial Intelligence (AI) techniques have been utilized as robust alternative technique for engineering analysis problems. Artificial intelligence emerged as a computers science discipline in the mid 1950s. Since then, a number of handful tools has been produced for practical use in engineering to figure out sophisticated problems which normally require human intelligence (Pham and Pham, 1999). AI can be described as the simulation of human intelligence on a machine, so that the machine effectively to identifies and uses the right part of “Knowledge” at a specified step of solving a problem. Therefore, AI alternatively might be defined as object orientation with computational models that can think and act rationally. AI has broad spectrum of research fields. It tackles various types of knowledge representation modes, different methods of intelligent search, various techniques for resolving fuzzy data and knowledge (Konar, 1999). Several AI tools that are widely utilized for engineering problems are knowledge-based systems, fuzzy logic, inductive learning, neural networks and genetic algorithms (Pham and Pham, 1999).

## 6.2 Genetic Programming

A genetic algorithm (GA) is a search technique that has been used in computing for finding precise or approximate solutions to optimization or search problems. Genetic algorithms can be categorized as global search heuristics. Genetic algorithms are a particular class of evolutionary computation. The techniques used by GA are inspired by evolutionary biology such as; inheritance, mutation, selection, crossover (recombination).

Genetic programming (GP), proposed by Koza (1992) is essentially an application of genetic algorithms to computer programs. GP has been applied successfully to solve discrete, non-differentiable, combinatorial, and general nonlinear engineering optimization problems (Goldberg, 1989). It is an evolutionary algorithm based methodology inspired by biological evolution to find computer that performs a task defined by a user. Therefore, it is a machine learning technique used to construct a population of computer programs according to a fitness landscape determined by a program's ability to perform a given computational task. Similar to GA, the GP needs only the problem to be defined. Then, the program searches for a solution in a problem-independent manner (Goldberg, 1989; Zadeh, 1984).

Gene expression programming (GEP) is a natural development of genetic algorithms and genetic programming. GEP was introduced by Ferreira (2001). GEP is a natural development of GP. GEP evolves computer programs of different sizes and shapes encoded in linear chromosomes of fixed-length. GEP algorithm begins with the random generation of the fixed-length chromosomes of each individual for the initial population. Then, the chromosomes are expressed and the fitness of each individual is evaluated based on the quality of the solution it represents (Özbay et al., 2008).

GP reproduces computer programs to solve problems by executing the following steps (Fig. 6.1):

- (1) Generate an initial population of random compositions of the functions and terminals of the problem (computer programs),

- (2) Execute each program in the population and assign it a fitness value according to how well it solves the problem, and
- (3) Create a new population of computer programs:
- (i) Copy the best existing programs (reproduction),
  - (ii) Create new computer programs by mutation,
  - (iii) Create new computer programs by crossover (sexual reproduction).

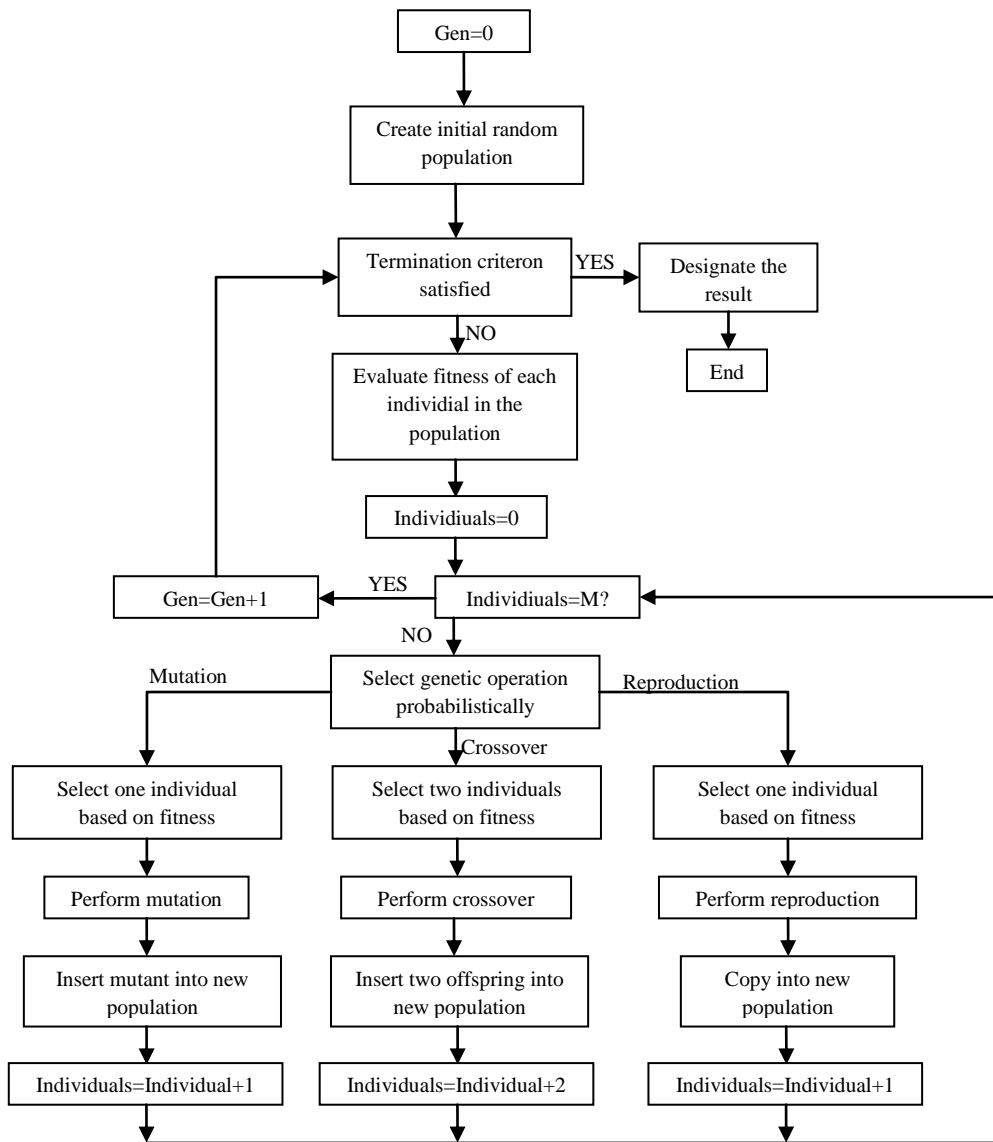


Figure 6.1 Flowchart for the genetic programming paradigm (Koza, 1992)

A significant advantage of GEP is that it makes it possible to infer exactly the phenotype given the sequence of a gene, and vice versa which is termed as Karva

language. For example, the following algebraic expression (Eq 6.1) can be represented by a diagram which is the expression tree as follows (Fig. 6.2).

$$Y = \sqrt{\sqrt{\frac{d_3}{\sin d_2 + c_1 - \ln c_1}} \times d_1} \quad (6.1)$$

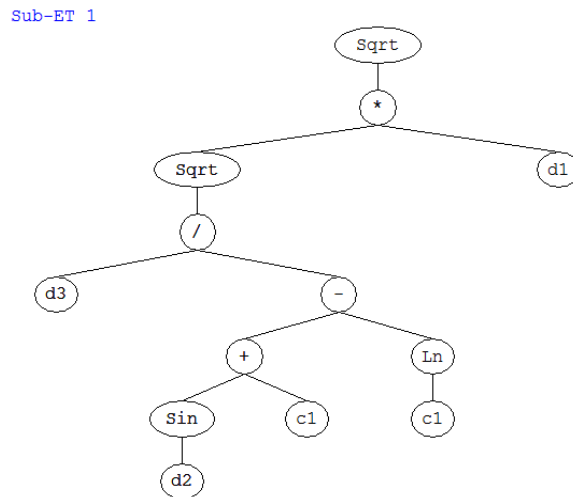


Figure 6.2 A sample sub-expression tree for a mathematical operation

### 6.3 Multiple linear regression (MLR)

In a simple linear regression model, a single response measurement  $Y$  is related to a single predictor (covariate, regressor)  $X$  for each observation. The critical assumption of the model is that the conditional mean function is linear. Multiple linear regression (MLR) is mathematical method that examines the linear relationship between 1 dependent ( $Y$ ) and 2 or more independent variables ( $X_i$ ). In most problems, more than one predictor variable will be available. This leads to the following “multiple regression” mean function (Fig. 6.3)

$$Y_i = \beta_0 + \beta_1 X_{1i} + \beta_2 X_{2i} + \dots + \beta_k X_{ki} + \epsilon$$

Y-intercept
Population slopes
Random Error

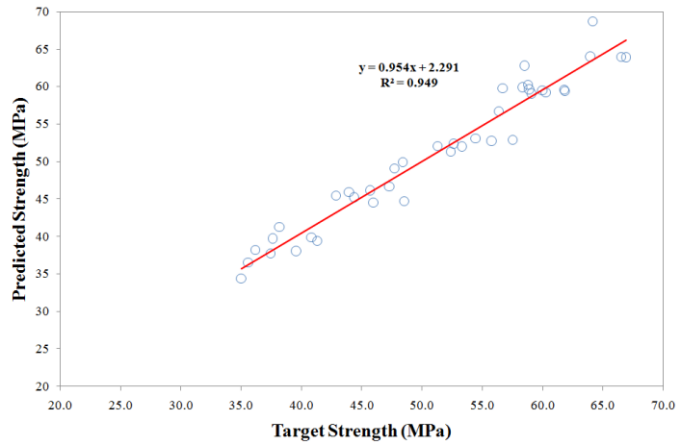
Figure 6.3 Components of MLR model

In this method, there are two main components; the dependent variable which is generally called the predictand, and the independent variables called the predictors. This method is based on least squares: the model is fit such that the sum-of-squares of differences of observed and predicted values are minimized (Arizona, 2012).

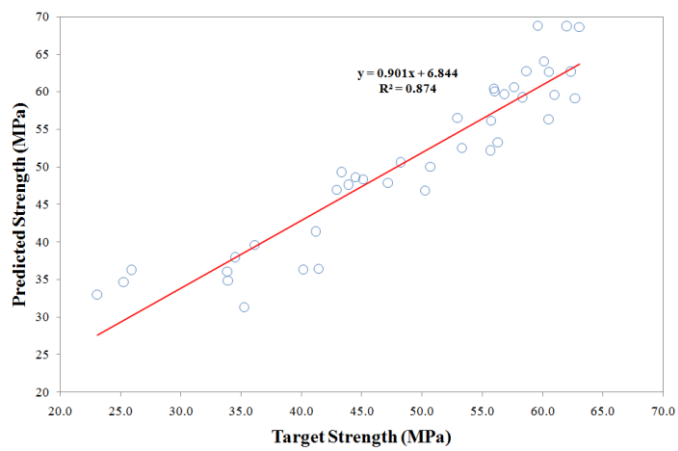
#### **6.4 Derivation of the mathematical models**

Software named GeneXproTools.4.0 was utilized for derivation of the mathematical model from gene expression programming. However for multiple linear regression model a statistical software "Minitab V15" was utilized. For GEP models the database was randomly divided in two sections to form training database and testing database. However for MLR model the whole database was used for each model. The details of the databases for prediction models were presented in "Appendix A". For constructing the prediction models the experimental results presented in this study were used. For derivation of shrinkage model, additional database from literature was also used.

Various input variables such as the chemical and mineralogical compositions of the materials, finenesses, replacement levels, testing age of concrete, chloride exposure period, number of freezing thawing cycles etc. were used for derivation of the models. The models developed for each property contain only the critical input parameter. GEP and MLR models were presented in "Appendix B". Linear correlations of the experimental and predicted data were graphically depicted in Figs. 6.4 through 6.23. On those figures correlation coefficient were also given. From critical observation of the figures, it can be inferred that GEP prediction values are highly correlated with the experimental results. The highest correlation was observed at test database for gas permeability model as  $R^2=0.962$  (Fig 6.10b) while the lowest was observed at MLR prediction model for corrosion current density  $R^2=0.433$  (Fig. 6.23)



a)



b)

Figure 6.4 Experimental vs. predicted compressive strength values from gene expression programming (GEP) model: a) Training data set and b) Testing data set

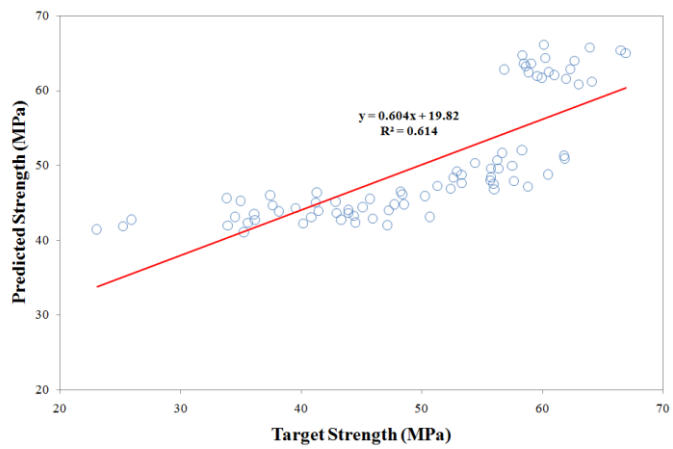
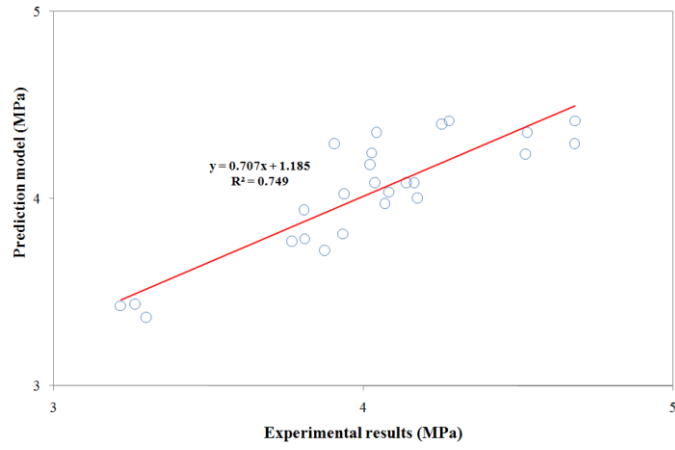
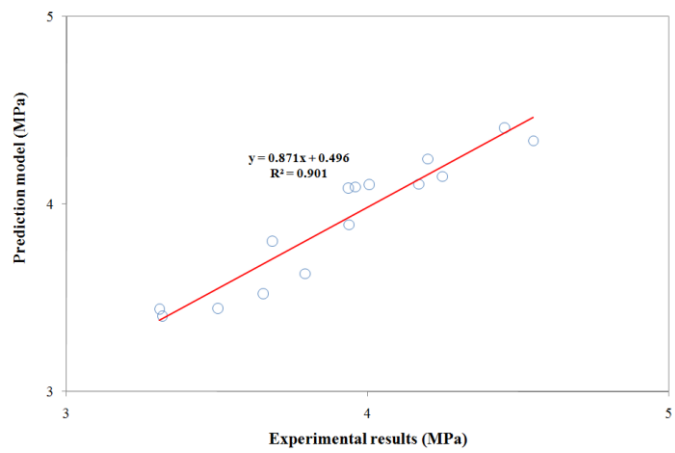


Figure 6.5 Experimental vs. predicted compressive strength values from MLR model



a)



b)

Figure 6.6 Experimental vs. predicted splitting tensile strength values from gene expression programming (GEP) model: a) Training data set and b) Testing data set

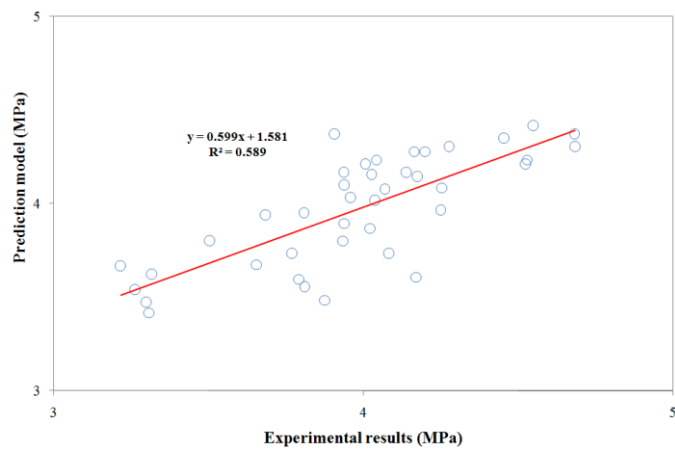
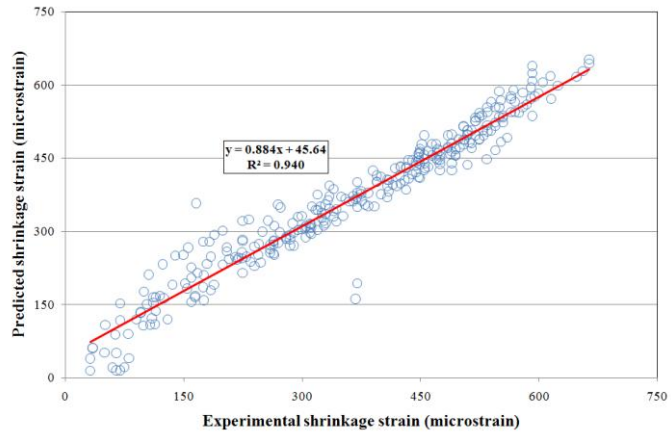
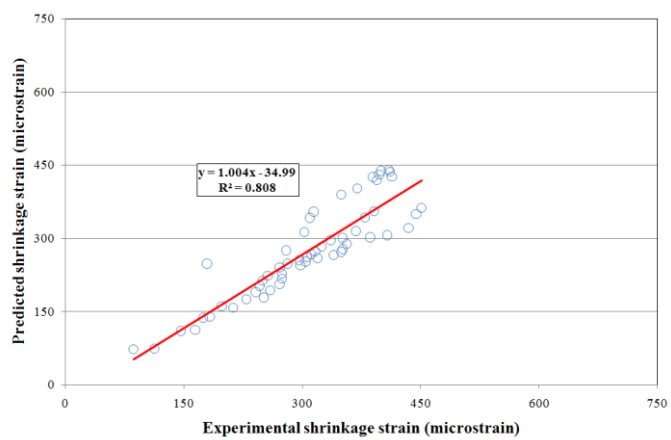


Figure 6.7 Experimental vs. predicted splitting tensile strength values from MLR model



a)



b)

Figure 6.8 Experimental vs. predicted shrinkage strain values from gene expression programming (GEP) model: a) Training data set and b) Testing data set

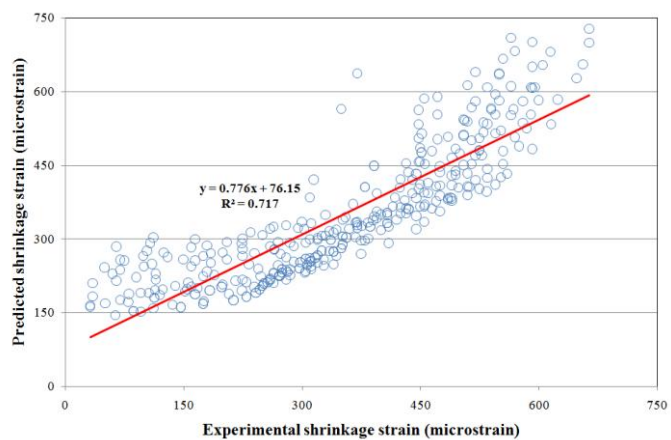
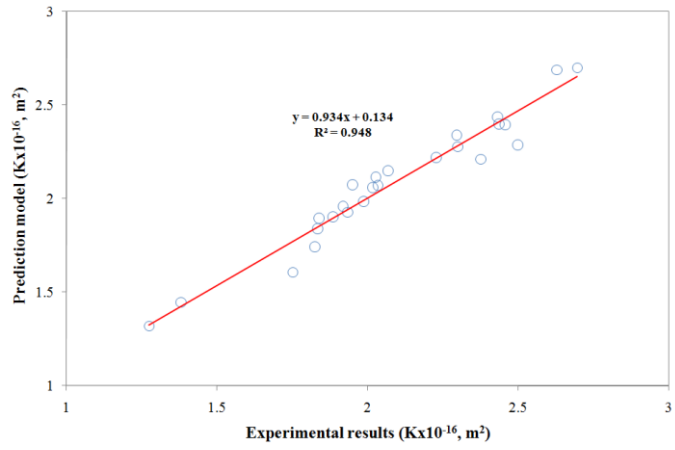
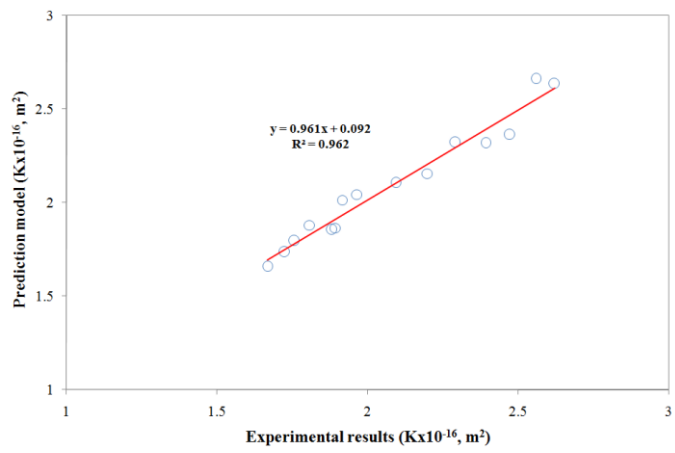


Figure 6.9 Experimental vs. predicted shrinkage strain values from MLR model





a)



b)

Figure 6.10 Experimental vs. predicted gas permeability values from gene expression programming (GEP) model: a) Training data set and b) Testing data set

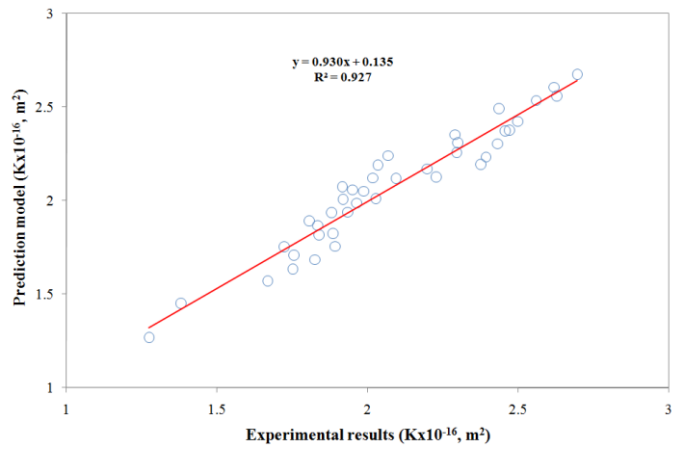
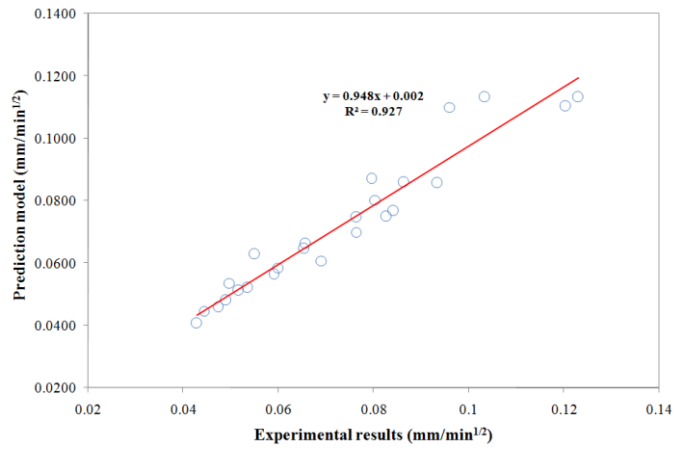
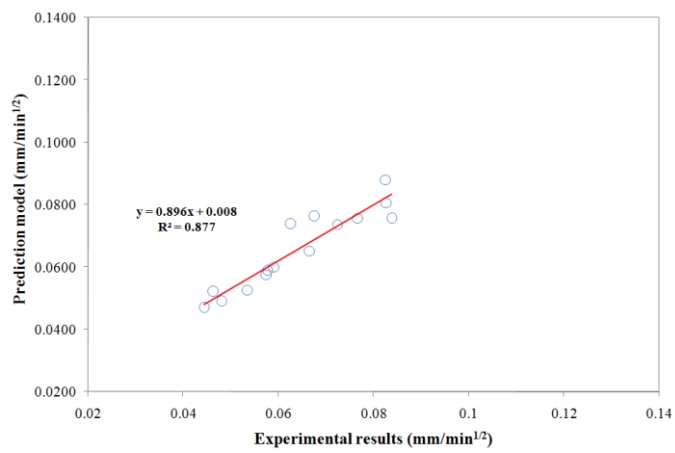


Figure 6.11 Experimental vs. predicted gas permeability values from MLR model



a)



b)

Figure 6.12 Experimental vs. predicted sorptivity values from gene expression programming (GEP) model: a) Training data set and b) Testing data set

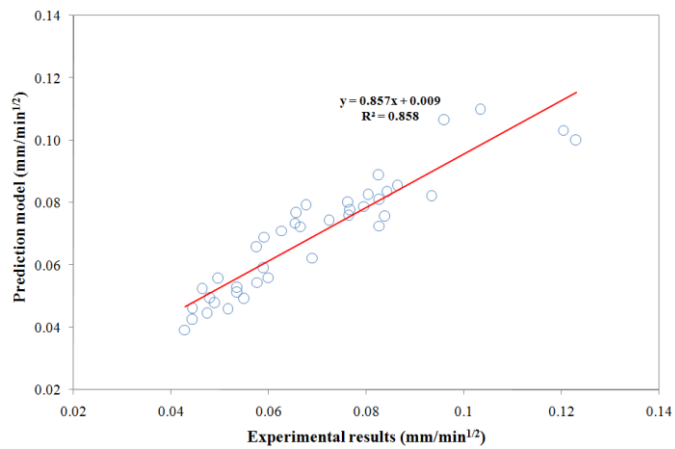
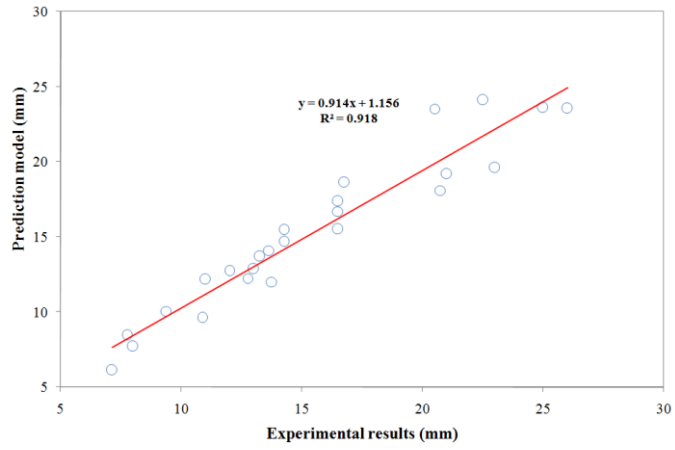
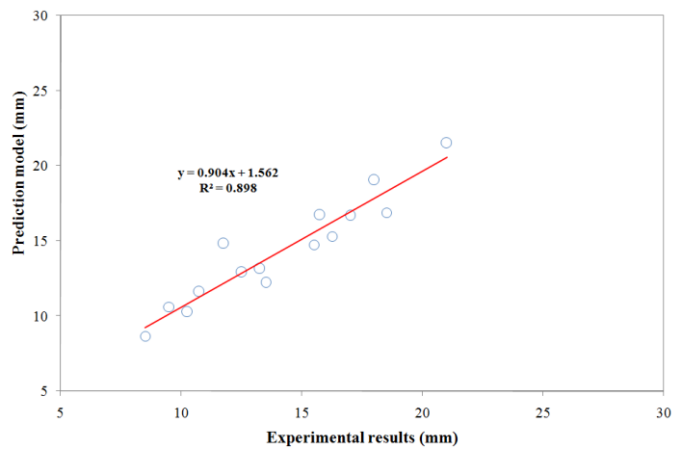


Figure 6.13 Experimental vs. predicted sorptivity values from MLR model



a)



b)

Figure 6.14 Experimental vs. predicted water permeability values from gene expression programming (GEP) model: a) Training data set and b) Testing data set

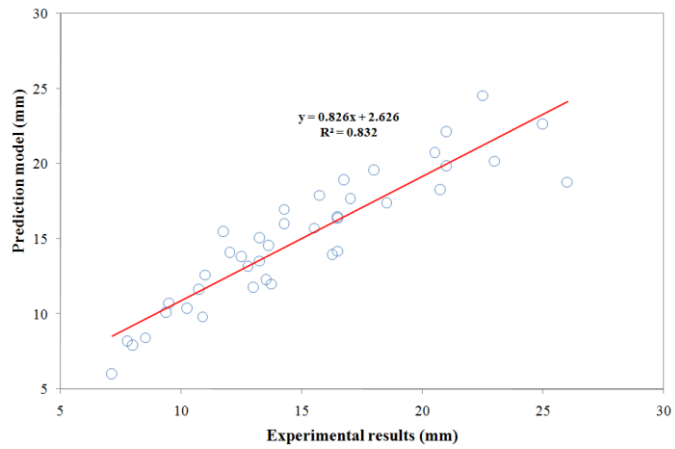
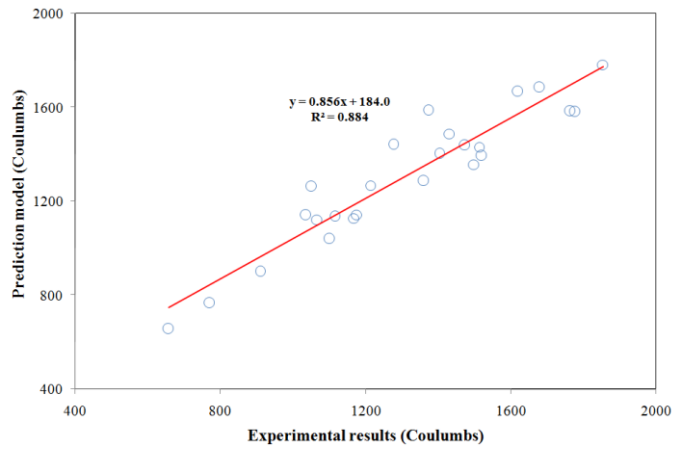
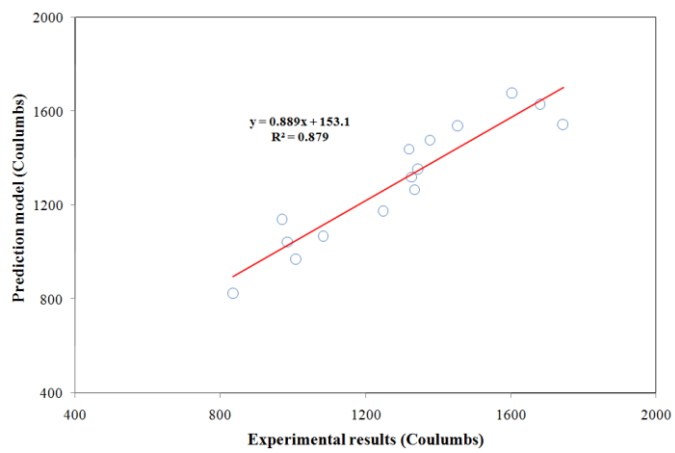


Figure 6.15 Experimental vs. predicted water permeability values from MLR model



a)



b)

Figure 6.16 Experimental vs. predicted total charge values from gene expression programming (GEP) model: a) Training data set and b) Testing data set

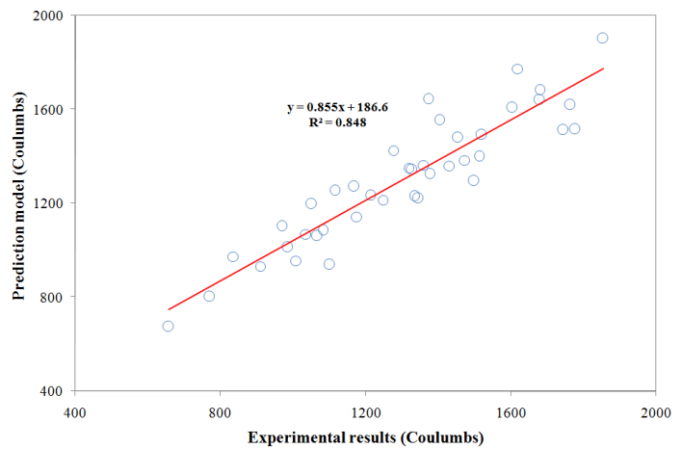
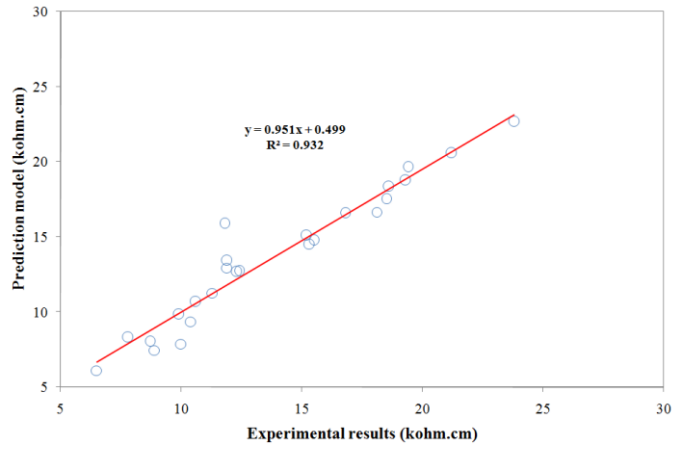
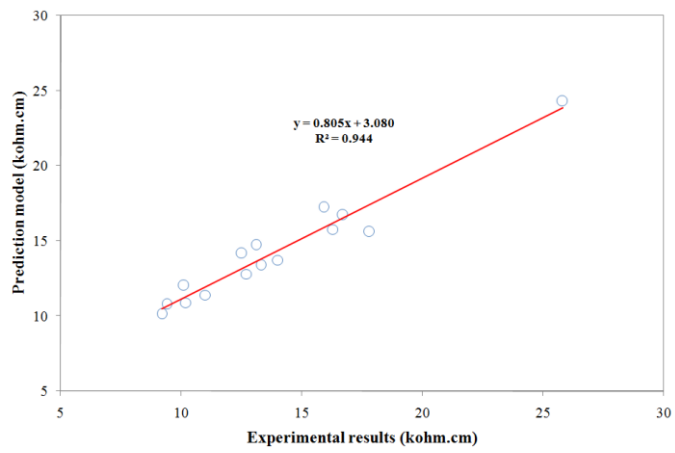


Figure 6.17 Experimental vs. predicted total charge values from MLR model



a)



b)

Figure 6.18 Experimental vs. predicted resistivity values from gene expression programming (GEP) model: a) Training data set and b) Testing data set

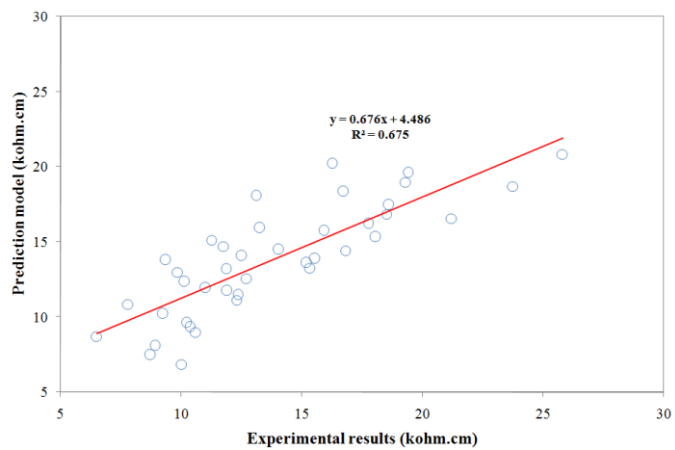
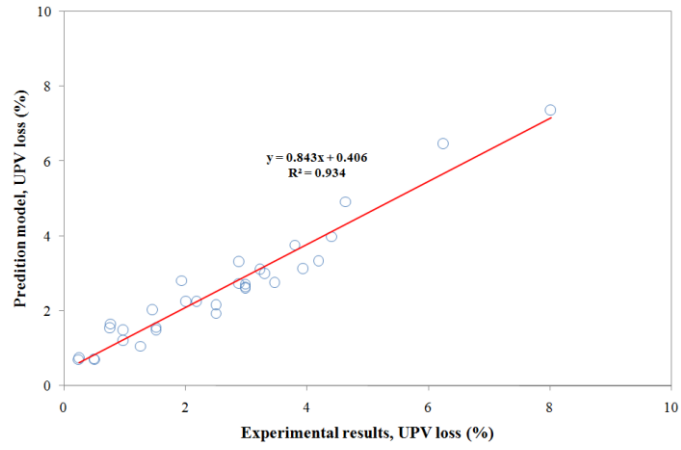
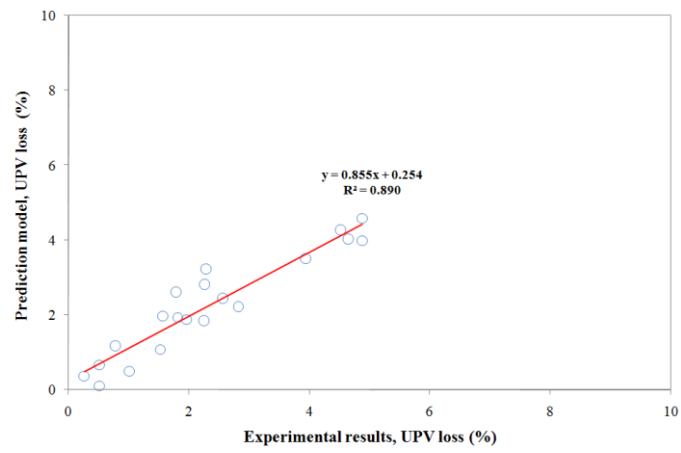


Figure 6.19 Experimental vs. predicted resistivity values from MLR model



a)



b)

Figure 6.20 Experimental vs. predicted UPV loss values from gene expression programming (GEP) model: a) Training data set and b) Testing data set

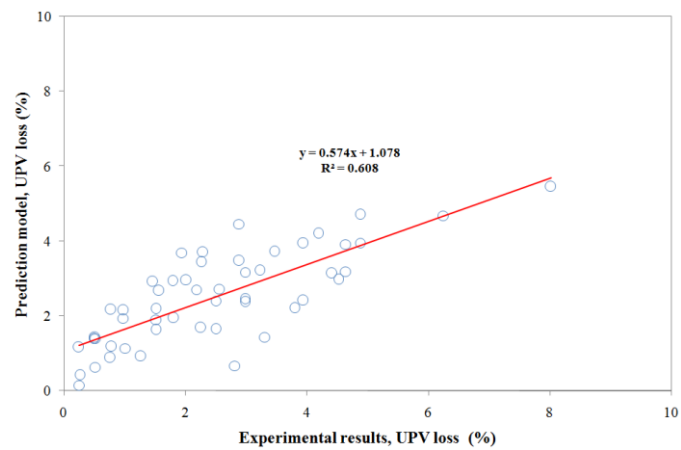
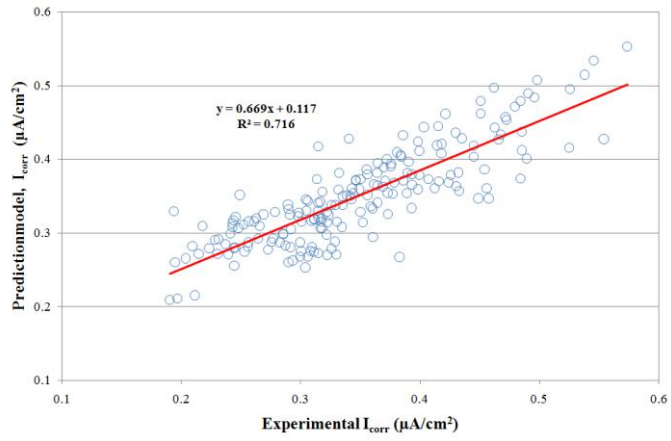
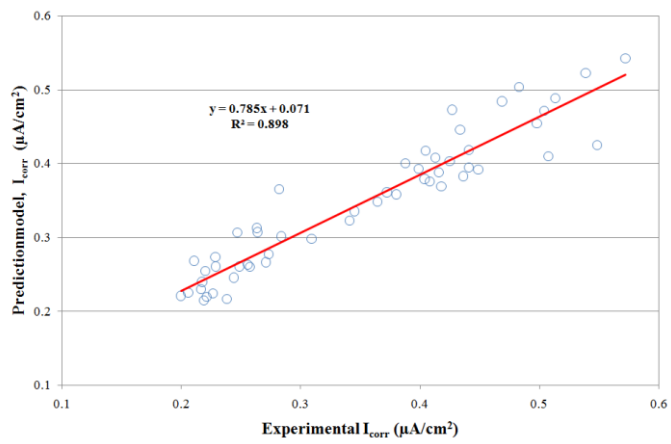


Figure 6.21 Experimental vs. predicted UPV loss values from MLR model



a)



b)

Figure 6.22 Experimental vs. predicted  $I_{corr}$  values from gene expression programming (GEP) model: a) Training data set and b) Testing data set

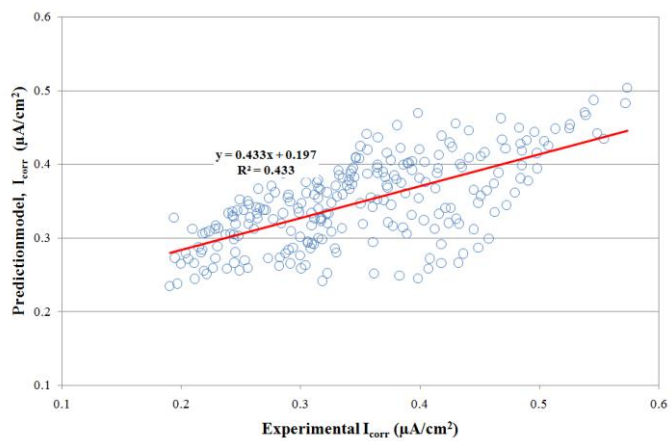


Figure 6.23 Experimental vs. predicted  $I_{corr}$  values from MLR model

## 6.5 Prediction performances of the models

The prediction performances of the developed models were evaluated through normalization of the experimental data. For this, the predicted values are divided by the experimental data to observe the robustness of the prediction model. Perfect estimation corresponds to normalized value of 1. However, the normalized values less than 1 are considered as underpredicted while the greater values are overpredicted. Experimental vs. normalized values are plotted on the graphs in Figs. 6.24 through 6.33.

For the compressive strength values lower than 30 MPa both of the models gave higher results. However the predicted compressive strength values for GEP model are generally between  $\pm 10\%$  limits of the actual value. MLR model had a decreasing tendency in prediction as the actual compressive strength values increases from 25 to 60 MPa. Unlike compressive strength prediction performance, the normalized values observed for splitting tensile strength seemed to be close to each other for GEP and MLR models (Fig 6.25).

Fig. 6.26 shows that, most of the predicted values revealed a close trend to the actual values for the GEP model. However, for the shrinkage strain values less than 250 microstrain, some of the predicted values were either underestimated or overestimated. On the other hand, for the MLR model, for the shrinkage strain values below 400 microstrain, the predicted values were generally overestimated.

Observing the prediction performances of the prediction models on permeability properties the best can be detected for gas permeability (Fig 6.27). Electrical resistivity values for GEP model were generally scattered around 1 while MLR model ranged between 0.61 and 1.48 (Fig. 6.31).

Irregular distribution of the data was observed for UPV loss values while more uniform trend in the scatter of the normalized  $I_{\text{corr}}$  values were monitored for both models (Figs. 6.32 and 6.33).



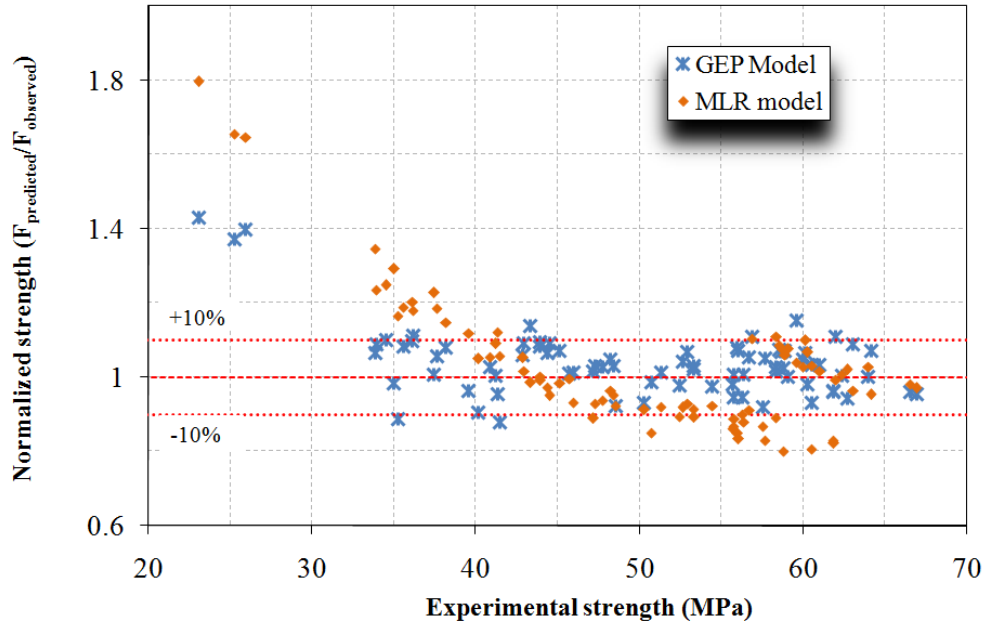


Figure 6.24 Prediction performances of GEP and MLR analytical models for compressive strength

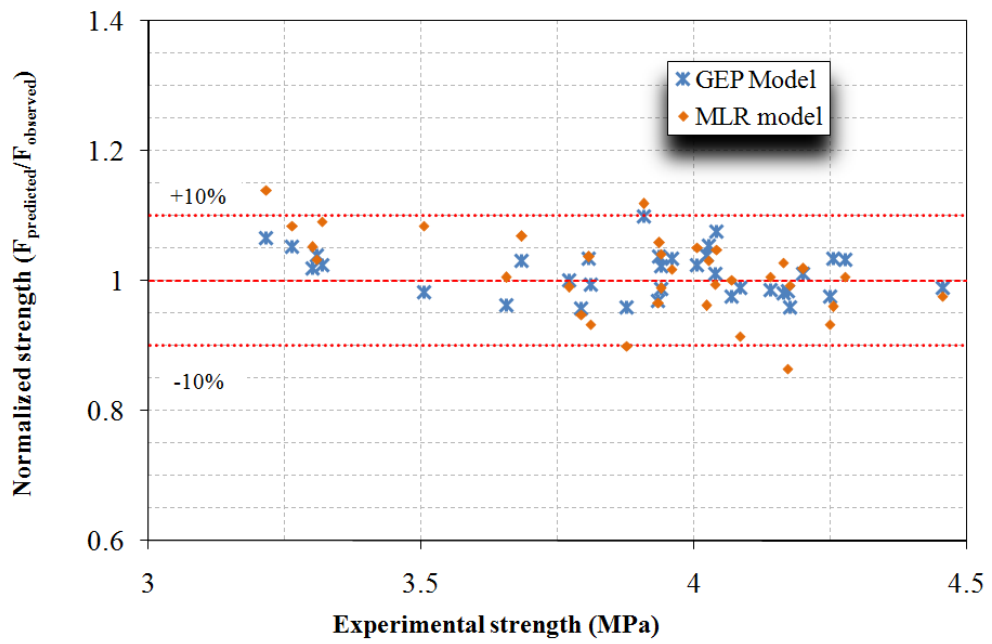
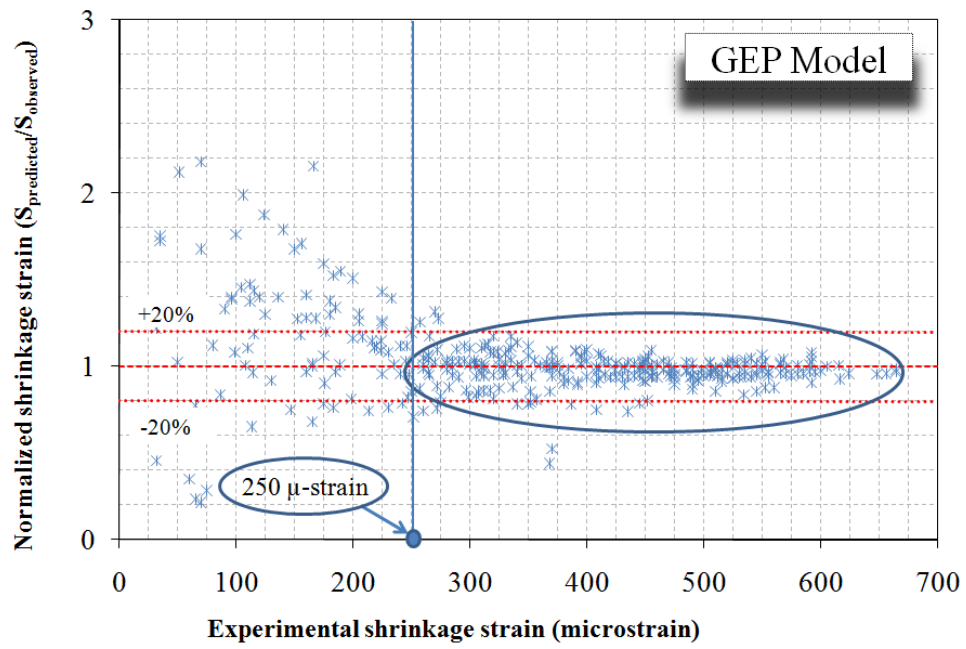
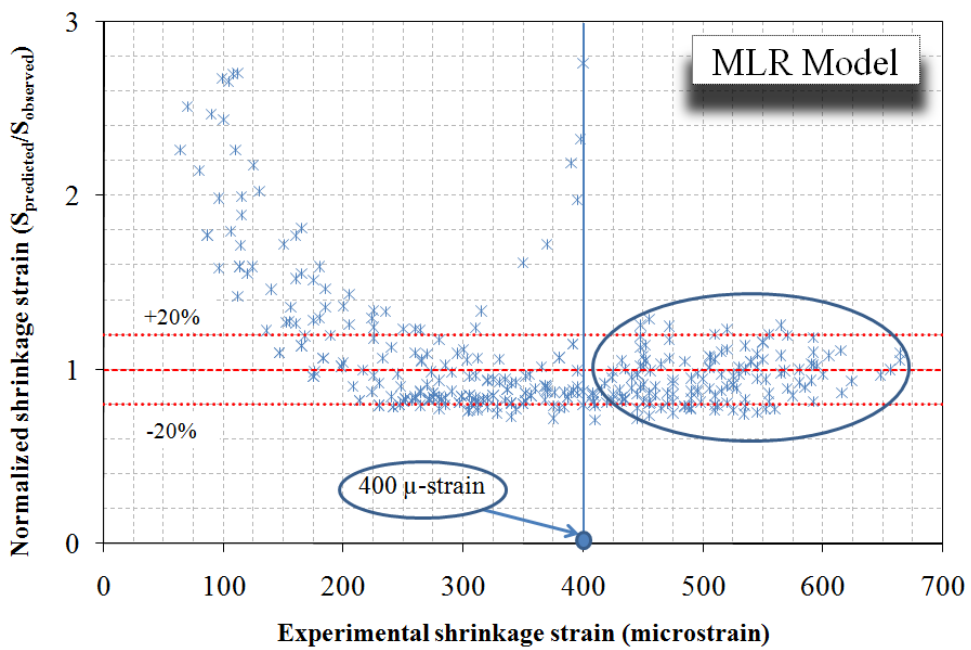


Figure 6.25 Prediction performances of GEP and MLR analytical models for splitting tensile strength



a)



b)

Figure 6.26 Prediction performances of a) GEP and b) MLR analytical models for shrinkage strain

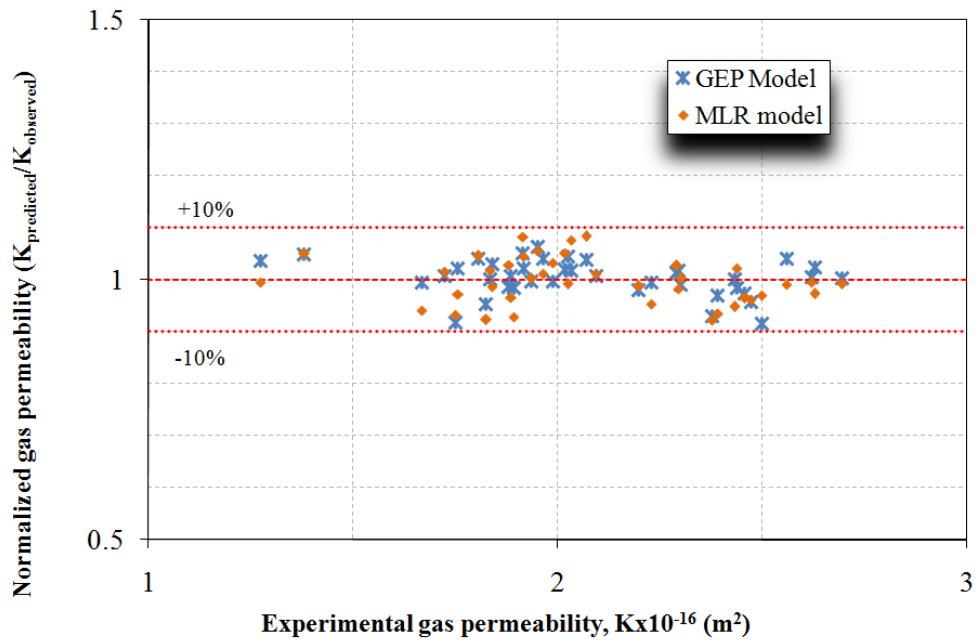


Figure 6.27 Prediction performances of GEP and MLR analytical models for gas permeability

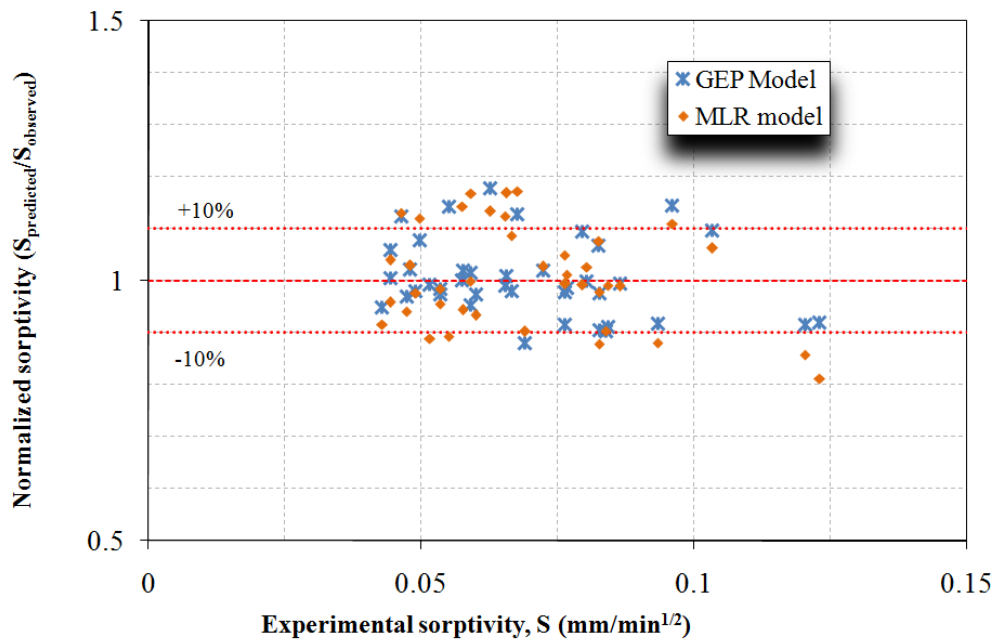


Figure 6.28 Prediction performances of GEP and MLR analytical models for water sorptivity

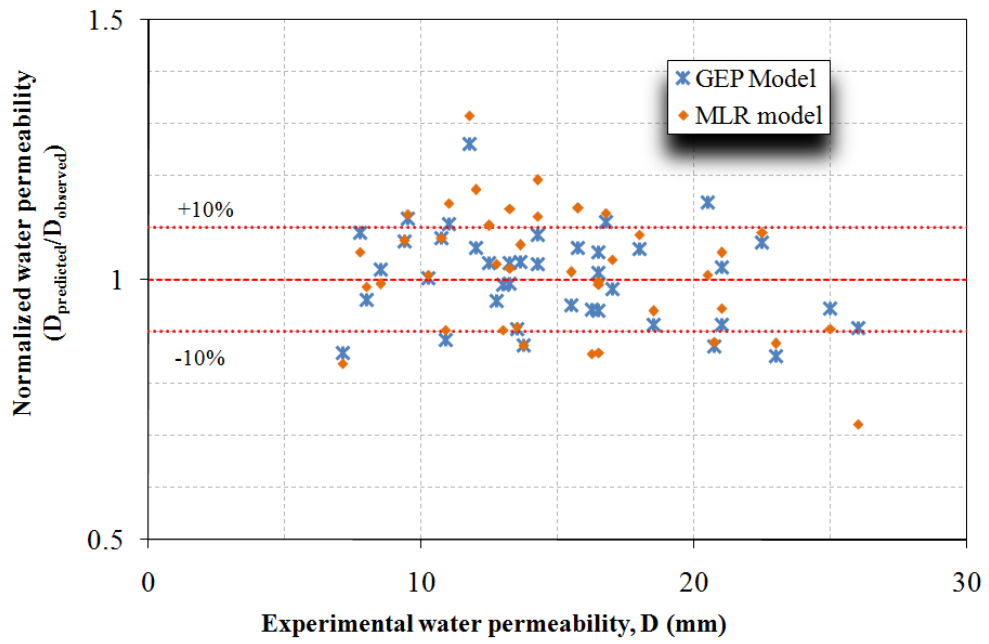


Figure 6.29 Prediction performances of GEP and MLR analytical models for water permeability

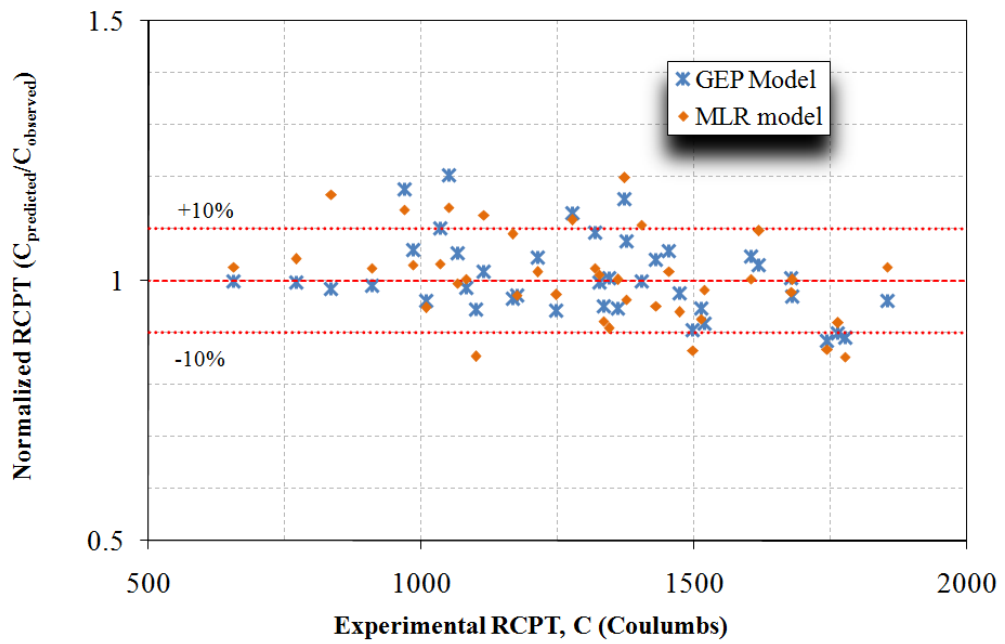


Figure 6.30 Prediction performances of GEP and MLR analytical models for rapid chloride permeability test

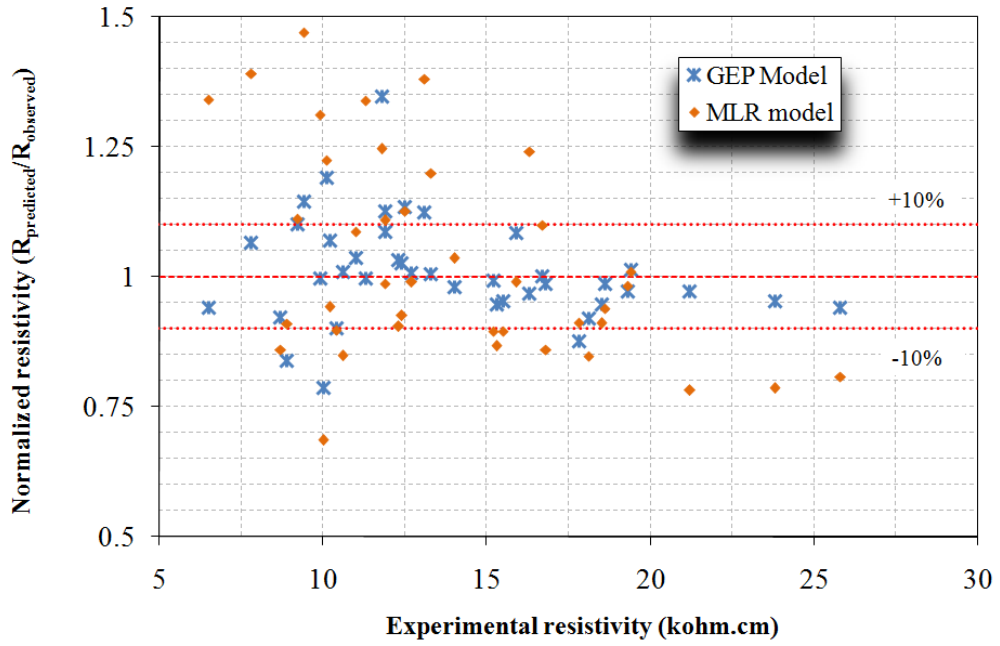


Figure 6.31 Prediction performances of GEP and MLR analytical models for electrical resistivity

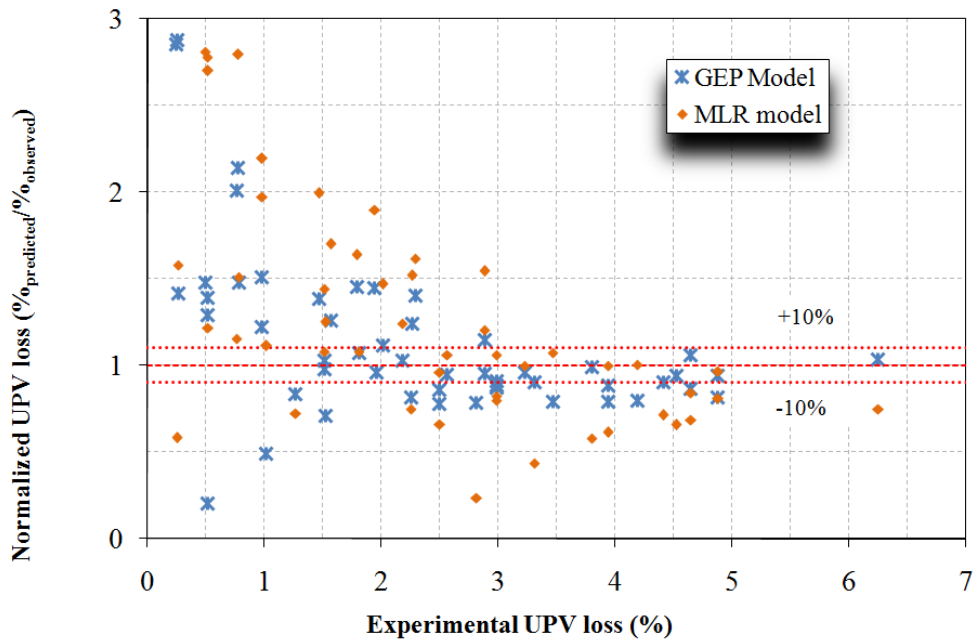
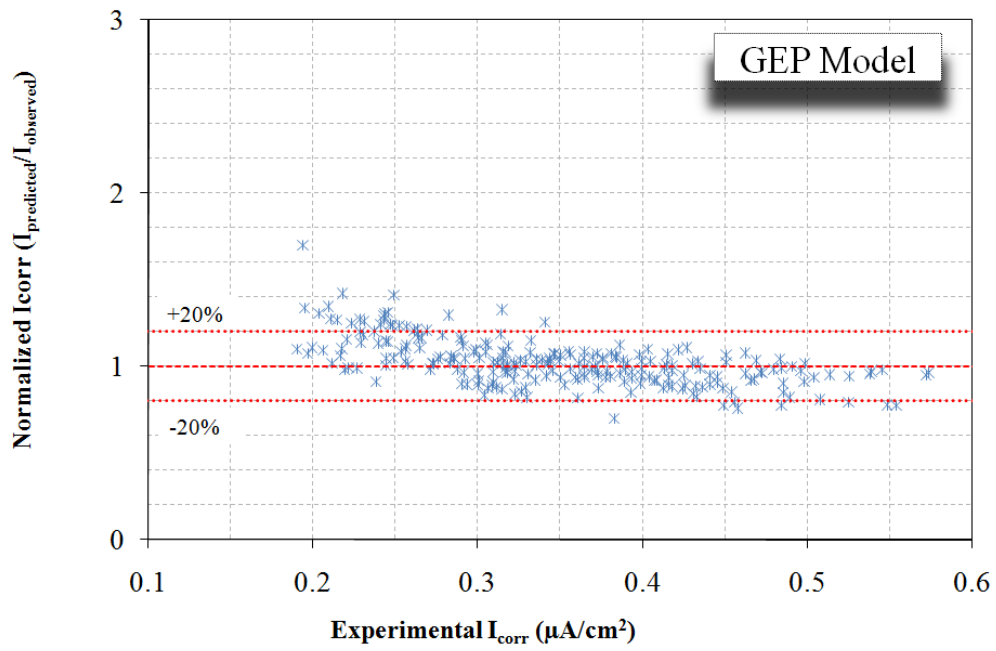
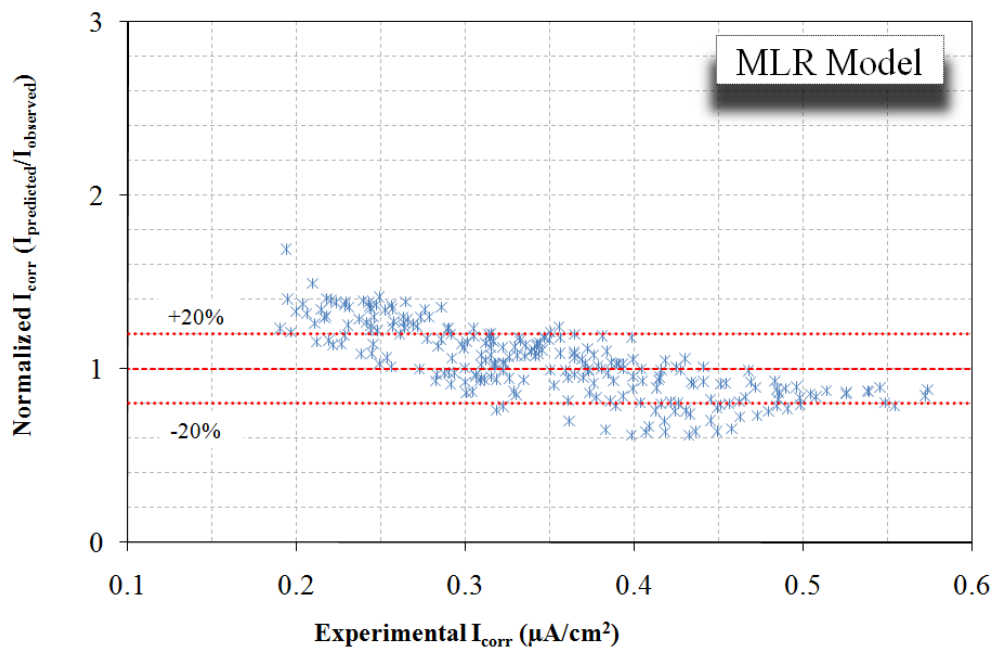


Figure 6.32 Prediction performances of GEP and MLR analytical models for UPV loss after 300 cycles of freezing and thawing



a)



b)

Figure 6.33 Prediction performances of a) GEP and b) MLR analytical models for corrosion current density ( $I_{corr}$ ) values

## **CHAPTER 7**

### **CONCLUSIONS**

#### **7.1 Introduction**

Four types of Turkish kaolins obtained from different quarries located at Balıkesir-Düvertepe (DV), Balıkesir-Danaçayırı (DC), Çanakkale-Çan (CC), and Bursa-Mustafa Kemal (BMK) were investigated in terms of microstructural properties and pozzolanic activity. After proper heat treatment, concretes containing calcined impure kaolins and commercially available high reactivity metakaolin were produced to examine mechanical and durability properties. Based on the experimental findings and analytical evaluations presented in this thesis, the following conclusions can be summarized:

#### **7.2 Microstructural characterization and pozzolanic activity of kaolins**

The following conclusions may be drawn from the first stage of the experimental study carried out on the characterization of raw and calcined kaolins.

- All of the kaolin types consist of mainly kaolinite and quartz minerals. However, BMK kaolin has a high amount of alunite (28%) and highly well-ordered crystalline structure. This situation leads to much higher calcination temperature requirement for BMK kaolin. Kaolinite content of each kaolin was plenty enough to gain pozzolanic activity.
- Because of its high alunite content, BMK kaolin had double endothermic peaks in DTA analysis, while others had single ones. The minimum and maximum endothermic peaks were respectively observed at CC and BMK kaolins as, 500 °C for the former and 780 °C for the latter. TG analysis showed that kaolins DV, DC, and CC were almost fully dehydroxylated between 700-750 °C. On the other hand, BMK kaolin maintained decomposition up to 850 °C.

- The pozzolanic activity index (PI) of the calcined kaolins revealed that maximum contribution to the compressive strength was achieved at 750 °C for calcined DV, DC, CC kaolins and at 850 °C for calcined BMK kaolin. All of the calcined kaolins satisfied ASTM C618 limit (75%) in terms of PI. The maximum PI values obtained for calcined DV, CC, DC, and BMK kaolins were 107%, 107%, 104%, and 102%, respectively.
- The weight losses of the kaolins during the calcination process were almost same as those found in TG analysis. For example, according to TG analysis, DV kaolin had 9.5% weight loss. At the end of the calcination process applied (750 °C, 3h) the weight loss of 9.2% was achieved. This situation can be taken as an evidence for the satisfactory dehydroxylation/amorphization of the kaolinite minerals existing within the kaolin.
- According to the XRD test results of the calcined kaolin samples, it was observed that kaolinite and alunite peaks were diminished, while some amount of quartz were still detected.
- When observing the fineness and particle size distribution of calcined kaolins, it was found that the major change occurred in CC kaolins at both average particle size (from 9.2 μm to 33.2 μm) and BET specific surface area (20% decrease). The other kaolins had similar reduction of the BET surface area and minor change in particle size distributions. The decreases in BET surface area were measured as 7%, 12%, and 10% for DV, DC, and BMK kaolins.
- SEM image analyses show that the particles of the kaolins become coarser due to agglomeration and formation of new bonds as a consequence of amorphization. Surface textures of the kaolins were deformed due to the physical and/or chemical decomposition.
- Based on GLM-ANOVA test result, it was seen that the calcination temperature and kaolin type were found to be effective on the pozzolanic behavior within 5% level of significance. When sequential sum of squares are taken into consideration, the contribution of the kaolin type seems to have a great importance for the pozzolanic behavior.



### 7.3 Properties of the concretes

- All four types of calcined kaolins, which were derived from unprocessed Turkish kaolins, provided similar behavior to that of the commercial metakaolin, with respect to the concrete strength development. Moreover, strength enhancement of MK modified concretes, even at early ages, were proved to be comparatively better than control concrete.
- When considering calcined kaolin incorporated concretes, 15% replacement was found to be the most effective substitution level for improving the concrete strength for 28 and 90 days of curing.
- GLM-ANOVA analysis proved that type and amount of thermally treated kaolin as well as age of concrete are effective parameters on concrete strength.
- The inclusion of MK and CK in concrete provided noticeable enhancement in gas permeability of concretes at 28 and 90 days. Calcined DV kaolin had the closest trend to MK in reduction of the gas permeability coefficients, at all replacement levels.
- The highest water penetration depth was observed for control concrete at 28 days as 26.5 mm. At 20% replacement level, CK and MK proved to be the most effective substitution level, especially at 90 days. The water penetration depth was dropped to 38%.
- Sorptivity test results revealed that 15 and 20% replacement of calcined BMK kaolin caused an increase at 28 day testing. However, at 90 days CK included concretes had systematic decrease in sorptivity with the increase in amount of the mineral admixtures used. On the other hand, the concretes with calcined DV, DC, and CC kaolins had very close sorptivity coefficients to that of MK concretes.
- The inclusions of MK and CKs had significant effect on the improvement of chloride resistance of concretes. It was noted that DV and CC concretes revealed similar trend in decreasing the level total charge passed. Nonetheless, the slight divergence in the results of these CKs may be due to the differences in the finenesses of the mineral admixtures.

- GLM-ANOVA proved that the age of concrete, type of thermally treated kaolin used and the replacement level are significantly effective on the transport properties of the concretes investigated in this study. Particularly, the replacement level of mineral admixture was statistically observed to have the major contribution on the properties tested.
- Electrical resistivity (ER) test results revealed that inclusion of MK and CK provided improvement in concretes except for 5% replacement level of BMK. BMK5 had the lowest resistivity values at both ages. However for the other replacement levels ER values were enhanced. Considering 28 day ER values, the concretes incorporating calcined DV, DC, and CC kaolins revealed similar performance as MK incorporated ones did. However, at 90 days MK incorporated concretes had relatively higher ER values than CK incorporated ones.
- Freezing and thawing cycles resulted in maximum UPV reduction of 8% in control concrete. At early periods of cycles the reductions in UPV values were insignificant for CK and MK incorporated concretes. At the end of 300 cycles of freezing and thawing, there were remarkable strength deterioration in concretes especially in terms of flexural strength. However using CKs and especially MK mitigated the damaging effect of freezing and thawing.
- Variation of corrosion current density and corresponding corrosion rate due to the chloride attack was monitored over 40 weeks of exposure period. Control concrete revealed almost same behavior for both of the NaCl exposure conditions (2% and 5%). However, incorporation of MK and CK inhibited the sharp rise in corrosion current density as a result of improvement in microstructure of concrete.
- Calcined kaolins (CKs) having various chemical and physical properties revealed comparable performance in enhancement of shrinkage strain development of concretes to metakaolin (MK). The best performances of the mineral admixtures were observed at 15% replacement level. The levels of reductions measured were 27.5%, 17.2%, 12.4%, 9.2%, and 3.7% for the concretes designated as MK15, DV15, DC15, CC15, and BMK15, respectively. The low enhancement of calcined BMK kaolin incorporated concretes was due to lower reactivity of this material as compared to others.

- As the time passed, decrease in the shrinkage rates of plain and mineral admixed concretes were observed to be power and exponential type relationship, respectively. The average shrinkage strain developments of the concretes were quickly diminished within the first two weeks and then tend to be constant at later ages. Although at 5% replacement level MK showed similar shrinkage strain rate reduction as CKs, increasing the amount to 15% resulted in a slight divergence of MK from the others.
- Weight loss variation of the concretes illustrated very close tendency to shrinkage strain development. The correlation coefficients of 0.99 for both control and MK concretes and 0.98 for CKs can be considered as an indication of strong dependence between shrinkage and weight loss. One of the other noticeable findings of this analysis is that MK incorporated concretes revealed a different behavior from CK incorporated ones in terms of the change in the amount of weight loss corresponding to the same shrinkage strain. For example, for shrinkage of 400 microstrain MK5 had 75 gr of weight loss while those of 5% CK incorporated ones were measured as  $88 \pm 2$  gr.
- GLM-ANOVA analysis proved that the type and amount of thermally treated kaolin has significant effect on shrinkage behavior of concretes. Therefore, it can be claimed that the chemical, mineralogical, and physical properties of the crude kaolins should strictly be determined before utilizing for concrete production. Despite having the highest fineness when compared to other CKs, BMK did not have considerable contribution to the improvement of shrinkage behavior of concrete due to mineralogical composition of the raw material (high alunite content).

#### **7.4 Mathematical modeling**

- A mathematical model to predict the compressive strength of concrete was derived using GEP and MLR. Since the type and fineness of the materials have noticeable effect on the concrete strength development as well as age of

concrete and replacement level, the GEP model approved the parameters regarding the material property ( $\text{SiO}_2$ ,  $\text{Al}_2\text{O}_3$ , kaolinite, alunite contents).

- The prediction models from gene expression programming (GEP) and multiple linear regression were obtained using total 358 data samples from the current study and available ones presented in the literature. The parameters considered for constructing the prediction models were calcined kaolin and concrete related properties as well as drying period. When considering training database, the models with 0.94 and 0.77 correlation coefficients for the GEP and MLR model were obtained, respectively. However, the correlation coefficient of the MLR model for testing data base was relatively less than that of the GEP model. The normalization of the predicted values has shown that for the experimental shrinkage strain values above 250 and 400 microstrain, the predicted values fell between  $\pm 20\%$  bands of the GEP and MLR models, respectively.
- The mathematical models derived for prediction of the permeability properties, demonstrated high correlation with actual values. Especially the models for gas permeability seemed to be best among the other transport properties. However both of the models developed for electrical resistivity and UPV loss revealed the poorest performance in terms of prediction capability. The predicted results were either underestimated or overestimated. Most of the predicted values obtained from GEP model for corrosion current density illustrated a close trend to that of experimental values, while MLR prediction model had decreasing tendency in estimation as actual values increased.

## REFERENCES

- Al-Amoudi, O.S.B., Maslehuddin, M., Lashari, A.N., Almusallam, A.A. (2003). Effectiveness of corrosion inhibitors in contaminated concrete. *Cem Concr Compos.* **25**,439–49.
- Aldea, C.M., Young, F., Wang, K., Shah, S.P. (2000). Effects of curing conditions on properties of concrete using slag replacement. *Cement and Concrete Research.* **30**, 465-472.
- Al-Sibahy, A., Edwards, R. (2012). Mechanical and thermal properties of novel lightweight concrete mixtures containing recycled glass and metakaolin. *Construction and Building Materials.* **31**, 157–167.
- Andrade, C., Alonso, C. (2001) On-site measurements of corrosion rate of reinforcements. *Constr Build Mater*, **15**, 141–5.
- Andrade, C., Alonso, C., Gonzalez, J.A. (1990) An initial effort to use corrosion rate measurements for estimating rebar durability. In: Berke NS, Chaker V, Whiting D, editors. *Corrosion rates of steel in concrete. ASTM STP 1065. Philadelphia: American Society for Testing and Materials*,. p. 29–37.
- Andrade, C., Alonso, C., Gonzallez, J.A. (1986) Some laboratory experiments on the inhibitor effect of sodium nitrite on reinforcement corrosion. *Cement Concrete Aggr*, **8**:110–6.
- Arazi, S.C., Krenkel T.G. (1970). Dehydroxilation heat of alunite. *The American Mineralogist*, **55**: 1329-1337.
- Arıkan, M., Sobolev, K., Ertün, T., Yeğınobalı, A., Turker, P. (2009). Properties of blended cements with thermally activated kaolin. *Construction and Building Materials*, **23**, 62-70.
- Arizona (2012) [http://www.ltrr.arizona.edu/~dmeko/notes\\_11.pdf](http://www.ltrr.arizona.edu/~dmeko/notes_11.pdf)

Asbridge, A.H., Page, C.L., Page, M.M. (2002). Effects of metakaolin, water/binder ratio and interfacial transition zones on the micro hardness of cement mortars. *Cement and Concrete Research* **32**, 1365–1369.

Asbridge, A.H., Walters, G.V., Jones, T.R. (1994) Ternary blended concretes- OPC/GGBFS/metakaolin. *Denmark: Concrete Across Borders*, pp. 547–557.

ASTM C1202 (2012) Standard Test Method for Electrical Indication of Concrete's Ability to Resist Chloride Ion Penetration. *American society for testing and materials. Annual book of ASTM standards*, **vol. 04.02**. West Conshohocken, PA: ASTM.

ASTM C157 (2008) Standard Test Method for Length Change of Hardened Hydraulic-Cement Mortar and Concrete. *American society for testing and materials. Annual book of ASTM standards*, **vol. 04.02**. West Conshohocken, PA: ASTM.

ASTM C311. (2005) Standard methods of sampling and testing fly ash or natural pozzolans for use as a mineral admixture in portland cement concrete. *American society for testing and materials. Annual book of ASTM standards*, **vol. 04.02**. West Conshohocken, PA: ASTM.

ASTM C39 (2012) Standard Test Method for Compressive Strength of Cylindrical Concrete Specimens. *American society for testing and materials. Annual book of ASTM standards*, **vol. 04.02**. West Conshohocken, PA: ASTM.

ASTM C496 (2011) Standard Test Method for Splitting Tensile Strength of Cylindrical Concrete Specimens. *American society for testing and materials. Annual book of ASTM standards*, **vol. 04.02**. West Conshohocken, PA: ASTM.

ASTM C597 (2010) Standard Test Method for Pulse Velocity Through Concrete. *American society for testing and materials. Annual book of ASTM standards*, **vol. 04.02**. West Conshohocken, PA: ASTM.

ASTM C618-08. (2008) Standard Specification for Coal Fly Ash and Raw or Calcined Natural Pozzolan for Use in Concrete 2008. *American society for*

*testing and materials. Annual book of ASTM standards*, vol. **04.02**, West Conshohocken, PA: ASTM.

ASTM C666 (2008) Standard Test Method for Resistance of Concrete to Rapid Freezing and Thawing, *American society for testing and materials. Annual book of ASTM standards*, vol. **04.02**, West Conshohocken, PA: ASTM.

Ateşok, M.G., Eygi, M.S., Özer, O. (2008) Kaolenin, polimer kullanımıyla uygun fiziksel özellikte seramik hammaddesi haline getirilebilirliğinin araştırılması. *TÜBİTAK MAG Proje 106M178*, ss 1-145.

Badogiannis, E., Kakali, G., Dimopoulou, G., Chaniotakis, E., Tsivilis, S. (2005). Metakaolin as a main cement constituent: exploitation of poor Greek kaolins. *Cem Concr Compos*, **27**, 197–203.

Badogiannis, E., Kakali, G., Tsivilis, S. (2005). Metakaolin as a supplementary cementitious material; optimization of kaolin to metakaolin conversion. *Journal of Thermal Analysis and Calorimetry*, **81**, 457–462.

Batis G., Pantazopoulou, P., Tsivilis, S., Badogiannis, E. (2005). The effect of metakaolin on the corrosion behavior of cement mortars. *Cement and Concrete Composites*, **27**, 458-467.

Bissonette, B., Pierre, P., Pigeon, M. (1999). Influence of key parameters on drying shrinkage of cementitious materials. *Cement and Concrete Research*, **29**, 1655-1662.

Bredy, P., Chabannet, M., Pera, J. (1989). Microstructural and porosity of metakaolin blended cements. *Mater. Res. Soc. Symp. Proc.* **137**, 431– 436.

Brooks, J.J., Johari M.A.M. (2001). Effect of metakaolin on creep and shrinkage of concrete. *Cement and Concrete Composite*, **23**, 495-502.

Brooks, J.J., Johari, M.A.M., Mazloom, M. (2000) Effect of admixtures on the setting times of high-strength concrete. *Cement Concr Compos*, **2**, 2293–301.

Caldarone, M.A., Gruber, K.A., Burg, R.G. (1994). High-reactivity metakaolin: a new generation mineral admixture. *Concrete International*, **16**, 37-40.

- Cassagnabère, F., Escadeillas, G., Mouret, M. (2009). Study of the reactivity of cement/metakaolin binders at early age for specific use in steam cured precast concrete. *Construction and Building Materials*, **23**, 775-784.
- Chan, S.Y.N., Ji, X. (1998). Water sorptivity and chloride diffusivity of oil shale ash concrete. *Construction and Building Materials* **12**,177-183.
- Chandrasekhar, S., Ramaswamy, S. (2002). Influence of mineral impurities on the properties of kaolin and its thermally treated products. *Applied Clay Science*, **21**, 133– 142.
- Chen, D., Mahadevan, S. (2008) Chloride-induced reinforcement corrosion and concrete cracking simulation. *Cement & Concrete Composites*, **30**, 227–238.
- Chen, W., Liu, J., Brue, F., Skoczylas, F., Davy, C.A., Bourbon, X., Talandier, J. (2012).Water retention and gas relative permeability of two industrial concretes. *Cement and Concrete Research* **42**, 1001–1013.
- Chindaprasirt, P., Chotithanormç, C., Cao, H.T., Sirivivatnanon, V. (2007) Influence of fly ash fineness on the chloride penetration of concrete. *Cons Build Mat*, **21**, 356-61.
- Chindaprasirt, P., Homwuttiwong, S., Sirivivatnanon, V. (2004) Influence of fly ash fineness on strength, drying shrinkage and sulfate resistance of blended cement mortar. *Cement and Concrete Research*, **34**, 1087-1092.
- Coleman, N.J., Page, C.L. (1997) Aspects of the pore solution chemistry of hydrated cement pastes containing metakaolin. *Cement & Concrete Research*, **27**, 147-154.
- Cook, D.J. (1986). Calcined Clay, Shale, and Other Soils. *In: R.N. Swamy (Ed.), Cement Replacement Materials*, Surrey University Press, 40-72
- DIN 1048 Part 5 (1991) Testing concrete, Testing of hardened concrete
- Ding, J., Li, Z. (2002) Effects of metakaolin and silica fume on properties of concrete. *ACI Mat. Journal*, **99**, 393-398.



- El-Gelany, M.A. (2001). Short-term corrosion rate measurement of OPC and HPC reinforced concrete specimens by electrochemical techniques. *Materials and Structures*, **34**, 426–32.
- Elsener, B. (2002). Macrocell corrosion of steel in concrete-implications for corrosion monitoring. *Cement and Concrete Composites*, **24**, 65–72.
- Ferreira, C. (2001). Gene expression programming: a new adaptive algorithm for solving problems. *Complex Systems*, **13**, 87-129.
- Frias, M., Cabrera, J. (2001). Influence of MK on the reaction kinetics in MK/lime and MK-blended cement systems at 20 °C. *Cement and Concrete Research*, **31**, 519-527.
- Gamiz, E., Melgosa, M., Maranon, M.S., Garcia, J.M.M., Delgado, R. (2005). Relationships between chemico-mineralogical composition and color properties in selected natural and calcined Spanish kaolins. *Applied Clay Science*, **28**, 269-282
- Goldberg, D. (1989) Genetic Algorithms in search, optimization and machine learning. MA: Addison-Welsley.
- Gonzalez, J.A., Feliu, S., Rodriguez, P., Ramirez, E., Alonso, C., Andrade, C. (1996). Some questions on the corrosion of steel in concrete Part I: when, how and how much steel corrodes. *Mater Struct*, **29**, 40–46.
- Güneyisi, E., Gesoğlu, M., Karaoğlu, S., Mermerdaş, K. (2012) Strength, permeability and shrinkage cracking of silica fume and metakaolin concretes. *Construction and Building Materials*, **34**, 120-130.
- Güneyisi, E., Gesoğlu, M., Karaboğa, F., Mermerdaş, K. (2012). Corrosion behaviour of reinforcing steel embedded in chloride contaminated concretes with and without metakaolin. *Composites Part B: Engineering*, **45**, 1288-1295.
- Güneyisi, E., Gesoğlu, M., Mermerdaş, K. (2008). Improving strength, drying shrinkage, and pore structure of concrete using metakaolin. *Material and Structures*, **41**, 937-949.

Güneyisi, E., Gesoğlu, M., Mermerdaş, K. (2010). Strength deterioration of plain and metakaolin concretes in aggressive sulfate environments. *ASCE Journal of Materials in Civil Engineering*, **22**, 403-407.

Güneyisi, E., Gesoğlu, M., Özbay, E. (2010) Strength and drying shrinkage properties of self-compacting concretes incorporating multi-system blended mineral admixtures. *Construction and Building Materials*, **24**, 1878–1887.

Güneyisi, E., Gesoğlu, M., Özbay, E. (2011) Permeation Properties of Self-Consolidating Concretes with Mineral Admixtures. *ACI Materials Journal* **108**, 150-158.

Güneyisi, E., Mermerdaş, K. (2007). Comparative study on strength, sorptivity, and chloride ingress characteristics of air-cured and water-cured concretes modified with metakaolin. *Materials and Structures*, **40**, 1161-1171.

Güneyisi, E., Özturan, T., Gesoğlu, M. (2005). A study on reinforcement corrosion and related properties of plain and blended cement concretes under different curing conditions. *Cement and Concrete Composites*, **27**: 449-461.

Hassan, A.A.A., Lachemi, M., Hossain, K.M.A. (2012) Effect of metakaolin and silica fume on the durability of self-consolidating concrete. *Cement & Concrete Composites*, **34**, 801–807

Hope, B.B., Page, J.A., Ip A.K.C. (1986). Corrosion rates of steel in concrete. *Cement and Concrete Research*, **16**, 771–81.

Ismail, M., Ohtsu, M. (2006) Corrosion rate of ordinary and high-performance concrete subjected to chloride attack by AC impedance spectroscopy. *Construction and Building Materials*, **20**, 458–469.

Kakali, G., Perraki, T., Tsivilis, S., Badogiannis, E. (2001). Thermal treatment of kaolin: the effect of mineralogy on the pozzolanic activity. *Applied Clay Science*, **20**, 73-80.

- Kaloumenou, M., Badogiannis, E., Tsvivilis, S., Kakali, G. (1999). Effect of the kaolin particle size on the pozzolanic behaviour of the metakaolinite produced. *Journal of Thermal Analysis and Calorimetry*, **56**: 901–907.
- Khatib, J.M, Clay, R.M (2004). Absorption characteristics of metakaolin concrete. *Cement and Concrete Research*, **34**, 19-29.
- Khatib, J.M. and Wild, S. (1996). Pore size distribution of metakaolin paste. *Cement and Concrete Research*, **26**, 1545–1553.
- Khatri, R.P., Sirivivatnanon, V., Yu, L.K. (1997). Effect of curing on water permeability of concretes prepared with normal Portland cement and with slag and silica fume. *Magazine of Concrete Research*, **49**, 162-172.
- Kim, H.S., Lee, S.H., Moon, H.Y. (2007). Strength properties and durability aspects of high strength concrete using Korean metakaolin. *Construction and Building Materials* **21**, 1229-1237.
- Konar , A. (1999). Artificial Intelligence and Soft Computing , CRC Press
- Kostuch, J.A., Walters, G.V., Jones, T.R. (1993). High performance concrete incorporating metakaolin – a review. *Concrete 2000*, University of Dundee, pp. 1799–1811.
- Koza, J.R. (1992). Genetic programming: On the programming of computers by means of natural selection. MIT Press.
- Krieg, W. (2008). Rapid chloride permeability testing, a critical review. *Proc Concr Hot Aggressive Environ*, 147–56.
- Lambert, P., Page, C.L., Vassie, P.R.W. (1991) Investigations of reinforcement corrosion: electrochemical monitoring of steel in chloride contaminated concrete. *Materials and Structures*, **24**, 351–8.
- Larbi. J.A., Bijen, J.M. (1992). Influence of pozzolans on the portland cement paste– aggregate interface in relation to diffusion of ions and water absorption in concrete. *Cement and Concrete. Research*. **22**, 551–562.

- Lee, S.T., Moon, H.Y., Hooton, R.D., Kim, J.P. (2005). Effect of sodium concentration and replacement levels of metakaolin on the resistance of mortars exposed to magnesium sulfate solutions. *Cement and Concrete Research*, **35**, 1545-1553.
- Liu, T., Weyers, R.W. (1998) Modeling the dynamic corrosion process in chloride contaminated concrete structures. *Cem Concr Res*, **28**, 365–79.
- Liu, Y. (1996) Modeling the Time-to-Corrosion Cracking of the Cover Concrete in Chloride Contaminated Reinforced Concrete Structures. *PhD thesis*, Virginia Polytechnic Institute and State University, USA.
- Madandoust, R., Mousavi, S.Y. (2012) Fresh and hardened properties of self-compacting concrete containing metakaolin. *Construction and Building Materials* **35**, 752–760.
- Maheswaran, T., Sanjayan, J.G. (2004) A semi-closed-form solution for chloride diffusion in concrete with time-varying parameters. *Magazine of Concrete Research*, **56**, 359–66.
- Maslehuddin, M., Al-Amoudi, O.S.B. (1992). Corrosion of reinforcing steel in concrete: its monitoring and prevention. *Preprint, Symposium on Corrosion and its Control, King Saud University, Riyadh*, 80–90.
- Mehta, P.K., Monteiro, P. (1997). *Concrete*. Indian Edition, University of California, Berkeley.
- Melo, K.A., Carneiro, A.M.P. (2010). Effect of Metakaolin's finesses and content in self-consolidating concrete. *Construction and Building Materials*, **24**, 1529–1535.
- Menadi, B., Kenai, S., Khatib, J., Ait-Mokhtar, A. (2009). Strength and durability of concrete incorporating crushed limestone sand. *Construction and Building Materials*, **23**, 625–633.

- Mermerdaş, K. (2006). Effectiveness of metakaolin on the strength and durability properties of air-cured and water-cured concretes. *MSc thesis*, Gaziantep University, Gaziantep.
- Mermerdaş, K., Gesoğlu, M., Güneyisi, E., Özturan, T. (2012) Strength development of concretes incorporated with metakaolin and different types of calcined kaolins. *Construction and Building Materials*, **37**, 766–774.
- Moon, H.Y., Shin, K.J. (2007). Frost attack resistance and steel bar corrosion of antiwashout underwater concrete containing mineral admixtures, *Construction and Building Materials*, **21**, 98-108
- Moulin, E., Blanc, P., Sorrentino, D. (2001). Influence of key cement chemical parameters on the properties of metakaolin blended cements. *Cem Concr Compos*, **23**, 463–9.
- Murat, M. (1983). Hydration reaction and hardening of calcined clays and related minerals: II. Influence of mineralogical properties of the raw-kaolinite on the reactivity of metakaolinite. *Cement and Concrete Research*, **13**, 511–518.
- Naveen, K.C., John, K.V., Vengala, J., and Ranganath, R.V. (2006). Self-compacting concrete with fly ash and metakaolin. *Indian Concrete Journal*, **80**, 33-39
- Neville, A.M. (1996). Properties of Concrete, 4<sup>th</sup> and final ed. Addison Wesley Logman, England
- Oriol, M., Pera, J. (1995). Pozzolanic activity of metakaolin under microwave treatment. *Cement and Concrete Research* **25**, 265–270.
- Özbay, E., Gesoğlu, M., Güneyisi, E. (2008) Empirical modeling of fresh and hardened properties of self-compacting concretes by genetic programming. *Construction and Building Materials*, **22**, 1831–1840.
- Parande, A.K., Babu, B.R., Karthik, M.A., Deepak, K.K.K., Palaniswamy, N. (2008). Study on strength and corrosion performance for steel embedded in

metakaolin blended concrete/mortar. *Construction and Building Materials*, **22**, 127–134.

Pham, D.T. and Pham, P.T.N. (1999). Artificial intelligence in engineering, *International Journal of Machine Tools & Manufacture*, 937–949

Poon, C.S., Kou, S.C., Lam, L. (2006). Compressive Strength, Chloride Diffusivity and Pore Structure of High Performance Metakaolin and Silica Fume Concrete. *Construction and Building Materials*, **10**, 858-865

Poon, C.S., Lam, L., Kou, S.C., Wong, Y.L., Wong, R. (2001). Rate of pozzolanic reaction of metakaolin in high-performance cement pastes. *Cement and Concrete Research* **31**, 1301–1306.

Pradhan, B., Bhattacharjee, B. (2009) Performance evaluation of rebar in chloride contaminated concrete by corrosion rate. *Construction and Building Materials*, **23**, 2346–2356.

Qian, X., Li, Z. (2001) The relationships between stress and strain for high-performance concrete with metakaolin. *Cement and Concrete Research*, **31**, 1607–1611.

Ramezani pour, A.A., Jovein, H.B. (2012) Influence of metakaolin as supplementary cementing material on strength and durability of concretes. *Construction and Building Materials* 30 (2012) 470–479

Ramezani pour, A.A., Malhotra, V.M. (1995). Effect of curing on the compressive strength, resistance to chloride ion penetration and porosity of concretes incorporating slag, fly ash, or silica fume. *Cement and Concrete Composites*, **17**, 125–33.

Ramezani pour, A.A., Pilvar, A., Mahdikhani, M., Moodi, F. (2011) Practical evaluation of relationship between concrete resistivity, water penetration, rapid chloride penetration and compressive strength. *Constr Build Mater*, **25**, 2472–9.

RILEM TC 116-PCD. (1999). Permeability of concrete as a criterion of its durability. *Mat Struc*, **32**, 174-179.

Rodriguez, P, Ramirez, E., Gonzalez, J.A. (1994). Methods for studying corrosion in reinforced concrete. *Mag Concr Res*, **46**, 81–90.

Sabir, B.B., Wild, S, Khatib, J.M. (1996). On the Workability and Strength Development of Metakaolin Concrete, *Concrete for Environmental Enhancement and Protection*, R. K. Dhir and T. D. Dyer, eds., E&FN Spon, London, UK, pp. 651-656.

Sabir, B.B., Wild, S., Bai, J. (2001). Metakaolin and Calcined Clay as Pozzolans for Concrete: A Review. *Cement and Concrete Composites* **23**, 441-454.

Shekarchi M., Bonakdar A., Bakhshi M., Mirdamadi A., Mobasher B. (2010) Transport properties in metakaolin blended concrete. *Construction and Building Materials*, **24**, 2217–2223.

Shvarzman, A., Kovler, K., Grader. G.S., Shter, G.E. (2003). The effect of dehydroxylation/amorphization degree on pozzolanic activity of kaolinite. *Cement and Concrete Research*, **31**, 405-416.

Singh, M., Garg, M. (2006). Reactive pozzolana from Indian clays—their use in cement mortars. *Cement and Concrete Research*, **36**, 1903–1907

Snyder, K.A. (2000). Effect of drying shrinkage cracks and flexural cracks on concrete bulk permeability. *National Institute of Standards and Technology*. Technology Administration U.S. Department of Commerce

Stern, M., Geary, A.L. (1957) A theoretical analysis of the slope of the polarization curves. *J Electrochem Soc*, **104**:56–63.

Taylor, H.F.W (1997) *Cement Chemistry* (2nd edition), *Thomas Telford Publishing*.

Thomas, M.D.A, Hooton, R.D., Scott, A., Zibara, H. (2012) The effect of supplementary cementitious materials on chloride binding in hardened cement paste. *Cement and Concrete Research*, **42**, 1-7.

TS EN 12390-8 (2002) Testing Hardened Concrete—Part 8: Depth of Penetration of Water under Pressure. *Institute of Turkish Standards*, Ankara, Turkey

Tuutti, K. (1982) Corrosion of Steel in Concrete. CBI *Swedish Cement and Concrete Research Institute*, Stockholm, Sweden 159 pp.

Vejmelkova, E., Keppert, M., Grzeszczyk, S., Skalinski, B., Cerny, R. (2011). Properties of self-compacting concrete mixtures containing metakaolin and blast furnace slag. *Construction and Building Materials*, **25**, 1325–1331.

Vejmelková, E., Pavlíková, M., Keppert M, Keršner Z, Rovnaníková P, Ondráček M, Sedlmajer M, Cerný R. (2010). High performance concrete with Czech metakaolin: Experimental analysis of strength, toughness and durability characteristics. *Construction and Building Materials*, **24**, 1404–1411.

Vizcayno, C., de Gutiérrez, R.M., Castello, R., Rodriguez, E., Guerrero, C.E. 2010. Pozzolan obtained by mechanochemical and thermal treatments of kaolin. *Applied Clay Science* 49:405-413.

Wee, T.H., Suryavanshi, A.K., Tin, S.S. (2000) Evaluation of rapid chloride permeability test (RCPT) results for concrete containing mineral admixtures. *ACI Mater J*, **97**, 221–32.

Wiegink, K., Marikunte, S., Shah, S.P. (1996) Shrinkage cracking of high-strength concrete. *ACI Mater J*, **93**, 1–8.

Wikipedia (2008) [http://en.wikipedia.org/wiki/Mathematical\\_model](http://en.wikipedia.org/wiki/Mathematical_model)

Wild, S., Khatib, J.M. (1997). Portlandite consumption in metakaolin cement pastes and mortars. *Cement and Concrete Research*, **27**, 127–146.

Wild, S., Khatib, J.M., Jones, A. (1996). Relative strength, pozzolanic activity and cement hydration in superplasticized metakaolin concrete. *Cement and Concrete Research*, **26**, 1537–1544.

Yanık, G., Esenli, F., Uz, V., Esenli, V., Uz, B., Külah, T. (2010). Ceramic properties of kaolinized tuffaceous rocks in Kesan region, Thrace, NW Turkey. *Applied Clay Science*, **48**, 499–505.

Zadeh, L.A. (1994) Soft computing and fuzzy logic. *IEEE Software*, **11**, 48–56



Zhang M.H., V.M. Malhotra (1995). Characteristics of a thermally activated alumino-silicate pozzolanic material ant its use in concrete. *Cement and Concrete Research*, **25**, 1713-1725.

**APPENDIX A**  
**Input and output databases**

Table A1 Input and output database for compressive strength (training set)

Replacement level	Age	SiO <sub>2</sub> *	Al <sub>2</sub> O <sub>3</sub> *	Kaolinite *	Alunite *	Fineness	Compressive strength
5	3	63.7	22.1	54	2	7.3	38.2
5	7	63.7	22.1	54	2	7.3	47.7
5	28	63.7	22.1	54	2	7.3	56.4
5	90	63.7	22.1	54	2	7.3	58.5
5	3	53	43	95	0	18	41.3
5	7	53	43	95	0	18	51.3
5	28	53	43	95	0	18	58.3
5	3	44.8	26.7	46	28	7.4	40.8
5	7	44.8	26.7	46	28	7.4	47.3
10	3	62.9	23.6	54	4	4.5	37.6
10	7	62.9	23.6	54	4	4.5	45.7
10	28	62.9	23.6	54	4	4.5	54.4
10	90	62.9	23.6	54	4	4.5	60.3
10	3	53	43	95	0	18	37.4
10	7	53	43	95	0	18	52.4
10	28	53	43	95	0	18	56.7
10	90	53	43	95	0	18	64
10	3	44.8	26.7	46	28	7.4	36.2
10	7	44.8	26.7	46	28	7.4	43.9
10	28	44.8	26.7	46	28	7.4	52.6
10	90	44.8	26.7	46	28	7.4	58.9
15	28	73.3	15.1	38	0.5	6.5	58.8
15	90	73.3	15.1	38	0.5	6.5	64.1
15	3	62.9	23.6	54	4	4.5	39.6
15	7	62.9	23.6	54	4	4.5	42.9
15	28	62.9	23.6	54	4	4.5	57.5
15	28	53	43	95	0	18	61.8
15	90	53	43	95	0	18	66.5
15	3	44.8	26.7	46	28	7.4	35.6
15	7	44.8	26.7	46	28	7.4	44.4
20	7	62.9	23.6	54	4	4.5	48.5
20	28	62.9	23.6	54	4	4.5	55.8
20	90	62.9	23.6	54	4	4.5	59.1
20	3	53	43	95	0	18	35
20	7	53	43	95	0	18	48.4
20	28	53	43	95	0	18	61.9
20	90	53	43	95	0	18	66.9
20	7	44.8	26.7	46	28	7.4	46
20	28	44.8	26.7	46	28	7.4	53.3
20	90	44.8	26.7	46	28	7.4	60

\*The properties of kaolins before calcination

Table A2 Input and output database for compressive strength (testing set)

Replacement level	Age	SiO <sub>2</sub> *	Al <sub>2</sub> O <sub>3</sub> *	Kaolinite*	Alunite*	Fineness	Compressive strength
5	3	73.3	15.1	38	0.5	6.5	40.2
5	7	73.3	15.1	38	0.5	6.5	50.7
5	28	73.3	15.1	38	0.5	6.5	57.6
5	90	73.3	15.1	38	0.5	6.5	59.6
5	3	62.9	23.6	54	4	4.5	41.2
5	7	62.9	23.6	54	4	4.5	50.3
5	28	62.9	23.6	54	4	4.5	56.3
5	90	62.9	23.6	54	4	4.5	58.3
5	90	44.8	26.7	46	28	7.4	56.8
5	90	53	43	95	0	18	60.1
5	28	44.8	26.7	46	28	7.4	53.3
10	3	63.7	22.1	54	2	7.3	36.1
10	7	63.7	22.1	54	2	7.3	45.1
10	28	63.7	22.1	54	2	7.3	52.9
10	90	63.7	22.1	54	2	7.3	58.7
10	3	73.3	15.1	38	0.5	6.5	25.3
10	7	73.3	15.1	38	0.5	6.5	43.3
10	28	73.3	15.1	38	0.5	6.5	56
10	90	73.3	15.1	38	0.5	6.5	62
15	3	63.7	22.1	54	2	7.3	34.5
15	7	63.7	22.1	54	2	7.3	43.9
15	28	63.7	22.1	54	2	7.3	60.5
15	90	63.7	22.1	54	2	7.3	62.3
15	3	73.3	15.1	38	0.5	6.5	23.1
15	7	73.3	15.1	38	0.5	6.5	44.5
15	28	44.8	26.7	46	28	7.4	55.7
15	90	44.8	26.7	46	28	7.4	61
15	90	62.9	23.6	54	4	4.5	62.7
15	3	53	43	95	0	18	33.8
15	7	53	43	95	0	18	48.2
20	3	63.7	22.1	54	2	7.3	25.9
20	7	63.7	22.1	54	2	7.3	42.9
20	28	63.7	22.1	54	2	7.3	55.7
20	90	63.7	22.1	54	2	7.3	60.5
20	3	73.3	15.1	38	0.5	6.5	35.3
20	7	73.3	15.1	38	0.5	6.5	47.2
20	28	73.3	15.1	38	0.5	6.5	56
20	90	73.3	15.1	38	0.5	6.5	63
20	3	62.9	23.6	54	4	4.5	41.5
20	3	44.8	26.7	46	28	7.4	33.9

\*The properties of kaolins before calcination

Table A3 Input and output database for splitting tensile strength

Replacement Level (%)	Age	SiO2	Al2O3	Kaolinite	Alunite	Fineness	Splitting tensile strength
5	28	63.73	22.06	54	2	7.34	3.77
10	28	63.73	22.06	54	2	7.34	3.93
15	28	63.73	22.06	54	2	7.34	4.02
20	28	63.73	22.06	54	2	7.34	3.68
5	90	63.73	22.06	54	2	7.34	4.05
10	90	63.73	22.06	54	2	7.34	4.20
15	90	63.73	22.06	54	2	7.34	4.45
20	90	63.73	22.06	54	2	7.34	4.55
5	28	73.29	15.14	38	0.5	6.45	3.3
10	28	73.29	15.14	38	0.5	6.45	3.26
15	28	73.29	15.14	38	0.5	6.45	4.17
20	28	73.29	15.14	38	0.5	6.45	3.65
5	90	73.29	15.14	38	0.5	6.45	3.80
10	90	73.29	15.14	38	0.5	6.45	4.03
15	90	73.29	15.14	38	0.5	6.45	4.25
20	90	73.29	15.14	38	0.5	6.45	4.02
5	90	62.9	23.61	54	4	4.45	4.06
10	90	62.9	23.61	54	4	4.45	4.17
15	90	62.9	23.61	54	4	4.45	4.52
20	90	62.9	23.61	54	4	4.45	4.16
5	28	62.9	23.61	54	4	4.45	3.79
10	28	62.9	23.61	54	4	4.45	3.21
15	28	62.9	23.61	54	4	4.45	4.08
20	28	62.9	23.61	54	4	4.45	3.50
5	28	44.76	26.7	46	28	7.4	3.30
10	28	44.76	26.7	46	28	7.4	3.87
15	28	44.76	26.7	46	28	7.4	3.81
20	28	44.76	26.7	46	28	7.4	3.31
5	90	44.76	26.7	46	28	7.4	3.93
10	90	44.76	26.7	46	28	7.4	4.24
15	90	44.76	26.7	46	28	7.4	3.95
20	90	44.76	26.7	46	28	7.4	3.93
5	90	53	43	95	0	18	3.93
10	90	53	43	95	0	18	4.04
15	90	53	43	95	0	18	4.27
20	90	53	43	95	0	18	3.90
5	90	53	43	95	0	18	4.14
10	90	53	43	95	0	18	4.52
15	90	53	43	95	0	18	4.68
20	90	53	43	95	0	18	4.68

Table A4 Input and output database used for constructing the models for permeability properties

INPUT VARIABLES						OUTPUT VARIABLES			
Kaolinite (%)	SiO <sub>2</sub> (%)	Al <sub>2</sub> O <sub>3</sub> (%)	Fineness (m <sup>2</sup> /gr)	Age (days)	Replacement (%)	Gas			Water
						Permeability, Kx10 <sup>-16</sup> (m <sup>2</sup> )	RCPT (Coulombs)	Sorptivity (mm/min <sup>1/2</sup> )	Permeability (mm)
54	69.8	24.2	7.3	28	5	2.63	1678	0.0803	21.0
54	69.8	24.2	7.3	28	10	2.47	1744	0.0676	15.8
54	69.8	24.2	7.3	28	15	2.38	1473	0.0763	14.3
54	69.8	24.2	7.3	28	20	2.03	1115	0.0827	12.0
54	69.8	24.2	7.3	90	5	2.29	1430.5	0.0600	16.5
54	69.8	24.2	7.3	90	10	1.91	1334	0.0535	13.5
54	69.8	24.2	7.3	90	15	1.81	969	0.0480	10.3
54	69.8	24.2	7.3	90	20	1.76	835	0.0443	8.5
38	77.7	15.1	6.5	28	5	2.62	1679.5	0.0825	21.0
38	77.7	15.1	6.5	28	10	2.50	1403	0.0863	23.0
38	77.7	15.1	6.5	28	15	2.07	1276.5	0.0933	20.8
38	77.7	15.1	6.5	28	20	1.95	1498	0.0795	16.5
38	77.7	15.1	6.5	90	5	2.43	1512.5	0.0690	16.5
38	77.7	15.1	6.5	90	10	2.02	1167.5	0.0590	13.6
38	77.7	15.1	6.5	90	15	1.93	1175.5	0.0497	11.0
38	77.7	15.1	6.5	90	20	1.89	985	0.0463	9.5
54	68.2	25.6	4.5	28	5	2.56	1604	0.0827	18.0
54	68.2	25.6	4.5	28	10	2.29	1454	0.0767	17.0
54	68.2	25.6	4.5	28	15	2.20	1318.5	0.0723	15.5
54	68.2	25.6	4.5	28	20	1.96	1344.5	0.0626	12.5
54	68.2	25.6	4.5	90	5	2.39	1376	0.0577	16.3
54	68.2	25.6	4.5	90	10	1.99	1050	0.0535	13.8
54	68.2	25.6	4.5	90	15	1.84	1035	0.0490	9.4
54	68.2	25.6	4.5	90	20	1.83	1100	0.0473	7.8
46	59.9	29.3	7.4	28	5	2.69	1854	0.1033	22.5
46	59.9	29.3	7.4	28	10	2.44	1618.5	0.0960	25.0
46	59.9	29.3	7.4	28	15	2.30	1372.5	0.1203	20.5
46	59.9	29.3	7.4	28	20	2.23	1776	0.1230	26.0
46	59.9	29.3	7.4	90	5	2.46	1763.5	0.0842	16.8
46	59.9	29.3	7.4	90	10	2.03	1519	0.0763	14.3
46	59.9	29.3	7.4	90	15	1.92	1359.5	0.0657	13.3
46	59.9	29.3	7.4	90	20	1.89	1213	0.0653	12.8
95	53.0	43.0	18.0	28	5	2.09	1326.5	0.0838	18.5
95	53.0	43.0	18.0	28	10	1.88	1247.5	0.0666	11.8
95	53.0	43.0	18.0	28	15	1.72	1082	0.0591	13.3
95	53.0	43.0	18.0	28	20	1.67	1008.5	0.0575	10.8
95	53.0	43.0	18.0	90	5	1.84	1065.5	0.0550	13.0
95	53.0	43.0	18.0	90	10	1.75	909.5	0.0516	10.9
95	53.0	43.0	18.0	90	15	1.38	770.5	0.0444	8.0
95	53.0	43.0	18.0	90	20	1.27	656.5	0.0428	7.1

Table A5 Summary of input and output database used for shrinkage modeling

Data	MK replacement level (%)	w/b ratio	Binder content (kg/m <sup>3</sup> )	Fineness of MK (m <sup>2</sup> /gr)	Al <sub>2</sub> O <sub>3</sub> content (%)	SiO <sub>2</sub> content (%)	Overall Drying period (days)	Shrinkage (microstrain)	
Current study (200 samples)	5%, 15%	0.4	350	18	43	53	60	32-510	
				7.34	24.2	69.8		50-555	
				6.45	15.1	77.7		35-595	
				4.45	25.2	68.2		65-570	
				7.43	29.3	59.9		60-615	
Training data	10%, 20%	0.35 0.55	450	8.6	45.8	52.8	60	104-664	
			350					32-472	
	Güneyisi et al. (2010) (24 samples)	5%, 15%	0.32	550	12	36.3	52.7	50	183-370
Testing data	Güneyisi et al. (2012a) (42 samples)	5%, 15%	0.35	470	12	36.3	52.7	42	86-451
	Brooks and Johari (2001) (14 samples)	15%	0.28	450	15	41.3	51.6	200	180-414

Table A6 Input and output database used for electrical resistivity modeling

Calcined kaolins	Type of mineral admixture	Replacement Level (%)	Age (days)	ER (kohm.cm)
DV	1	5	28	10.0
	1	10	28	10.6
	1	15	28	12.3
	1	20	28	15.3
	1	5	90	11.0
	1	10	90	12.5
	1	15	90	17.8
	1	20	90	16.7
CC	3	5	28	8.9
	3	10	28	9.2
	3	15	28	10.1
	3	20	28	14.0
	3	5	90	11.9
	3	10	90	18.1
	3	15	90	18.6
	3	20	90	19.4
DC	2	5	28	8.7
	2	10	28	10.2
	2	15	28	11.9
	2	20	28	15.5
	2	5	90	12.7
	2	10	90	11.8
	2	15	90	18.5
	2	20	90	19.3
BMK	4	5	28	6.5
	4	10	28	7.8
	4	15	28	9.9
	4	20	28	11.3
	4	5	90	9.4
	4	10	90	13.3
	4	15	90	13.1
	4	20	90	16.3
MK	5	5	28	10.4
	5	10	28	12.4
	5	15	28	15.2
	5	20	28	15.9
	5	5	90	16.8
	5	10	90	21.2
	5	15	90	23.8
	5	20	90	25.8

Table A7 Summary of input and output database used for corrosion current density modeling

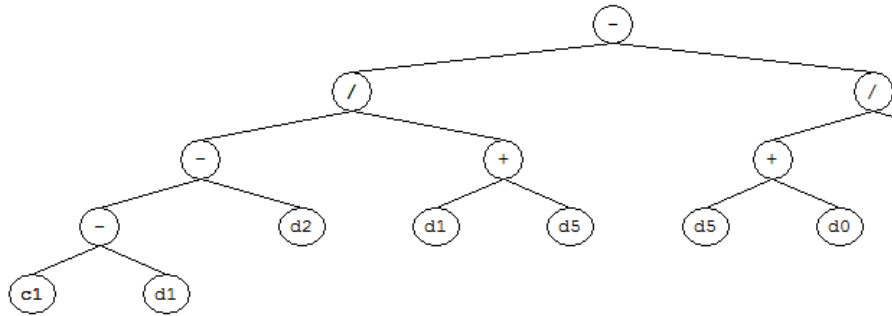
Kaolin type	NaCl Concentration	Replacement	Exposure period (weeks)	Icorr ( $\mu\text{A}/\text{cm}^2$ )
0:Control				
1: DV				
2: DC	2%	0%		
3:CC	5%	5%	0-40	0.19-0.57
4: BMK		15%		
5:MK				



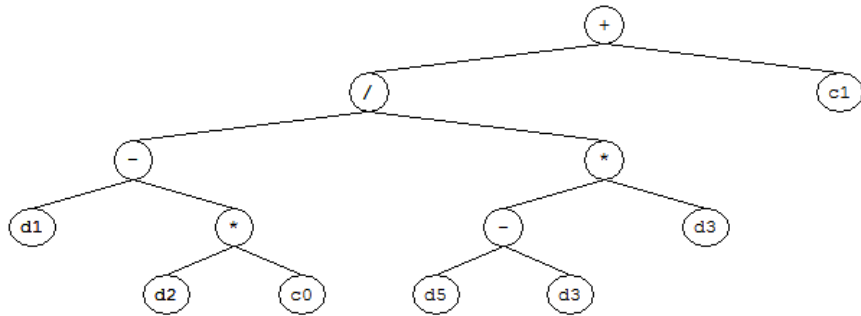
**APPENDIX B**  
**Mathematical models**

## B.1. Analytical models for compressive strength

Sub-ET 1



Sub-ET 2



Sub-ET 3

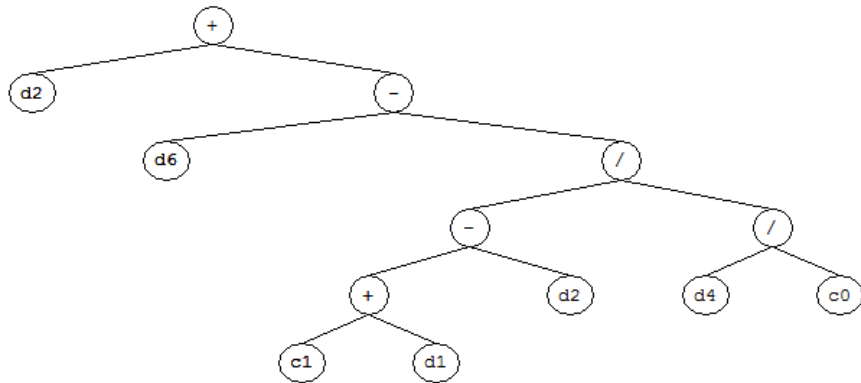


Figure B1 GEP expression tree for prediction of compressive strength [ $c_0$ - $c_1$ : constants,  $d_0$ : replacement level of CK or MK (%),  $d_1$ : age of concrete (days),  $d_2$ :  $\text{SiO}_2$  content of uncalcined kaolin,  $d_3$ :  $\text{Al}_2\text{O}_3$  content of uncalcined kaolin (%)  $d_4$ : kaolinite content of uncalcined kaolin (%),  $d_5$ : alunite content of uncalcined kaolin (%), and  $d_6$ : fineness of calcined kaolin ( $\text{m}^2/\text{gr}$ )].

### **GEP MODEL**

$$F=F1+F2+F3$$

$$F1 = (((G1C1-d[1])-d[2])/(d[1]+d[5]))-((d[5]+d[0])/d[1]))$$

$$F2= (((d[1]-(d[2]*G2C0))/((d[5]-d[3])*d[3]))+G2C1);$$

$$F3= (d[2]+(d[6]-(((G3C1+d[1])-d[2])/(d[4]/G3C0))))$$

$$G1C1 = -7.517456$$

$$G2C0 = -9.998871$$

$$G2C1 = -6.01538$$

$$G3C0 = -3.939331$$

$$G3C1 = -9.952881$$

### **MLR MODEL**

$$F= -976 -0.075*(Replacement\ level) +0.227*(Age) +10.9*SiO_2-15.8*Al_2O_3 \\ +12.2*(Kaolinite\ content) +14.5*(Alunite\ content)-1.96*(Fineness)$$

## B.2. Analytical models for splitting tensile strength

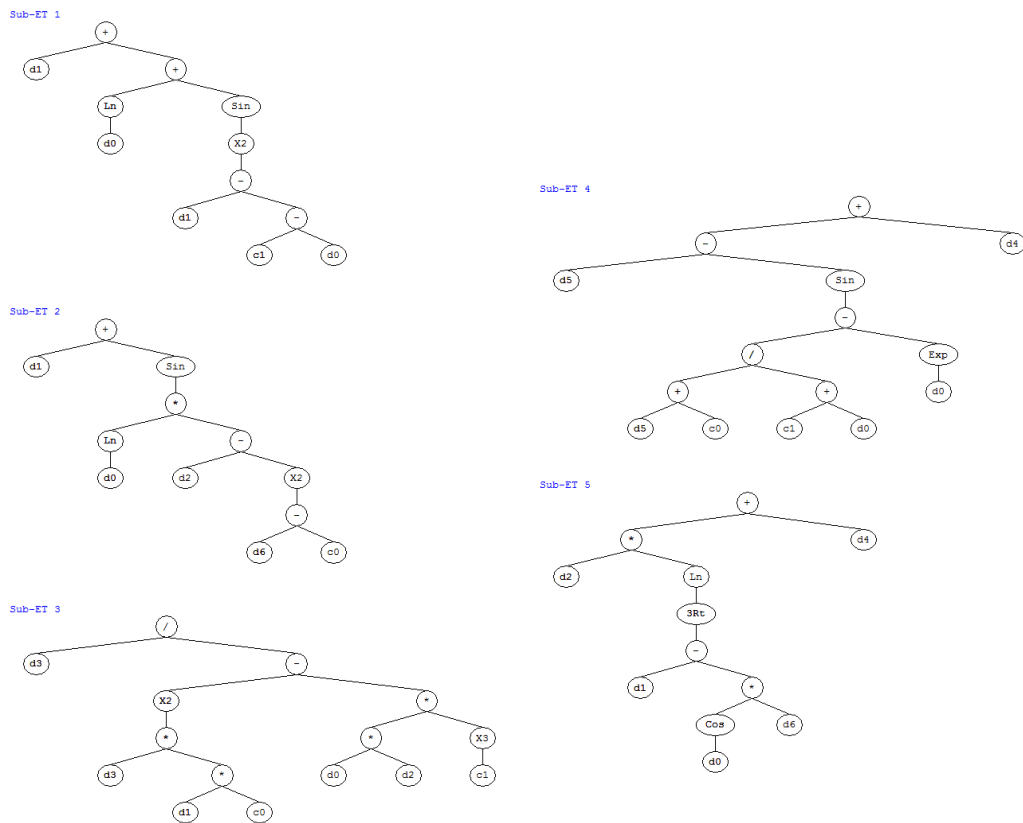


Figure B2 GEP expression tree for prediction of splitting tensile strength [ $c_0$ - $c_1$ : constants,  $d_0$ : replacement level of CK or MK (%),  $d_1$ : age of concrete (days),  $d_2$ : $\text{SiO}_2$  content of uncalcined kaolin,  $d_3$ : $\text{Al}_2\text{O}_3$  content of uncalcined kaolin (%),  $d_4$ : kaolinite content of uncalcined kaolin (%),  $d_5$ : alunite content of uncalcined kaolin (%), and  $d_6$ : fineness of calcined kaolin ( $\text{m}^2/\text{gr}$ )].

## GEP MODEL

$$F=F1 *F2 *F3 *F4 *F5$$

$$F1 = (d[1]+(\log(d[0]))+\sin(\text{pow}((d[1]-(G1C1-d[0])),2))))$$

$$F2= (d[1]+\sin((\log(d[0])*(d[2]-\text{pow}((d[6]-G2C0),2))))))$$

$$F3= (d[3]/(\text{pow}((d[3]*(d[1]*G3C0)),2)-((d[0]*d[2])*\text{pow}(G3C1,3))))$$

$$F4= ((d[5]-\sin((((d[5]+G4C0)/(G4C1+d[0]))-\exp(d[0]))))+d[4])$$

$$F5= ((d[2]*\log(\text{pow}((d[1]-(\cos(d[0])*d[6])),(1.0/3.0))))+d[4])$$

$$G1C1 = 7.525055$$

$$G2C0 = 7.025665$$

$$G3C0 = 9.624634$$

$$G3C1 = 7.927216$$

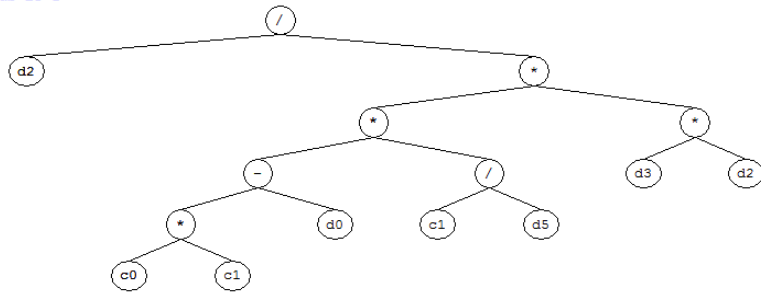
$$G4C1 = -2.66211$$

## MLR MODEL

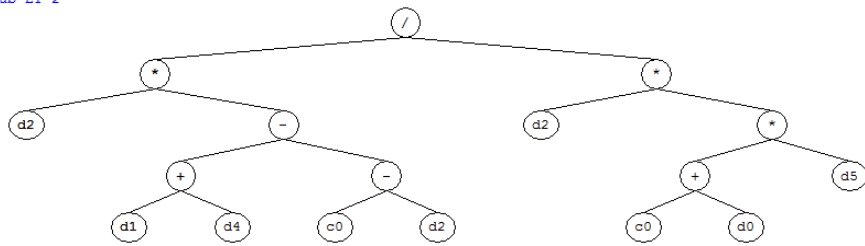
$$F=5.38+0.0136*(\text{Replacement level}) +0.00771*(\text{Age})-0.0308* \text{SiO}_2-0.099* \text{Al}_2\text{O}_3+0.0412*(\text{Kaolinite content})-0.0043*(\text{Fineness})$$

### B.3. Analytical models for gas permeability

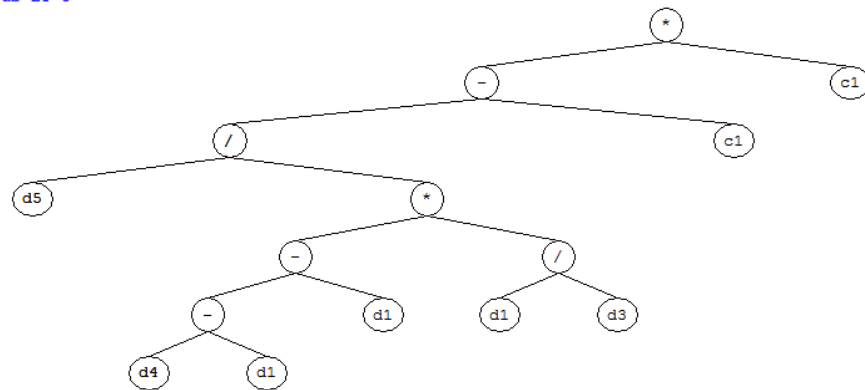
Sub-ET 1



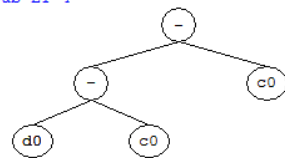
Sub-ET 2



Sub-ET 3



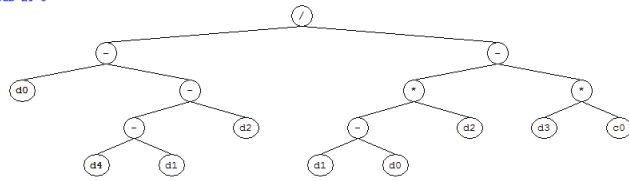
Sub-ET 4



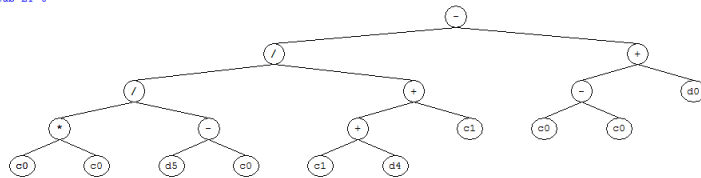
(Next page)

(Continued)

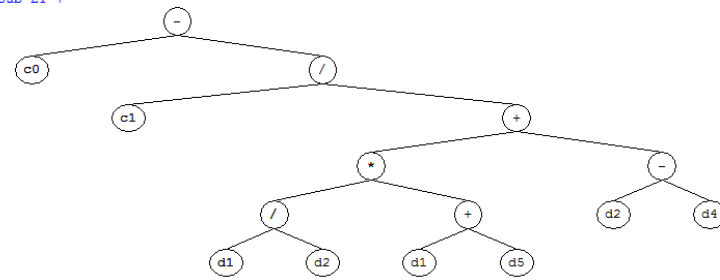
Sub-ET 5



Sub-ET 6



Sub-ET 7



Sub-ET 8



Figure B3 GEP expression tree for prediction of gas permeability [ $c_0$ - $c_1$ : constants,  $d_0$ : kaolinite content of uncalcined kaolin,  $d_1$ :  $\text{SiO}_2$  content of uncalcined kaolin (%),  $d_2$ :  $\text{Al}_2\text{O}_3$  content of uncalcined kaolin (%),  $d_3$ : fineness of calcined kaolin ( $\text{m}^2/\text{gr}$ ),  $d_4$ : age of concrete (days),  $d_5$ : replacement level of CK or MK (%)]

## GEP MODEL

$$K=K1+K2+K3+K4+K5+K6+K7+K8$$

$$K1 = (d[2]/((((G1C0*G1C1)-d[0])*(G1C1/d[5]))*(d[3]*d[2])))$$

$$K2 = ((d[2]*((d[1]+d[4])-(G2C0-d[2])))/(d[2]*((G2C0+d[0])*d[5])))$$

$$K3 = (((d[5]/(((d[4]-d[1])-d[1])*(d[1]/d[3]))) - G3C1)*G3C1)$$

$$K4 = ((d[0]-G4C0)-G4C0)$$

$$K5 = ((d[0]-((d[4]-d[1])-d[2]))/(((d[1]-d[0])*d[2])-(d[3]*G5C0)))$$

$$K6 = (((G6C0*G6C0)/(d[5]-G6C0))/((G6C1+d[4])+G6C1))-((G6C0-G6C0)+d[0])$$

$$K7 = (G7C0-(G7C1/(((d[1]/d[2])*(d[1]+d[5]))+(d[2]-d[4]))))$$

$$K8 = G8C1$$

$$G1C0 = 6.001434$$

$$G1C1 = 8.44635$$

$$G2C0 = 9.652466$$

$$G3C1 = 0.813416$$

$$G4C0 = 1.467438$$

$$G5C0 = 9.880127$$

$$G6C0 = -6.336639$$

$$G6C1 = -9.52417$$

$$G7C0 = 6.028015$$

$$G7C1 = -1.736511$$

$$G8C1 = -0.858368$$

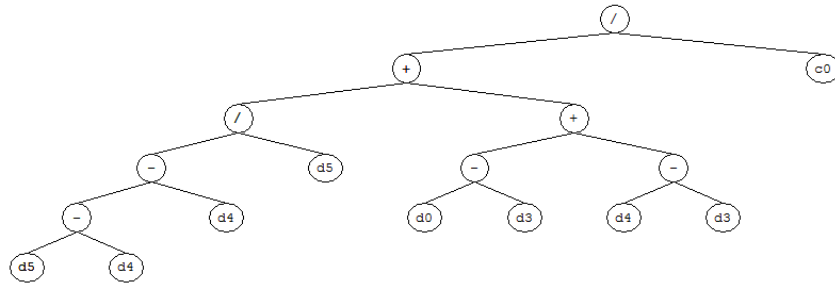
## MLR MODEL

$$K = -21.9-0.0978*(Kaolinite)+0.283 SiO_2+ 0.411*(Al_2O_3)+0.0537*(Fineness)-0.00488*(Age)-0.0366*(Replacement)$$

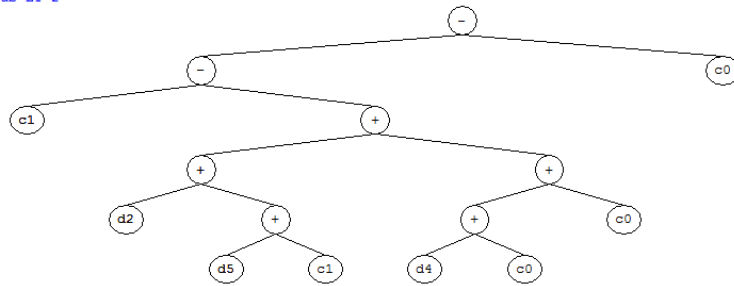


## B.4. Analytical models for water permeability

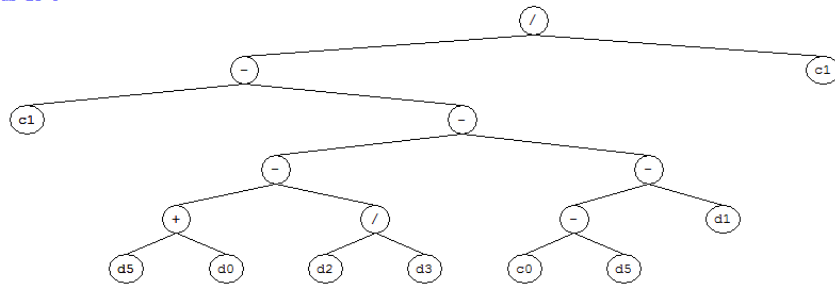
Sub-ET 1



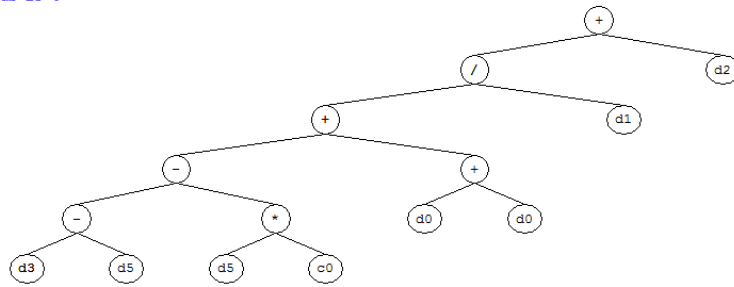
Sub-ET 2



Sub-ET 3



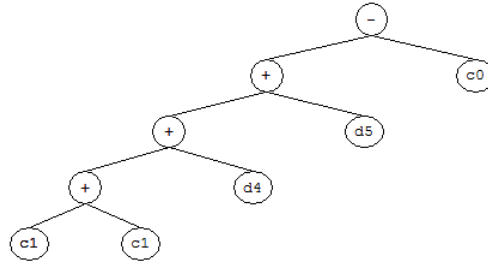
Sub-ET 4



(Next page)

(continued)

Sub-ET 5



Sub-ET 6

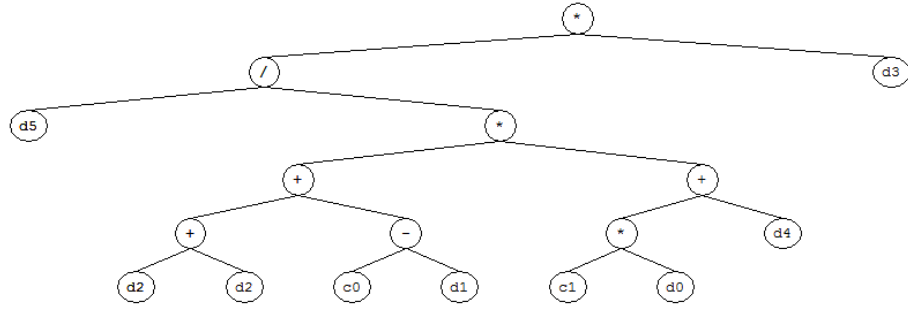


Figure B4 GEP expression tree for prediction of water permeability [ $c_0$ - $c_1$ : constants,  $d_0$ : kaolinite content of uncalcined kaolin (%),  $d_1$ :  $\text{SiO}_2$  content of uncalcined kaolin (%),  $d_2$ :  $\text{Al}_2\text{O}_3$  content of uncalcined kaolin (%),  $d_3$ : fineness of calcined kaolin ( $\text{m}^2/\text{gr}$ ),  $d_4$ : age of concrete (days),  $d_5$ : replacement level of CK or MK (%)]

### GEP MODEL

$$D=D1+D2+D3+D4+D5+D6$$

$$D1= (((((d[5]-d[4])-d[4])/d[5])+((d[0]-d[3])+(d[4]-d[3])))/G1C0)$$

$$D2= ((G2C1-((d[2]+(d[5]+G2C1)))+(d[4]+G2C0)+G2C0))-G2C0)$$

$$D3= ((G3C1-(((d[5]+d[0])-(d[2]/d[3]))-(G3C0-d[5])-d[1])))/G3C1)$$

$$D4= (((((d[3]-d[5])-(d[5]*G4C0))+(d[0]+d[0]))/d[1])+d[2])$$

$$D5= (((G5C1+G5C1)+d[4])+d[5])-G5C0)$$

$$D6= ((d[5])/(((d[2]+d[2])+(G6C0-d[1]))*((G6C1*d[0])+d[4]))) * d[3])$$

$$G1C0 = -8.816498$$

$$G2C0 = -7.967621$$

$$G2C1 = -0.204864$$

$$G3C0 = 0.688721$$

$$G3C1 = 9.213226$$

$$G4C0 = 1.054321$$

$$G5C0 = 4.903351$$

$$G5C1 = 9.422241$$

$$G6C0 = 4.908783$$

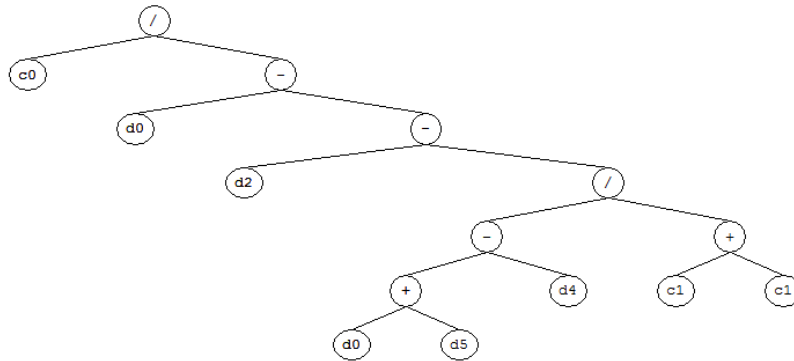
$$G6C1 = -0.450195$$

### MLR MODEL

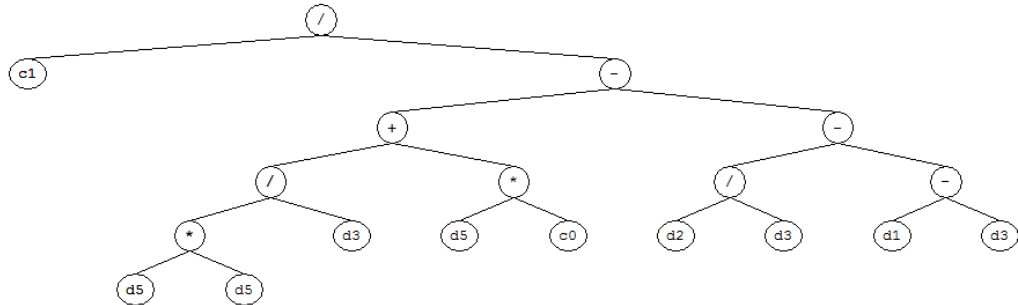
$$D = 209+0.27*(\text{Kaolinite})-2.0*(\text{SiO}_2)+ 2.49*(\text{Al}_2\text{O}_3)-0.030*(\text{Fineness})-0.091*(\text{Age})-0.3846*(\text{Replacement})$$

## B.5. Analytical models for water sorptivity

Sub-ET 1



Sub-ET 2



Sub-ET 3

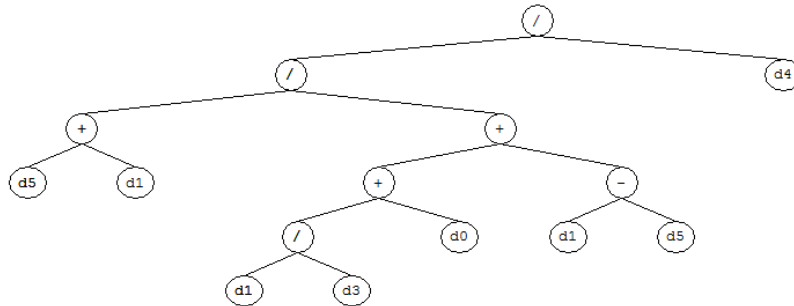


Figure B5 GEP expression tree for prediction of water sorptivity [ $c_0$ - $c_1$ : constants,  $d_0$ : kaolinite content of uncalcined kaolin,  $d_1$ :  $\text{SiO}_2$  content of uncalcined kaolin (%),  $d_2$ :  $\text{Al}_2\text{O}_3$  content of uncalcined kaolin (%),  $d_3$ : fineness of calcined kaolin ( $\text{m}^2/\text{gr}$ ),  $d_4$ : age of concrete (days),  $d_5$ : replacement level of CK or MK (%)]

### **GEP MODEL**

$$S1 = (G1C0/(d[0]-(d[2]-(((d[0]+d[5])-(d[4])/(G1C1+G1C1))))))$$

$$S2 = (G2C1/((((d[5]*d[5])/d[3])+(d[5]*G2C0))-((d[2]/d[3])-(d[1]-d[3]))))$$

$$S3 = (((d[5]+d[1])/(((d[1]/d[3])+d[0])+(d[1]-d[5])))/d[4])$$

$$G1C0 = 0.839814$$

$$G1C1 = -4.012603$$

$$G2C0 = 3.566986$$

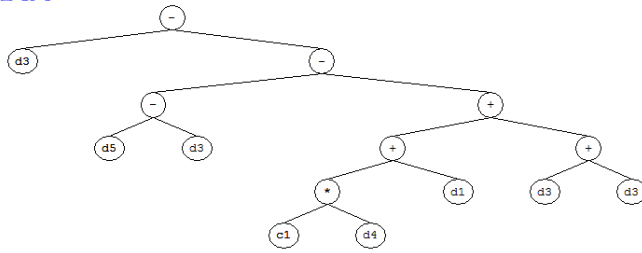
$$G2C1 = 2.173706$$

### **MLR MODEL**

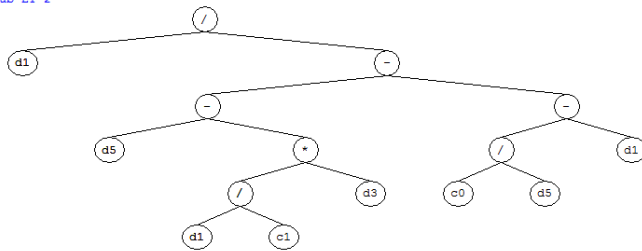
$$S = 0.46 - 0.00065 * (\text{Kaolinite}) - 0.0038 * (\text{SiO}_2) - 0.0030 * (\text{Al}_2\text{O}_3) + 0.00117 * (\text{Fineness}) - 0.000427 * (\text{Age}) - 0.000661 * (\text{Replacement})$$

## B.6. Analytical models for rapid chloride permeability test

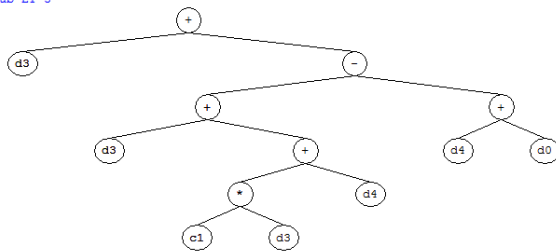
Sub-ET 1



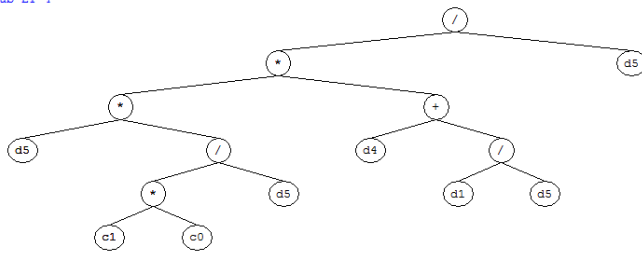
Sub-ET 2



Sub-ET 3



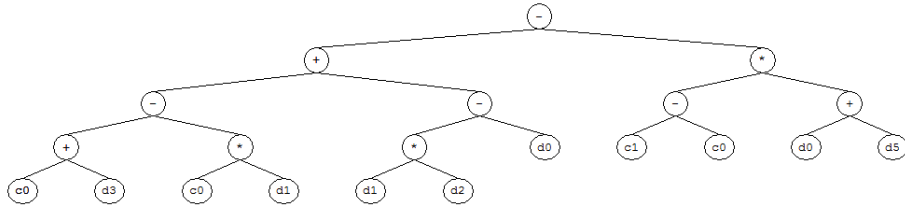
Sub-ET 4



(Next page)

(continued)

Sub-ET 5



Sub-ET 6

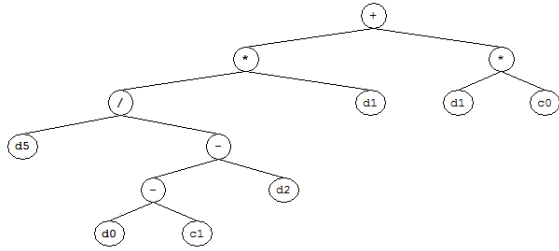


Figure B6 GEP expression tree for prediction of rapid chloride permeability [ $c_0$ - $c_1$ : constants,  $d_0$ : kaolinite content of uncalcined kaolin,  $d_1$ :  $\text{SiO}_2$  content of uncalcined kaolin (%),  $d_2$ :  $\text{Al}_2\text{O}_3$  content of uncalcined kaolin (%),  $d_3$ : fineness of calcined kaolin ( $\text{m}^2/\text{gr}$ ),  $d_4$ : age of concrete (days),  $d_5$ : replacement level of CK or MK (%)]

## GEP MODEL

$$C=C1+C2+C3+C4+C5+C6$$

$$C1= (d[3]-((d[5]-d[3])-(((G1C1*d[4])+d[1])+(d[3]+d[3])))))$$

$$C2= (d[1]/((d[5]-((d[1]/G2C1)*d[3]))-((G2C0/d[5])-d[1])))$$

$$C3= (d[3]+((d[3]+((G3C1*d[3])+d[4]))-(d[4]+d[0])))$$

$$C4= (((d[5]*((G4C1*G4C0)/d[5]))*(d[4]+(d[1]/d[5])))/d[5])$$

$$C5= (((G5C0+d[3])-(G5C0*d[1]))+((d[1]*d[2])-d[0]))-((G5C1-G5C0)*(d[0]+d[5]))$$

$$C6= (((d[5]/((d[0]-G6C1)-d[2]))*d[1])+(d[1]*G6C0))$$

$$G1C1 = -5.658722$$

$$G2C0 = 5.341186$$

$$G2C1 = 5.702454$$

$$G3C1 = 9.843811$$

$$G4C1 = -5.007781$$

$$G5C0 = -8.821442$$

$$G5C1 = 9.848786$$

$$G6C0 = 6.544708$$

$$G6C1 = 9.795014$$

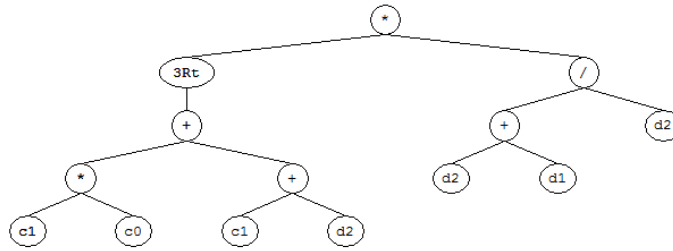
## MLR MODEL

$$C = -17093-85.7*(\text{Kaolinite}) +217*(\text{SiO}_2) +333*(\text{Al}_2\text{O}_3) +55.5*(\text{Fineness}) -4.55*(\text{Age})-25.8*(\text{Replacement})$$

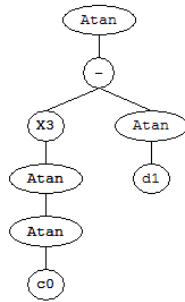


## B.7. Analytical models for electrical resistivity test

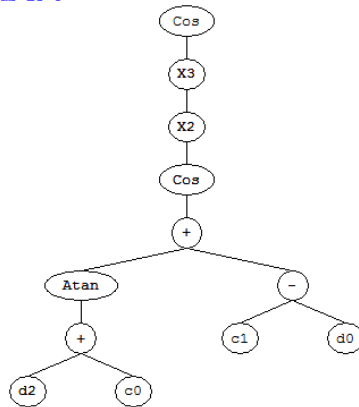
Sub-ET 1



Sub-ET 2



Sub-ET 3



Sub-ET 4

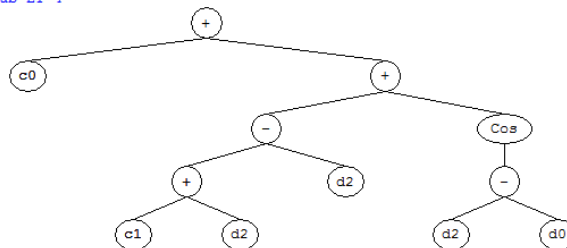


Figure B7 GEP expression tree for prediction of electrical resistivity [ $c_0$ - $c_1$ : constants,  $d_0$ : type of mineral admixture (1:DV, 2:DC, 3:CC, 4:BMK, and 5:MK),  $d_1$ : replacement level of CK or MK (%),  $d_2$ : age of concrete (days)]

## GEP MODEL

$$R=R1*R2*R3*R4$$

$$R1 = (\text{pow}(\text{pow}(\text{pow}(\text{G1C1} * \text{G1C0}) + (\text{G1C1} + \text{d}[2])), (1.0/3.0)) * ((\text{d}[2] + \text{d}[1]) / \text{d}[2]))$$

$$R2 = \text{atan}(\text{pow}(\text{atan}(\text{atan}(\text{G2C0})), 3) - \text{atan}(\text{d}[1]))$$

$$R3 = \text{cos}(\text{pow}(\text{pow}(\text{cos}(\text{atan}(\text{d}[2] + \text{G3C0}) + (\text{G3C1} - \text{d}[0])), 2), 3))$$

$$R4 = (\text{G4C0} + (((\text{G4C1} + \text{d}[2]) - \text{d}[2]) + \text{cos}(\text{d}[2] - \text{d}[0])))$$

$$\text{G1C0} = -4.848084$$

$$\text{G1C1} = 4.39032$$

$$\text{G2C0} = 8.967347$$

$$\text{G3C0} = -9.884491$$

$$\text{G3C1} = -4.113372$$

$$\text{G4C0} = -9.515717$$

$$\text{G4C1} = 1.794709$$

## MLR MODEL

$$R = 1.8 + 0.62 * (\text{Type of mineral admixture}) + 0.427 * (\text{Replacement level}) \\ + 0.0822 * (\text{Age})$$

## B.8. Analytical models for UPV loss due to freezing and thawing

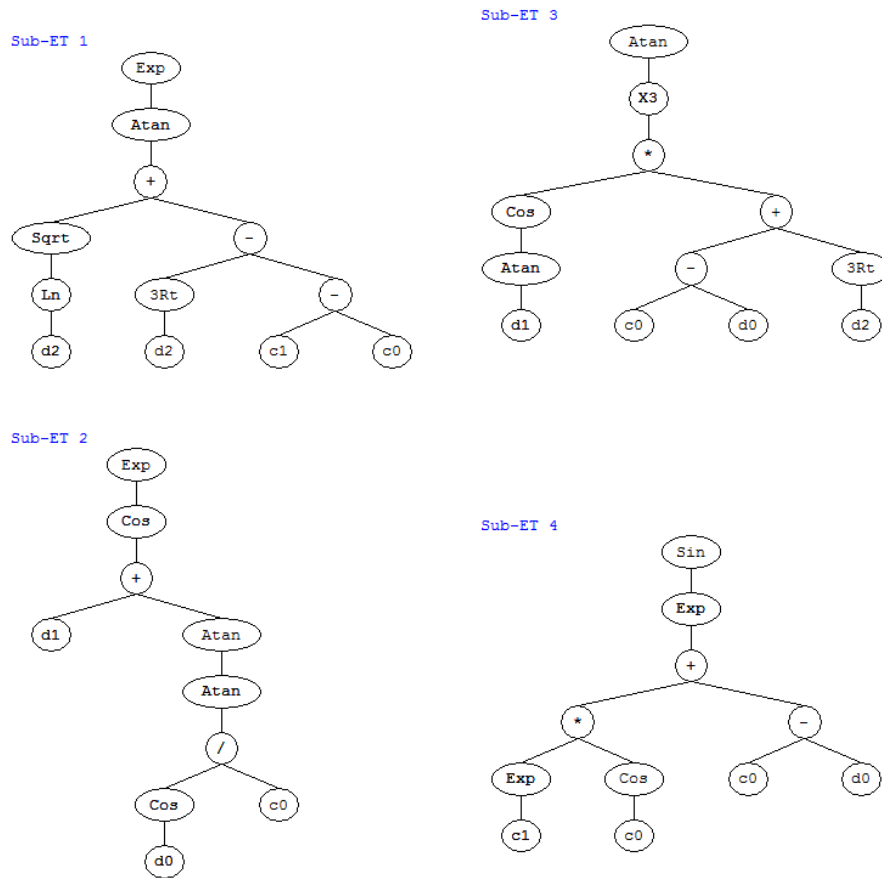


Figure B8 GEP expression tree for prediction of UPV loss as a result of freezing - thawing [c<sub>0</sub>-c<sub>1</sub>: constants, d<sub>0</sub>: type of mineral admixture (0:Control, 1:DV, 2:DC, 3:CC, 4:BMK, and 5:MK), d<sub>1</sub>: replacement level of CK or MK (%), d<sub>2</sub>: Number of freezing-thawing cycles]

### **GEP MODEL**

$$L=L1+L2+L3+L4$$

$$L1= \exp(\operatorname{atan}(\sqrt{\log(d[2])}+(\operatorname{pow}(d[2],(1.0/3.0))-(G1C1-G1C0))))$$

$$L2= \exp(\cos((d[1]+\operatorname{atan}(\operatorname{atan}(\cos(d[0])/G2C0))))))$$

$$L3= \operatorname{atan}(\operatorname{pow}(\cos(\operatorname{atan}(d[1]))*((G3C0-d[0])+\operatorname{pow}(d[2],(1.0/3.0))),3))$$

$$L4= \sin(\exp(((\exp(G4C1)*\cos(G4C0))+(G4C0-d[0])))$$

$$G1C0 = 1.394318$$

$$G1C1 = 8.933381$$

$$G2C0 = 2.175842$$

$$G2C1 = -9.278106$$

$$G3C0 = -5.113433$$

$$G3C1 = 7.802368$$

$$G4C0 = 8.583893$$

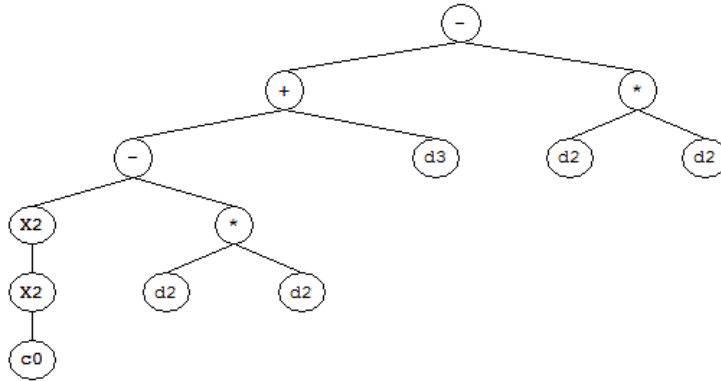
$$G4C1 = -3.53894$$

### **MLR MODEL**

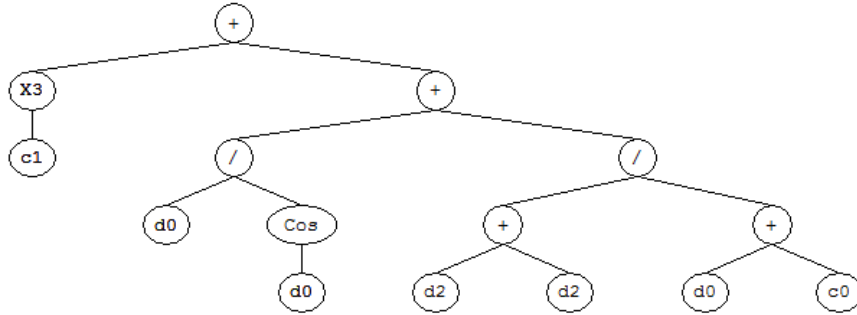
$$L= 1.61-0.251*(\text{Type of mineral admixture})-0.0984*(\text{Replacement level}) \\ +0.0128*(\text{Number of cycles})$$

## B.9. Analytical models for corrosion current density

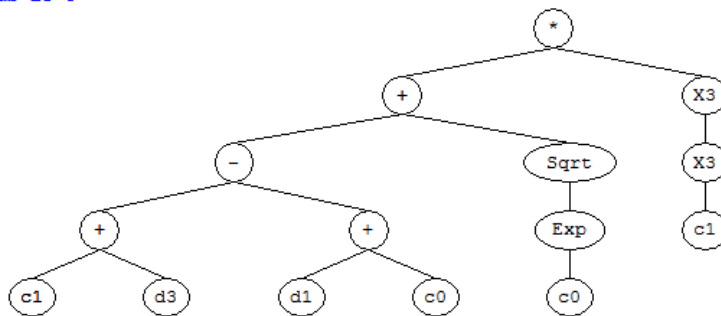
Sub-ET 1



Sub-ET 2



Sub-ET 3



(Next page)

(continued)

Sub-ET 4

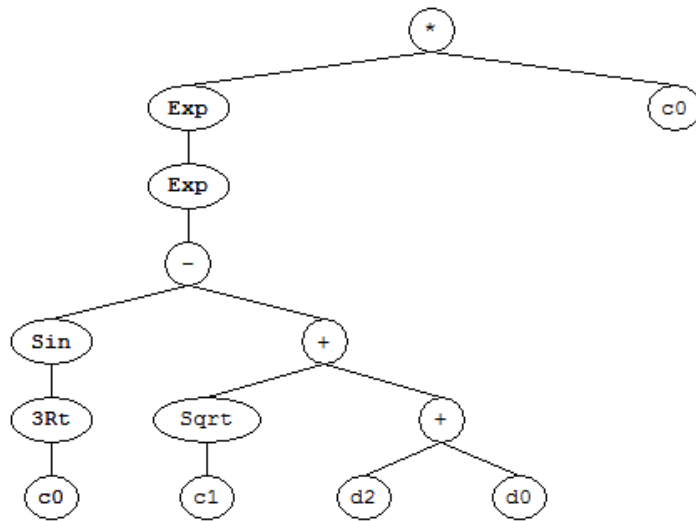


Figure B9 GEP expression tree for prediction of corrosion current density [ $c_0$ - $c_1$ : constants,  $d_0$ : type of mineral admixture (0:Control, 1:DV, 2:DC, 3:CC, 4:BMK, and 5:MK),  $d_1$ : concentration of NaCl solution,  $d_2$ : replacement level of CK or MK (%),  $d_3$ : exposure period (days)]

### GEP MODEL

$$I=I1*I2*I3*I4$$

$$I1= (((\text{pow}(\text{pow}(G1C0,2),2)-(\text{d}[2]*\text{d}[2]))+\text{d}[3])-(\text{d}[2]*\text{d}[2]))$$

$$I2= (\text{pow}(G2C1,3)+((\text{d}[0]/\cos(\text{d}[0]))+((\text{d}[2]+\text{d}[2])/(\text{d}[0]+G2C0))))$$

$$I3= (((((G3C1+\text{d}[3])-(\text{d}[1]+G3C0))+\text{sqrt}(\exp(G3C0))))*\text{pow}(\text{pow}(G3C1,3),3))$$

$$I3= (\exp(\exp((\sin(\text{pow}(G4C0,(1.0/3.0)))-(\text{sqrt}(G4C1)+(\text{d}[2]+\text{d}[0]))))))*G4C0$$

$$G1C0 = 7.042175;$$

$$G1C1 = -8.319;$$

$$G2C0 = -4.20343;$$

$$G2C1 = -7.065612;$$

$$G3C0 = 9.61792;$$

$$G3C1 = -0.089569;$$

$$G4C0 = 8.729584;$$

$$G4C1 = 5.159515;$$

### MLR MODEL

$$I= 0.385-0.00711*(\text{Type of mineral admixture})-0.00685*(\text{NaCl concentration}) - 0.00538*(\text{Replacement})+0.0033*(\text{Exposure period})$$

## B.9. Analytical models for drying shrinkage

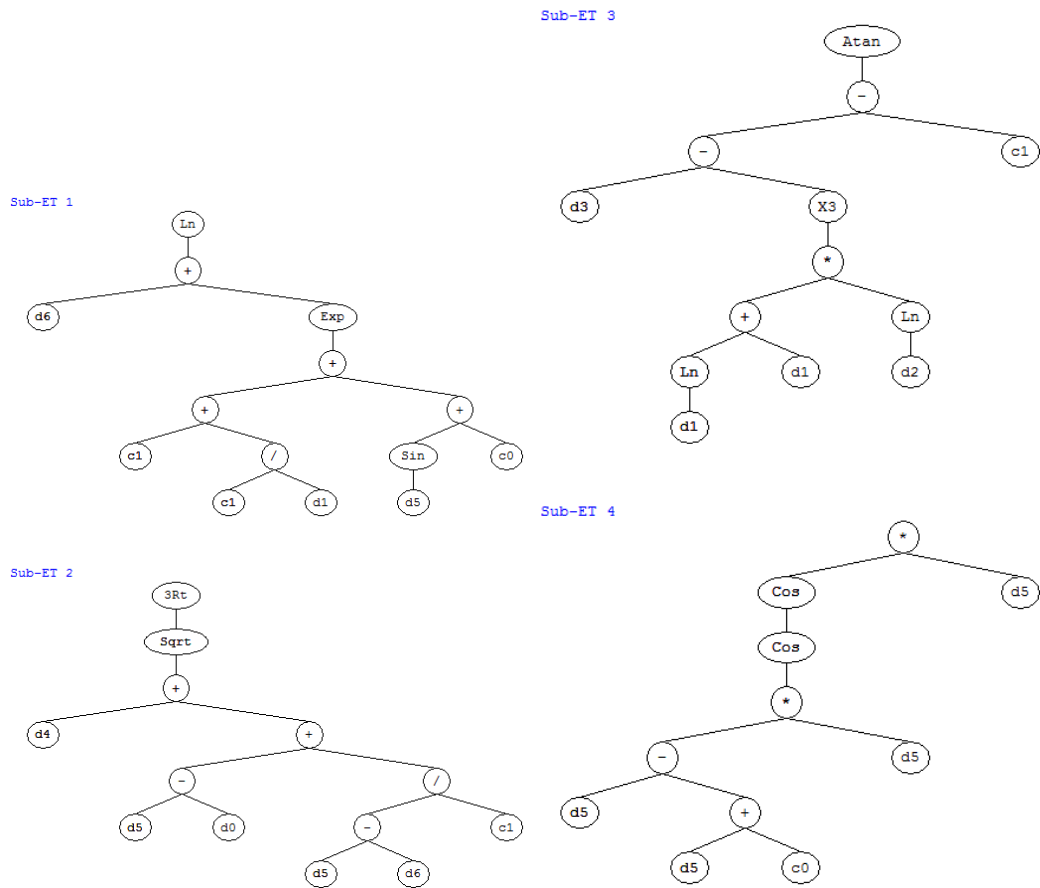


Figure B10 GEP expression tree for prediction of drying shrinkage [ $d_0$  is replacement level (%);  $d_1$  is w/b content;  $d_2$  is binder content ( $\text{kg}/\text{m}^3$  of concrete);  $d_3$  is fineness of MK or CK ( $\text{m}^2/\text{gr}$ );  $d_4$  is  $\text{Al}_2\text{O}_3$  content (%);  $d_5$  is  $\text{SiO}_2$  content (%);  $d_6$  is drying period (days) and  $c_0$  and  $c_1$  are constants]



### **GEP MODEL**

$$S=S1*S2*S3*S4$$

$$S1 = \log((d[6]+\exp(((G1C1+(G1C1/d[1]))+(\sin(d[5])+G1C0))))))$$

$$S2= \text{pow}(\text{sqrt}((d[4]+((d[5]-d[0])+((d[5]-d[6])/G2C1)))),(1.0/3.0))$$

$$S3= \text{atan}(((d[3]-\text{pow}((\log(d[1])+d[1])*\log(d[2])),3))-G3C1))$$

$$S4= (\cos(\cos(((d[5]-(d[5]+G4C0))*d[5]))) * d[5])$$

$$G1C0 = -9.738892$$

$$G1C1 = 2.379333$$

$$G2C1 = 2.861298$$

$$G3C1 = 6.534363$$

$$G4C0 = 8.285644$$

### **MLR MODEL**

$$S= 239-2.68*(\text{Replacement level})-692*(\text{w/b ratio}) -0.501*(\text{Binder content})-13.2*(\text{Fineness})+9.0*(\text{Al}_2\text{O}_3)+4.87*(\text{SiO}_2)+7.2*(\text{Drying period})$$

## PERSONAL INFORMATION

Name and Surname: Kasım MERMERDAŞ  
Nationality : T.C.  
Birth place and date : Şanlıurfa/1981  
Marital status : Married-2 children  
Phone number : 505 9044441/342 3172442  
Fax : 342 3601107  
Email : mermerdas@gantep.edu.tr

## EDUCATION

	Graduate school	Year
Master	University of Gaziantep	2007
Bachelor	University of Gaziantep	2004
High School	Şanlıurfa İHL	1999

## WORK EXPERIENCE

Years	Place	Enrollment
2004-Present	University of Gaziantep	Research Assistant

## PUBLICATIONS

### A. International Journals

1. Mehmet Gesoglu, Erhan Güneyisi, Radhwan Alzebaree, **Kasım Mermerdaş** (2013). "Effect of silica fume and steel fiber on the mechanical properties of the concretes produced with cold bonded fly ash aggregates" Construction and Building Materials Vol. 40 pp. 982-990.
2. Erhan Güneyisi, Mehmet Gesoğlu, Fatih Karaboğa, **Kasım Mermerdaş** (2013) "Corrosion behavior of reinforcing steel embedded in chloride contaminated concretes with and without metakaolin" Composites Part B: Engineering Vol. 45 pp.1288-1295.
3. **Kasım Mermerdaş**, Mehmet Gesoğlu, Erhan Güneyisi, Turan Özturan (2012) "Strength development of concretes incorporated with metakaolin and different types of calcined kaolins" Construction and Building Materials Vol. 37 pp. 766-774.
4. Erhan Güneyisi, Mehmet Gesoğlu, Turan Özturan, **Kasım Mermerdaş** (2012) "Microstructural properties and pozzolanic activity of calcined kaolins as supplementary cementing materials" Canadian Journal of Civil Engineering Vol. 39 pp.1274-1284
5. Erhan Güneyisi, Mehmet Gesoğlu, Seda Karaoğlu, **Kasım Mermerdaş** (2012) "Strength, permeability and shrinkage cracking of silica fume and metakaolin concretes" Construction and Building Materials Vol. 34 pp. 120-130.
6. Mehmet Gesoğlu, Erhan Güneyisi, M. Erkan Kocabağ, Veysel Bayram, **Kasım Mermerdaş** (2012) "Fresh and hardened characteristics of self compacting concretes made with combined use of marble powder, limestone filler, and fly ash" Construction and Building Materials Vol. 37 pp. 160-170.

7. Mehmet Gesođlu, Erhan Güneyisi, Swara Fuad Mahmood, H. Öznur Öz, **Kasım Mermerdaş** (2012) "Recycling ground granulated blast furnace slag as cold bonded artificial aggregate partially used in self-compacting concrete" Journal of Hazardous Material Vol. 235 pp. 352-358.
8. Erhan Güneyisi, Mehmet Gesođlu, Turan Özturan, **Kasım Mermerdaş**, Erdoğan Özbay (2011) "Properties of mortars with natural pozzolana and limestone based blended cements" ACI Materials Journal Vol. 108 pp. 493-500.
9. Erhan Güneyisi, Mehmet Gesođlu, **Kasım Mermerdaş**. Strength deterioration of plain and metakaolin concretes in aggressive sulfate environments. ASCE Journal of Materials in Civil Engineering Vol. 22 pp.403-407
10. Erhan Güneyisi, Mehmet Gesođlu, **Kasım Mermerdaş** (2008) "Improving strength, drying shrinkage, and pore structure of concrete using metakaolin" Materials and Structures Vol. 41 pp.937-949.
11. Erhan Güneyisi, **Kasım Mermerdaş** (2007) "Comparative study on strength, sorptivity, and chloride ingress characteristics of air-cured and water-cured concretes modified with metakaolin" Materials and Structures Vol. 40 pp.1161-1171.

## **B. International Congress, Conference, and Symposium**

1. Shimal J. Younus, Erhan Güneyisi, Mehmet Gesođlu, **Kasım Mermerdaş**, Süleyman İpek (2012) "Resistance of natural rubber latex modified lightweight concrete to chloride ingress" 7th Asian Symposium on Polymers in Concrete (ASPIC 2012) Proc. pp. 473-480.
2. Erhan Güneyisi, Mehmet Gesođlu, **Kasım Mermerdaş**, Süleyman İpek (2012) "Transport properties of plain and silica fume concretes incorporating waste tire rubber" 27th International Conference on Solid Waste Technology and Management, USA CD pp. 599-608.
3. Faruk Geyik, Mehmet Gesođlu, Erhan Güneyisi, **Kasım Mermerdaş**, Hatice Öznur Öz (2012) "Predicting the crushing strength of cold-bonded artificial aggregates by genetic algorithms" 27th International Conference on Solid Waste Technology and Management, USA, CD pp. 276-283.
4. Erhan Güneyisi, Mehmet Gesođlu, Turan Özturan, **Kasım Mermerdaş** (2012) "Comparing pozzolanic activity of metakaolin and calcined kaolin, and their effects on strength of concrete" 10th International Congress on Advances in Civil Engineering (ACE 2012) CD version.
5. **Kasım Mermerdaş**, Faruk Geyik (2010) "Use of Genetic Programming for Prediction of Compressive Strength of the Concretes Modified with Metakaolin" 9th International Congress on Advances in Civil Engineering (ACE 2010) CD version.
6. Önder Ökmen, Ahmet Öztaş, **Kasım Mermerdaş** (2006) "İnşaat Proje Süre Tespitinde PERT, Stokastik CPM, ve Sübjektif Kararlı Risk Analizi Tabanlı CPM

uygulaması: Karşılaştırmalı bir vaka çalışması" Uluslararası GAP V. Mühendislik Kongresi Cilt 2 ss. 1255-1262.

### **C. National Journals**

1. Mehmet Gesoğlu, Erhan Güneyisi, **Kasım Mermerdaş** (2007) "Metakaolin Miktarının ve Kür Koşullarının Betonun Basınç Dayanımı ve Elektriksel Direnci Üzerine Etkileri" Hazır Beton Dergisi Vol. 14 ss. 72-76.

### **D. National Congress, Conference, and Symposium**

1. Erhan Güneyisi, Mehmet Gesoğlu, Seda Karaoğlu, **Kasım Mermerdaş** (2011) "Silis Dumanı ve Metakaolinin Betonların Gaz Geçirimsizliği ve Kısıtlanmış Rötresine Etkileri" 8. Ulusal Beton Kongresi Bildiriler Kitabı ss. 55-66.

2. Mehmet Gesoğlu, Erhan Güneyisi, M. Erkan Kocabağ, Veysel Bayram, **Kasım Mermerdaş** (2011) "Mermer Tozu ve Uçucu Kül Katkılı Kendiliğinden Yerleşen Betonların Taze ve Sertleşmiş Özelliklerinin İncelenmesi" 8. Ulusal Beton Kongresi Bildiriler Kitabı ss. 109-119.

3. Erhan Güneyisi, Mehmet Gesoğlu, **Kasım Mermerdaş** (2007) "Metakaolin Katkılı Betonların Sülfat Dayanıklılığının İncelenmesi" 7. Ulusal Beton Kongresi Bildiriler Kitabı ss. 259-269.

### **RESEARCH PROJECTS**

1. Puzolan ve kalker katkıli çimentolu harçların geçirimsizlik, elektriksel direnç ve sülfat ortamındaki dayanıklılık özelliklerinin araştırılması (TÇMB, Completed, 2008)

2. Türkiye kökenli kaolenlerin kalsine edilerek betonda dayanım ve geçirimsizlik özelliklerinin iyileştirilmesi amaçlı kullanımının araştırılması. (GAZÜ BAP, Completed 2009)

### **FOREIGN LANGUAGE**

Turkish (Mother language), English

### **HOBBIES**

Chess, Computer, Reading